UNIVERSITÀ DEGLI STUDI DI PALERMO

Dottorato in ingegneria dell'innovazione tecnologica.
Dipartimento dell'innovazione industriale e digitale-DIID
Ingegneria Chimica, Gestionale, Informatica, Meccanica

Xyloglucan-based hydrogels: A biomaterials chemistry contribution towards advanced wound dressings

IL DOTTORE
ALESSIA AJOVALASIT

IL COORDINATORE
Prof. ANTONIO CHELLA

IL TUTOR
Prof. CLELIA DISPENZA

CICLO XXX
2018

CONTENTS

ABSTRACT

The last two decades have witnessed the introduction of several new wound dressings, with many of them being hydrogels for the advantages that these materials can offer in the application. However, despite the advancements and the wide range of dressings available, wound management is still an extremely challenging task due to its subjectivity, complexity and scarce knowledge of the wound healing process itself, and patient variability. For this reason, an interdisciplinary approach to wound care that can help reducing the incidence and prevalence of wounds is needed.

One important goal would be to develop "smart" wound dressings that are easy to apply, wear and be removed, that are able to maintain a good balance between hydration of the wound bed and fluid absorption, that can act as a barrier against bacteria to prevent infections, yet allowing oxygenation, that are able to provide the physician with relevant information on physico-chemical and biological parameters to monitor the state of the wound and the healing process without requiring direct inspection, that can (eventually) release drugs or play regeneration functions to sustain and enhance the healing process.

This very ambitious goal can only be achieved by merging contributions from different fields of research and expertise. In particular, the field of (bio)materials science and technology for the development of materials with the required combination of physico-chemical, mechanical and barrier properties, skin electronics for the integration of sensors and actuators, and tissue engineering to explore the possibility of including in the "smart" dressing also tissue regeneration functions (Fig. I).

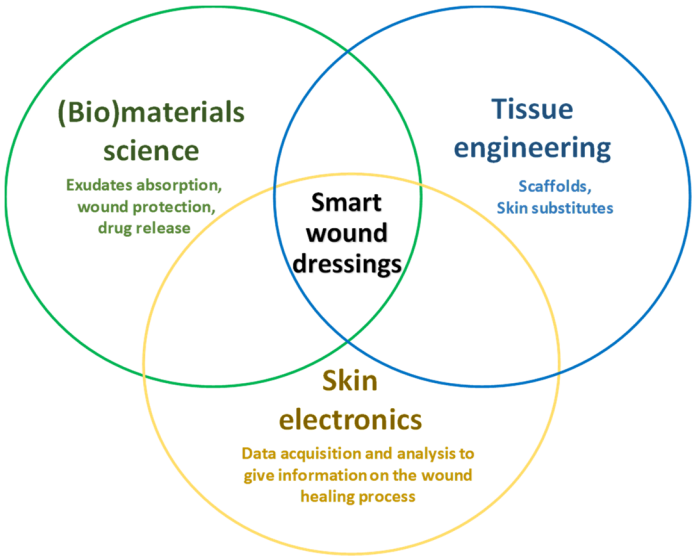

Fig. I Schematic representation of the approach chosen to design a "smart" wound dressing

The design of new materials for wound management applications can, in principle, benefit from the use of an intrinsically active polymer.

Among all the available polymers, xyloglucan (XG) combines several favourable properties, which make it a suitable candidate for the scope:

- It is abundant in nature, thus low-cost and its extraction is easy and high yield,
- it is characterized by a very interesting self-assembly behaviour,
- it is biodegradable and biocompatible; due to its vegetal origin it should not elicit the response of the human immune system,
- there are a few studies concerning the possibility to employ this polysaccharide for biomedical applications, and it has been shown to have intrinsic activity such as anti-inflammatory properties for application through the skin and potential beneficial effect in reepithelization and remodelling,
- it has film-forming properties,

- and it is approved by FDA as food additive.

For all of these reasons, xyloglucan is believed to have great potential on wound healing, making its application worth to be investigated.

KEY OBJECTIVES

This study intends to attempt the merge of some elements from (bio)materials science, skin electronics and tissue engineering for the production of dressings and materials which could stimulate wound healing.
In particular, it is aimed to:

- develop a new platform of materials using xyloglucan to produce hydrogel as wound dressings and/or scaffolds;
- investigate co-assembly as method to produce fibrous scaffolds that are known to favour wound healing;
- identify a suitable technology that can allow the development of a wearable sensor for advanced wound management.

STRUCTURE OF THE THESIS

An introduction about hydrogels, wound healing process, commercially available wound dressings and polysaccharides generally used for wound dressings is provided in Chapter 1, 2 and 3. Chapter 3 discusses also structure and properties of the main polysaccharide used in this thesis: xyloglucan.

Chapter 4 presents the experimental work carried out for the development of physically and chemically crosslinked xyloglucan-based hydrogel films to be used as wound dressings. Structure-properties relationships were investigated through different complementary techniques: FTIR, rheology, thermal analysis,

morphological analysis, moisture retention and swelling measurements. Selected formulations were also subjected to *in vitro* cytotoxicity tests and hemocompatibility tests.

In Chapter 5, the carboxylation of xyloglucan, performed to introduce ionisable groups that can drive its co-assembly with oppositely charged molecules and macromolecules is presented. Physico-chemical characterisations of the carboxylated xyloglucan (CXG) were performed using FTIR, thermal analysis, rheology and light scattering. *In vitro* cytotoxicity tests were performed in order to confirm the cytocompatibility of the polysaccharide after the modification. Furthermore, a preliminary study on the interactions of the obtained xyloglucan variant with oppositely charged molecules, in particular poly-D-lysine, polyethylenimine, and a peptide amphiphile, was conducted using dynamic light scattering.

In Chapter 6, the study of the co-assembly of CXG with peptide amphiphiles (PAs) aimed to obtain wound healing fibrous scaffolds is presented. A PA sequence, able to co-assemble with CXG to yield tough and resilient gels was identified among a library of different PA sequences synthetized. Interactions between the two building blocks were probed through different experimental techniques (i.e. circular dichroism spectroscopy, IR spectroscopy, dynamic mechanical analysis, transmission and scanning electron microscopy,). Biological *in vitro* evaluations were performed in order to evaluate the suitability of the co-assembled gel for tissue engineering applications, with a specific focus on wound healing. Preliminary *in vivo* wound closure experiments using wild-type mouse model were performed in order to assess an eventual enhancement of the wound healing process.

In Chapter 7, it was proved the concept of the integration of one of the hydrogel film presented in Chapter 4 with inexpensive, lightweight ultra-high frequency radiofrequency identification (UHF RFID) tags to produce a hydrogel wound dressing

device that can battery-less monitor temperature and moisture level of the bandage in contact with the skin. The characterisation of the hydrogel film was complemented with measurements of electrical properties and radio frequencies response, mechanical properties, study of hydrolytic degradation, swelling in serum as simulated exudate, and also with studies on the film protein retention ability and barrier properties against bacteria.

In APPENDIX A, all the experimental procedures will be described in detail.

ACKNOWLEDGMENTS

Firstly, I would like to express my sincere gratitude to my supervisor Prof. Clelia Dispenza for the support of my PhD study and related research, for her guidance that helped me in all the time of research and writing of this thesis. Nonetheless, I wish to gratefully thank Prof. Giuseppe Spadaro who introduced me this group of research, giving me the opportunity to take up this career.

I would like to thank Dr. Maria Antonietta Sabatino, who trained me in most of the techniques I used during these three years and most of all for her friendship; she was always present with good advices and encouragements when I needed.

My sincere thanks goes to Prof. Alvaro Mata, who provided me the opportunity to join his team at Queen Mary University of London (U.K.), and who gave access to the laboratory and research facilities. The year spent in its group significantly contributed to my professional and personal growth.

I would like also to express my gratitude to Dr. Estelle Collin, who trained me in cell culture and then gave me support and advice for my research and most of all for her moral support and friendship.

I gratefully acknowledge DSP Gokyo, Food and Chemical Co. (Japan), and particularly K.Yamatoya, M.Shirakawa, A. Tabuchi for supplying xyloglucan powder.

My gratefulness goes to Dr. Daniela Giacomazza and Dr. Donatella Bulone from National Institute of Research-Institute of Biophysics (CNR-IBF, Palermo,Italy) who gave me the possibility to use their equipment and were always available to kindly give advice for my research and contributed to the editing of the paper I have published and to the others that are in preparation.

Then, I wish to thank Dr. Marta Di Carlo and Dr. Pasquale Picone from National Institute of Research-Biomedicine and molecular immunology institute (CNR-IBIM, Palermo, Italy) for their valuable contribution in biological assessments that helped me to validate most of the new materials I am presenting in this thesis.

I extend my thanks to all of my colleagues and friends both from Laboratory of BioNanomaterials and Composites (Università degli studi di Palermo, Italy) and of Matagroup (Queen Mary University of London, UK): Lorena, Simona, Maria, Gastòn, Carlos, Clara and Anna, who make this PhD a not only professional but also an extraordinary personal experience.

Last but not least, my immense gratitude to my family and to my boyfriend Leonardo, thank you for the endless support, comprehension, patience and love that kept me strong and motivated.

LIST OF ABBREVIATIONS

bFGF	beta- Fibroblast growth factor
CBD-VEGF	Collagen-targeting vascular endothelial growth factor
CTGF	Connective tissue growth factor
CX	Crosslinked
CXG	Carboxylated xyloglucan
DA	Degree of acetylation
DAPI	4',6-diamidino-2-phenylindole
Deg-XG	Degalactosylated xyloglucan
DIC	N,N′-Diisopropylcarbodiimide
DLS	Dynamic light scattering
DS	Degree of substitution
DSC	Differential scanning calorimetry
ECM	Extracellular matrix
FBS	Fetal bovin serum
FDA	Food and Drug Administration
FTIR	Fourier Transform Infrared Spectroscopy
GA	Glutaraldehyde
GF	Gel fraction

GFC	Gel filtration chromatography
GL	Glycerol
HA	Hyaluronic acid
HEPES	4-(2-Hydroxyethyl)piperazine-1-ethanesulfonic acid
HOBT	1-Hydroxybenzotriazole hydrate
HPMC	Hydroxypropyl methylcellulose
INR	International normalized ratio
IPN	Interpenetrating network
KGF	Keratinocyte growth factor
LB	Luria-Bertani broth
LCTS	Lower critical solution temperature
MCH	Mean corpuscular hemoglobin
MCHC	Mean corpuscular hemoglobin concentration
MCV	Mean Corpuscular Volume
MU	Moisture uptake
MW	Molecular weight
Mw	Weight average molecular weight
PA	Peptide amphiphile
PBS	Phosphate buffer solution

PCL	Polycaprolactone
PCT	Procalcitonin test
PDL	Poly-D-Lysine
PDGF	Platelet-derived growth factor
PDLLA	Poly(lactic acid)
PDMS	Poly(dimethylsiloxane)
PEE	Poly(ester elastomer)
PEG	Poly(ethylene glycol)
PEI	Poly(ethylenimine)
PEO	Poly(ethylene oxide)
PGA	Poly(glycolic acid)
PHEMA	Poly(2-hydroxyethyl methacrylate)
PI	Polydispersity index
PNIPAM	Poly(N-isopropylacrylamide)
PT	Prothrombin time
PTT	Partial thromboplastin time
PS	Polystyrene
PVA	Poly(vinyl alcohol)
PVP	Poly(vinyl pirrolidone)
RBC	Red blood cell count
RDW	Red cell distribution width
RFID	Radio frequency identifiction
RH	Relative humidity
ROS	Reactive oxygen species

SDS-PAGE	Sodium Dodecyl Sulphate - PolyAcrylamide Gel Electrophoresis
SD	Swelling degree
SEM	Scanning electron microscopy
SLS	Static light scattering
TEM	Trasmission electron microscopy
TEMPO	2,2,6,6-Tetramethyl-1-piperidinyloxy
TGA	Thermal gravimetric analysis
TGF	Transforming growth factor
UCTS	Upper critical solution temperature
UHF	Ultra high frequencies
XG	Xyloglucan

LIST OF FIGURES

5. Synthesis and characterisation of carboxylated xyloglucan

FUTURE DEVELOPMENTS

APPENDIX A

LIST OF TABLES

4. Xyloglucan-based hydrogel films for wound dressing: structure-property relationships

5. Synthesis and characterisation of carboxylated xyloglucan

LIST OF SCHEMES

1. Hydrogels for wound healing applications

1.1. Hydrogels definition and classification

Hydrogels are defined as three-dimensional hydrophilic networks that exhibit the ability to swell and retain a significant fraction of water within their structure, without dissolving.[1,2] This ability arises from the presence of hydrophilic functional groups attached to the polymeric backbone, such as -OH, -CONH-, $-CONH_2$ and $-SO_3H$, while their resistance to dissolution is due to the presence of crosslinks between network chains.[3,4]

Several classifications have been proposed for hydrogels depending on their preparation method, ionic charge, or physical structure. They can be distinguished in single-polymer hydrogels (composed of a single species of polymer), multi-polymer hydrogels (composed of two or more different polymers), and interpenetrating polymer networks (IPN) comprising two or more networks of natural or synthetic polymers, which are at least partially interlaced but not covalently bonded to each other.[5,6]

Furthermore, the nature of the crosslinking permits to classify hydrogels as chemical or physical hydrogels. Crosslinking is characterized by the presence of junctions, which may be formed by chemical linkages, such as covalent or ionic bonds in so-called chemical hydrogels, or physical interactions such as ionic interactions, hydrogen bonds, or hydrophobic interactions in so-called physical hydrogels.

Depending on the nature of the polymer, different techniques can be used to induce crosslinking. Crosslinking may occur by covalent bonding between polymeric chains triggered by initiators and catalysts, by exposure to a radiation source, including electron beam exposure[7], gamma-radiation [8], or UV light [4,9] or by adding different chemicals (e.g., glutaraldehyde, epichlohydrin, etc.) in conjunction with heating and, sometimes, pressure (Fig. 1.1a-b). Otherwise, physical crosslinking may be obtained through coacervation or precipitation methods exploiting ionic interaction, crystallization, stereocomplex formation, hydrophobic interactions and

hydrogen bonds (Fig. 1.1c).

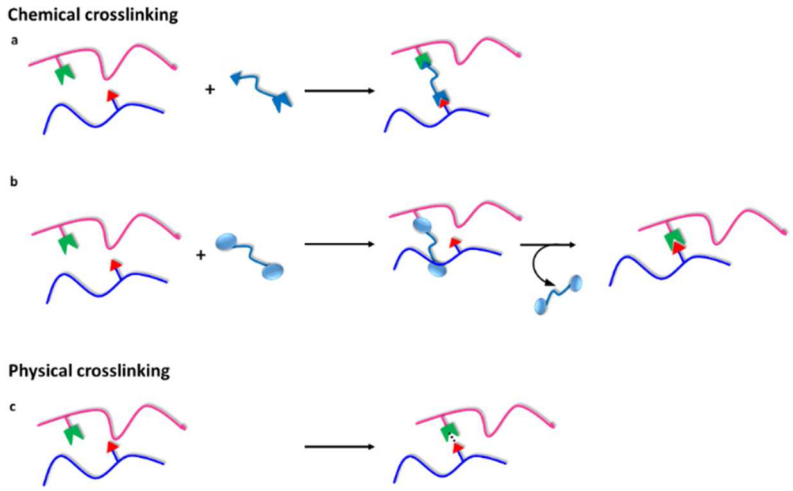

Fig. 1.1 Schematic representation of different type of crosslinking: chemical crosslinking with the crosslinker incorporated into the bond (a), chemical crosslinking with the crosslinker not incorporated into the bond (b), and physical crosslinking (c)

Crosslinking interconnect polymer chains, increase molecular weight and provide better mechanical properties.[10]

Network properties such as swelling degree, elastic modulus and transport of molecules are also influenced by the type and degree of crosslinking. Different degrees of crosslinking and presence or absence of crystallinity, can give rise to elasticity, decrease of viscosity, insolubility of the polymer, increased T_g, increase strength and toughness, lower melting point, etc.[10]

According to hydrogel physical structure and chemical composition they can be distinguished in amorphous (non-crystalline), semi-crystalline and crystalline hydrogels. Furthermore, they could be either neutral or ionic depending on the ionisations of their pendant groups.[1]

Hydrogels can also be classified as “smart” or stimuli-responsive when they are able to respond to changes in their environment. “Smart” hydrogels undergo gelation due

to one or a combination of different external stimuli such as temperature variation, pH change, swelling, solvent exchange, photo-crosslinking, stereocomplexation, ionic crosslinking and synergic interactions among different polymers.[11]

Among all this stimuli, temperature is the most widely used. The thermodynamic principle at the basis of thermo-responsive polymer solubilisation-insolubilisation equilibrium, which is affected by the change in the solubility of the polymer chain or by the formation of a complex among polymer chains that may accompany temperature variations. Generally, the solubility of solute molecules changes drastically with the change in temperature. Besides, the behaviour of polymer in a given medium reflects the balance of interactions among its own segments and the surrounding solvent molecules.[12] In a positive thermo-reversible system, polymers having an upper critical solution temperature (UCST) shrink by cooling below the UCST. While in a negative thermo-reversible hydrogel, polymers have a lower critical solution temperature (LCST) and they contract by heating above the LCST. Namely, they can be tuned to be liquid at room temperature (20-25°C) and to undergo gelation when in contact with body fluids (36-37°C), due to the increase in temperature.

Hydrogels constituted by polymers containing weakly acidic (anionic) or basic (cationic) groups are defined pH-responsive. Protonation-deprotonation mechanism is at the basis of their gelation. Stimuli-responsive polymers can be blended with polysaccharides, such as chitosan, alginate, cellulose, dextran for the development of stimuli-responsive hydrogels with properties like biocompatibility, biodegradability and biological functionality.[13]

Hydrogels may be obtained in different forms including matrices, micro- or nano-particles, coatings, films depending on the preparation method. [14]

1.2. Hydrogels in biomedical applications

The first hydrogel with potential for biomedical application was synthesized in 1955 by Professors Lim and Wichterle. It was a synthetic poly-2-hydroxyethyl methacrylate (PHEMA) used, soon after its discovery, in contact lens production.[15] Since then, hydrogels gained an increasing attention from the scientific community and industry, so that they became widely used in biomedicine and several products are already in the market.[14] Indeed, hydrogels are extremely suitable for various applications in pharmaceutical and medical industries because they offer a combination of favorable properties, among them biocompatibility, hydrophilicity, non-toxicity, biodegradability, super-absorbency, high storage capacity for small and large molecules, and whole cells; and because they can be intrinsically stimuli-responsive and interactive.[16–18] Thanks to their structural similarity to macromolecular-based components present in the human body they have generally satisfying performance on *in vivo* implantation when in contact with either blood or living tissue.[19]
Mechanical properties and structural stability in aqueous environment are necessary requirements for hydrogels used in biomedical applications. For this reason, hydrogels are generally crosslinked for these applications, and they need complete removal of materials breakdown products and/or residual unreacted crosslinking agents (glutaraldehyde, epichloridin, genepin etc.) to guarantee biocompatibility.[20]

Several polymers have been proposed for the preparation of hydrogels for biomedical applications, both from natural or synthetic origin. They can be polysaccharides (cellulose, starch, alginate, chitin, hyaluronate etc.), proteins (collagens, pectins, caseins, albumins) and/or synthetic and biodegradable polymers (poly(vinyl alcohol) (PVA), poly(vinylpyrrolidone) (PVP), poly(ethyleneglycol) (PEG), PHEMA etc.).[21]
Synthetic polymers are man-made polymers, produced by chemical reactions and do have good mechanical properties and thermal stability, much better than several naturally occurring polymers. However, they can contain residues of initiators or other

agents coming from polymerization reactions, and other compounds/impurities that prevent cytocompatibility. PVA is one of the most frequent and oldest synthetic polymers used for hydrogels fabrication; due to its biocompatibility it has been applied in several advanced biomedical applications, and particularly in wound dressing.[22]

On the other hand, natural polymers, also called biopolymers,[23] are generally abundant in nature, extracted from renewable sources and thus they are obtained at a relatively low cost due to their easy availability.[24] Natural polymers have several promising applications in drug delivery, tissue engineering, biomedical sensing, skin grafting, medical adhesives, textiles etc.[25,26]

In the last decades, the development of hydrogels based on the blends of a natural and a synthetic polymer have gained increasing attention. Polymer blends allow to synergically combine different properties into one versatile material. Indeed, synthetic and natural polymers have complementary properties. Synthetic polymers are easier to use owning to their well-defined structure and tunable polydispersity, but natural polymers are generally more biodegradable. [24] Several examples of blends have been reported for the fabrication of hydrogels for biomedical applications with improved elasticity, stiffness, hydrophilicity, etc.. For instance, PVA and gelatin superabsorbent hydrogel membranes as drug delivery systems and moist wound dressing have been produced by esterification reaction.[27] Blending can come also with three components. For instance, agar, gelatin and κ-carrageenan as well as their two-components blends, have been used for the development of hydrogels for controlled release of drugs.[28]

Moreover, thermoresponsive hydrogels are very interesting for biomedical applications because they can undergo gelation upon physiological condition, having the LCST below human body temperature. Among the thermoresponsive polymers used for biomedical applications there are both synthetic polymers such as poly(N-isopropylacrylamide (PNIPAM) or natural polymers (degalactosylated xyloglucan,

gelatin, cellulose derivatives etc.).[29] These hydrogels are generally used for injectable applications but they find also use in drug delivery [30] or wound dressings.[31]

1.2.1. Hydrogels as drug delivery systems

Hydrogels are considered excellent candidates for controlled release applications. Their structure allows drug diffusion, sensitivity to surrounding environment, or recognition of a specific target by incorporation of specific functional groups within the matrix.[18] Their typical porous structure facilitates the drug loading into the matrix and also allows subsequent drug release at a rate dependent on the diffusion coefficient of the small molecule or macromolecule through the gel network.
However, the homogeneity of drug loading within the matrix can result difficult to achieve due to hydrophobic nature of most of the drug molecules.[32]
The benefit of using hydrogels as drug delivery systems is mainly pharmacokinetic: hydrogels can be employed as a depot formulation from which the active molecule can slowly diffuse, either maintaining a high local concentration of the drug in the surrounding tissues or for systemic delivery over a prolonged period.

In general, hydrogels for drug delivery are formed outside the body and impregnated with drug before placement or implantation in the body.[32] For many applications, especially oral-delivery, drug-loaded hydrogels are employed in the dehydrated form. In this form they usually appear glassy, thus the release of water-soluble drugs involves a simultaneous absorption of water and desorption of the drug. They can show different diffusion kinetics ranging from Fickian to Case II extremes, depending on many variables such as temperature, polymer relaxation, thermodynamic compatibility between the solvent and the hydrogel, drug distribution in the matrix, etc.[33,34]
This characteristic is very interesting in hydrogel wound dressings, because they can be loaded with antimicrobial or antibiotic agents [35,36] as it will be discussed in detail in Chapter 2.

Furthermore, thermoresponsive hydrogels are of great interest in therapeutic delivery systems as injectable depot systems. For instance, crosslinked chitosan with PNIPAAM forms a thermoresponsive IPN for the delivery of diclofenac with improved drug loading capacity and sustained release behaviour. In fact, the presence of the cationic chitosan network in the IPN provides the high affinity for anionic drugs in an aqueous medium. In the presence of a relatively high concentration of ions, a competition with the drug for the binding to the network occurs and the drug can be released. Under these conditions, the drug diffusion is delayed by the collapsed PNIPAM network at 37°C.[30]

1.2.2. Hydrogels as scaffolds in regenerative medicine

Regenerative medicine is a promising field of research, aiming to improve current medical options, especially in the field of tissue replacement or repair of damaged tissues with an enhancement of healing processes. Hydrogels have been proposed as tissue scaffolds not only for their structural and compositional similarities to extracellular matrix (ECM) and their exceptional framework function for cells proliferation and survival, but also because their mechanical properties can be tailored to mimic those of natural living tissues.[17] Hydrogel scaffolds are able to provide bulk and mechanical backing to the tissue construct they are in contact with, either if cells are adhered on them or suspended within their 3D network.[1]

The design of a hydrogel for tissue engineering requires the control of a number of criteria to be appropriately effective. These criteria involve physico-chemical and mechanical parameters and biological activity.[37] Starting from physical parameters that must be taken into account, mechanical properties of hydrogel-based biomaterials are important parameters and, in general, they vary depending on anatomical location, cell types, and special applications they are addressed for. For example, relatively strong mechanical properties may be required in situations where the device may be subjected to weight-loading or strain, or where the maintenance of a specific cytoarchitecture is needed, such as for cartilage or bone scaffolds. In other situations,

looser networks may be needed or even preferable.[38] For instance, hydrogels elasticity plays a critical role in engineering soft and elastic tissues such as skin and blood vessels.

Synthetic polymeric hydrogels provide a good control over mechanical properties, but other desirable features such as degradability or cell adhesion are lacking and must be further incorporated into these matrices.[39]

Degradation is a critical requirement in tissue engineering; in fact, scaffold has a time-limited architectural role and after the accomplishment of that function it will disappear, leaving a pure biological system. This mechanism can be due to hydrolysis, enzymatic reaction, and/or dissolution. [20]

Biological activity is one more parameter that must be considered to provide guidance cues to improve cells adhesion and proliferation. Indeed, it is well-known that specific biochemical and physical signals can enhance the "bioactivity" of the scaffold, rendering them instructive for cells and promoting tissue regeneration.[37] Biosignals can be either specific amino acid sequences, like the well-known RGDS-sequence, which promote cell-adhesion, others such as topography, elasticity, and porosity, or stiffness of the materials which are known to direct cell differentiation and function.[16,39,40]

Hydrogel scaffolds for regenerative medicine can come both with or without cells inside, being classified as cellular scaffolds and acellular scaffolds, respectively.[41] Cellular scaffolds combine cells from the body of patients with highly porous hydrogels. This approach is quite expensive due to the process of extraction of cells from patient's body, generally stem cells, followed by seeding and growth in the scaffold before its implantation. There are many examples in literature of cellular scaffolds, they mostly use collagen as main polymer because it is the most common protein in the body and provides strength and structural stability to several tissues including skin, blood vessels, tendons, cartilages and bones.[41,42]

On the other hand, acellular scaffolds aim to influence cellular processes such as apoptosis, angiogenesis or recruitment of stem cells, inducing at last the regeneration of the damaged tissue they are in contact with. An example of acellular scaffold is a dextran crosslinked hydrogel that was developed for the treatment of third-degree burns, showing remarkable improvements of the healing process *in vivo* over 3 weeks, and promoting neovascularisation and skin regeneration.[43] Some scaffolds for tissue regeneration can be loaded with active compounds or growth factors for the enhancement of the healing. For instance, a collagen scaffold loaded with collagen binding vascular endothelial growth factor (CBD-VEGF) was proposed and tested in *in vivo* diabetic rat model for chronic wound healing. It was demonstrated that CBD-VEGF scaffold induced the formation of blood vessels and cell migration, which accelerated tissue regeneration in chronic wound.[44] Other examples of release of growth factors that led to a speeding up of wound healing include the release of fibroblast growth factor (bFGF) from nitrocinnamate-derived polyethylene glycol (PEG-NC) [45] or collagen-mimetic engineered proteins from PEG-diacrylate (PEGDA) microspheres. [46]

1.2.3. Hydrogel sensors

Hydrogel sensors are commonly made by stimuli-responsive polymers.[47] These "smart" biomaterials have a high potential not only for their special properties but also for technological and biomedical applications. Sensing is triggered by chemical signals, such as pH, metabolites and ionic factors which alter molecular interactions between polymer chains or between polymer chain and solutes present in a system as well as by a physical stimulus such as temperature or electrical potential that may provide various energy sources for altering molecular interactions. These interactions modify the properties of polymeric materials like solubility, swelling behaviour, configurations of conformational change, redox (reduction-oxidation) state and crystalline/amorphous transition.

Among these “smart” hydrogels, temperature- and pH-responsive hydrogels have been the most widely investigated for their biomedical applications, including wound dressings, because these two factors have a physiological significance.
Furthermore, there is another type of hydrogels used for sensing applications that are hydrogel-based biosensors. They exploit the ability of certain hydrogel to sense their environment on a molecular level, through the detection or reaction with biological molecules which lead to a change of swollen volume. Biomolecules such as receptors or enzymes are usually immobilized within a stimuli-responsive hydrogel matrix to yield to a biosensing material. The most common example of these is glucose-oxidase within pH-responsive hydrogels to make glucose-sensors.[47]
Hydrogels or stimuli-responsive hydrogels can be integrated in devices for developing sensors. Some examples specifically addressed to wound management will be mentioned in Chapter 2.

References

[1] B.B. V Slaughter, S.S. Khurshid, O.Z. Fisher, A. Khademhosseini, N.A. Peppas, Hydrogels in Regenerative Medicine, Adv. Mater. 21 (2009) 3307–3329. doi:10.1002/adma.200802106.

[2] N.A. Peppas, J.Z. Hilt, A. Khademhosseini, R. Langer, Hydrogels in biology and medicine: From molecular principles to bionanotechnology, Adv. Mater. 18 (2006) 1345–1360. doi:10.1002/adma.200501612.

[3] S.P. Nagam, A.N. Jyothi, J. Poojitha, S. Aruna, R.R. Nadendla, A comprehencive review on hydrogel, Int. J. Curr. Pharm. Res. 8 (2016) 19–23.

[4] K. Deligkaris, T.S. Tadele, W. Olthuis, A. Van den Berg, Hydrogel-based devices for biomedical applications, Sensors Actuators B Chem. 147 (2010) 765–774. doi:10.1016/j.snb.2010.03.083.

[5] E.M. Ahmed, Hydrogel: Preparation, characterization, and applications: A review, J. Adv. Res. 6 (2015) 105–121. doi:10.1016/j.jare.2013.07.006.

[6] B.D. Ratner, A.S. Hoffman, F.J. Schoen, eds., Biomaterial science. An Introduction to Materials in Medicine, 1st ed., Academic press, 1996.

[7] D. Xu, J. Hong, K. Sheng, L. Dong, S.D. Yao, M.A. Sabatino, D. Bulone, M. Veres, A. Spinella, G. Spadaro, C. Dispenza, Structure of e-beam sculptured poly(N-vinylpyrrolidone) networks across different length-scales, from macro to nano, Polymer (Guildf). 54 (2013) 1606–1611. doi:10.1016/j.radphyschem.2007.02.007.

[8] Z. Ajji, I. Othman, J.M. Rosiak, Production of hydrogel wound dressings using gamma radiation, Nucl. Instruments Methods Phys. Res. Sect. B Beam Interact. with Mater. Atoms. 229 (2005) 375–380. doi:10.1016/j.nimb.2004.12.135.

[9] K. Pal, A.K. Banthia, D.K. Majumdar, Preparation and characterization of polyvinyl alcohol-gelatin hydrogel membranes for biomedical applications., AAPS PharmSciTech. 8 (2007) E1–E5. doi:10.1208/pt080121.

[10] J. Maitra, V.K. Shukla, Cross-linking in Hydrogels - A Review, Am. J. Polym. Sci. 4 (2014) 25–31. doi:10.5923/j.ajps.20140402.01.

[11] H.B. Nirmal, S.R. Bakliwal, S.P. Pawar, In-Situ gel: New trends in controlled and sustained drug delivery system, Int. J. PharmTech Res. 2 (2010) 1398–1408.

[12] Y. Osada, J. Ping Gong, Y. Tanaka, Polymer Gels, J. Macromol. Sci. Part C Polym. Rev. 44 (2004) 87–112. doi:10.1081/mc-120027935.

[13] M. Prabaharan, J.F. Mano, Stimuli-responsive hydrogels based on polysaccharides incorporated with thermo-responsive polymers as novel biomaterials, Macromol. Biosci. 6 (2006) 991–1008.

doi:10.1002/mabi.200600164.

[14] E. Caló, V. V. Khutoryanskiy, Biomedical applications of hydrogels: A review of patents and commercial products, Eur. Polym. J. 65 (2015) 252–267. doi:10.1016/j.eurpolymj.2014.11.024.

[15] I. Gibas, H. Janik, Review : Synthetic Polymer Hydrogels for Biomedical Applications, Chem. Technol. 4 (2010) 297–304. http://www.nbuv.gov.ua/Portal/Chem_Biol/Chemistry/2010_4/07.pdf.

[16] N. Gadegaard, E. Martines, M.O. Riehle, K. Seunarine, C.D.W. Wilkinson, Applications of nano-patterning to tissue engineering, Microelectron. Eng. 83 (2006) 1577–1581. doi:10.1016/j.mee.2006.01.147.

[17] M.R. Huglin, Hydrogels in medicine and pharmacy Edited by N. A. Peppas, CRC Press Inc., Boca Raton, Florida, 1986 (Vol. l), 1987 (Vols 2 and 3)., 1989. doi:10.1002/pi.4980210223.

[18] N.A. Peppas, Y.Huang, M. Torres-Lugo, J. H.Ward, and J. Zhang, Physicochemical foundations and structural design of hydrogels in medicine and biology, Annu.Rev.Biomed.Eng. (2000) 9–29.

[19] Y. Osada, J.P. Gong, Y. Tanaka, Polymer Gels, J. Macromol. Sci. - Polym. Rev. 44 (2004) 87–112. doi:10.1081/MC-120027935.

[20] D.S. Kohane, R. Langer, Polymeric biomaterials in tissue engineering, Pediatr. Res. 63 (2008) 487–491. doi:10.1203/01.pdr.0000305937.26105.e7\r00006450-200805000-00006 [pii].

[21] T. Coviello, P. Matricardi, C. Marianecci, F. Alhaique, Polysaccharide hydrogels for modified release formulations, J. Control. Release. 119 (2007) 5–24. doi:10.1016/j.jconrel.2007.01.004.

[22] E.A. Kamoun, E.R.S. Kenawy, X. Chen, A review on polymeric hydrogel membranes for wound dressing applications: PVA-based hydrogel dressings, J. Adv. Res. 8 (2017) 217–233. doi:10.1016/j.jare.2017.01.005.

[23] M. Vert, Y. Doi, K.-H. Hellwich, M. Hess, P. Hodge, P. Kubisa, M. Rinaudo, F. Schué, Terminology for biorelated polymers and applications (IUPAC Recommendations 2012), Pure Appl. Chem. 84 (2012) 1. doi:10.1351/PAC-REC-10-12-04.

[24] A. Sionkowska, Current research on the blends of natural and synthetic polymers as new biomaterials: Review, Prog. Polym. Sci. 36 (2011) 1254–1276. doi:10.1016/j.progpolymsci.2011.05.003.

[25] C.K. Simi, T.E. Abraham, Biodegradable biocompatible xyloglucan films for various applications, Colloid Polym. Sci. 288 (2010) 297–306. doi:10.1007/s00396-009-2151-8.

[26] S.E. Yannas IV, Burke JF, Orgill DP, Wound tissue can utilize a polymeric template to synthesize a functional extension of skin, Science. 215 (1982) 174–176. doi:10.1126/science.7031899.

[27] K. Pal, A.K. Banthia, D.K. Majumdar, Preparation and characterization of polyvinyl alcohol-gelatin hydrogel membranes for biomedical applications., AAPS PharmSciTech. 8 (2007) 21. doi:10.1208/pt080121.

[28] J. Liu, S. Lin, L. Li, E. Liu, Release of theophylline from polymer blend hydrogels, Int. J. Pharm. 298 (2005) 117–125. doi:10.1016/j.ijpharm.2005.04.006.

[29] L. Klouda, A.G. Mikos, Thermoresponsive hydrogels in biomedical applications A seven-year update, Eur. J. Pharm. Biopharm. 68 (2008) 34–45. doi:10.1016/j.ejpb.2015.05.017.

[30] C. Alvarez-Lorenzo, A. Concheiro, A.S. Dubovik, N. V. Grinberg, T. V.

Burova, V.Y. Grinberg, Temperature-sensitive chitosan-poly(N-isopropylacrylamide) interpenetrated networks with enhanced loading capacity and controlled release properties, J. Control. Release. 102 (2005) 629–641. doi:10.1016/j.jconrel.2004.10.021.

[31] L. Mi, H. Xue, Y. Li, S. Jiang, A thermoresponsive antimicrobial wound dressing hydrogel based on a cationic betaine ester, Adv. Funct. Mater. 21 (2011) 4028–4034. doi:10.1002/adfm.201100871.

[32] T.R. Hoare, D.S. Kohane, Hydrogels in drug delivery : Progress and challenges *, Polym. with Aligned Carbon Nanotub. Act. Compos. Mater. 49 (2008) 1993–2007. doi:10.1016/j.polymer.2008.01.027.

[33] P.I. Lee, C. Kim, Probing the mechanism of drug release from hydrogels, J. Control. Rel. 16 (1991) 229–236.

[34] P.I. Lee, Kinetics of drug release from hydrogel matrices, J. Control. Release. 2 (1985) 277–288. doi:10.1016/0168-3659(85)90051-3.

[35] E.R. Kenawy, E. a. Kamoun, M.S. Mohy Eldin, M. a. El-Meligy, Physically crosslinked poly(vinyl alcohol)-hydroxyethyl starch blend hydrogel membranes: Synthesis and characterization for biomedical applications, Arab. J. Chem. 7 (2014) 372–380. doi:10.1016/j.arabjc.2013.05.026.

[36] T.R. Anderson, M.E. Marquart, A. V. Janorkar, Effective release of a broad spectrum antibiotic from elastin-like polypeptide-collagen composite, J. Biomed. Mater. Res. Part A. 103 (2015) 782–790. doi:10.1002/jbm.a.35219.

[37] R. Jin, P.J. Dijkstra, Hydrogels for Tissue Engineering, Chem. Rev. 101 (2001) 1869–1879. doi:10.1007/978-1-4419-5919-5_11.

[38] A. Mata, L. Hsu, R. Capito, C. Aparicio, K. Henrikson, S.I. Stupp, Micropatterning of bioactive self-assembling gels, Soft Matter. 5 (2009) 1228–1236. doi:10.1039/b819002j.

[39] Y.-N. Zhang, R.K. Avery, Q. Vallmajo-Martin, A. Assmann, A. Vegh, A. Memic, B.D. Olsen, N. Annabi, A. Khademhosseini, A Highly Elastic and Rapidly Crosslinkable Elastin-Like Polypeptide-Based Hydrogel for Biomedical Applications, Adv. Funct. Mater. 25 (2015) 4814–4826. doi:10.1002/adfm.201501489.

[40] C.N. Grover, J.H. Gwynne, N. Pugh, S. Hamaia, R.W. Farndale, S.M. Best, R.E. Cameron, Crosslinking and composition influence the surface properties, mechanical stiffness and cell reactivity of collagen-based films, Acta Biomater. 8 (2012) 3080–3090. doi:10.1016/j.actbio.2012.05.006.

[41] J. Glowacki, S. Mizuno, Collagen scaffolds for tissue engineering, Biopolymers. 89 (2008) 338–344. doi:10.1002/bip.20871.

[42] B.B. Nguyen, R.A. Moriarty, T. Kamalitdinov, J.M. Etheridge, J.P. Fisher, Collagen Hydrogel Scaffold Promotes Mesenchymal Stem Cell and Endothelial Cell Coculture for Bone Tissue Engineering, J. Biomed. Mater. Res. Part A. 105 (2017) 1123–1131. doi:10.1002/jbm.a.36008.

[43] G. Sun, X. Zhang, Y.-I. Shen, R. Sebastian, L.E. Dickinson, K. Fox-Talbot, M. Reinblatt, C. Steenbergen, J.W. Harmon, S. Gerecht, Dextran hydrogel scaffolds enhance angiogenic responses and promote complete skin regeneration during burn wound healing, Proc. Natl. Acad. Sci. 108 (2011) 20976–20981. doi:10.1073/pnas.1115973108.

[44] X.H. and J.D. Qian Tan, Bing Chen, Xin Yan, Yue Lin, Zhifeng Xiao, Promotion of diabetic wound healing by collagen scaffold with collagen-binding vascular endothelial growth factor in a diabetic rat model, J. Tissue Eng. Regen. Med. 4 (2012) 524–531. doi:10.1002/term.

[45] F.M. Andreopoulos, I. Persaud, Delivery of basic fibroblast growth factor (bFGF) from photoresponsive hydrogel scaffolds, Biomaterials. 27 (2006) 2468–2476. doi:10.1016/j.biomaterials.2005.11.019.

[46] S. Cereceres, T. Touchet, M.B. Browning, C. Smith, J. Rivera, M. Höök, C. Whitfield-Cargile, B. Russell, E. Cosgriff-Hernandez, Chronic Wound Dressings Based on Collagen-Mimetic Proteins, Adv. Wound Care. 4 (2015) 444–456. doi:10.1089/wound.2014.0614.

[47] N.A. Peppas, D.S. Van Blarcom, Hydrogel-based biosensors and sensing devices for drug delivery, J. Control. Release. 240 (2016) 142–150. doi:10.1016/j.jconrel.2015.11.022.

2. Wound management

2.1. Wound healing physiology

A wound is a type of circumscribed injury of the skin caused by a physical or thermal damage or due to a pathological condition. The specific biological process that leads to tissue regeneration is defined as wound healing. This process is very complex and involves different stages[1,2]:

- *Haemostasis:* It is characterized by bleeding with the role to flush out bacteria, but it is immediately followed by the activation of platelets, which start the coagulation cascade. Platelets start to release factors that initiate the healing process, like platelet-derived growth factor (PDGF) or transforming growth factors (TGFs), the fibroblast growth factors (FGFs), and vascular endothelial growth factor (VEGF).
- *Inflammation*: This phase lasts from 3 to 7 days in which the wound presents pain, redness, warmth, and swelling due to specific enzymes and various mediators that are secreted by inflammatory cells on the wound bed. The main active cells at this stage are phagocytic cells, such as neutrophil and macrophages. Neutrophils secrete reactive oxygen species (ROS) and proteases for preventing bacteria contamination and for cleaning the wound bed from debris, while blood monocytes arrive to the wound site and differentiate in macrophages, which remove bacteria and non-viable tissue by phagocytosis. The latter also release growth factors and cytokines to recruit fibroblast, endothelial cells and keratinocytes for repairing the tissue.
- *Proliferation:* This phase is characterized by granulation, new blood vessels formation (angiogenesis) and epithelisation. All of these processes are stimulated by the presence of growth factors, like TGF-β, connective

tissue growth factor (CTGF), VEGF, keratinocyte growth factors (KGFs) and TGF-α.

- *Remodelling:* This is the last phase of healing. At this stage, inflammatory cells leave the wound bed; cells releasing growth factor are diminishing and the provisional matrix is remodelled into organized collagen bundles.

All these phases occur in an ordered manner overlapping one with each other and involving well-connected biochemical and cellular processes and, in particular, interactions among cytokines, growth factors, blood and the extracellular matrix. The important role of cytokines includes the stimulation and the production of components of the basement membrane, prevention from dehydration, increasing inflammation and formation of granulation tissue.[3] Furthermore, the healing process could be altered by local factors such as hypothermia, pain, infection, radiation and tissue oxygen tension that can affect directly the characteristic of the wound, otherwise could be influenced by systemic factors including the overall health or the presence of comorbidities that can affect the ability to heal. In addition, poor nutrition, age and protein, vitamins and/or mineral deficiency can delay the wound healing.[4]

Depending on the nature of the healing process, wounds can be classified in *acute* or *chronic*. An acute wound is a wound that heals completely within an expected period of time, usually 8-12 weeks, with an expected rate and according to a normal healing process. The primary cause of acute wounds is mechanical injures, including penetrating wounds caused by knives and gun shots, and surgical wounds caused by surgical incisions. Burns and chemical injures are considered another category of acute wounds, they can be caused by chemicals, electricity, radiations or thermal sources. Depending on the temperature of the thermal sources or the time of the exposure, it is possible to distinguish different degree of burns.

Chronic wounds are those that do not progress through a normal healing process due to the presence of physiological conditions such as diabetes, obesity, cancer, persistent infections or other patient related conditions. Chronic wounds also include diabetic foot ulcers, venous leg ulcers and pressure ulcers. These ulcers can last over 12 months and they can cause to loss of function and decreased quality of life, leading in some cases to amputation of limbs or death. [5]
In conclusion, the time of the wound healing process strongly depends on the type of wounds and on the presence of some disease, but the selection of the right material for the dressing is also critical to have a faster healing.

2.2. Chronic wound management: economic and social impact

Among all the type of wounds, chronic non-healing wounds represent a substantial economic issue to healthcare systems in western countries.

Older people are subjected to a higher risk for chronic wounds, also due to the slowing down of the healing process related with aging. Furthermore, chronic wounds are also related to other diseases such as cardiovascular diseases, diabetes or obesity, incidence of which is significantly increased in the last decades.[6]
Because chronic wounds are generally treated as co-morbidities, the importance of the development of new treatments is often hidden. Clinicians are not specialised in wound care and there is a lack of effective treatments and adequate approaches for the prevention of those medical conditions. These inefficiencies are also surrounded by a lack of deep knowledge on the biological processes associated with wound healing, which make this issues also a scientific challenge.[7]
The costs of these treatments are very high also due to the prolonged time of treatment that is related with the long time that these wounds can take to heal, from several years to decades.[8] Costs estimated in USA can reach US$20 billion, while in UK they represent the 3% of the total healthcare expense.[8]

The rate of amputation of limbs as consequence of chronic wounds is frightful (globally there is one amputation every 30 seconds) and the 5-years mortality after amputation is between 40% and 70%. Infections are another main drawback of these type of wounds, being the major causes of amputation and they could be avoided with early stage diagnosis and an accurate care.[9]
In the following paragraphs it will be given an overview of the different type of existent wound dressings and wound healing scaffolds.

2.3. Wound dressings

The progress on wound dressing has led from the crude application of plant herbs, animal fat and honey to new materials for tissue engineering. Design of effective wound dressings needs a deep understanding of the healing process taking into account several parameters such as the conditions of the patient, the presence of comorbidities and the effect that each of the materials used may have on the wound.
A summary of all the type of dressings is reported in Fig. 2.1 and they will be discussed individually in the following paragraphs.

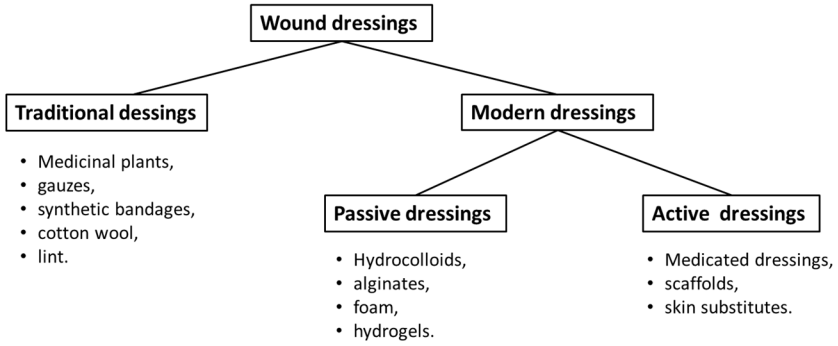

Fig. 2.1 Scheme of the different types of wound dressings

2.3.1. Traditional dressings

In the past, many traditional medicinal plants have been employed for the treatments of wounds thanks to their antibacterial and antioxidant properties, i.e. *Guiera senegalensis, Commelina diffusa* and *Spathodea campanulata*, etc. However, these plants or their crude extracts applied directly on the wounds may contain microorganisms that can cause infections, and also some potentially harmful chemical components that may affect the healing process. Other traditional wound dressings were natural or synthetic bandages, cotton wool, lint and gauzes all with varying degrees of absorbency. Their primary function was to keep the wound dry by allowing evaporation of wound exudates and preventing bacterial infection.

Plain gauze is still one of the most commonly employed products in hospitals because is certainly cheap, readily available and suitable for different types of wounds. It can be also impregnated with some active ingredients such as iodine, zinc oxide/zinc ions, or petrolatum to enhance their performance. Iodine provides antimicrobial properties, whereas zinc oxide could promote wound cleansing and re-epithelialization.[10] However, the use of gauze often produce discomfort and side effect related to its removal, as it may cause trauma by stripping off newly formed epidermis.

To overcome these limitations, research has been focused on the design and development of new wound dressings, and it has produced advanced materials with better physical and chemical properties, that are discussed in the following sections.

2.3.2. Modern dressings

Studies on wounds and wound healing have indicated the optimal features of a wound dressing.

In particular, in early ‘60s, Winter announced the first generation of wound dressings that represented a breakthrough in the field.[11] In his pioneering work, he

discovered that maintaining the wound hydrated improved the epithelial repair of wounded pig skin at least twice compared to the air-exposed wounds.[12] On the basis of his studies it was designed for the first time the ideal wound dressings, which should keep a wet environment with high biocompatibility and prohibit the bacterial infection for accelerating the tissue regeneration.[13]

Thus, the ideal dressing needs to fulfil the following requirements:

- absorb excess of exudates and toxins,
- provide or maintain moist environment,
- enhance epidermal migration,
- allow gas exchange between wounded tissue and environment,
- maintain appropriate tissue temperature to improve the blood flow to the wound bed and enhances epidermal migration,
- promote angiogenesis and connective tissue synthesis,
- provide protection against bacterial infection,
- be easy to remove without further trauma to the wound,
- provide debridement action to enhance leucocytes migration and support the accumulation of enzyme and
- must be sterile, non-toxic and non-allergenic.

Modern dressings can be divided in two categories: *passive* and *bioactive* dressings. The formers fulfil the above mentioned functions, while the latters can enhance the healing process through more advanced functions (e.g. drug delivery or scaffolds). Furthermore, they are themselves classified according to the materials from which they are composed, including hydrocolloids, alginates and hydrogels and generally they occur in the form of gels, thin films and foam sheets.[6]

2.3.2.1. Passive dressings

2.3.2.1.1. Hydrocolloids

Hydrocolloids are a class of wound dressings obtained from colloidal (gel forming agents) materials combined with other materials, such as elastomers and adhesives. They are composed by an active surface which is coated with a crosslinked adhesive matrix containing a dispersion of gelatin, pectin and carboxy-methylcellulose together with other polymers and adhesives forming a flexible wafer, for instance polyurethane foam or film carrier, to create an absorbent and self-adhesive sheet. Several hydrocolloid dressings are already in the market, for instance Granuflex™ and Aquacel™ (Conva Tec, Hounslow, UK), Comfeel™ (Coloplast, Peterborough, UK) and Tegasorb™ (3M Healthcare, Loughborough, UK). These dressings are capable of absorbing low to moderate levels of fluids and can be used to promote autolytic debridement of dry, exuding, or necrotic wounds. They are indicated for light to moderately exuding wounds, such as pressure sores, minor burns and traumatic injuries. Thinner versions are generally used on wounds that are dry or have low levels of exudate. Additionally, hydrocolloids are suitable for promoting granulation tissue. The presence of an occlusive outer cover in this type of dressing prevents water vapour exchange between the wound and its surroundings and this can be disadvantageous for infected wounds that require a certain amount of oxygen to rapidly heal. Furthermore, these dressings can release residuals that are deposited in the wound and often have to be removed during dressing change.[1]

2.3.2.1.2. Alginates

Another class of modern dressings are the alginates. They are produced starting from sodium and calcium salts of alginic acid, a polysaccharide composed by mannuronic and guluronic acid units. Alginate dressings have a high absorbency and they are able to form gels upon contact with wound exudates, thus they are indicated

in the treatment of unshaped wounds that present cavities. They are usually employed as sodium salt alginate and in the dry state. When administered to the wound, the gelling property of the sodium alginates is attributed to the exchange of the sodium ions with calcium ions present in exudate and blood which help to form a crosslinked polymeric gel that degrades slowly.[14] Various alginate dressings are already in the market and they can be distinguished in those rich in mannuronate, such as Sorbsan™ (Maersk, Suffolk, UK), which form soft flexible gels upon hydration, and those rich in guluronic acid, like Kaltostat™ (Conva Tec), which form firmer gels upon absorbing wound exudate. Others commercial products include Silvercel®, Sorbalgon®, Algicell®. Furthermore, it has been demonstrated that calcium ions present in alginate dressings may help the healing process, stimulating fibroblasts proliferation and having haemostatic properties. However, if the amount of exudates is not sufficient to gel the polymer, they may require further moisturizing, which could lead to infections. They can be subjected to autoclaving for their sterilisation. They also require a support, generally in fabric to maintain them in place.[4]

2.3.2.1.3. Foams

Foams are porous dressings commonly composed by polyurethane, which come sometimes with adhesive borders. They are easy to handle and provide thermal insulation and high absorbency. Foam dressings available in the market include Tielle™, 3M Adhesive Foam™, or Allevyn™. Thanks to their high absorbance these dressings are indicated for the treatment of heavily exuding wounds. The absorbance capacity can be controlled by foam properties, such as texture, thickness and pore size, and their open structure guarantees high vapour transmission, which is important to maintain the wound environment with the right level of oxygenation and moisture.[1]

2.3.2.1.4. Hydrogels

Hydrogels have been applied for many years in wound management, since they combine the features of moist wound with good fluid absorbance.[15,16] Thanks to their unique properties, they are considered as the closest to an ideal dressing and they are suitable for use in all stages of wound healing, i.e, haemostasis, inflammation, granulation, epithelialization and reconstruction phase.[1] Their moisturizing effect of the wound environment can promote granulation, epithelialization, autolytic debridement and the high water content of hydrogel dressings cools the wound, giving pain relief and soothing that can last for long.[17]
However, the moisture that they provide can cause maceration of peri-wound tissue, (tissue surrounding the wound) and the exudate accumulation may lead to bacterial proliferation. For this reason, it is important that they can act as barrier for bacterial infections. Moreover, it is important to guarantee a good mechanical strength to avoid difficulties in handling.
Hydrogels can be applied in different forms, such as a gel, gauzes impregnated with hydrogel or as elastic films. The latter have the remarkable advantage to be self-standing, and their partial adhesion to the wound surface reducing the dressing-change discomfort and pain.
Crosslinking of polymeric components in order avoid the dissolution of the matrix is one of the common methods to produce wound dressings. [18,19]
Various polymers from both natural and synthetic origin have been proposed in the preparation of hydrogels wound dressings, such as hyaluronic acid, alginate, collagen, chitosan, PVA, PVP, etc.[14,20,21] They can be used alone or in blends, especially PVA has been extensively investigated in blends with natural polymer (chitosan, gelatin, glucans, dextran, startch..) or synthetic ones (PVP, PEG, poly-N-isopropylacrylamide (NIPAAm), etc.).[11,22–24]

Furthermore, several hydrogel dressings are already commercially available, such as Nu-gel™, Purilon™, Aquaform™ polymers and Intrasite™.[21] Tegaderm® is a widely used array of commercial hydrogels that is sold in different forms, like films or wound filler gel.

Although hydrogels are the closest materials to the ideal wound dressings, wound healing process is very complex and advanced functions are required specially to target the complex chronic wounds. For this reason, scientific efforts have been focused in the development of advanced hydrogel materials, that are able to provide multiple functions beside their usual barrier, moisturizing and absorbent functions and they are classified as bioactive dressings.

2.3.2.2. Bioactive dressings

2.3.2.2.1. Medicated dressings

Medicated dressings, which incorporate therapeutic agents, play an important role in the wound healing, helping and speeding up the process. Generally, the incorporated compounds are antiseptic agents that prevent infections and promote tissue regeneration. Medicated dressings with antiseptic activity usually are silver- or iodine-impregnated, but the prolonged use of these substances can cause skin irritation and staining.[3] For instance, Das et al. have produced an amorphous hydrogel based on carboxymethylcellulose (CMC) and silver nanoparticles as a new cost-effective hydrogel wound dressing. It was demonstrated to have good antimicrobial properties with a good absorbency of exudates to maintain the moist environment.[25] Some of these hydrogel dressings loaded with antimicrobial agents are already available in the market, among all Silvasorb® gel, SilverMed®, Iodosorb® etc., contain colloidal silver, iodine or others antimicrobial agents. However, the number of commercial dressings in the form of hydrogel films is not elevated; one of those is Silverseal® that is commercialized in only in U.S.

In addition to antimicrobial agents, also antibiotics resulted to be efficacious and to help the healing process. For instance, cross-linked hydrogel films composed by PVA and dextran obtained through the freezing–thawing method have been reported as new potential wound dressings loaded with gentamicin. These films resulted swellable, flexible, and elastic and they displayed a good *in vivo* enhancement of the healing due to the delivery of the antibiotic.[26] Moreover, ciprofloxacin, that is a water insoluble drug, has been embedded into a PVP matrix by using acetic acid as co-solvent in water. The obtained transparent films showed good plasticity and softness, together with a good antiseptic properties coming from the residual acetic acid in the matrix and antibacterial activity against *Escherichia coli* and *Bacillus subtilis.*[27] Also PVA/chitosan-based crosslinked hydrogel films shown a significant improvement of the wound healing due to the embedding of minocycline as antibiotic.[22]
However, while the use of antiseptics is not related with bacterial resistance, the release of topical antibiotics needs to be carefully controlled so that it can prevent wound infection without contributing to the emergence of antibiotic-resistance.[28]

A more recent approach is based on the incorporation of cell-signalling elements such as growth factors or stem cells. This method is particularly suitable for the treatment of chronic wounds in which the normal wound healing process is disrupted. These elements allow an external modulation of the wound environment taking an active physiological role in the wound healing process. They usually act stimulating angiogenesis and cellular proliferation, which affect both the production and the degradation of the extracellular matrix and also play a role in inflammation cells and fibroblasts activity. Several growth factor-loaded dressings have been reported and the most commonly used growth factors for skin regeneration include EGF, bFGF, KGF, VEGF, PDGF, TGF-β, etc. each one involved in a different step of the complex healing process. Some reported examples of those dressings are

spongy sheets of crosslinked hyaluronic acid (HA) embedded with arginine and EGF that have shown to promote epithelialisation;[21] a photo-crosslinked hydrogel composed by the mixture of glycidyl methacrylated chito-oligosaccharide (COS), di-acrylated pluronic and a recombinant human epidermal growth factor (rhEGF) that has been reported to significantly enhance *in vivo* epidermal differentiation during the wound healing process;[29] star-poly-ethylene glycol (PEG)-heparin hydrogels functionalized with TGF-β that have been demonstrated to release the growth factor with consequent growth and differentiation of fibroblast.[30]

Furthermore, also some supplements such as vitamins or minerals such as vitamins A, C and E as well as zinc and copper, can be added to dressings to improve the healing and the type of dressings used for this delivery include oil based liquid emulsions, creams, ointments, gauze and silicone gel sheets.[1]

2.3.2.2.2. Tissue engineered scaffold and skin substitutes

The field of regenerative skin tissue engineering aims to facilitate faster wound healing and consequently restoration of skin, either generating novel or biocompatible substitutes or by reconstruction of the tissues. In the last decade, the invention of numerous skin substitutes represented a significant advancement in skin regeneration. These bioengineered skin substitutes not only repair the wounds, but can also be embedded with therapeutic agents, such as growth factors, antibiotics, anti-inflammatory drugs that can eventually enhancing the healing process.[31]

Skin regeneration benefits mainly from the use of suitable scaffold matrices, which are considered the best materials for restoring, maintaining and improving tissue functions. These scaffolds can be composed by natural (i.e. proteins and/or polysaccharides) or synthetic polymers, but can also be composite materials that include both natural and synthetic polymers. There are several different techniques to fabricate a scaffold including the use of extracellular matrix (ECM)-secreting cell

sheets, pre-made porous scaffolds of synthetic, natural and biodegradable biomaterials, decellularized ECM scaffolds, and cells entrapped in hydrogels. There are also different types of scaffolds, i.e. porous, fibrous, microspheres (each of which can be in the form of hydrogel), and acellular, etc. (Fig. 2.2).[32] All of these scaffolds can be seeded with cells in order to enhance the biological response.

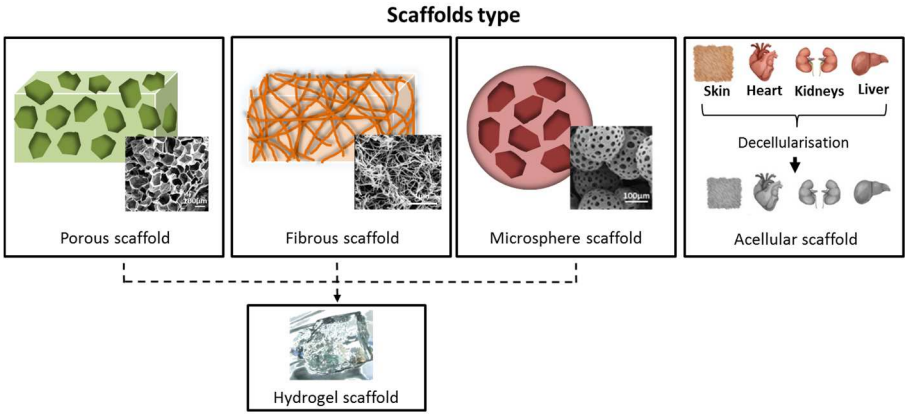

Fig. 2.2 Different categories of scaffolds for wound healing

An ideal porous scaffold in skin engineering is the one that mimics the natural environment for skin growth through appropriate cell infiltration, proliferation and differentiation. It should be biodegradable, permeable to oxygen, water and nutrient exchange and should be protective against infection and mechanical damage. However, different pore sizes are required for the specific cell types. Most of these porous scaffolds are composed of collagen and keratinocytes or fibroblasts are seeded into them. There are also several synthetic biodegradable polymers, such as (PEG, poly(lactic acid) (PLA), poly(glycolide) (PGA), poly(lactic-co-glycolic acid) (PLGA), poly(caprolactone) (PCL), poly(D,L-lactic acid or D,L-lactide) (PDLLA), poly(ester) elastomer (PEE) based on poly(ethylene oxide) (PEO), and

poly(butylene terephthalate) (PBT)[33–35] used for the fabrication of porous scaffolds. Some commercial products are already into the market, such as Orcel®, Biobrane®, Terudermis® and Pelnac® that is made up of collagen of porcine origin, differently from all the others which are composed mainly by bovine-collagen. All of these products are particularly indicated for the treatment of burns.

Nano-fibrous scaffolds can be also included in the category of porous scaffolds. Their highly microporous structure is particularly suitable for cell adhesion, proliferation and differentiation. Some of the techniques commonly used for the synthesis of nanofibres are self-assembly, phase separation, drawing, template synthesis and the most common electrospinning technique**.**[36] Nanofibres can also be functionalised to carry biosignals by simple blending or coating techniques or by surface grafting to physically attach through non-covalent interactions, or covalently bind on the fibres adhesive proteins or ligand molecules that can help and speed up the healing process.[37,38] Recently, nanofibrous scaffolds based on a blend of mussel adhesive protein (MAP) as natural biomaterial and PCL to provide mechanical reinforcement have been fabricated through electrospinning process. These scaffolds have shown to accelerate wound regeneration, also suggesting that the successful application of these mats for wound healing is due to the adhesive property of the scaffold conferred by MAP. Another mat for wound dressing applications loaded with an antibiotic has been produced by electrospinning of a water/acetic acid PVP and ciprofloxacin solution.[27] All of these electrospun mats are generally non-transparent, hindering a direct visual inspection of the wound, thus requiring the dressing to be removed for check-ups.

Another category of scaffolds for skin regeneration is the collagen rich matrices created by removing all cellular components from living tissues, such as kidneys, skin, etc., commonly called “acellular scaffolds”. These scaffolds are not only used

for skin regeneration; indeed, depending on the type of cells seeded on them, they can be used also for other tissue types. These scaffolds require a careful and complete decellularization to avoid immune response and rejection after implantation and, even if they are very promising, they rise up ethical concerns.
In recent years, other scaffolding approaches involving microspheres have gained increasing attention mainly for the possibility that they offer to effective deliver drugs, such as antibiotics. The microspheres approach has several benefits, such as easy fabrication, controlled morphology and physicochemical properties, resulting in versatile use of the pharmacokinetics of the encapsulated molecules and the size of the microspheres can be adjusted to obtain an optimal controlled release of the actives molecules.[32]

2.3.2.2.3. Wound management sensors and actuators devices

"Smart" dressings are an emerging field that is going to revolutionize wound care. These dressings are similar to "wearable" or "epidermal" electronics and exploit biochemical signals that are immediately converted to readable outputs, with diagnostic value for wound management.[39] The complexity of the wound healing process offers an abundance of these biochemical targets, such as pH, temperature, reactive oxygen species (ROS), bacterial load, growth factors, hormones, inflammatory mediators, etc. and they can be used to develop sensors for wound management. This new generation of dressings are believed to have an enormous potential and their popularity is rapidly growing due to the possibility to apply this technology to both acute and chronic wounds. Benefits in sensing the wound environment include reduction of hospitalization time, prevention of amputations and better understanding of the processes which impair healing.[39]

Sensors that detect infection at the wound site have been developed and use very different approaches. Zhou et al. have developed a sensor which use toxins produced by bacteria in wounds as biochemical signal indicating early infections. Using the same mechanisms, as phospholipase-A2 and α-haemolysin toxins from *S. aureus* and *P. aeruginosa* permeabilize or hydrolyse cell membranes, they proposed Trojan-like phospholipid vesicles, which are recognized by the bacteria as eukaryotic cells but instead release a fluorescent dye cargo when attached by bacteria-secreted toxins. Thus, the occurrence of fluorescence is directly related with the presence of infection.[40]

Another indicator of infection is the temperature of the wound site that is possible to measure it with hand-held infrared thermometers. A novel approach is to use dressing which change colour upon heating with high sensitivity, reportedly ± 0.5 ºC. This approach is possible using stimuli-responsive polymers attached to poly-Si, which change conformation depending on the temperature and resulting in a change of colour of the matrix.

Another stimulus that can be monitored is the pH. For example, a pH-sensitive poly(vinyl alcohol)/poly(acrylic acid) hydrogel was studied for the development of a passive hydrogel-based device. This device resulted able to wirelessly track the pH of the wound and the moisture level (Fig. 2.3).[41]

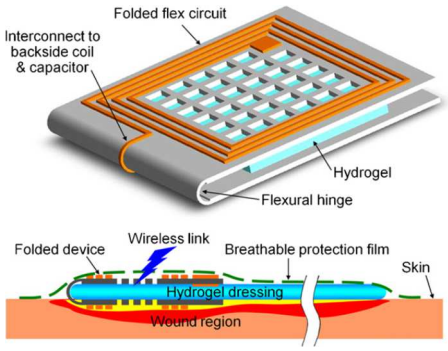

Fig. 2.3 pH sensitive gel between inductance coils for continuous *in situ* pH monitoring; figure reproduced from [41]

Moisture of wounds is another parameter that can be monitored in order to have useful information about the healing process and about the state of the wound itself. Indeed, it is well-know that an excessive or insufficient moisture levels can lead to maceration or drying out, respectively, and both these conditions are not favourable for a normal healing pathway.[42] For this reason, sensors based on electrical impedance have been developed for real-time monitoring moisture levels in a wound.[43] In addition, it was experimentally demonstrated that the uptake of biological fluids by a hydrogel membrane sensibly impacts on the matching and radiation performance of a RFID tag, which can be exploited as a wireless battery-less epidermal radio-sensor. The significant advantage of using RFID antennas is related to their extremely low-cost and their lightweight; moreover, these antennas do not need any battery to be integrated with them because they passively collect the data and return them when asked by an external source. In contrast to all the other devices and technologies, this is an important characteristic that make these technology wearable and comfortable. Thus, as described by Occhiuzzi et al., the coupling of a hydrogel and a RFID antenna can be exploited for the development of a sensor to monitor the amount of exudate loss from a wound (Fig. 2.4). The plaster-

sensor designed is a passive device that can measure the wound bed temperature, pH and fluid loss, and remotely transmit this information when interrogated by another radio-emitting/absorbing device near to wound dressing.[44]

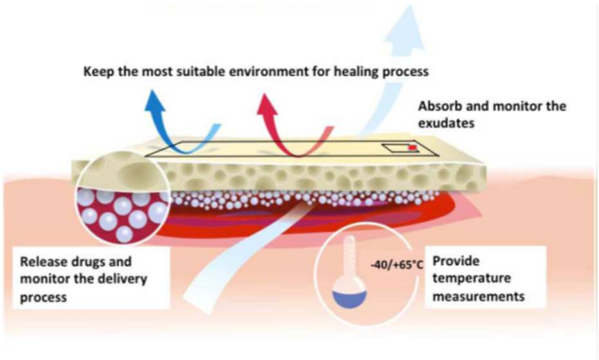

Fig. 2.4 Pictorial representation of the RFID epidermal sensor working as intelligent plaster for wound treatment.[44]

Another class of wound management device is represented by actuators.

In this field, a very important advancement has been recently reached by Mostafalu et al.[45] They developed a textile patch able to release different therapeutic agents or growth factors for the treatment of chronic wounds. The patch is made up by composite conductive fibres coated with a hydrogel layer of poly(ethylene glycol) diacrylate (PEGDA)-alginate containing thermoresponsive drug carriers. The fibres are loaded with different drugs and growth factors and are then assembled into fabrics and connected to a microcontroller that will individually power them up. Each of the fibres can be individually heated to enable on-demand the release of different drugs with a controlled temporal profile using an external input from a smartphone. The *in vitro* and *in vivo* experiments confirmed the effectiveness of the release of antibiotics (cefazolin and vancomycin) and of the growth factor (VEGF) proving the enhancement of angiogenesis and the eradication of bacteria.[45]

Although this report results very innovative, the presence of the microcontroller does not answer to the need of a lightweight device, as battery-less RFID antennas do.

References

[1] J.S. Boateng, K.H. Matthews, H.N.E. Stevens, G.M. Eccleston, Wound Healing Dressings and Drug Delivery Systems: A Review, J. Pharm. Sci. 97 (2008) 2892–2922. doi:10.1002/jps21210.

[2] P. Martin, Wound healing--aiming for perfect skin regeneration., Science. 276 (1997) 75–81. doi:10.1126/science.276.5309.75.

[3] S. Dhivya, V.V. Padma, E. Santhini, Wound dressings - a review., BioMedicine. 5 (2015). doi:10.7603/s40681-015-0022-9.

[4] C. Daunton, S. Kothari, L. Smith, D. Steele, A history of materials and practices for wound management, Wound Pract. Res. 20 (2012) 174.

[5] G. Han, R. Ceilley, Chronic Wound Healing: A Review of Current Management and Treatments, Adv. Ther. 34 (2017) 599–610. doi:10.1007/s12325-017-0478-y.

[6] Z. Moore, S. Cowman, The need for EU standards in wound care : an Irish survey, Wounds UK. (2002) 20–28.

[7] R.G. Frykberg, J. Banks, Challenges in the Treatment of Chronic Wounds, 4 (2015) 560–582. doi:10.1089/wound.2015.0635.

[8] M. Turns, The diabetic foot: an overview of assessment and complications., Br. J. Nurs. 20 (2011) S19–S25. doi:10.12968/bjon.2011.20.Sup8.S19.

[9] K. Järbrink, G. Ni, H. Sönnergren, A. Schmidtchen, C. Pang, R. Bajpai, J. Car, The humanistic and economic burden of chronic wounds : a protocol for a systematic review, Syst. Rev. 6 (2017) 1–7. doi:10.1186/s13643-016-0400-8.

[10] P.S. Murphy, G.R.D. Evans, Advances in Wound Healing: A Review of Current Wound Healing Products, Plast. Surg. Int. 2012 (2012) 1–8. doi:10.1155/2012/190436.

[11] E.A. Kamoun, X. Chen, M.S. Mohy Eldin, E.-R.S. Kenawy, Crosslinked poly(vinyl alcohol) hydrogels for wound dressing applications: A review of remarkably blended polymers, Arab. J. Chem. 8 (2015) 1–14. doi:10.1016/j.arabjc.2014.07.005.

[12] G.D. Winter, Formation of the Scab and the Rate of Epithelization of Superficial Wounds in the Skin of the Young Domestic Pig, Nature. 193 (1962) 293–294. doi:10.1038/193293a0.

[13] G.D. Winter, J.T. Scales, Effect of Air drying and Dressings on the Surface of a Wound, Nature. 4862 (1963) 91–92. doi:10.1038/197091b0.

[14] S. Thomas, Alginate dressings in surgery and wound management – part 1, J. Wound Care. 9 (2000) 9–13. doi:10.12968/jowc.2000.9.2.26338.

[15] K. Deligkaris, T.S. Tadele, W. Olthuis, A. Van den Berg, Hydrogel-based devices for biomedical applications, Sensors Actuators B Chem. 147 (2010) 765–774. doi:10.1016/j.snb.2010.03.083.

[16] N.A. Peppas, Y.Huang, M. Torres-Lugo, J. H.Ward, and J. Zhang, Physicochemical foundations and structural design of hydrogels in medicine and biology, Annu.Rev.Biomed.Eng. (2000) 9–29.

[17] J.C. Dumville, S. O'Meara, S. Deshpande, K. Speak, Hydrogel dressings for healing diabetic foot ulcers., Cochrane Database Syst. Rev. 9 (2011) 1–46. doi:10.1002/14651858.CD009101.pub2.

[18] K.R. Kirker, Y. Luo, J.H. Nielson, J. Shelby, G.D. Prestwich, Glycosaminoglycan hydrogel films as bio-interactive dressings for wound healing, Biomaterials. 23 (2002) 3661–3671. doi:10.1016/S0142-9612(02)00100-X.

[19] J. Wang, J. Wei, Interpenetrating network hydrogels with high strength and transparency for potential use as external dressings, Mater. Sci. Eng. C. 80 (2017) 460–467. doi:10.1016/j.msec.2017.06.018.

[20] C.N. Grover, J.H. Gwynne, N. Pugh, S. Hamaia, R.W. Farndale, S.M. Best, R.E. Cameron, Crosslinking and composition influence the surface properties, mechanical stiffness and cell reactivity of collagen-based films, Acta Biomater. 8 (2012) 3080–3090. doi:10.1016/j.actbio.2012.05.006.

[21] Y.M.& Y. Kuroyanagi, Development of a Wound Dressing Composed of Hyaluronic Acid and Collagen Sponge with Epidermal Growth Factor, J. Biomater. Sci. 21 (2010) 715–726. doi:10.1163/156856209X435844.

[22] J.H. Sung, M.R. Hwang, J.O. Kim, J.H. Lee, Y. Il Kim, J.H. Kim, S.W. Chang, S.G. Jin, J.A. Kim, W.S. Lyoo, S.S. Han, S.K. Ku, C.S. Yong, H.G. Choi, Gel characterisation and in vivo evaluation of minocycline-loaded wound dressing with enhanced wound healing using polyvinyl alcohol and chitosan, Int. J. Pharm. 392 (2010) 232–240. doi:10.1016/j.ijpharm.2010.03.024.

[23] Z. Ajji, I. Othman, J.M. Rosiak, Production of hydrogel wound dressings using gamma radiation, Nucl. Instruments Methods Phys. Res. Sect. B Beam

Interact. with Mater. Atoms. 229 (2005) 375–380. doi:10.1016/j.nimb.2004.12.135.

[24] J.M. Yang, W.Y. Su, T.L. Leu, M.C. Yang, Evaluation of chitosan/PVA blended hydrogel membranes, J. Memb. Sci. 236 (2004) 39–51. doi:10.1016/j.memsci.2004.02.005.

[25] A. Das, A. Kumar, N.B. Patil, C. Viswanathan, D. Ghosh, Preparation and characterization of silver nanoparticle loaded amorphous hydrogel of carboxymethylcellulose for infected wounds., Carbohydr. Polym. 130 (2015) 254–61. doi:10.1016/j.carbpol.2015.03.082.

[26] M. Hwang, J.O. Kim, J.H. Lee, Y. Il Kim, J.H. Kim, S.W. Chang, S.G. Jin, J.A. Kim, W.S. Lyoo, S.S. Han, S.K. Ku, C.S. Yong, H. Choi, Gentamicin-Loaded Wound Dressing With Polyvinyl Alcohol / Dextran Hydrogel : Gel Characterization and In Vivo Healing Evaluation, AAPS PharmSciTech. 11 (2010) 1092–1103. doi:10.1208/s12249-010-9474-0.

[27] M. Contardi, J.A. Heredia-Guerrero, G. Perotto, P. Valentini, P.P. Pompa, R. Spanò, L. Goldoni, R. Bertorelli, A. Athanassiou, I.S. Bayer, Transparent ciprofloxacin-povidone antibiotic films and nanofiber mats as potential skin and wound care dressings, Eur. J. Pharm. Sci. 104 (2017) 133–144. doi:10.1016/j.ejps.2017.03.044.

[28] D.J. Leaper, P. Durani, Topical antimicrobial therapy of chronic wounds healing by secondary intention using iodine products, Int. Wound J. 5 (2008) 361–368. doi:10.1111/j.1742-481X.2007.00406.x.

[29] J.S. Choi, H.S. Yoo, Pluronic/chitosan hydrogels containing epidermal growth factor with wound-adhesive and photo-crosslinkable properties, J. Biomed. Mater. Res. - Part A. 95 A (2010) 564–573.

doi:10.1002/jbm.a.32848.

[30] A. Watarai, L. Schirmer, S. Thönes, U. Freudenberg, C. Werner, J.C. Simon, U. Anderegg, TGFβ functionalized starPEG-heparin hydrogels modulate human dermal fibroblast growth and differentiation, Acta Biomater. 25 (2015) 65–75. doi:10.1016/j.actbio.2015.07.036.

[31] S.J. Juris, A. Mueller, B.T.L. Smith, S. Johnston, R. Walker, R.D. Kross, Biodegradable Polysaccharide Gels for Skin Scaffolds, J. Biomater. Nanobiotechnol. 2 (2011) 216–225. doi:10.4236/jbnb.2011.23027.

[32] A.A. Chaudhari, K. Vig, D.R. Baganizi, R. Sahu, S. Dixit, V. Dennis, S.R. Singh, S.R. Pillai, Future prospects for scaffolding methods and biomaterials in skin tissue engineering: A review, Int. J. Mol. Sci. 17 (2016) 1–31. doi:10.3390/ijms17121974.

[33] M. Vahidi, M. Frounchi, S. Dadbin, Porous gelatin/poly(ethylene glycol) scaffolds for skin cells, Soft Mater. 15 (2017) 95–102. doi:10.1080/1539445X.2016.1268623.

[34] H.M. Yin, J. Qian, J. Zhang, Z.F. Lin, J.S. Li, J.Z. Xu, Z.M. Li, Engineering porous poly(lactic acid) scaffolds with high mechanical performance via a solid state extrusion/porogen leaching approach, Polymers (Basel). 8 (2016) 1–13. doi:10.3390/polym8060213.

[35] N. Thadavirul, P. Pavasant, P. Supaphol, Development of polycaprolactone porous scaffolds by combining solvent casting, particulate leaching, and polymer leaching techniques for bone tissue engineering, J. Biomed. Mater. Res. - Part A. 102 (2014) 3379–3392. doi:10.1002/jbm.a.35010.

[36] A. Dehsorkhi, V. Castelletto, I.W. Hamley, Self-assembling amphiphilic

peptides, J. Pept. Sci. 20 (2014) 453–467. doi:10.1002/psc.2633.

[37] B.J. Kim, Y.S. Choi, H.J. Cha, Reinforced multifunctionalized nanofibrous scaffolds using mussel adhesive proteins, Angew. Chemie - Int. Ed. 51 (2012) 675–678. doi:10.1002/anie.201105789.

[38] B.J. Kim, H. Cheong, E.S. Choi, S.H. Yun, B.H. Choi, K.S. Park, I.S. Kim, D.H. Park, H.J. Cha, Accelerated skin wound healing using electrospun nanofibrous mats blended with mussel adhesive protein and polycaprolactone, J. Biomed. Mater. Res. - Part A. 105 (2017) 218–225. doi:10.1002/jbm.a.35903.

[39] T.R. Dargaville, B.L. Farrugia, J. a. Broadbent, S. Pace, Z. Upton, N.H. Voelcker, Sensors and imaging for wound healing: A review, Biosens. Bioelectron. 41 (2013) 30–42. doi:10.1016/j.bios.2012.09.029.

[40] J. Zhou, T.N. Tun, S. ha Hong, J.D. Mercer-Chalmers, M. Laabei, A.E.R. Young, A.T.A. Jenkins, Development of a prototype wound dressing technology which can detect and report colonization by pathogenic bacteria, Biosens. Bioelectron. 30 (2011) 67–72. doi:10.1016/j.bios.2011.08.028.

[41] V. Sridhar, K. Takahata, A hydrogel-based passive wireless sensor using a flex-circuit inductive transducer, Sensors Actuators, A Phys. 155 (2009) 58–65. doi:10.1016/j.sna.2009.08.010.

[42] G.D. Winter, Formation of the Scab and the Rate of Epithelization of Superficial Wounds in the Skin of the Young Domestic Pig, Nature. 193 (1962) 293–294. doi:10.1038/193293a0.

[43] D. McColl, B. Cartlidge, P. Connolly, Real-time monitoring of moisture levels in wound dressings in vitro: An experimental study, Int. J. Surg. 5

(2007) 316–322. doi:10.1016/j.ijsu.2007.02.008.

[44] C. Occhiuzzi, A. Ajovalasit, M.A. Sabatino, C. Dispenza, G. Marrocco, RFID Epidermal Sensor including Hydrogel Membranes for Wound Monitoring and Healing, in: 2015 IEEE Int. Conf. RFID, 2015: pp. 227–233.

[45] P. Mostafalu, G. Kiaee, G. Giatsidis, A. Khalilpour, M. Nabavinia, M.R. Dokmeci, S. Sonkusale, D.P. Orgill, A. Tamayol, A. Khademhosseini, A Textile Dressing for Temporal and Dosage Controlled Drug Delivery, Adv. Funct. Mater. 1702399 (2017) 1–10. doi:10.1002/adfm.201702399.

3. Polysaccharide as candidates for wound dressing and wound healing applications

3.1. Polysaccharides used in wound dressing applications

Polysaccharides are polymers composed of carbohydrate monomers attached by glycosidic linkages. They offer a wide range of different compositions and structures; they can be linear or branched, and depending on the monosaccharides that constitute the chain, their composition, and source, they can offer a variety of different properties.[1] In particular, their structural characteristics, such as degree of substitution (DS) and molecular weight (MW), etc., have a big impact on their properties like solubility, physiological activity, chemical reactivity, and biodegradability.[2]

Polysaccharide are abundantly present in nature and readily available from a number of natural sources such as algae, plants, animals, and microorganisms.[3]. They represent the most abundant renewable source of polymers for several applications, ranging from eco-commodities, to food supplements, cosmetics, pharmaceuticals, and biomedical devices.[4]

Many polysaccharides are approved in the U.S. by FDA (Food and Drug Administration) and this may speed up the process of commercialisation of polysaccharide-based biomedical products with a wide range of polysaccharides products already in the market.[3]

These natural polymers are broadly used in pharmaceutical, biomedical and cosmetic industries. In particular, they have been used for drug delivery, tissue engineering, wound healing, skin hydration and protection, ocular preparations etc.[4]

In wound healing applications, polysaccharide biopolymers are slowly becoming popular as modern wound dressings materials because they are absorbent, non-toxic and non-allergenic. Their ample structural diversity gives the opportunity to exploit their wide range of properties to prepare wound dressing specific to a wound aetiology.[5]

Natural polysaccharides can also provide intrinsic bioactivity towards wounds which can enhance the healing process. Indeed, they are able to trigger non-specific immune response by activating the macrophages that clean up the wound site after the injury. In particular, macrophages can be activated for initiating the healing process by galectin receptors, that are able to recognise β-1,3-D-glycan bonds present in many natural polysaccharide.[6]

Furthermore, polysaccharides containing glycosaminoglycans (e.g. hyaluronic acid) are present in the extracellular matrix. They participate during the healing process by binding to proteins with hierarchical specificity and are mainly involved in cell differentiation, cell adhesion, cell signalling and cell-matrix interactions.[7]

Alginate, gellan, chitosan and hyaluronic acid are the most widely used polysaccharides to produce hydrogel wound dressings, and also used for drug delivery systems and tissue engineering. Some of these polysaccharides, such as alginate, are present in commercial products in the form of gels or as film dressings coupled with a textile support (see Chapter 2, paragraph 2.3.2.1.2.), while many others polysaccharides such as cellulose, starch or xyloglucan have intrinsic film-forming properties themselves so they can be formulated as self-standing films. However, these films are usually brittle and with poor mechanical properties. For this reason they are generally blended with plasticizers, that are small molecules added to soften the polymer by lowering its glass transition temperature or reducing its degree of crystallinity or crystal size.[8]

Polysaccharides commonly used in wound dressing include:

- Hyaluronic acid (HA); also called hyaluronan, is an anionic, non-sulfated glycosaminoglycan distributed widely throughout connective, epithelial, and neural tissues. It is composed of alternating units of D-glucuronic acid and D-N-acetylglucosamine, linked together via alternating β-1,4 and β-1,3 glycosidic bonds. HA has been widely studied for drug delivery, for dermal but also nasal, pulmonary or parenteral delivery. It has recently gained more attention for wound dressing fabrication because of its presence in the

extracellular matrix and involvement in the inflammation and proliferation stages of wound healing. Furthermore, glycosaminoglycans have been demonstrated to improve the wound healing process through re-epithelialization and increased vascularization.[9] It is also widely used in tissue engineering for skin regeneration [10,11]

- Alginic acid; also called algin or alginate, is an anionic polysaccharide widely distributed in the cell walls of brown algae, composed of β-D-mannuronic acid and R-L-guluronic acid units. It is able to undergo ionotropic gelation in presence of multivalent cations. The mechanism of gelation of alginate and its application in wound dressings have been already discussed in Chapter 2 (paragraph 2.3.2.1.2). Its biocompatibility, non-immunogenity and mucoadhesivity are well known and they have been exploited for the development of alginate-based drug delivery systems, wound dressings and scaffolds.

- Cellulose; is the most abundant organic polymer on Earth, consisting of a linear chain of several hundred to many thousands of β-(1→4) linked D-glucose units. Cellulose is an important structural component of the primary cell wall of green plants and many forms of algae. Some species of bacteria secrete it to form biofilms.

  It is not soluble in water and for this reason its derivatives (carboxymethyl-cellulose, hydroxymethyl-cellulose etc.) are preferred for biomedical applications. They have been extensively used for the development of bioactive wound dressings with drug delivery and scaffold functions. For instance, carboxymethylcellulose backed by a film has been used as hydrocolloid dressing.[12] The use of cellulose as hydrogel wound dressings is relatively recent and it is often used in blend with other polymers such as collagen.[13,14]

- Chitin and chitosan are linear polysaccharides composed of randomly distributed β-(1→4)-linked D-glucosamine (deacetylated unit) and N-acetyl-D-glucosamine (acetylated unit). The two terms chitin and chitosan are employed to define different degree of acetylation (DA) of this polysaccharide, which represents a percentage of N-acetyl-D-glucosamine unit with respect to the total number of the two units; however, even though the term chitosan is usually considered when DA is below 50%, there is no clear limit which unequivocally defines chitosan and chitin.[15] Can primarily be extracted from the exoskeleton of arthropods (e.g., shells of crabs and shrimp) and from the cuticles of insects, however it has been found also in the cell walls of fungi and yeast. Chitosan is used in wound bandages thanks to its haemostatic and antibacterial properties. In particular, in *in vivo* experiments it has been shown to improve healing of both infected and non-infected wounds.[16]

3.2. Polysaccharide modification

3.2.1. Crosslinking of polysaccharide for wound dressings fabrication

Crosslinking is a common method to produce polysaccharide-based wound dressings that do not disintegrate when in contact with biological fluids.

Although crosslinking improves polysaccharide properties, most of the crosslinkers causes undesirable changes to the polymer chain or results in high cytotoxicity. Glutharaldehyde (GA) has been widely used to crosslink most of the polysaccharides employed in biomedical applications including wound dressings. GA is a bifunctional crosslinker able to react both with amino and hydroxyl groups, and for this reason, it has been particularly used to crosslink blends of polysaccharide both with protein or with synthetic polymers.[17] For instance, GA has been used to crosslink alginate/collagen [18] or collagen/hyaluronic acid wound dressing membranes.[19] GA has been also used to immobilize chitosan hydrogel onto poly(N-

isopropylacrylamide) gel/polypropylene unwoven surface, in order to enhance antibacterial ability in wound dressings.[20]

Crosslinking with GA was also used for other biomedical applications to obtain drug delivery systems such as chitosan beads for the release of diclofenac, interpenetrated microbeads of xyloglucan and alginate for the prolonged release of diltiazem or kappa carrageenan pH-sensitive hydrogels.[21–23]

However, contradictory results are reported in literature regarding the *in vitro* cytotoxicity of glutaraledehyde-crosslinked materials, so a careful characterisation of materials is necessary for their biomedical applications.[17]

In addition to glutaraldehyde, several other reagents including epichloridin, genepin and carbodiimide have been used for the crosslinking of polysaccharide but with poor improvement of mechanical properties and resilience due to their low crosslinking efficiency. For instance, genepin possesses significantly less cytotoxicity compared to GA and it has been used to crosslink chitosan films as wound dressings. The antimicrobial activity of chitosan was maintained after crosslinking, was found that crosslinking of a chitosan membrane using genipin increased the ultimate tensile strength of the film increased and the strain-at-fracture and swelling ratio decreased, as one would expect from a crosslinked film.[24]

Recently, citric acid was proposed as benign crosslinking agent of polysaccharides: in particular cellulose and starch, leading to improvements of the mechanical properties and the chemical and mechanical stability of the crosslinked films without compromising the cytotoxicity.[25,26]

Furthermore, high energy irradiation is a well-established technology that allows gel manufacturing and its sterilization in one process. Recently, the fabrication of a hydrogel dressing based on poly(N-vinyl pyrrolidone) (PVP) and agar containing also chitosan as antimicrobial compound has been reported. [27]

Polysaccharide for wound healing applications can also be physically crosslinked. The gelation of alginate in presence of calcium ions described in Chapter 2 (paragraph 2.3.2.1.2) is an example of physical hydrogel wound dressing.

Another recent example is the physical crosslinking of sacran (a megamolecular natural polysaccharide newly extracted from cyanobacterium Aphanothece sacrum) hydrogel films by a solvent-casting method. These films showed a considerably improved wound healing ability, probably due to not only the moisturing effect but also the anti-inflammatory effect of sacran.[28]

3.2.2. Polysaccharide functionalization

Polysaccharides can be modified to meet the specific needs of medical applications, bearing even greater potential for tissue engineering.

Functionalisation of polysaccharides can change their chemical structures, for instance, making them more hydrophobic or hydrophilic, depending on the desired application.

Other reactions on polysaccharide may lead to the introduction of different functionalities, such as carboxyl, carboxymethyl, esters, sulfonate groups etc. and for these reactions it is preferable to react homogeneous solutions to have a uniform derivatisation of the polymer, hence it is very important to choose the appropriate solvent for polysaccharide substrates.[29]

Typical reactions on polysaccharides use the saccharide oxygen as nucleophile that reacts and is retained in the product which may be either an ester or an ether, or the substitution of saccharide oxygen with a heteroatomic nucleophile. The latter approach requires in the first instance that the saccharide oxygen is transformed into a good leaving group, thus susceptible to a nucleophilic attack.[29]

Another very common reaction for polysaccharide functionalisation is the oxidation which may lead to different structures depending on the way of oxidation. Polysaccharides may be oxidized at the primary alcohol simply giving the aldehyde or further to the carboxylic acid level, or they may be subjected to an oxidative cleavage of 1,2-diols which lead to a dicarbonyl compound. Oxidation of primary alcohol to carboxylic acid results in a polysaccharide chain with uronic acid similar

to natural occurring polyuronic polysaccharides such as pectin or alginate. This topic will be discussed in details in Chapter 5 (paragraph 5.1).

Another method to obtain the oxidation at primary hydroxyl groups is the enzymatic oxidation and the enzyme commonly used for this purpose is galactose-6-oxidase, which is selective for the C6 of galactose residues.

Grafting of synthetic monomer on a polysaccharide chains represents another way to control polymer solubility in desired solvents, water uptake and degradation. These semi-synthetic polymers offer the best features of both natural and synthetic polymers.

3.3. Xyloglucan

Xyloglucan (XG) was used in this PhD project due to the combination of several favourable properties that make it particularly suitable for biomedical applications such as wound healing. It is very abundant in nature and this determines its low cost, is able to form either films or gels depending on the processing conditions, is biocompatible and biodegradable and has been already studied for some tissue engineering applications.[30,31] An overview on XG origins, physico-chemical properties and biomedical applications will be provided in the following paragraphs.

3.3.1. Origin, composition and physico-chemical properties

Xyloglucan is a hemicellulose found in the primary cell walls of dicotyledons and non-graminaceous monocotyledons. It can also be found as a storage polysaccharide in different seeds, such as *Tamarindus, Impatiens, Annona, Tropaeolum, Hymenaea, and Detarium*. In these seeds it represents 50% (w/w) of the storing energetic resources.[32]

Xyloglucan backbone is formed by β-(1→4)-D-glucan, similar to cellulose. The glucose backbone it partially substituted by α-(1→6)-linked xylose branches that in turn may be further derivatized by β-(1→2)-linked galactose residues. In Fig. 3.1 is reported an idealized chemical structure, because, as for all the polysaccharide from natural sources, the real distribution of the repeating units is not homogenous and varies according to many external conditioning factors, such as the polysaccharide

origin, the extraction process from seeds and so on.[33] In particular, the branching pattern in xyloglucan is strongly dependent on the natural source.

Xyloglucans extracted from different seeds have different chain flexibility, that are at the basis of the different physiological activities or physico-chemical properties.

Xyloglucan from *Tamarind* seeds, which is the most studied xyloglucan is that extracted from *Tamarindus Indica*, thanks to its commercial availability, has a high molecular weight, with reported average molecular weight (Mw) values in the range 650 to 2,500 kDa. This is a marked difference compared with wood-derived hemicelluloses, which have lower molecular weights, in the order of 10,000 – 50,000 Da after the extraction process.[34]

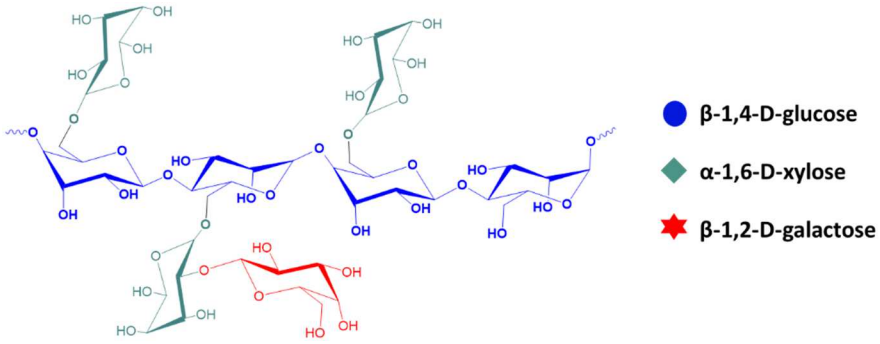

Fig. 3.1 One representative xyloglucan repeating unit

Four different monomers have been identified in xyloglucan from *Tamarind* seeds, that differ for the number and the distribution of galactose residues (Fig. 3.2). These different monomers are Glc_4Xyl_3 heptamer, two types of Glc_4Xyl_3Gal octamers and $Glc_4Xyl_3Gal_2$ nonamer. The molar ratio of these repeating units in *Tamarind* seed xyloglucans is typically 1:0.42:2.08:6.20.[35,36]

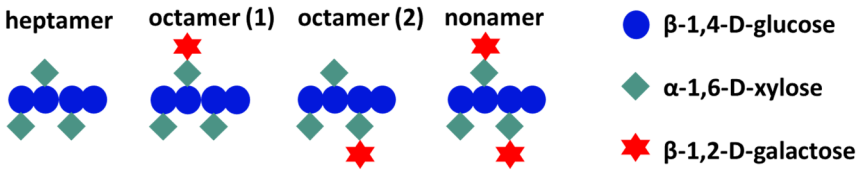

Fig. 3.2 Chemical structure of four monomers of xyloglucan

Differently from cellulose, that is insoluble in water because of its crystaline structure that involves intra- and inter-molecular hydrogen bonding, xyloglucan is water-soluble due to the presence of xylose and galactose residues of its side chain that causes steric hindrance, preventing the cellulose-like chain crystallization.

However, xyloglucan tendency to self-assembly in aqueous solution prevents its complete dissolution, as also observed for other biopolymers. Xyloglucan shows a balance between hydrophilic and hydrophobic character: macromolecules do not fully hydrate and supramolecular, flat, ribbon-like aggregates form even in very dilute solutions.[30]

In aqueous solutions, xyloglucan molecules behave as flexible random coil polymer and they do not show any conformational change such as coil-helix transition like other polysaccharides, i.e. xantan gum, gellan or carrageenan. Solutions of XG (>0.5 %w) have a non-Newtonian (pseudo-plastic or shear-thinning) rheology and it shows random-coil polymer.[37]

Hindered rotation and the specific aggregation in solution are responsible for the stiffness of the polymer and the “hyper-entangled” behaviour.[34]

The thermal stability of xyloglucan at high temperature (below 280°C) is also attributed to its “hyper-entangled” structure, while chemical the stability in mild acids and bases can be attributed to the high degree of substitution of the backbone, which, to some extent, shields it from hydrolysing agents.[30,34,38]

Xyloglucan can form a gel in cold water only in the presence of alcohols or high levels of sugar. Gelation is the result of a localized increase of polymer concentration due to water sequestration by the alcohol, leading to polymer chain association and is strongly dependent on the type of alcohol.[39] Similarly, gelation mechanism in high concentrated sucrose systems involves the aggregation of "dehydrated" chains.[40] Sugar substituents along polymer chains limit the degree of aggregation, thus preventing polymer precipitation and promoting gelation, instead.
Other ways to induce xyloglucan gelation are the addition of polyphenols, such as epigallocatechin gallate, or mixing with helix-forming polysaccharides, such as galactomannans or xantan gum. Also the addition of iodine to xyloglucan solution can promote the formation of a coloured weak gel.[34]
On the other hand, the partial removal of galactose residues using the enzyme β-galactosidase, induces the ability to undergo gelation reversibly upon heating without the addition of any substance.

Xyloglucan is biodegradable and in suitable biological environments it can be subjected to hydrolytic and/or enzymatic degradations. Its degradation products should be non-toxic since they should consist in naturally occurring saccharides. However, while fungi or plants produce the enzyme endo-β-(1,4)-glucanase, that is able to degrade xyloglucan, the human genome doesn't contain the genes coding for xyloglucan degradation, even though xyloglucans are important components of most human diets. It has been recently found that degradation of xyloglucan in humans is attributable to a common human gut symbiont, called *Bacteroidetes* that contain in their genome a polysaccharide utilization locus (PUL) appointed to the expression of the enzyme for the degradation of different polysaccharide linkage.[41]

3.3.2. Xyloglucan biomedical applications

While a relevant number of publications and patents are reported for the use of xyloglucan as a food additive, being approved by FDA for use as food additive,

stabilizing and thickening agent, [38] much less has been published about its use in the pharmaceutical and biomedical fields. However, the already published works indicate its potential for a wide variety of applications with numerous advantages compared with other macromolecular systems.[42,43]

Xyloglucan, thanks to its somewhat amphiphilic nature, has been extensively used in drug delivery as vehicle of a variety of both hydrophobic and hydrophilic active molecules. In particular, it has been used to produce tablets for the sustained release of both water-soluble (acetaminophen, caffeine, theophylline and salicylic acid) and water insoluble (indomethacin) drugs.[44]

Its intrinsic mucoadhesive properties result particularly attractive for drug delivery. Furthermore, the combination of xyloglucan with appropriate amounts of glycerol lead to an increase of its mucoadhesiveness. Xyloglucan-glycerol formulations suitable for the application in human mucosae such as nasal, oral, vaginal as moisturizers or for the release of therapeutic agent have been patented by Alfawassermann in 2005.[45] A similar approach was used to produce xyloglucan mucoadhesive films for the release of rizatriptan benzoate for the treatment of migraine.[46]

Xyloglucan has been shown also safe for the ocular mucosa that is really sensitive and, recently, a xyloglucan film for the ocular release of ciprofloxacin has been described. The use of a safe polymeric film for ophthalmic drug release can significantly improve the effectiveness of the drug compared to common ophthalmic drops, increasing the precorneal residence of the drug.[47]

Other films for drug delivery have been prepared using combination of xyloglucan and chitosan or starch. The combination of xyloglucan and chitosan gives place to a strong, stable and flexible film due to the inter-intramolecular hydrogen bonding established between the two polysaccharide. This film was able to encapsulate streptomycin (as a model drug) and successfully release the active in a controlled fashion by changing the pH suitably.[48]

Xyloglucan has also been used for tissue regeneration purposes. In this case, partially degalactosylated thermoresponsive xyloglucan has been used to form in-situ gels, incorporating the growth factor FGF-18 for the regeneration of cartilage. The growth factor is never released by xyloglucan matrix, in this way the uncontrolled cartilage growth also in healthy areas is avoided.[31]

For some biomedical applications i.e. wound dressing, chemical crosslinking may be required in order to form permanent and stable networks. In the literature, there are just few reports of xyloglucan chemical crosslinking. Sravani et al. reported the chemical crosslinking of xyloglucan using epichlorohydrin. The crosslinking was considered as a release retardant of diclofenac sodium and ketoprofen.[49] Otherwise, more recently citric acid as chemical crosslinker was used for the fabrication of a hydroxypropyl methylcellulose (HPMC) and xyloglucan. These films loaded with gentamicin show very good antibacterial properties against *Staphylococcus aureus* and *Escherichia coli* and thus they have been proposed for biomedical applications.[50]

Although xyloglucan is a very versatile excipient for pharmaceutical applications, in the last two decades, several studies have revealed that xyloglucan owns also intrinsic biological activity. For instance, it now recognized the anti-inflammatory effect of xyloglucan, in particular, for topical administration in the treatment of inflammatory diseases of the skin and mucosa.[51] Xyloglucan has also been suggested as natural additive compound in sun creams because it has been shown that it has immune-protective and DNA-protective effect from ultraviolet damage.[52]

The wound healing properties of tamarind extracts or xyloglucan have been sufficiently investigated but there is still a lack for bringing these properties into functional materials.

Wound healing properties of tamarind seed extracts containing 65% of xyloglucans have been *in vivo* tested. The reported results show that all extracts exhibited

significant increase in the rate of healing and this effect was attributed to the various components present in those extracts, among which alkaloids, flavonoids, saponin and tannin.[53]

However, solely xyloglucan healing properties have been further investigated. Tamarind xyloglucans was proven to improve processes of wounds reepithelialisation and remodelling. This result suggests again that xyloglucan can be more than a simple excipient and also be beneficial for tissue regeneration.[54]

Xyloglucan has been also demonstrated to be effective in promoting corneal wound healing, probably due to its influence in integrin recognition system.[55]

It has been used also for tissue engineering applications to produce a synthetic extracellular matrix for hepatocytes. Indeed, the presence of galactose residues in the side chains of xyloglucan favour cell adhesion because they can be recognized by asialoglycoprotein receptors that are present in certain type of cells, such as hepatocytes.[56] For the same reason, XG was also used as coating for alginate capsules, to promote hepatocytes attachment;[57] Seo et al. also compared the rate of cell adhesion of collagen type-I-coated, XG-coated and uncoated polystyrene (PS) surfaces and discover that xyloglucan induce an adhesion rate that is very similar to collagen type-I.[57]

Another application of xyloglucan in tissue engineering involves the use of its thermoresponsive version to produce hydrogel for neural tissue engineering of the spinal cord. These hydrogels have been functionalized with poly-D-lysine to promote neurone adhesion and neurite outgrowth with the aim to support neural stem cells with a scaffold that acted as a proliferative niche to support differentiation and reduce glial scarring, thus facilitating repair by direct cell replacement. Xyloglucan has been proved to be not toxic and able to support neuronal differentiation. Degalactosilation of xyloglucan yielded biological scaffolds that had superior capacity to support *in vitro* neuronal survival, differentiation, and neurite extension.[58] Following this work, these xyloglucan-based scaffolds have been directly implanted within the brain, in particular in the caudate putamen of adult rats. The inflammatory response after the

implantation, as well as scaffolds capability to promote the controlled infiltration of axons, have been investigated and resulted non-toxic and able to support the growth and the differentiation of neurites.[59]

3.3.3. Xyloglucan modification

Thermoresponsive degalactosilated xyloglucan is not the only variant of xyloglucan that has been produced for biomedical applications. Several xyloglucan functionalisations are under investigation in order to replace xyloglucan hydroxyl groups with more reactive functional groups, such as carboxyl, amino, alkyloamino, thiol and carboxymethyl groups.[35,60]

These derivative usually show different physico-chemical properties; for instance, they can show better water solubility, increased mucoadhesivity and they may result in a modification drug release profile.

Carboxylation of xyloglucan hydroxyl groups has been performed with different methods. Galactose oxidase has been used to form formyl residues followed by further oxidation to carboxylate groups by addition of alkaline I_2/I^-.[35] Another way to obtain this modification is the regioselective TEMPO-mediated oxidation that selectively oxidizes primary hydroxyl groups. This reaction has been successfully performed on both *Hymanea cubaril* and *Tamarind indica* xyloglucan and the mechanism of the reaction will be discussed in Chapter 5 (paragraph 5.1).

Another way to introduce carboxyl groups in XG polymer chain is the carboxymethylation. This reaction has been performed with sodium salt of monochloro acetic acid in the presence of sodium hydroxide. This functionalization was used to produce matrices for controlled drug release.[61]

On the other hand, amination of xyloglucan has been obtained through reaction with ethylene diamine. The resulting product in which hydroxyl groups of XG in the C2, C3 and C6 position were substituted by $-NHCH_2CH_2NH_2$ which was further reduced to $-NH_2$ using $NaBH_4$ as reducing agent. This xyloglucan was able to self-assemble in spherical nanoparticles at low concentration and form irreversible hydrogels with a

characteristic blue fluorescence at higher concentration, showing an anti-microbial activity higher than chitosan.[62]

Another finest xyloglucan modification has involved the coupling of a short peptide sequence on the polymer chain. In this case, xyloglucan was first partially degraded in order to obtain xyloglucan oligosaccharides and then coupled with –GRGDS sequence. These modified oligosaccharides have been finally integrated with bacterial cellulose nanofibrils to obtain a composite material that promote cell adhesion and proliferation.[63]

More recently, xyloglucan has also been functionalised with the addition of thiol groups by esterification of its hydroxyl groups with thioglycolic acid. This functionalisation led to a remarkable increase of the mucoadhesive strength of this polymer that encourage further evaluations for new formulations of different pharmaceutical dosage form.[64]

References

[1] J. Liu, S. Willför, C. Xu, A review of bioactive plant polysaccharides: Biological activities, functionalizatison, and biomedical applications, Bioact. Carbohydrates Diet. Fibre. 5 (2014) 31–61. doi:10.1016/j.bcdf.2014.12.001.

[2] N.B. Shelke, R. James, C.T. Laurencin, S.G. Kumbar, Polysaccharide biomaterials for drug delivery and regenerative engineering, Polym. Adv. Technol. 25 (2014) 448–460. doi:10.1002/pat.3266.

[3] E. Muntimadugu, D.E. Ickowicz, A.J. Domb, W. Khan, Polysaccharide Biomaterials, 91120 (2013) 787–794. doi:10.1002/ijch.201300062.

[4] P. Laurienzo, J.C. Fernandes, S. Colliec-Jouault, J.H. Fitton, The Use of Natural Polysaccharides as Biomaterials, Biomed Res. Int. 2015 (2015) 1–2. doi:10.1155/2015/242378.

[5] D. Aduba, H. Yang, Polysaccharide Fabrication Platforms and

Biocompatibility Assessment as Candidate Wound Dressing Materials, Bioengineering. 4 (2017) 1–16. doi:10.3390/bioengineering4010001.

[6] N. Panjwani, Role of galectins in re-epithelialization of wounds., Ann. Transl. Med. 2 (2014) 1–11. doi:10.3978/j.issn.2305-5839.2014.09.09.

[7] K. Senni, J. Pereira, F. Gueniche, C. Delbarre-Ladrat, C. Sinquin, J. Ratiskol, G. Godeau, A.M. Fischer, D. Helley, S. Colliec-Jouault, Marine polysaccharides: A source of bioactive molecules for cell therapy and tissue engineering, Mar. Drugs. 9 (2011) 1664–1681. doi:10.3390/md9091664.

[8] Y.O. S. Gungor, M.S. Erdal, Recent advances in Plasticizers, Luqman M, InTech, Rijeka, Croatia, 2012.

[9] K.R. Kirker, Y. Luo, J.H. Nielson, J. Shelby, G.D. Prestwich, Glycosaminoglycan hydrogel films as bio-interactive dressings for wound healing, Biomaterials. 23 (2002) 3661–3671. doi:10.1016/S0142-9612(02)00100-X.

[10] P.B. Malafaya, G.A. Silva, R.L. Reis, Natural–origin polymers as carriers and scaffolds for biomolecules and cell delivery in tissue engineering applications, Adv. Drug Deliv. Rev. 59 (2007) 207–233. doi:10.1016/j.addr.2007.03.012.

[11] C.B. Highley, G.D. Prestwich, J.A. Burdick, Recent advances in hyaluronic acid hydrogels for biomedical applications, Curr. Opin. Biotechnol. 40 (2016) 35–40. doi:10.1016/j.copbio.2016.02.008.

[12] C. Daunton, S. Kothari, L. Smith, D. Steele, A history of materials and practices for wound management, Wound Pract. Res. 20 (2012) 174.

[13] S. Kiselioviene, O. Baniukaitiene, V. Harkavenko, N.A. Babenko, J. Liesiene, C. Chemistry, Cellulose Hydrogel Sheets for Wound Dressings, Cellul. Chem. Technol. 50 (2016) 915–923.

[14] P.R.F. de S. Moraes, S. Saska, H. Barud, L.R. de Lima, V. da C.A. Martins, A.M. de G. Plepis, S.J.L. Ribeiro, A.M.M. Gaspar, Bacterial Cellulose/Collagen Hydrogel for Wound Healing, Mater. Res. 19 (2016) 106–116. doi:10.1590/1980-5373-MR-2015-0249.

[15] W. Wang, Y. Du, Y. Qiu, X. Wang, Y. Hu, J. Yang, J. Cai, J.F. Kennedy, A new green technology for direct production of low molecular weight chitosan, Carbohydr. Polym. 74 (2008) 127–132. doi:10.1016/j.carbpol.2008.01.025.

[16] M. Burkatovskaya, A.P. Castano, T.N. Demidova-Rice, G.P. Tegos, M.R. Hamblin, Effect of chitosan acetate bandage on wound healing in infected and noninfected wounds in mice, Wound Repair Regen. 16 (2008) 425–431. doi:10.1111/j.1524-475X.2008.00382.x.

[17] N. Reddy, R. Reddy, Q. Jiang, Crosslinking biopolymers for biomedical applications, Trends Biotechnol. 33 (2015) 362–369. doi:10.1016/j.tibtech.2015.03.008.

[18] L. Bao, W. Yang, X. Mao, S. Mou, S. Tang, Agar/collagen membrane as skin dressing for wounds, Biomed. Mater. 3 (2008) 1–7. doi:10.1088/1748-6041/3/4/044108.

[19] R.R. Cobb, Mechanical and biocompatible characterization of a cross-linked collagen-hyaluronic acid wound dressing, Biomatter. 3 (2013) 1–14. doi:10.4161/biom.25633.

[20] K.S. Chen, Y.A. Ku, C.H. Lee, H.R. Lin, F.H. Lin, T.M. Chen, Immobilization of chitosan gel with cross-linking reagent on PNIPAAm gel/PP nonwoven composites surface, Mater. Sci. Eng. C. 25 (2005) 472–478. doi:10.1016/j.msec.2004.12.006.

[21] V.H. Kulkarni, P. V. Kulkarni, J. Keshavayya, Glutaraldehyde-crosslinked chitosan beads for controlled release of diclofenac sodium, J. Appl. Polym.

Sci. 103 (2007) 211–217. doi:10.1002/app.25161.

[22] S. Distantina, M. Fahrurrozi, Preparation of Hydrogel Based on Glutaraldehyde-Crosslinked Carrageenan, in: 3rd Int. Conf. Chemestry Chem. Eng., 2012: pp. 150–154.

[23] R. V Kulkarni, S. Mutalik, B.S. Mangond, U.Y. Nayak, Novel interpenetrated polymer network microbeads of natural polysaccharides for modified release of water soluble drug: in-vitro and in-vivo evaluation, J. Pharm. Pharmacol. 64 (2012) 530–540. doi:10.1111/j.2042-7158.2011.01433.x.

[24] R.A.A. Muzzarelli, Genipin-crosslinked chitosan hydrogels as biomedical and pharmaceutical aids, Carbohydr. Polym. 77 (2009) 1–9. doi:10.1016/j.carbpol.2009.01.016.

[25] M.G. Raucci, C. Demitri, D. Giugliano, V. De Benedictis, A. Sannino, L. Ambrosio, Effect of citric acid crosslinking cellulose-based hydrogels on osteogenic differentiation, (2014) 2045–2056. doi:10.1002/jbm.a.35343.

[26] N. Reddy, Citric acid cross-linking of starch films, Food Chem. 118 (2009) 702–711. doi:10.1016/j.foodchem.2009.05.050.

[27] W. Mozalewska, R. Czechowska-Biskup, A.K. Olejnik, R.A. Wach, P. Ulański, J.M. Rosiak, Chitosan-containing hydrogel wound dressings prepared by radiation technique, Radiat. Phys. Chem. 134 (2017) 1–7. doi:10.1016/j.radphyschem.2017.01.003.

[28] N. Wathoni, K. Motoyama, T. Higashi, M. Okajima, T. Kaneko, H. Arima, Physically crosslinked-sacran hydrogel films for wound dressing application, Int. J. Biol. Macromol. 89 (2016) 465–470. doi:10.1016/j.ijbiomac.2016.05.006.

[29] I. Cumpstey, Chemical Modification of Polysaccharides, ISRN Org. Chem. 2013 (2013) 1–27. doi:10.1155/2013/417672.

[30] S. Todaro, C. Dispenza, M.A. Sabatino, M.G. Ortore, R. Passantino, P.L. San Biagio, D. Bulone, Temperature-induced self-assembly of degalactosylated xyloglucan at low concentration, J. Polym. Sci. Part B Polym. Phys. 53 (2015) 1727–1735. doi:10.1002/polb.23895.

[31] C. Dispenza, S. Todaro, D. Bulone, M.A. Sabatino, G. Ghersi, P.L. San Biagio, C. Lo Presti, Physico-chemical and mechanical characterization of in-situ forming xyloglucan gels incorporating a growth factor to promote cartilage reconstruction, Mater. Sci. Eng. C. 70 (2017) 745–752. doi:10.1016/j.msec.2016.09.045.

[32] N.B. Shankaracharya, Tamarind - chemistry, technology and uses - a critical appraisal, J. Food Sci. Technol. 335 (1998) 193–208.

[33] M. Hoffman, Z. Jia, M.J. Peña, M. Cash, A. Harper, A.R. Blackburn, A. Darvill, W.S. York, Structural analysis of xyloglucans in the primary cell walls of plants in the subclass Asteridae, Carbohydr. Res. 340 (2005) 1826–1840. doi:10.1016/j.carres.2005.04.016.

[34] G.O. Phillips, P.A. Williams, Handbook of hydrocolloids, Woodhead publishing limited, 2009.

[35] P. Lang, G. Masci, M. Dentini, V. Crescenzi, D. Cooke, J. Gidley, C. Fanutti, J.S.G. Reid, Tamarind seed polysaccharide : preparation , characterisation and solution properties of carboxylated , sulphated and alkylaminated derivatives, Carbohydr. Polym. 17 (1992) 185–198. doi:10.1016/0144-8617(92)90003-9.

[36] A.D. Kulkarni, A.A. Joshi, C.L. Patil, P.D. Amale, H.M. Patel, S.J. Surana, V.S. Belgamwar, K.S. Chaudhari, C. V. Pardeshi, Xyloglucan: A functional biomacromolecule for drug delivery applications, Int. J. Biol. Macromol. 104 (2017) 799–812. doi:10.1016/j.ijbiomac.2017.06.088.

[37] K. Khounvilay, W. Sittikijyothin, Rheological behaviour of tamarind seed

gum in aqueous solutions, Food Hydrocoll. 26 (2012) 334–338. doi:10.1016/j.foodhyd.2011.03.019.

[38] A. Mishra, A.V. Malhotra, Tamarind xyloglucan : a polysaccharide with versatile application potential †, J. Mater. Chem. 19 (2009) 8528–8536. doi:10.1039/b911150f.

[39] Y. Yuguchi, T. Kumagai, M. Wu, T. Hirotsu, J. Hosokawa, Gelation of xyloglucan in water/alcohol systems, Cellulose. 11 (2004) 203–208. doi:10.1023/B:CELL.0000025427.60557.40.

[40] K. Ogawa, T. Hayashi, K. Okamura, Conformational analysis of xyloglucans, Int. J. Biol. Macromol. 12 (1990) 218–222. doi:10.1016/0141-8130(90)90036-A.

[41] J. Larsbrink, T.E. Rogers, G.R. Hemsworth, L.S. McKee, A.S. Tauzin, O. Spadiut, S. Klinter, N.A. Pudlo, K. Urs, N.M. Koropatkin, A.L. Creagh, C.A. Haynes, A.G. Kelly, S.N. Cederholm, G.J. Davies, E.C. Martens, H. Brumer, A discrete genetic locus confers xyloglucan metabolism in select human gut Bacteroidetes, Nature. 506 (2014) 498–502. doi:10.1038/nature12907.

[42] T. Coviello, P. Matricardi, C. Marianecci, F. Alhaique, Polysaccharide hydrogels for modified release formulations, J. Control. Release. 119 (2007) 5–24. doi:10.1016/j.jconrel.2007.01.004.

[43] P. Kuru, Tamarindus indica and its health related effects, Asian Pac. J. Trop. Biomed. 4 (2014) 676–681. doi:10.12980/APJTB.4.2014APJTB-2014-0173.

[44] S. Sumathi, A.R. Ray, Release behaviour of drugs from tamarind seed polysaccharide tablets, J. Pharm. Pharm. Sci. 5 (2002) 12–18.

[45] G. Bottoni, P. Maffei, A. Sforzini, M. Federici, C. Caramella, S. Rossi, G.C. Viscomi, Mucoadhesive xyloglucan-containing formulations useful in medical devices and in pharmaceutical formulations, WO2006131262A1,

2005.

[46] A.M. Avachat, K.N. Gujar, K. V. Wagh, Development and evaluation of tamarind seed xyloglucan-based mucoadhesive buccal films of rizatriptan benzoate, Carbohydr. Polym. 91 (2013) 537–542. doi:10.1016/j.carbpol.2012.08.062.

[47] H.S. Mahajan, S.R. Deshmukh, Development and evaluation of gel-forming ocular films based on xyloglucan, Carbohydr. Polym. 122 (2015) 243–247. doi:10.1016/j.carbpol.2015.01.018.

[48] C.K. Simi, T.E. Abraham, Biodegradable biocompatible xyloglucan films for various applications, Colloid Polym. Sci. 288 (2010) 297–306. doi:10.1007/s00396-009-2151-8.

[49] B. Sravani, R. Deveswaran, S. Bharath, B. V Basavaraj, V. Madhavan, Release characteristics of drugs from cross linked tamarind seed polysaccharide matrix tablets, Pelagia Res. Libr. 2 (2011) 67–76.

[50] S. Kondaveeti, T.C. Damato, A.M. Carmona-Ribeiro, M.R. Sierakowski, D.F.S. Petri, Sustainable hydroxypropyl methylcellulose/xyloglucan/gentamicin films with antimicrobial properties, Carbohydr. Polym. 165 (2017) 285–293. doi:10.1016/j.carbpol.2017.02.066.

[51] I. Giori, A., Arpini, S., & Togni, S., Tamarind seed polysaccharide for use in the treatment of inflammatory diseases, WO2011147768 A1, 2011.

[52] F. Strickland, P. Ronald, P. Albersheim, A. Darvill, M. Pauly, S. Eberhard, Inhibition Of Uv-Induced Immune Suppression And Interleukin-10 Production By Cytoprotective Tamarind Oligosaccharides, US006251878B1, 2001.

[53] M. Yusof bin Mohamad, H.B. Akram, D. Najwa Bero, M. Tariqur Rahman, Tamarind Seed Extract Enhances Epidermal Wound Healing, Int. J. Biol. 4 (2012) 81–88. doi:10.5539/ijb.v4n1p81.

[54] W. Nie, a. M. Deters, Tamarind seed xyloglucans promote proliferation and migration of human skin cells through internalization via stimulation of proproliferative signal transduction pathways, Dermatol. Res. Pract. 2013 (2013) 1–14. doi:10.1155/2013/359756.

[55] S. Burgalassi, L. Raimondi, R. Pirisino, G. Banchelli, E. Boldrini, M.F. Saettone, Effect of xyloglucan (tamarind seed polysaccharide) on conjunctival cell adhesion to laminin and on corneal epithelium wound healing, Eur. J. Ophthalmol. 10 (2000) 71–76. doi:1120-6721/071.

[56] T.A.& C.-S.C. Seog-Jin Seo , In-Kyu Park , Mi-Kyoung Yoo , Mayumi Shirakawa, Xyloglucan as a synthetic extracellular matrix for hepatocyte attachment, Biomater. Sci. 15 (2004) 1375–1387. doi:10.1016/S0142-9612(03)00108-X.

[57] S.J. Seo, T. Akaike, Y.J. Choi, M. Shirakawa, I.K. Kang, C.S. Cho, Alginate microcapsules prepared with xyloglucan as a synthetic extracellular matrix for hepatocyte attachment, Biomaterials. 26 (2005) 3607–3615. doi:10.1016/j.biomaterials.2004.09.025.

[58] D.R. Nisbet, D. Moses, T.R. Gengenbach, J.S. Forsythe, D.I. Finkelstein, M.K. Horne, Enhancing neurite outgrowth from primary neurones and neural stem cells using thermoresponsive hydrogel scaffolds for the repair of spinal cord injury, J. Biomed. Mater. Res. - Part A. 89 (2009) 24–35. doi:10.1002/jbm.a.31962.

[59] D.R. Nisbet, A.E. Rodda, M.K. Horne, J.S. Forsythe, D.I. Finkelstein, Implantation of Functionalized Thermally Gelling Xyloglucan Hydrogel Within the Brain: Associated Neurite Infiltration and Inflammatory Response, Tissue Eng. Part A. 16 (2010) 2833–2842. doi:10.1089/ten.tea.2009.0677.

[60] R. Manchanda, S.C. Arora, R. Manchanda, Tamarind Seed Polysaccharide

and its Modifications- Versatile Pharmaceutical Excipients – A Review, Int. J. PharmaTech Res. 6 (2014) 412–420.

[61] P. Goyal, V. Kumar, P. Sharma, Carboxymethylation of tamarind kernel powder, Carbohydr. Polym. 69 (2007) 251–255. doi:10.1016/j.carbpol.2006.10.001.

[62] C.K. Simi, T.E. Abraham, Physico chemical properties of aminated tamarind xyloglucan, Colloids Surfaces B Biointerfaces. 81 (2010) 513–520. doi:10.1016/j.colsurfb.2010.07.051.

[63] A. Bodin, L. Ahrenstedt, H. Fink, H. Brumer, B. Risberg, P. Gatenholm, Modification of nanocellulose with a xyloglucan-RGD conjugate enhances adhesion and proliferation of endothelial cells: Implications for tissue engineering, Biomacromolecules. 8 (2007) 3697–3704. doi:10.1021/bm070343q.

[64] H. Kaur, S. Yadav, M. Ahuja, N. Dilbaghi, Synthesis, characterization and evaluation of thiolated tamarind seed polysaccharide as a mucoadhesive polymer, Carbohydr. Polym. 90 (2012) 1543–1549. doi:10.1016/j.carbpol.2012.07.028.

4. Xyloglucan-based hydrogel films for wound dressing: structure-property relationships

4.1. Introduction and aim

As discussed in Chapter 1 and 2, hydrogels are the best suitable for wound dressing applications, because they can offer a combination of favourable properties, including high absorbency of biological fluids, biocompatibility, biodegradability, stimuli-responsiveness, high storage capacity and release ability of small and large therapeutic molecules.[1–3] Their tuneable network density allows engineering their mechanical properties to get an optimal balance among softness, conformability, strength, swelling degree, permeability and barrier properties.

The hydrogels designed for wound dressing may accomplish several functions, playing an important role in the healing processes. They can absorb and retain the wound exudates, stimulating fibroblast proliferation and keratinocyte migration and promoting re-epithelialization.[4,5] They can protect the wound bed from contaminations and infection, by preventing microorganisms as bacteria to reach the damaged area, and from impact and abrasion by being resilient and compliant. They can incorporate, protect and release antibiotics or growth factors to the wound in a controlled fashion.[6]

As mentioned in Chapter 1 and 2, materials traditionally used to make hydrogels for wound dressing are both synthetic polymers (i.e. such as poly(methacrylates), poly(vinlypyrrolidone), poly(vinyl alcohol), natural (i.e. alginate or gelatin collagen, hyaluronic acid and chitosan)[2,7] or a combination of both.[8]

The main component of the formulations here presented is xyloglucan (XG) due to the combination of several favourable properties that have been introduced in Chapter 3, section 3.2, including abundancy, low cost, biocompatibility, drug loading capacity etc. XG has been also demonstrated to have also intrinsic anti-inflammatory properties and exerts a synergic effect in combination with other anti-inflammatory agents,

especially when used for topical administration to the skin or the buccal mucosa [9]. In wound healing applications, tamarind seed XG extracts, that contain about 65% of xyloglucan, have shown to promote skin regeneration favouring the processes of re-epithelialization and remodelling.[10,11]

Likewise for many other polysaccharides, pure XG films have poor mechanical properties in terms of tensile strength and toughness. The addition of plasticizers to polysaccharides, such as glycerol (GL) or polyethylene glycerol, is a way to overcome these limitations.[12,13] As mentioned in Chapter 1, improvements in mechanical properties can be achieved by blending polysaccharides with synthetic polymers.
To the best of my knowledge, there are no previous reports on XG-based wound dressings.
In this work, the influence of PVA, chemical crosslinking induced by glutaraldehyde, and glycerol content on the XG-based hydrogel film molecular structure were investigated by rheological and thermal analyses. The changes in hydrogel morphology, water retention and swelling behaviour in water and physiologic buffer were also studied. The aim of the present work was the elucidation of the network architecture and the specific role of the various components, that is key to further optimization of their applications, in particular the incorporation of Radio Frequency Identification (RFID) antennas to transform them in epidermal sensors able to gather and remotely transmit information on the conditions of human skin. Biological *in vitro* tests were also carried out to assess the cytotoxicity of the films and the eventually released components or degradation products. Furthermore, a study on the hemocompatibility of the obtained films was also carried out.

4.2. Materials and methods

4.2.1. Materials

Xyloglucan (XG) was kindly provided by DSP Goyko Food and Chemical Co. (Japan). Poly(vinylalcohol) (PVA, MW=16kDa, 98% degree of deacetylation), aqueous glutaraldehyde at 25% (GA, containing 3%w monomer, 22%w hemiacetal

and oligomers), glycerol (GL), HCl (1M), NaOH (1M), NaCl, KH_2PO_4, anhydrous Na_2HPO_4, were all purchased from Sigma-Aldrich. All the reagents used in this work were employed as received.

4.2.2. Methods

Preparation of the hydrogel films

Precursors solution of XG and PVA were prepared at 4 %wt and 2 %wt, respectively and their preparation is described in Appendix A.1.1. Films based on XG or on XG/PVA (50% v/v) with glycerol were prepared by mixing the various components for 30 min and casting weighed amounts of the resulting solution into a glass petri dish to air-dry. Chemically crosslinked films were prepared from either XG or XG/PVA aqueous solutions by mixing with GA for 1 hour at room temperature and in acidic environment. Then, pH was neutralized, glycerol added and the solution casted in a petri dish. The two amounts of glycerol in the mixture are denoted with GL05 (the lower) and GL1 (the higher). Compositions of the casted solutions are reported in Tab. 4.1.

The amount of residual water (H_2O-i) was determined by weighing the samples after air drying. The thicknesses of the obtained films were in the range of 35-50 µm. The amount of unreacted GA was estimated by UV-Vis spectroscopy and resulted under 1% with respect to the initial amount of GA (details in Appendix A.2.1).

Tab. 4.1 Composition of solutions for casting

Solutions	XG (%wt)	PVA (%wt)	GA_{tot} (%wt)	GL (%wt)
XG(GL05)_sol	2.8	-	-	5.9
XG(GL1)_sol	2.6	-	-	11.1
XG-PVA(GL05)_sol	1.8	0.95	-	5.9
XG-PVA(GL1)_sol	1.7	0.88	-	11.1
XG(GL05)_CX_sol	2.4	-	3.3	4.9
XG(GL1)_CX_sol	2.2	-	3.1	9.4
XG-PVA(GL05)_CX_sol	1.6	0.79	3.3	4.9
XG-PVA(GL1)_CX_sol	1.5	0.75	3.1	9.4

Gel fraction

Pre-conditioned specimens of the various films (equilibrated at room temperature and RH 50%) were placed inside small filter-paper bags, soaked in MilliQ water for 48 hours at 70°C in order to remove the soluble fractions and dried in a thermo-ventilated oven at 40°C to a constant weight. The gel fraction (GF, %) was calculated as:

$$GF = W_f/(W_i - W_{GL}) \text{ x } 100$$

Where, W_i and W_f are the initial and the final weight of the specimen after extraction and air drying, respectively.

Water retention and swelling degree

The ability of films to absorb water from air was studied at 22 °C and 11, 50 and 75% relative humidity (RH), and at 37 °C for 50 % RH. Samples were weighed at several time intervals until a constant weight was reached. The moisture uptake (MU, %) was calculated as:

$$MU = \frac{W_f - (W_i - W_{water-i})}{Wf} \; x \; 100$$

Where, W_f is the final weight of the film and $W_i - W_{\text{water}-i}$ is the weight of all components of the films except water.

The swelling ability of the chemically crosslinked films was evaluated by immersing them in either MilliQ water or isotonic PBS at pH 7.4. Samples were weighed at predetermined time intervals, after the excess of water was removed by placing them on a filter paper.

The swelling degree (SD %) was calculated as:

$$\text{SD \%} = \frac{(W_s - W_i)}{W_i} \; x \; 100$$

Where, W_s corresponds to the weight of the swollen sample and W_i represents the initial weight.

Rheology

Shear viscosity and dynamic-mechanical measurements were performed on XG, PVA, XG/PVA and XG/PVA plus glycerol solutions using a stress-controlled Rheometer AR G2 (TA Instruments) with an acrylic cone-plate geometry at 25 ± 0.1 °C. Flow curves were collected by imposing logarithmic ramps in the 0.1-10000 sec^{-1} range of shear rate. Dynamic-mechanical measurements were performed on films precursor solutions with the same geometry and temperature conditions. Dynamic-mechanical spectra were recorded in the frequency range 0.01-100 Hz at 0.01 strain. Films were also subjected to frequency sweep tests, both "as prepared" and "swollen" (crosslinked films, only). Acrylic parallel plate geometry (diameter 2 cm) was employed and the gap was set at about 35-50 μm and 700 μm. for dry and swollen films, respectively.

Thermal Gravimetric Analysis

Thermal-gravimetric analysis (TGA) was conducted with a Setaram, Labsysevo, TGDTA/DSC. Samples were pre-conditioned at 20°C and 11% RH, and tested in a temperature range of 20−500 °C at a heating rate of 10 °C/min.

FTIR analysis

FTIR analysis was performed using a Fourier Transform Infrared Spectrometer (FTIR) (Spectrum Two, Perkin Elmer). Before the analysis, samples were washed with MilliQ water, lyophilised in the presence of KBr and then compressed into tablets. Spectra were collected by accumulation of 32 scans between 4000 and 450 cm^{-1}, with a resolution of 4 cm^{-1}.

Scanning Electron Microscopy (SEM)

Surface morphology was imaged by a Field Emission Scanning Electron Microscope (FESEM-JEOL) at an accelerating voltage of 10 kV. Samples were previously swollen in MilliQ water, frozen in liquid nitrogen and freeze-dried. Freeze-dried samples were cut to expose their inner structure, mounted on SEM aluminum stubs by means of a graphite adhesive layer and coated with a gold layer by JFC-1300 gold coater (JEOL) for 90 s at 30 mA before scanning.

Biological evaluations

Cell culture

For this work, A549 epithelial cells were used and the cell culture conditions are described in Appendix A3.1.

Determination of cell viability

For cytocompatibility experiments (MTS assay) 4 (8 mm^2) and 8 (16 mm^2) mg of XG-PVA and XG were layered on a A549 epithelial cells monolayer ($6x10^4$ per well) in a 96-well flat-bottom plate and incubated for 24 hours. For the release test, XG-PVA and XG films were incubated with cell culture medium at different times at 37°C.

After this incubation, the medium was collected and administered to a A549 epithelial cell monolayers at 37°C for 24 hours.

Cell viability was measured by MTS assay. After treatment, 20µL of the MTS solution was added to each well, and the incubation was continued for 1 h at 37°C in humidified incubator with 5% CO_2. Treated and untreated cultured cells were morphologically analyzed by microscopic inspection. More details are discussed in Appendix A.3.2.

Blood compatibility and immune response assays

A volume of 3 ml of blood from human volunteer donors were drawn directly into K2-EDTA-coated Vacutainer tubes to prevent coagulation, and incubated with XG and XG-PVA hydrogel (1 cm^2) for 3 hours and mixed by gentle manual inversion. An aliquot of the blood was utilized for cell count and another aliquot for thrombolytic and hemolytic assays. Total White Blood Cells (WBC) number and composition, Red Blood Cells (RBC) number and parameters, hemoglobin concentration (Hgb) Mean Corpuscular Volume(MCV), Mean Corpuscular Hemoglobin (MCH), Mean Corpuscular Hemoglobin Concentration (MCHC), Red Cell Distribution Width (RDW), platelet number and parameters mean platelet volume (MPV) and distribution with (PDW) and plateletcrit (PCT), were measured by a Beckman Z1 Coulter Particle Counter. For thrombolytic assays the blood was centrifuged at 4000 rpm for 5 min and the plasma collected and analyzed for: prothrombin time (PT) assay, expressed as international normalized ratio (INR); activated partial thromboplastin time assay (aPTT); fibrinogen concentration and antithrombin III assay by using the ACL Laboratory Instrumentation. For hemolysis assays, the blood was centrifuged at 500 *g* for 5 min, and hematocrit and plasma levels were marked on the tube. The plasma was eliminated and the hematocrit tube was filled with 150 mM NaCl solution to the level of a reference mark on the capillary tube and gently inverted a few times and centrifuged at 500 g for 5 min. After centrifugation the supernatant was removed and replaced with PBS at pH 7.4. Then, erythrocytes (1ml) were dilute 1:50 in PBS and

200 µl dispensed into a 96-well plate. Thereafter, XG-PVA and XG or 10 µl of 20 % Triton X-100, as positive control, were added to each well. The plate was incubated at 37 °C for 1 h. The RBCs were visualized at microscopy (Axio Scope 2 microscope; Zeiss) to ascertain their integrity. Successively, the plate was centrifuged at 500g for 5 min and the pellet, containing erythrocytes was eliminated and 100 µl of the supernatant transferred into a 96-well plate. The absorbance was measured with a plate reader (Wallack Instrument, wavelength 490 nm). All the experimental data were normalized with this mean absorbance value, which represents 100 % hemolysis (Triton). Moreover, we analyzed C3 and C4 to detect activation of the complement system, in the plasma, by an enzyme-linked immunosorbent assay (ELISA, Abcam)

4.3. Results and discussions

4.3.1. Preparation of XG-based hydrogel films and physico-chemical characterizations

Optical transparency for wound bed inspection and flexibility are important features of a hydrogel wound dressings. Therefore, a preliminary evaluation of various formulations and preparation conditions was focused on a visual assessment of the optical transparency and homogeneity of the produced films, and by testing their ability to withstand folding.

In this work, two type of films were produced: physical or chemical crosslinked hydrogel films. The first type relies only on physical interactions among the components to yield a network; the second type (CX-type) is obtained from the same polymer solutions with addition of GA as chemical crosslinking agent.

All the investigated formulations are reported in Tab. 4.2 and in particular they refer to four physical and four chemical hydrogels films either with XG or with XG/PVA and with two different amounts of glycerol.

Tab. 4.2 Composition of air-dried films

Films	XG (%wt)	PVA (%wt)	GA_{tot} (%wt)	GL (%wt)	H_2O-*i* (%wt)
XG(GL05)	25.8 ±0.1	0	0	53.0 ± 0.1	21.2 ± 1.0
XG(GL1)	15.38 ±0.2	0	0	62.6 ± 0.2	21.9 ± 1.5
XG-PVA(GL05)	16.75 ± 0.1	8.2 ± 0.1	0	55.3 ± 0.1	19.6 ± 0.2
XG-PVA(GL1)	10.3 ±0.1	5.3 ± 0.1	0	61.7 ± 0.2	22.5 ± 0.5
XG(GL05)_CX	20.15 ± 1.8	0	29.0 ± 1.3	40.9 ±1.5	9.9 ± 4.7
XG(GL1)_CX	13.8 ±0.8	0	18.8 ± 1.1	55.1 ± 2.7	11.2 ± 4.7
XG-PVA(GL05)_CX	13.07 ±0.3	6.8 ± 0.2	28.8 ± 0.7	40.7 ± 0.9	10.6 ± 2.1
XG-PVA(GL1)_CX	8.5 ±0.2	4.4 ±0.1	18.7 ± 0.5	52.9 ± 1.0	15.4 ± 1.9

The aqueous solutions of XG, PVA, their mixtures before and after addition of glycerol are optically clear and transparent. Upon casting and air-drying, XG films are still perfectly transparent (Fig. 4.1a) while XG/PVA films look homogeneous but slightly opaque (Fig. 4.1a). All these films are easy to handle, thanks to the glycerol in the formulation, and their flexibility and conformability increase at increasing glycerol content (Fig. 4.1b-c).

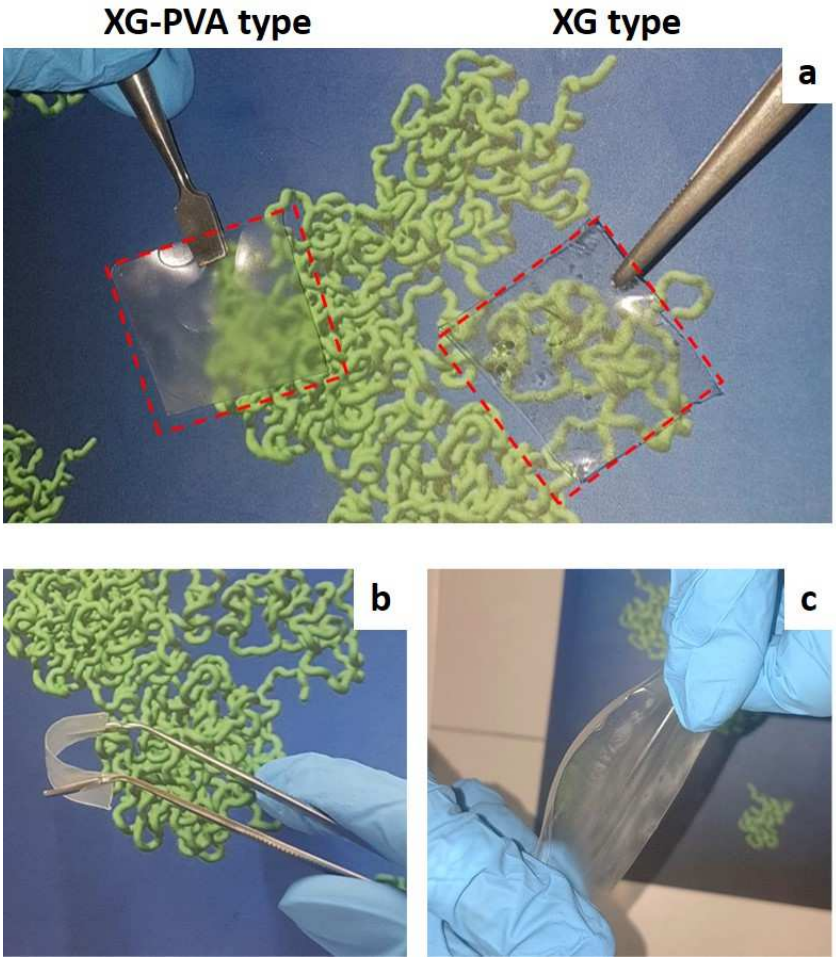

Fig. 4.1 Digital photographs of XG-PVA type and XG type hydrogel films (a) and of XG-PVA type hydrogel films folded (c) and stretched (c)

The glutaraldehyde-induced crosslinking reaction parameters, and more specifically (i) reaction time before addition of sodium hydroxide, (ii) GA content, (iii) modality of addition of GA, and (iv) the reaction temperature, were selected by visual inspection of the mixtures and obtained films. The screening of different reaction times showed that all systems that were kept reacting for longer than one hour before

casting formed white and dense granules dispersed into a viscous matrix, while mixtures that were basified after 1h of reaction resulted transparent and homogeneous. No benefits were obtained by increasing the reaction temperature above room temperature or by increasing the GA content, conditions that actually exacerbated the heterogeneity of the formed films. Indeed, prolonging the reaction time (before addition of sodium hydroxide and then glycerol), as well as increasing the reaction temperature or the concentration of crosslinking agent lead to the formation of densely crosslinked domains that may undergo phase-separation. The optimal temperature for the drying process was also investigated. While air-drying at room temperature leads to flexible films, drying at temperatures above 60 °C produces very brittle films. Non-crosslinked films are completely dissolved in water within two hours, while CX-type films have gel fractions in the 93- 96 % range, confirming that a permanent network is formed.

New chemical bond formation was investigated through FTIR analysis on the blend of PVA and XG as well as on the GA crosslinked films, after extraction of glycerol and other soluble fractions. Spectrum of XG-PVA blend obtained by drying the aqueous solution of the two polymers present in the same weight ratio as in the film, does not show any evidence of interaction between the two chemical species, resulting the mere superimposition of the spectra of the two individual components (Fig. 4.2).

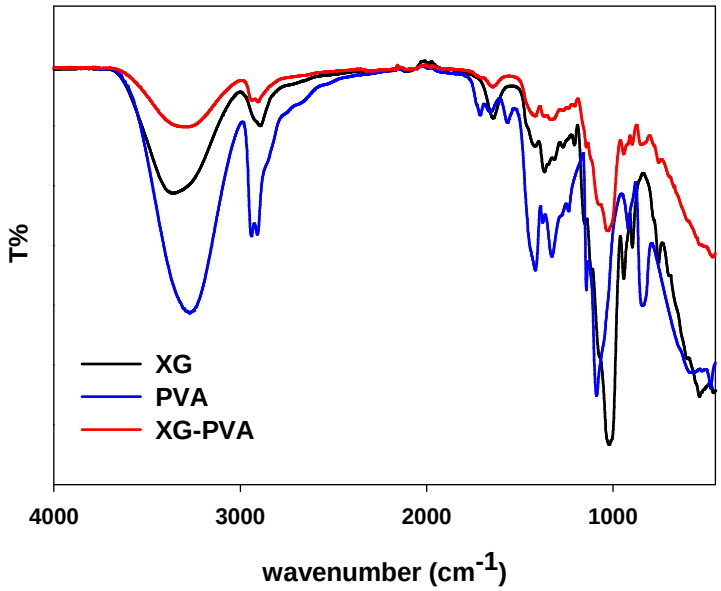

Fig. 4.2 FTIR spectra of XG, PVA and XG/PVA (50 %v/v) upon casting and air drying

Spectra of CX-type films containing only XG as polymeric component do not show significant differences with respect to pure XG spectrum (see Fig. 4.3a-b), except for the appearance of a peak at 1720 cm^{-1}, shown as a peak for XG(GL05)_CX and as a shoulder of the band at 1650 cm-1 for XG(GL1)_CX.

In the formulations containing PVA the new band at 1720 cm^{-1} is also present and increases in intensity for the lower glycerol content (Fig. 4.3c-d).

This peak can be assigned to the carbonyl group of glutaraldehyde grafted to the network and it becomes only a shoulder or disappear in systems with the higher glycerol content, probably because in this system the grafted GA can be more favourably end-capped by glycerol.

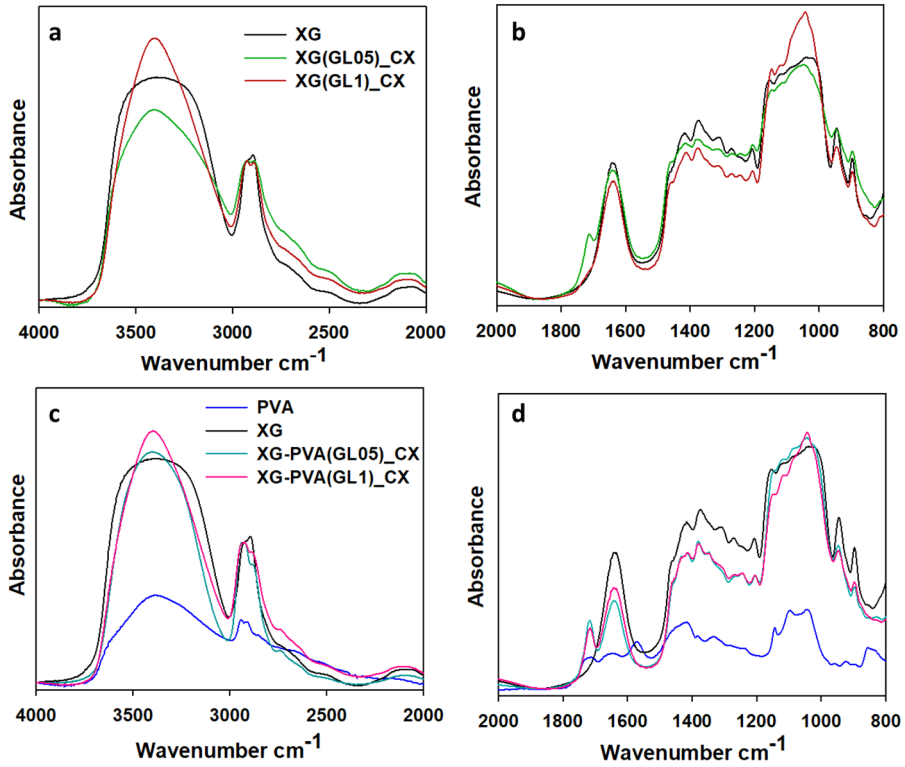

Fig. 4.3 FTIR spectra of crosslinked films; comparison between (a) XG-based chemically crosslinked gel with two glycerol contents (XG powder, as reference) from 4000 to 2000 cm^{-1} and from 2000 to 800 cm^{-1} and (b) XG-PVA based chemically crosslinked gels with two glycerol contents (XG and PVA powders, as reference) from 4000 to 2000 cm^{-1} (c) and from 2000 to 800 cm^{-1} (d)

These results suggest that GA can bind not only two XG chains (XG-GA-XG) or XG to PVA (XG-GA-PVA) by formation of hemiacetals and acetals, but also it could be simply grafted to XG (XG-GA) or to PVA (PVA-GA) and can also be end-capped by glycerol that is added after neutralization of the reaction mixture while the system is progressively concentrating due to water evaporation (XG-GA-GL). The possible reactions and the structures of the forming products are shown in Fig. 4.4.

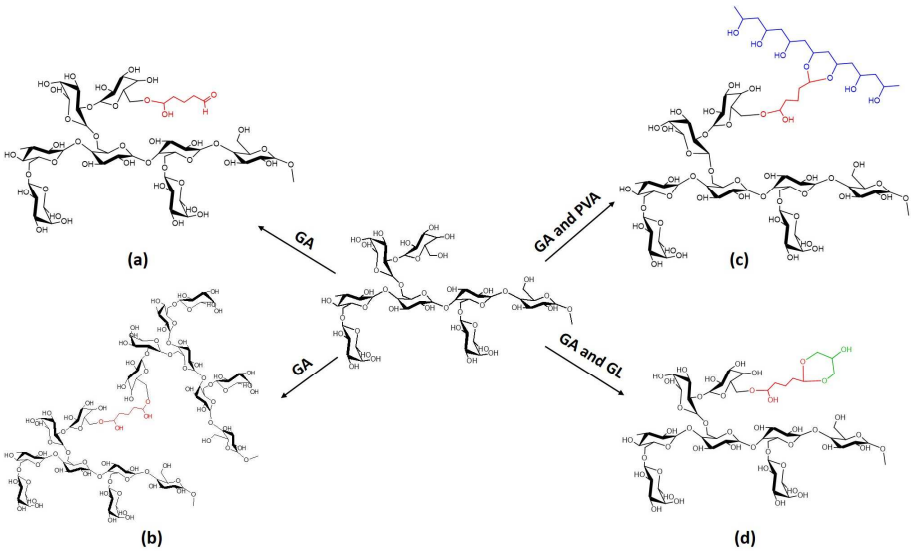

Fig. 4.4 Possible reaction products of xyloglucan (XG) with glutaraldehyde (GA), glycerol (GL) and poly(vinyl alcohol) (PVA): (a) GA-mediated XG crosslinking; (b) GA-mediated crosslinking between XG and PVA; (c) grafting GA to XG; (d) grafting of GA end capped GL to XG

The shear viscosity as a function of shear rate for the 1.8 %w XG solution and for the system obtained by mixing XG and PVA polymeric solutions and adding the same amount of glycerol used to prepare the XG-PVA(GL1) film is reported in Fig. 4.5. For the three systems, the flow curves are dominated by the characteristic shear thinning behavior of XG.[14–16] The presence of PVA does not change the viscosity while the presence of both PVA and glycerol causes only a slight reduction of viscosity.

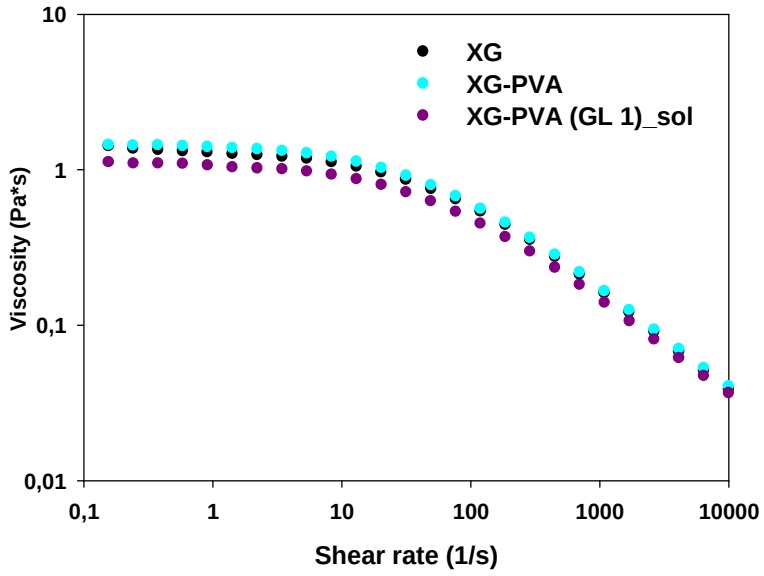

Fig. 4.5 Rotational shear viscosity of XG at 1.8 %w and XG-PVA aqueous solutions with the addition of glycerol XG-PVA(GL1)_sol

Aqueous XG or XG-PVA solutions before and after addition of GA and also after the addition of glycerol have been subjected to dynamic mechanical rheological analysis in frequency sweep mode (Fig. 4.6a-b). All the systems behave as viscoelastic liquid systems, showing the loss modulus, G" higher than the storage modulus, G', in the investigated frequency range, with the latter increase steeper than the former at the increase of frequency. Samples before and after the addition of glycerol do not show any significant difference. The crossover point between G' and G'' moves towards lower frequencies when GA is present in the blend. Finally, the addition of PVA lowers both G' and G'' values.

Dynamic mechanical spectra of physical and chemical films are reported in Fig. 4.6c and Fig. 4.6d, respectively. XG(GL05) shows the typical rheological behaviour of a weak gel; storage modulus is higher than loss modulus and almost invariant with frequency, while loss modulus increases with frequency. These results confirm the

ability of XG to form physical gels in the presence of glycerol.[12,17] The increase of the amount of glycerol has no effect on both storage and loss modulus. The addition of PVA (see XG-PVA(GL05) system) has no significant effect on both storage and loss modulus. This could be due to the relatively low molecular weight PVA that does not contribute to the physical gelation of the bulky XG chains, but actually favours XG chains slippage.[18]

The combined presence of PVA and a higher amount of glycerol (XG-PVA(GL1) system) causes a significant reduction of both G' and G", probably increasing further the distance among the polymer molecules and reducing their packing order.[18]

The influence of the chemical crosslinking on the mechanical spectra of the films is reported in Fig. 4.6d. With reference to the XG(GL05) sample, the presence of the crosslinker on the XG film casted with the lower amount of glycerol (XG(GL05)_CX) causes (i) a significant increase of both G' and G" and (ii) the invariance of G" with frequency, which is the typical behaviour of a strong (covalent) gel. Increasing the amount of added glycerol (see XG(GL1)_CX) results in a marked decrease of G' and a less pronounced decrease of G". Considering that the impact of glycerol in the G' and G" curves for the physical hydrogel films was much less significant, we can argue that glycerol interferes with the GA-mediated chemical crosslinking of xyloglucan, as suggested in the scheme in Fig. 4.3.

The effect of the presence of PVA on the chemically crosslinked films is also investigated. The presence of PVA in CX-type systems (XG-PVA(GL05)_CX system produces a significant decrease of storage modulus and a less marked decrease of loss modulus. This effect is similar to the effect of higher glycerol content in XG_CX films. Increasing glycerol content in XG-PVA CX-type films causes a further decrease of G".

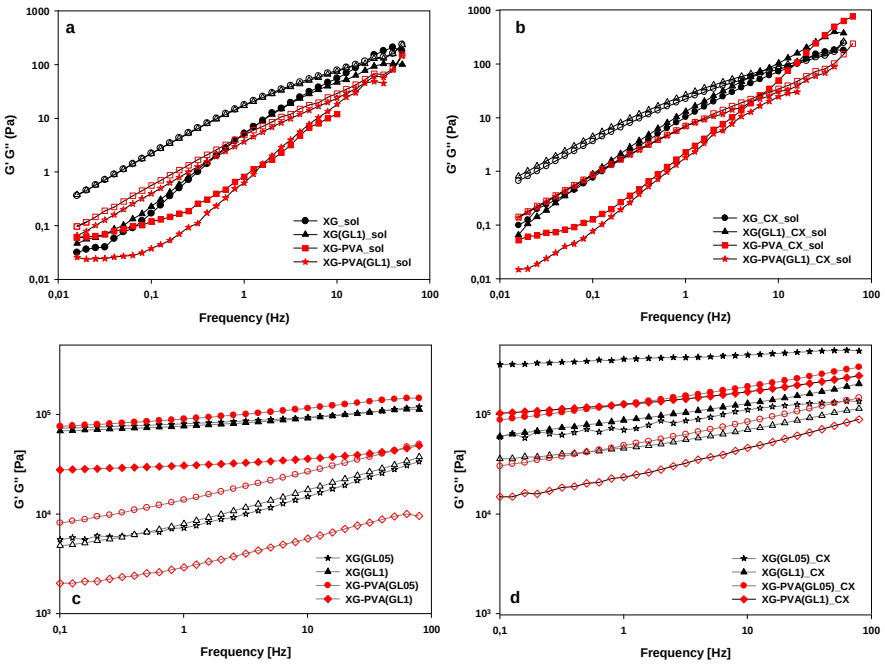

Fig. 4.6 Dynamic mechanical analysis in frequency sweep mode of precursor solutions and films. Solid symbols: storage modulus; open symbols: loss modulus. (a) Aqueous XG and XG/PVA before (XG_sol and XG-PVA_sol) and after addition of glycerol (XG(GL1)_sol and XG-PVA(GL1)_sol). (b) Precursor aqueous solutions of the chemical films obtained by addition of glutaraldehyde in the same samples illustrated in panel (a). (c) Comparison among the various physical hydrogels. (d) Chemically crosslinked films

Thermal analysis of physical and chemical films can be used to understand the interactions among the components of the formulation and the effect of crosslinking treatment.

Results of TGA analysis are reported in Fig. 4.7a-f. All systems show an initial mass loss in a range between 75°C and 120°C associated to the evaporation of the “residual water” and a more pronounced mass loss with multiple flexes at higher temperature (280°C-370°C), due to the thermal degradation of the various components present in the formulations. Glycerol and PVA do not leave any residual mass at 500°C [19],

therefore the residual masses in the various systems are strongly affected by the different content of XG and moisture content initially present in the system. A more detailed analysis of the curves reveals that xyloglucan (see Figure 4.7a) is fairly hydroscopic (water loss at about 75°C) and characterized by good thermal stability, with an onset of degradation at about 314°C and 38 %wt residual mass at 500°C. This exceptional high thermal stability could be attributable to its characteristic "hyper-entangled" supramolecular structure, which is responsible for its relatively high stiffness and high local packing density in the solid state.[20,21]

PVA (see Fig. 4.7b) shows the characteristic two-stage thermal degradation behavior with characteristic peaks at 300 °C and 440°C and the release of moisture occurs at higher temperature if compared with XG.[22]

In TGA curves of physical hydrogel films containing only XG as polymeric component (Fig. 4.7c), the temperature of the loss of water increases with respect to the pure polysaccharide, shifting from 75°C in pure XG to 105 °C and 115°C for XG(GL05) and XG(GL1).

This change suggests that the residual water shift from "free water" in XG powder to mainly "bound water" in the physical gels where also glycerol is present. This behavior supports the interpretation of XG gelation as the result of a localized increase of polymer concentration leading to association due to water sequestration by the alcohol. The films also show a second flex associated to glycerol vaporization and simultaneous thermal degradation (DTG peaks at 277 °C and at 288 °C for XG(GL05) and XG(GL1), respectively)[23], and a third flex due to the XG thermal degradation. XG decomposition is slightly shifted to higher temperature at 318°C and 320°C for XG(GL05) and XG(GL1), respectively, as a consequence of physical crosslinking.

The addition of GA to XG (Fig. 4.7e) induces profound modifications to the thermal degradation of the films. The two flexes associated to glycerol evaporation and xyloglucan degradation are much closer to each other (the glycerol evaporation is now detectable as a shoulder of the main peak of XG thermal decomposition in DTG curves) and significantly shifted to higher temperatures (295°C and 357°C for

glycerol and XG, respectively). This further supports the hypothesis that glycerol is partly grafted to the chemical network that binds also, as proposed in Fig. 4.3.

PVA has not significant influence either on glycerol or XG thermal degradation in both physical (Fig. 4.7d) and chemical gels (Fig. 4.7f). Only an evident increase of the water evaporation temperature due to the combined effect of crosslinking and presence of PVA (130-140°C) in GA-crosslinked films can be highlighted.

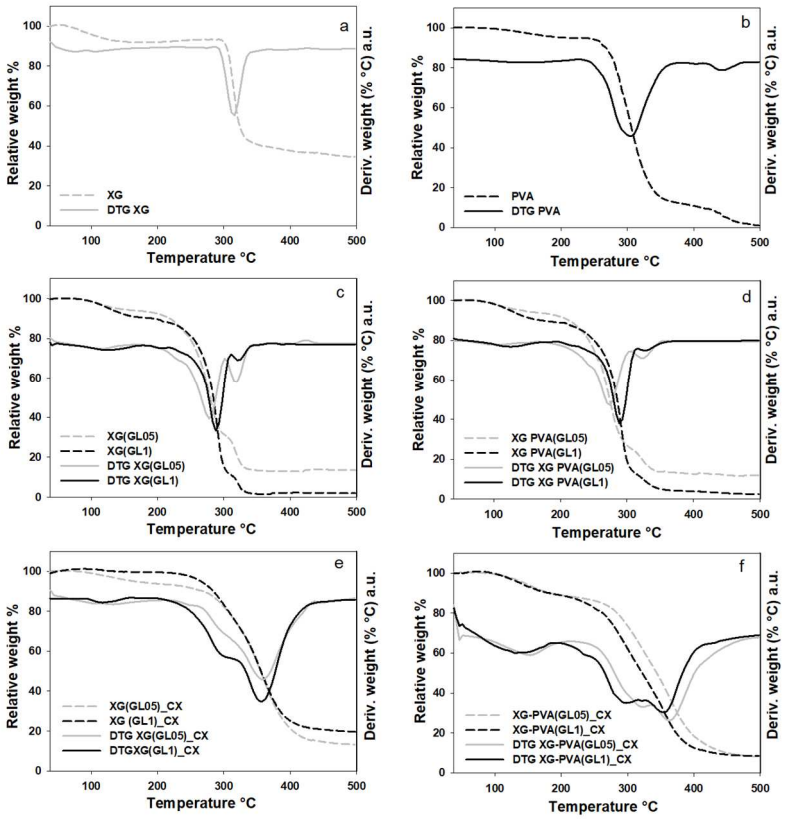

Fig. 4.7 Thermogravimetric analysis of air-dried films and the polymer powders. (a) XG-based physical and chemically crosslinked gels (XG powder, as reference). (b) comparison between the XG-based physical gel (XG(GL05)) and XG-PVA based physical gels with two glycerol contents (XG and PVA powders, as reference). (c) comparison between chemically crosslinked gels

SEM analysis on the fracture surfaces was performed in order to characterize the morphology of the films. Water-swollen chemically crosslinked gels, after extraction of glycerol and other soluble fractions, quenching with liquid nitrogen and freeze-drying have been analyzed and their representative micrographs are reported in Fig. 4.8.

XG-based films show a different morphology depending on the amount of GL. XG-based film with a lower content of glycerol (Fig. 4.8a) show a layered morphology with regularly stacked thin sheets connected by transverse walls, while the one with higher glycerol content results into a denser structure, made by closer sheets connected by thin filaments (Fig. 4.8b).

Interestingly, a similar lamellar morphology was observed for physical gels produced with a temperature-responsive, partially degalactosylated XG (Deg-XG). [24] This suggests that the obtained morphology is essentially governed by the xyloglucan self-assembly. For the aqueous solutions of Deg-XG the auto-organisation in lamellae is promoted by an increase of temperature that worsens the quality of the solvent and favors hydrophobic interactions. In the present contest, the role of temperature is played by glycerol, which competes with XG for the hydration water. The formed microstructure is then fixed by the chemical crosslinks promoted by GA.

The presence of PVA interferes with XG chain alignment yielding to a morphology with interconnected porosity. This porous microstructure has an average pore size of about 10 μm for the lower glycerol content (Fig. 4.8c), that increases to about 25 μm for the higher glycerol content (Fig. 4.8d).

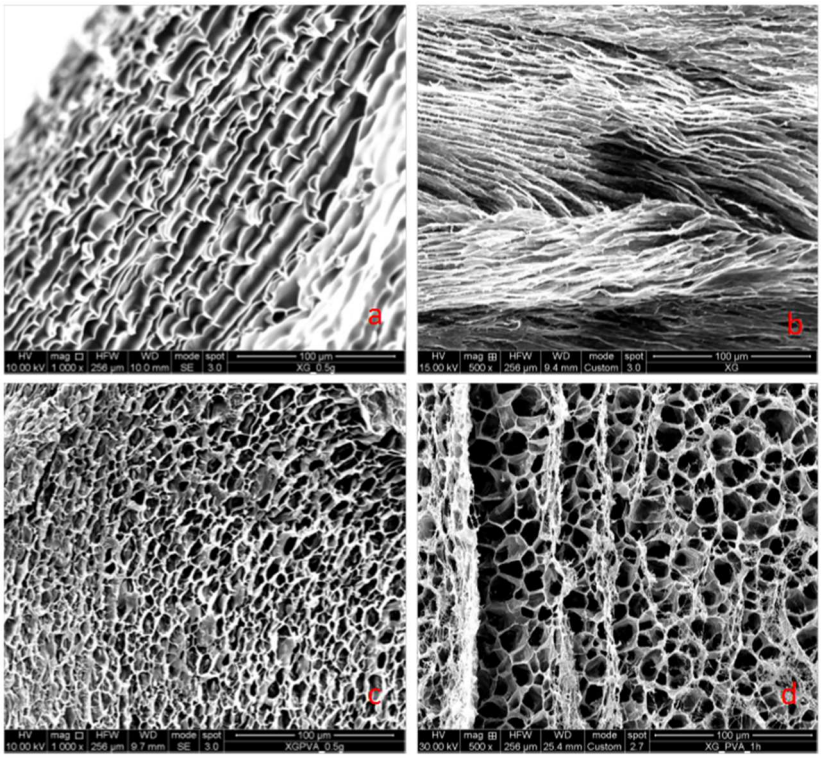

Fig. 4.8 Morphological characterization of (a) XG(GL05)_CX; (b) XG(GL1)_CX; (c) XG-PVA(GL05)_CX and (d) XG-PVA(GL1)_CX after equilibrium swelling, quenching and freeze-drying

In the perspective of the integration of those films in a device for the development of smart plasters for wound healing, their ability to retain moisture was investigated.

Results of the moisture retention in the various films, "as prepared" and after treatments at different temperatures and relative humidity % (RH%), are shown in Fig. 4.9.

First of all, it is important to notice that the initial moisture content of the "as prepared" chemical films is higher (ca. 20%w) than in the physical gel (ca. 10%w) (see also Tab. 4.2).

Furthermore, in systems containing PVA, the higher amount of glycerol results in slightly higher moisture retention than the corresponding formulations with lower

glycerol content. On the other hand, XG based films both with high and with low glycerol content, do not show significant differences. The incubation at 37°C for 2h and 50% RH, causes in all systems the loss of most of the water, leveling to a residual moisture content to 5 %wt, except for the two chemically crosslinked XG-PVA systems which almost completely dry out.

Upon incubation at room temperature (about 22°C) and 50% RH, all films progressively absorb humidity from the environment, reaching equilibrium in 24 h.

Thereafter, relative humidity of the environment was increased up to 75% leading to a significant further increase of the absorbed water that levels off in 24 h. One week cycles of moisture absorption (75% RH 22°C) and desorption (37°C RH 50%) were carried out for three months and beyond, showing no modification of the equilibrium water content in both conditions.

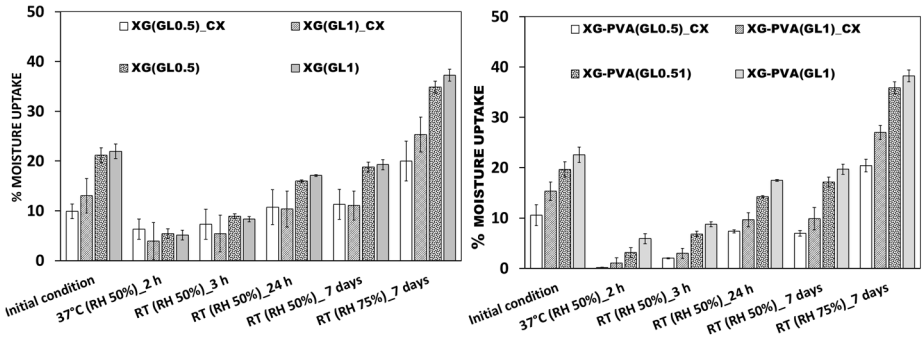

Fig. 4.9 Moisture uptake percentage as a function of the incubation time and relative humidity

The swelling behaviour was investigated only on chemically crosslinked variants, since all the physical hydrogels quickly swell and soon after dissolve when immersed in water. The swelling at plateaux percentages (SD%) of the chemically crosslinked films, both in MilliQ water and isotonic PBS, are reported in Tab. 4.3 and the corresponding swelling curves are shown in Fig. 4.10. Upon immersion, all systems take up water. The films containing more glycerol show higher SD% if compared with the corresponding systems with less glycerol.

The equilibrium swelling values of films with PVA and in particular with the higher glycerol content are even higher, in good agreement with their larger interconnected porosity observed by SEM.

The effect of saline solution is not very significant on the XG-based gels and the slight decrease in SD% at the increase of ionic strength is attributable to the reduction of the osmotic pressure. An opposite effect is shown by XG-PVA based systems, which show an increase of SD% at the increase of ionic strength. This behaviour could be explained with some degree of H-bonded interpolymer association between XG and PVA, which is perturbed by the presence of phosphate anions and other multivalent ions of the buffer.[25]

Tab. 4.3 Swelling degree (SD) percentage of chemically crosslinked films

System	SD % - water	SD % - PBS
XG(GL05)_CX	109 ± 20	90 ± 2
XG(GL1)_CX	210 ± 20	210 ± 15
XG-PVA(GL05)_CX	220 ± 25	250 ± 20
XG-PVA(GL1)_CX	325 ± 20	355 ± 25

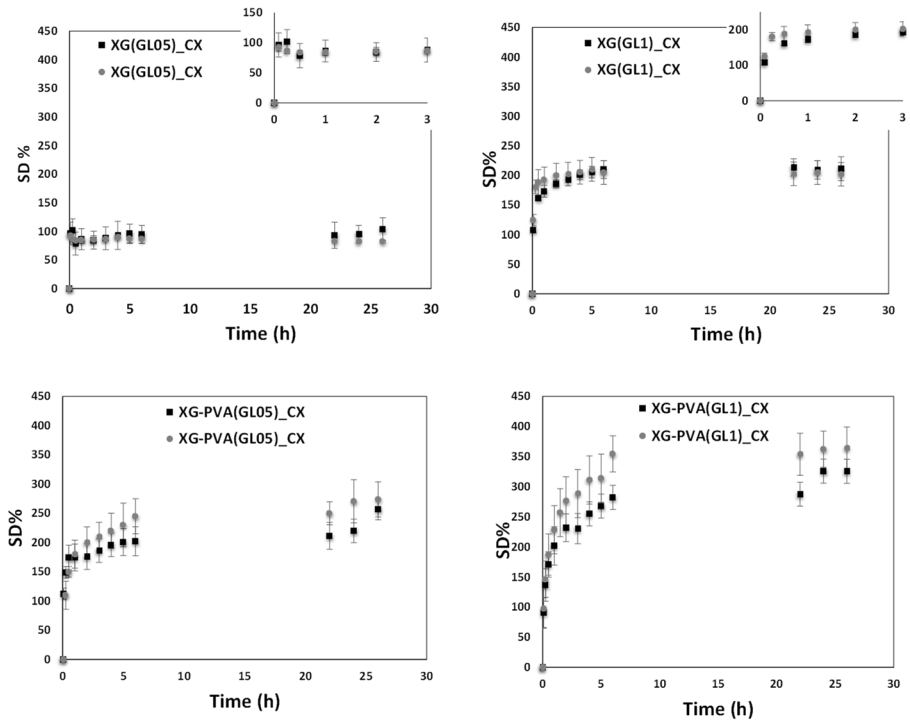

Fig. 4.10 Swelling degree in MilliQ water (black) and in PBS (grey)

The rheological behaviour of the equilibrium-swollen CX-type films was investigated and the dynamic mechanical spectra are reported in Fig. 4.11a-c. The corresponding curves of the "as prepared" films are also displayed for comparison. All the swollen systems still show the typical behaviour of chemical gels with G' curves being one order of magnitude higher than the corresponding G" curves, and invariant or slightly increasing with frequency. As expected, both G' and G" decrease for the softer swollen systems, when compared to the corresponding "as prepared "systems. The reduction of G" is more pronounced than the reduction of G', probably because water partially displaces the more viscous glycerol.

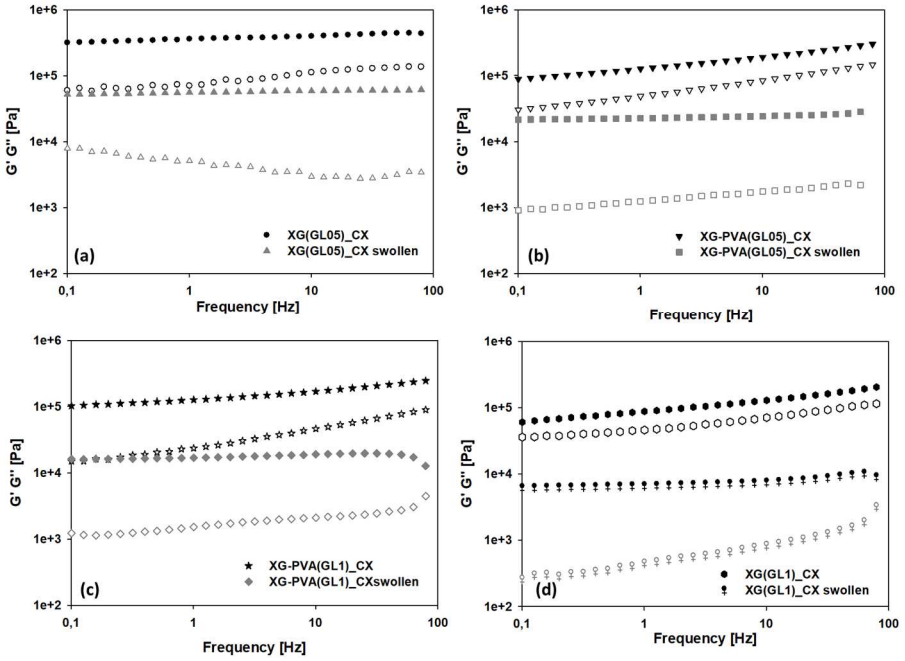

Fig. 4.11 Dynamic mechanical spectra of equilibrium-swollen CX-type films

4.3.2. Biological assessment

New biomaterials need to be firstly tested *in vitro* to evaluate their cytotoxicity. To this aim, it was performed a contact assay on four systems, namely XG(GL 1)_CX, XG-PVA(GL1)_CX, XG(GL1) and XG-PVA(GL1), selected for their superior performance in terms of flexibility and water retention ability. Samples were placed on A549 epithelial cells monolayers. After 24 hours the films were removed and the cells subjected to MTS viability assay. The obtained results are summarized in Fig. 4.12a-b. No cytotoxic behavior was detected for XG(GL1)_CX and XG-PVA(GL1)_CX films after the treatment, and the cell viability was as high as 90 %. In contrast, XG(GL1) and XG-PVA(GL1) films showed a moderate cytotoxicity (Fig. 4.12a). These results were confirmed by microscopic morphological inspection (Fig. 4.12b); cells incubated with both the CX-type films did not displayed altered

morphology compared to the control cells. In the contact area with the hydrogel and in its proximity no alteration in cellular outgrowth, extension of cellular body, morphology or proliferative behavior was observed. To test a possible toxic effect due to components that can be released by the crosslinked films during prolonged application on a wounded area, a viability assay was performed by using the cell medium in which both films were separately incubated. The medium was collected at different times, within a two-week time interval, and administered to cells. No cytotoxic behavior was detected for all the samples, the cells maintaining a viability value of about 90 % (Fig. 4.12c-e). It must be highlighted that no significant statistical difference was recorded between treated and control cells ($p \geq 0.05$), These results were confirmed by cells microscopic morphological inspection.

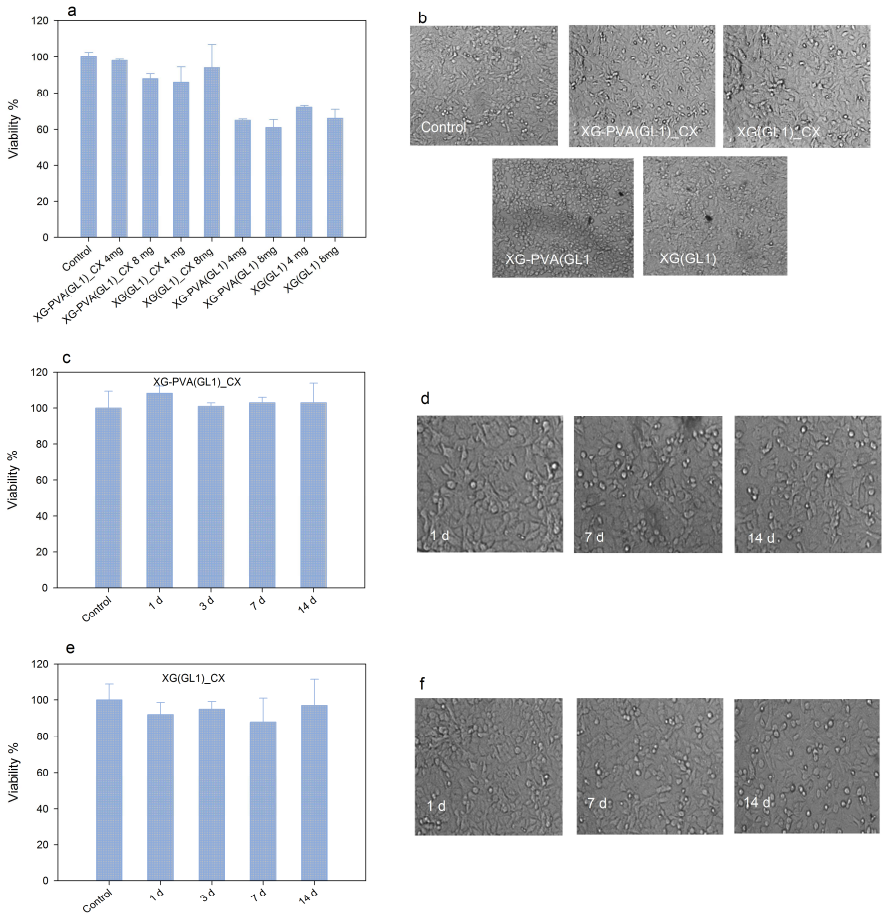

Fig. 4.12 MTS assay of A549 cells: untreated (Control), and incubated with XG(GL1)_CX, XG-PVA(GL1)_CX, XG(GL1) and XG-PVA(GL1) films at different concentrations (4 and 8 mg) for 24 h (a). Morphological images of A549 cells: untreated (Control) and incubated with the above films (b). MTS assay of A549 cells: untreated (Control) or treated with cell media in which XG(GL1)_CX and XG-PVA(GL1)_CX were immersed for different times (1, 3, 7, 14 days) (c and e); Morphological images of A549 cells treated with the cell media as described above (d and f)

On the basis of the better performance of the XG(GL1)_CX and XG-PVA(GL1)_CX films, only these two were used for further biological experiments.

The hemocompatibility test of the films is an essential step for the wound dressing manufacture. Ideally, films should neither induce hemolysis nor activate the blood defense systems, coagulation and fibrinolysis.

Hemolysis is a fundamental test to understand if the interaction of the material with erythrocytes affects the membrane integrity, leading to plasma hemoglobin release.[26] To investigate this effect of the films, they were incubated for 3 hours with blood (collected from healthy volunteers). The number of erythrocytes and their parameters were measured by a cell counter system. Results in Fig. 4.13a-b, show no significant difference with respect to the control. Moreover, hemolysis was analyzed by using a photometrical colorimetric test, which determines the amount of free hemoglobin (Hb). Results illustrated in Fig. 4.13c evidenced that the blood samples incubated with the films did not show any hemolysis if compared to the control. Triton was used as positive control. These results were confirmed by microscopic analysis of erythrocytes (Fig. 4.13d).

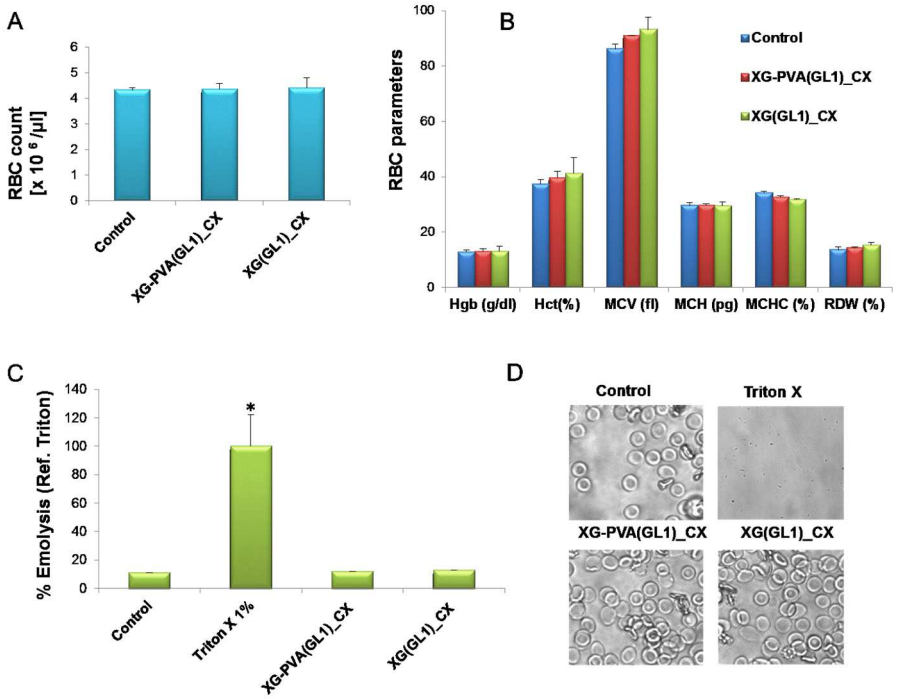

Fig. 4.13 Blood from a human volunteer donors was incubated or not (Control) with XG(GL1)_CX, XG-PVA(GL1)_CX films and the following analysis performed: Red blood cell (RBC) count (a); RBC parameters (MCV=Mean Corpuscolar Volume, MCH=Mean Corpuscolar Hemoglobin, MCHC=Mean Corpuscular Hemoglobin Concentration, RDW= Red Cell Distribution Width (b); Hemolysis assay of erythrocytes, Triton-X as positive control (c); Microscopic images of erythrocytes incubated or not (Control) with films or with Triton X. *p<0.05 vs. control (d)

Platelet activation and aggregation studies were performed to investigate the effect of the films on hemostasis, which is a multicomponent cascade that helps in maintaining the fluidity of the blood. As for hemolysis experiment, films were incubated for 3 hours with blood (collected from healthy volunteers). The platelet number and others parameters (Fig. 4.14) such as mean platelet volume (MPV), distribution width (PDW) and plateletcrit (Pct), resulted well within the normal range of the control. These results clearly demonstrated that the films did not prevent the normal platelet functions.

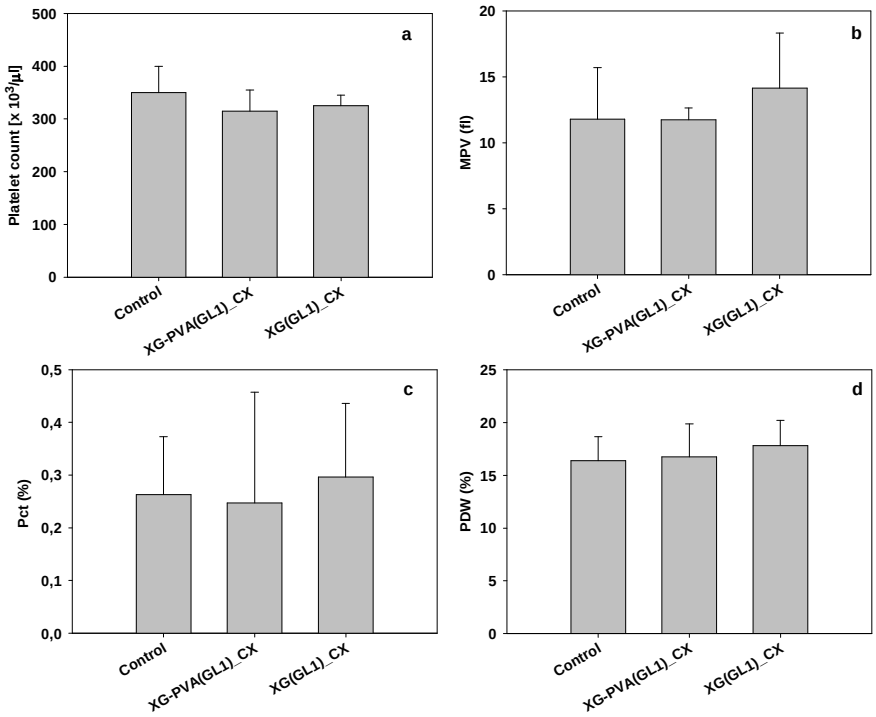

Fig. 4.14 Blood from a human volunteer donors was incubated or not (Control) with XG(GL1)_CX and XG-PVA(GL1)_CX films and the following analysis performed: platelet count (a); platelet indices including: mean platelet volume (MPV) (b), plateletcrit (Pct) (c), and distribution with (PDW) (d)

Plasma coagulation analysis is a sign of the thrombogenic potential.[27,28] The coagulation cascade includes intrinsic and extrinsic pathways leading to prothrombin activation and conversion of fibrinogen to fibrin.[27] It has been demonstrated that the interaction of biomaterials with blood, can induce in many cases negative effect on coagulation, platelet and hemostatic properties.[29,30] The effect of the films on the coagulation cascade was evaluated by the prothrombin time (PT) and activated partial thromboplastin time (aPTT) tests. PT measures the aberrations in the extrinsic pathway, aPTT is instead, a check for irregularities in the intrinsic pathway. The results (Fig. 4.15a-b) showed that both the PT and aPTT values were within the normal

range. Furthermore, to measure the occurrence of plasma coagulation, the antithrombin-III (atIII) and fibrinogen concentrations were measured and, as shown in Fig. 4.15c-d, the values of the film incubated samples were comparable to the control.

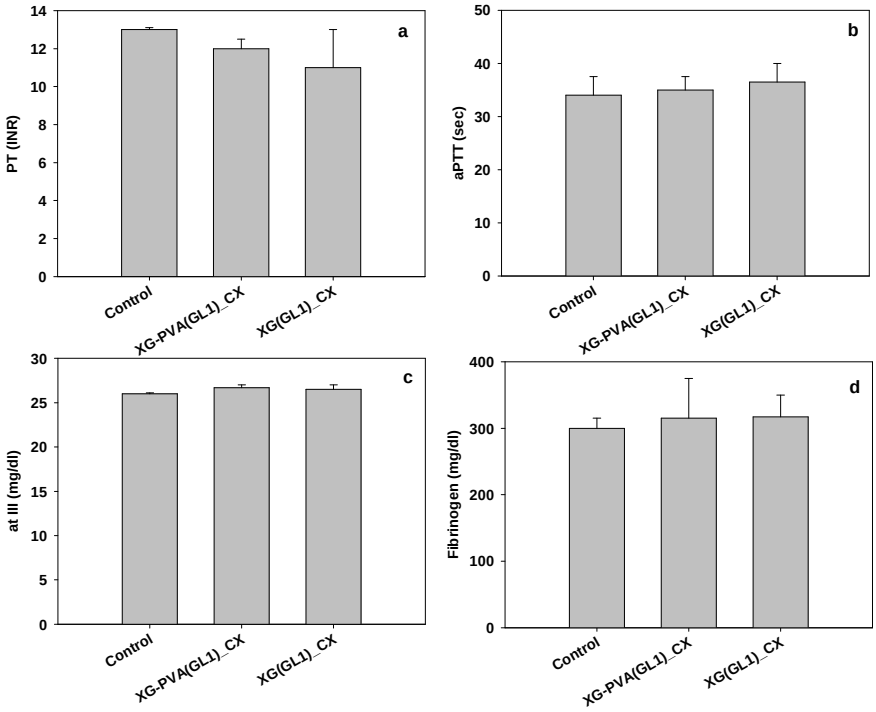

Fig. 4.15 Blood from a human volunteer donors was incubated or not (Control) with XG(GL1)_CX and XG-PVA(GL1)_CX films and the following analysis performed: Prothrombin time (PT) (a); Activated partial thromboplastin time (aPTT) (b); antithrombin-III (aTIII) (c); fibrinogen concentration (d)

Elicitation of immune response is another important parameter that has to be investigate.

For this reason, samples of XG(GL1)_CX, XG-PVA(GL1)_CX were incubated again in blood (collected from volunteers) and an *in vitro* test of the inflammatory response has been performed.[26]

Results in Fig. 4.16 show that no statistically relevant differences were revealed in the number (Fig. 4.16a), and composition of the white blood cells (WBC) (Fig. 4.16b), with respect to the control. Moreover, since contact of blood with pathological agents or foreign materials activates the complement pathway, as a body defense reaction [26], the levels of C3 and C4 were measured. No significant modifications of C3 and C4 plasma concentrations were detected in the samples incubated with XG and XG-PVA films (Fig. 4.16c-d). Thus, it may be concluded that the films are immunogenically silent because they do not cause any immune response *in vitro*.

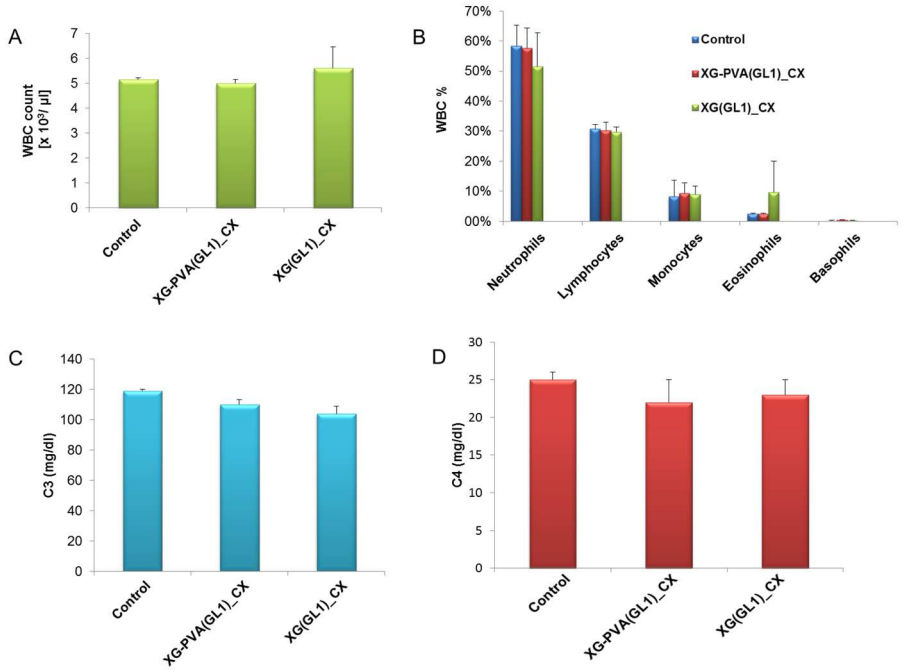

Fig. 4.16 White blood cell (WBC) count of human blood samples incubated or not (Control) with XG and XG-PVA films (a); Composition of the WBC population of human blood samples incubated or not (Control) with XG and XG-PVA films (b); C3 and C4 (c) and plasma concentrations of human blood samples incubated or not (Control) with XG and XG-PVA films (d)

4.4. Conclusions

Xyloglucan based thin hydrogel films were synthetized and fully characterized for their physico-chemical, thermal, rheological and morphological properties.

The films produced by adding glycerol to an aqueous solution of xyloglucan are physical hydrogels: gelation is relatively fast and the gel strength increases significantly upon drying. Physical films are perfectly transparent, relatively strong and resilient, but rapidly dissolve when exposed to aqueous solutions. Glutaraldehyde induces covalent crosslinking to XG chains, thus forming a permanent polymer network. Glycerol, that is required in the formulation to provide the necessary flexibility, is also partially grafted to the network through GA. In the chemically crosslinked variants, PVA can react with GA and graft to XG, modifying the lamellar structure formed by XG association into an open porous structure and increasing the network mesh size; this translates into higher swelling ratios if compared with systems with XG only and the same content of glycerol. All films can withstand repeated cycles of drying and rehydration by exposure to air at different temperature and humidity content. The chemically crosslinked films, both with and without PVA, displayed good cytocompatibility as demonstrated by *in vitro* test showing that viability is not affected by the presence of the film. It is also remarkable that no toxic components are released by the films. On other hand, the moderate cytotoxicity observed for the physical hydrogel films could be attributed to their rapid dissolution causing significant alteration of the composition of the culture medium. Furthermore, the tested chemically crosslinked films were also shown hemocompatible. These results encourage further investigations on both *in vitro* and *in vivo* biocompatibility and integration with RFID sensors, in order to transform this interesting material into a medical device for wound management (topic discussed in Chapter 7).

Contributions

The author wishes to point out the contribution of Dr. Simona Todaro for the help in the rheological measurements, Dr. Maria Antonietta Sabatino for the help in the FTIR and SEM measurements and the support in the design and interpretation of the results, and Dr. Pasquale Picone for all the biological evaluations presented in this chapter.

References

[1] E.M. Ahmed, Hydrogel: Preparation, characterization, and applications: A review, J. Adv. Res. 6 (2015) 105–121. doi:10.1016/j.jare.2013.07.006.

[2] J.S. Boateng, K.H. Matthews, H.N.E. Stevens, G.M. Eccleston, Wound Healing Dressings and Drug Delivery Systems: A Review, J. Pharm. Sci. 97 (2008) 2892–2922. doi:10.1002/jps21210.

[3] J.L. Drury, D.J. Mooney, Hydrogels for tissue engineering: Scaffold design variables and applications, Biomaterials. 24 (2003) 4337–4351. doi:10.1016/S0142-9612(03)00340-5.

[4] A. Bullock, P. Pickavance, D. Haddow, S. Rimmer, S. MacNeil, Development of a calcium-chelating hydrogel for treatment of superficial burns and scalds, Regen. Med. 5 (2010) 55–64. doi:10.2217/rme.09.67.

[5] G.D. Winter, Formation of the Scab and the Rate of Epithelization of Superficial Wounds in the Skin of the Young Domestic Pig, Nature. 193 (1962) 293–294. doi:10.1038/193293a0.

[6] E.A. Kamoun, E.R.S. Kenawy, X. Chen, A review on polymeric hydrogel membranes for wound dressing applications: PVA-based hydrogel dressings, J. Adv. Res. 8 (2017) 217–233. doi:10.1016/j.jare.2017.01.005.

[7] B. Balakrishnen, M. Mohanty, P. Umashankar, A. Jayakrishnan, Evaluation of an in situ forming hydrogel wound dressing based on oxidized alginate and gelatin, Biomaterials. 26 (2005) 6335–6342. doi:10.1016/j.biomaterials.2005.04.012.

[8] M. Hrynyk, M. Martins-green, A.E. Barron, R.J. Neufeld, Alginate-PEG Sponge Architecture and Role in the Design of Insulin Release Dressings, Biomacromolecules. (2012). doi:10.1021/bm300186k.

[9] I. Giori, A., Arpini, S., & Togni, S., Tamarind seed polysaccharide for use in the treatment of inflammatory diseases, WO2011147768 A1, 2011.

[10] M. Yusof bin Mohamad, H.B. Akram, D. Najwa Bero, M. Tariqur Rahman, Tamarind Seed Extract Enhances Epidermal Wound Healing, Int. J. Biol. 4 (2012) 81–88. doi:10.5539/ijb.v4n1p81.

[11] W. Nie, A.M. Deters, Tamarind seed xyloglucans promote proliferation and migration of human skin cells through internalization via stimulation of proproliferative signal transduction pathways, Dermatol. Res. Pract. (2013) 1–14. doi:10.1155/2013/359756.

[12] E.M. Bergstr̈m, L. Salmén, J. Kochumalayil, L. Berglund, Plasticized xyloglucan for improved toughness-Thermal and mechanical behaviour, Carbohydr. Polym. 87 (2012) 2532–2537. doi:10.1016/j.carbpol.2011.11.024.

[13] C.K. Simi, T.E. Abraham, Biodegradable biocompatible xyloglucan films for various applications, Colloid Polym. Sci. 288 (2010) 297–306. doi:10.1007/s00396-009-2151-8.

[14] A. Semenzato, A. Costantini, G. Baratto, Green Polymers in Personal Care Products: Rheological Properties of Tamarind Seed Polysaccharide, Cosmetics. 2 (2014) 1–10. doi:10.3390/cosmetics2010001.

[15] K. Khounvilay, W. Sittikijyothin, Rheological behaviour of tamarind seed gum in aqueous solutions, Food Hydrocoll. 26 (2012) 334–338. doi:10.1016/j.foodhyd.2011.03.019.

[16] R.A. De Freitas, V.C. Spier, M.R. Sierakowski, T. Nicolai, L. Benyahia, C. Chassenieux, Transient and quasi-permanent networks in xyloglucan solutions, Carbohydr. Polym. (2015) 216–223. doi:10.1016/j.carbpol.2015.04.066.

[17] Y. Yuguchi, T. Kumagai, M. Wu, T. Hirotsu, J. Hosokawa, Gelation of xyloglucan in water/alcohol systems, Cellulose. 11 (2004) 203–208. doi:10.1023/B:CELL.0000025427.60557.40.

[18] N.A. El-Gendy, Pharmaceutical Plasticizers for Drug Delivery Systems, Curr. Drug Deliv. 9 (2012) 148–163. doi:10.2174/156720112800234602.

[19] M. Mohsin, A. Hossin, Y. Haik, Thermal and Mechanical Properties of Poly (vinyl alcohol) Plasticized with Glycerol, J. Appl. Polym. Sci. 122 (2011) 3102–3109. doi:10.1002/app.

[20] S. Todaro, Xyolglucan self-assembled nanostructures and gels for biomedical application, 2014.

[21] G.O. Phillips, P.A. Williams, Handbook of hydrocolloids, Woodhead publishing limited, 2009.

[22] H. Yang, S. Xu, L. Jiang, Y. Dan, Thermal Decomposition Behavior of Poly (Vinyl Alcohol) with Different Hydroxyl Content, J. Macromol. Sci. Part B. 51 (2012) 464–480. doi:10.1080/00222348.2011.597687.

[23] A.Y. Maturana Cordoba, J.D. Pagliuso, Thermal Decomposition Behavior of Crude Glycerin, in: COBEM 2011, 2011: p. 6.

[24] S. Todaro, M. Antonietta, M. Rosalia, P. Picone, M. Laura, D. Giacinto, D. Bulone, C. Dispenza, Temporal control of xyloglucan self-assembly into layered structures by radiation-induced degradation, Carbohydr. Polym. 152 (2016) 382–390. doi:10.1016/j.carbpol.2016.07.005.

[25] F.J. O'Brien, Biomaterials & scaffolds for tissue engineering, Mater. Today. 14 (2011) 88–95. doi:10.1016/S1369-7021(11)70058-X.

[26] S. Krajewski, R. Prucek, A. Panacek, M. Avci-Adali, A. Nolte, A. Straub, R. Zboril, H.P. Wendel, L. Kvitek, Hemocompatibility evaluation of different silver nanoparticle concentrations employing a modified Chandler-loop in vitro assay on human blood, Acta Biomater. 9 (2013) 7460–7468. doi:10.1016/j.actbio.2013.03.016.

[27] D. Narayanan, S. Nair, D. Menon, A systematic evaluation of hydroxyethyl

starch as a potential nanocarrier for parenteral drug delivery, Int. J. Biol. Macromol. 74 (2015) 575–584. doi:10.1016/j.ijbiomac.2014.12.012.

[28] B. Kundu, C.J. Schlimp, S. Nürnberger, H. Redl, S.C. Kundu, Thromboelastometric and platelet responses to silk biomaterials., Sci. Rep. 4 (2014) 4945. doi:10.1038/srep04945.

[29] M. Jamnicki, A. Zollinger, B. Seifert, D. Popovic, T. Pasch, D.R. Spahn, Compromised Hydroxyethyl Blood Coagulation: An In vitro Comparison of Starch 130/0.4 and Hydroxyethyl Starch 200/0.5 Using Thrombelastography, Int. Anesth. Res. Soc. 87 (1998) 989–993. doi:10.1213/00000539-199811000-00002.

[30] X. Li-Chong, B. James, C.A. Siedlecki, Proteins, Platelets, and Blood Coagulation at Biomaterial Interfaces, Colloids Surfaces B Biointerfaces. 1 (2014) 49–68. doi:10.1016/j.colsurfb.2014.09.040.

5. Synthesis and characterisation of carboxylated xyloglucan

5.1. Introduction and aim

Several studies have investigated into the possibility of modifying the chemical structure of xyloglucan by replacing some of its hydroxyl groups with functional groups, such as carboxyl, thiol, amino, alkyloamino, sulphated and carboxymethyl groups, in order to ameliorate water solubility, increase mucoadhesivity and modify the release profile of an incorporated drug.[1–4]

Derivatisation of polysaccharides by oxidation is a common method to convert free primary alcohols into aldehydes and further into carboxylic acid groups (Scheme 5.1a). Oxidation to the carboxylic acid level results in polysaccharides based on uronic acids, which then resemble the structure of natural polyuronic acids, such as pectin or alginates. On the other hand, when the secondary alcohols are also oxidized the oxidative cleavage of 1,2-diols occurs, which leads to ring-opening and dicarboxyl compounds formation (Scheme 5.1b).[5]

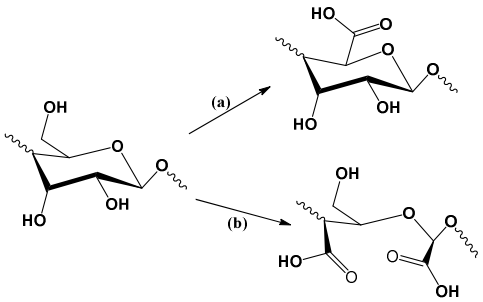

Scheme 5.1 Different modes of chemical oxidation, illustrated for a generic polysaccharide. (a) Oxidation of a primary alcohol; (b) Oxidative cleavage of a diol

Since these two oxidation modes are possible, when oxidative derivatisation of a native (unprotected) polysaccharide is performed, it is important to guarantee a good

selectivity on the primary alcohol, thus avoiding oxidation of the secondary alcohols to yield sugar ring opening reactions.
For instance, the oxidation of polysaccharides such as cellulose or xyloglucan with NaClO and NaBr results in a non-selective oxidation, meaning that both primary and secondary alcohols can be oxidised. The non-selective oxidation involves both oxidation modes described in Scheme 5.1, leading both to carboxylation of primary hydroxyl groups and oxidative cleavage of the sugar ring.[6,7]

Van Bekkum in early ‘90s was the first to report that the catalyst TEMPO could be used for the regioselective oxidation of primary alcohols in polysaccharides (starch and inulin were included in the initial report) to give the corresponding polyuronic acids with an almost complete conversion.[8]
A possible mechanism of reaction of TEMPO-NaClO-NaBr systems involves the initial oxidation of the persistent radical TEMPO by NaOCl, which is transformed in the active oxidant, an oxoammonium species. This species oxidizes the polysaccharide primary alcohol to aldehyde, being reduced in hydroxylamine. In aqueous solution, the aldehyde is hydrated and the hydrated form is then oxidized to carboxyl group by another oxoammonium molecule present in solution. NaOCl is responsible for the initial oxidative activation of TEMPO and also for the reoxidation of hydroxylamine in oxoammonium (see Scheme 5.2).
The TEMPO-mediated oxidation has been demonstrated to be a viable route to the selective oxidation of different polysaccharides, such as cellulose, pullulan, including xyloglucan extracted from *Hymanea Courbaril* seeds.[9,10]

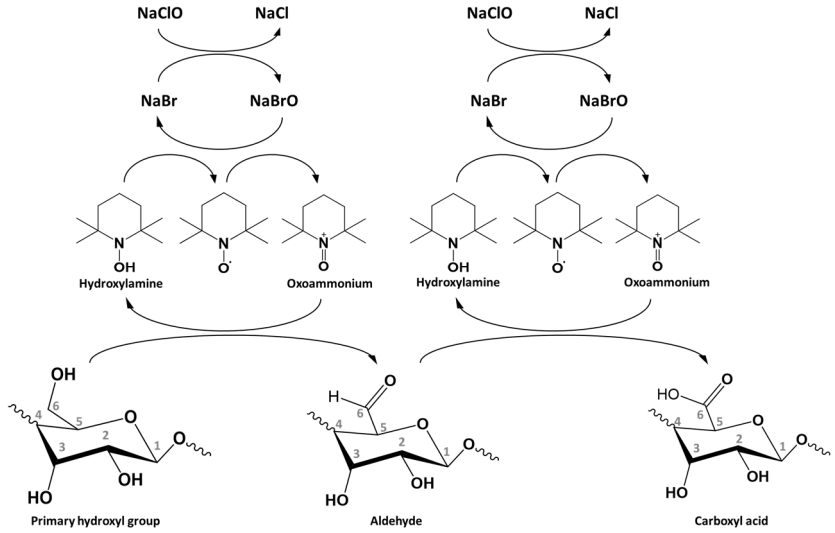

Scheme 5.2 Mechanism of TEMPO-mediated oxidation of a generic polysaccharide primary hydroxyl groups to carboxyl groups

Along with the above described oxidation reaction, a secondary reaction occurs which leads to scission of the polysaccharide chain. This secondary reaction has been mainly attributed to β-elimination.[11] Such reaction occurs preferentially under alkaline conditions, when in position C6 there is an aldehyde, which is the first product of the oxidation. This condition favours the increase of the acidity of the hydrogen at C5, which is deprotonated in the alkaline reaction, leading to the formation of a double bond between the carbohydrate C4 and C5 as intermediate, which then evolves with the elimination of the group linked to the β carbon (C4) (Scheme 5.3).[6] Hence, alkaline conditions are necessary for the occurrence of this β-elimination.

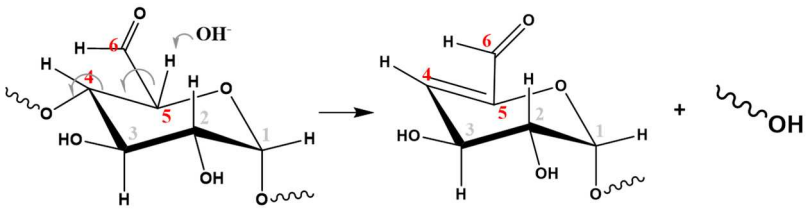

Scheme 5.3 Mechanism of β-elimination

However, it has been observed that chain scission occurs also when the oxidation is conducted at acidic pH (i.e. pH around 5), even though in this condition it is less emphasized and the products of the reaction are characterised by a lower decrease of molecular weight and a lower degree of carboxylation.[7,12] This observation suggests that β-elimination is not the only mechanism that leads to chain scission.

In order to investigate this aspect, Shibata et al. have studied the oxidation of celluronic acid, a variant of cellulose that is already carboxylated. They have suggested that hydroxyl radicals, formed from NaBrO and TEMPO at pH 10–11, cause chain scission during the oxidation (Scheme 5.4). Therefore, they have proposed the addition of radical scavengers to the system to suppress chain scission, but they have observed only a mitigation of this effect.[6]

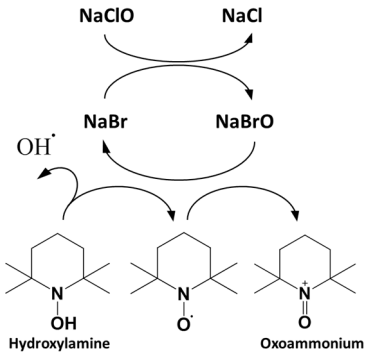

Scheme 5.4 Possible scheme of formation of hydroxyl radicals during TEMPO-mediated oxidation

The relationship between the presence of TEMPO catalyst and the chain scission reaction is still quite controversial.

In a more recent report focused on the mechanism of chain scission in xyloglucan, Spier et al. have studied the influence of TEMPO concentration on the molecular degradation of the polysaccharide, observing that increasing the catalyst concentration, the degree of chain scission was indeed reduced. In other words, they observed that the higher is the content of TEMPO, the lower is the chain scission, an observation that contradicts what previously reported by Shibata et al., that retains TEMPO responsible of the formation of hydroxyl radicals and of a higher chain scission because they did not study the effect of TEMPO concentration in the system. Thus, Spier et al. have suggested that TEMPO acts as a "sacrificial molecule": being a preferential substrate for the oxidation by NaBrO, it is oxidized at the place of the polysaccharide chain by this oxidant specie, protecting then the polysaccharide from chain scission and non-selective oxidations. This means not only that a higher concentration of TEMPO decreases the chain scission degree, but also decreases the degree of carboxylation.[7]

Beside the role of TEMPO in the oxidation reaction and, in particular, in the chain scission concurrent reaction, other authors have studied the influence of NaClO concentration and time of reaction on both carboxylation and chain scission levels.[10,13] In particular, it has been shown that in TEMPO-NaClO-NaBr reactions the increase of NaClO concentration causes an increase of the carboxylate groups content as well as an increase of the chain scission degree. But while the degree of carboxylation reaches a plateau, the degree of chain scission increases proportionally to the increase of the oxidant species, without reaching a plateau.[13] The increase of chain scission after complete carboxylation of primary hydroxyl groups may also be related to the presence of carboxyl groups at C6 (favoured primary hydroxyl groups position) that, in an alkaline environment, favours β-elimination due to the increase of the acidity of C5, as previously explained.

The increase of reaction time has been shown to produce similar effects. Lucyszyn et al. have observed that increasing the reaction time in the oxidation of xyloglucan from *Hymanea coubaril* seeds, both carboxylation and chain scission degrees increased.[10]

In conclusion, the TEMPO-mediated oxidation can be a viable strategy to introduce ionisable and reactive functional groups in xyloglucan chains and it also leads to reductions of its high molecular weight.
Degree of carboxylation and degree of chain scission are the most important measurable parameters to evaluate the effect of the oxidation reaction. The most widely used techniques to evaluate the reduction of molecular mass are size exclusion chromatography (SEC) and/or dynamic light scattering (DLS), while for the determination of the carboxyl groups content, different techniques have been proposed, including titration (conductimetric or pHmetric), nuclear magnetic resonance (^{13}C-NMR), high performance anion exchange chromatography. [7,14,15]
In most reported cases, the oxidation reaction is performed at temperature below 5 °C and at alkaline pH (between 9.5 and 11) in order to have a good balance between carboxylation and chain scission.[12,14]

In this work, the introduction of carboxyl groups in xyloglucan chains is aimed to promote electrostatic interactions with oppositely charge polyelectrolytes. Indeed, this type of non-covalent interactions are considered the main driving force of co-assembly in interfacial systems, leading to the assembly of building blocks from molecular- to macro-scale. Co-assembly offers the opportunity to form thermodynamically stable structures without the use of chemical crosslinking and is considered a powerful tool for the production of complex and adaptable biomaterials with highly tunable properties and significant biological effects.[16–19]
In particular, the assembly of anionic carboxylated-xyloglucan (CXG) with a positively charge peptide amphiphile (PA) sequence is a possible approach for the

fabrication of fibrous scaffolds for wound healing and this topic will be discussed in details in the following chapter (Chapter 6).

The obtained CXG was characterised for its molecular structure modification, its behaviour in solution, by dynamic light scattering and viscosity measurements, and its thermal stability.

In the prospect of its use to produce co-assembled hydrogel dressings/scaffolds for wound healing, a cytotoxicity test was also performed.

Furthermore, a preliminary study to verify the ability of CXG to interact with oppositely charge molecules and, in particular, with poly-D-lysine (PDL), polyethilenimine (PEI) and a positively charge peptide amphiphile (PA-H3), was performed.

5.2. Materials and Methods

5.2.1. Materials

Tamarind seeds xyloglucan (XG) was kindly provided by DSP Gokyo Food and Chemical Co. (Japan). 2,2,6,6-Tetramethyl-1-piperidinyloxy (TEMPO), sodium bromide (NaBr), sodium hypochlorite solution, sodium borohydride ($NaBH_4$), ethanol, and HCl (1M), NaOH (1 M) were purchased from Sigma Aldrich and used without further purification. Poly-D-Lysine (PDL, MW= 150-300 kDa) and polyethilen imine (PEI branched, MW=800 Da) were purchased by Sigma Aldrich. Peptide amphiphile $C_{16}(Val)_3(Ala)_3(His)_3$, named in this chapter PA-H3 was synthesized as described in Appendix A.1.3 and it will be presented in detail in Chapter 6.

5.2.2. Methods

Synthesis of the carboxylated variant of XG

The carboxylation reaction and the setup used are described in detail in Appendix A.1.2. Briefly, 0.2%wt XG aqueous solution was reacted with 0.128 mM TEMPO, 0.81 mM NaBr and 15% NaOCl solution for 4h at 5 °C under an inert atmosphere,

providing continuous magnetic stirring. During reaction, the pH was constantly monitored and maintained at the constant value of 9 ± 0.2 by addition of small volumes of 0.1M NaOH. The reaction was stopped by addition of $NaBH_4$ to the final concentration of 4 mM. The product was recovered by precipitation in ethanol followed by freeze drying.

Fourier-transform infrared spectroscopy (FTIR)

FTIR analysis was performed using a Fourier Transform Infrared Spectrometer (FTIR) (Spectrum Two FTIR spectrometer, Perkin Elmer). Samples were prepared starting from both the fully protonated and deprotonated CXG, prepared as described in Appendix A.2.3. All spectra have been normalized with respect to the peak correspondent to the stretching of methylene groups (2956 cm^{-1}).

Determination of carboxyl groups by titration

The quantitative analysis of carboxyl groups of CXG was performed by acid-base titration as described in Appendix A.2.6. In particular, CXG was titrated with 0.05M NaOH solution and the equivalent point was detected at pH 7.

Gel filtration chromatography

Gel filtration chromatography was conducted using a Shodex SB HQ (804 and 806) columns coupled with an Agilent 1260 Infinity HPLC with a refractive index detector (see also Appendix A.2.7 for detail on the equipment). All samples were eluted with a flux of 0.6 ml/min of 0.02%wt sodium azide aqueous solution. Prior to injection in the column, the polymer aqueous solution was filtered with 1.2 µm cellulose acetate (Millipore) syringe filters. Chromatograms of the samples were compared with chromatograms of pullulan standard solutions.

Static and Dynamic Light Scattering (SLS and DLS)

Static light scattering (SLS) measurements were performed using a Brookhaven Instrument BI200-SM goniometer (Biophysics Institute, Palermo Unit, National Research Council) Briefly, the scattered light intensity was measured at 10 scattering angles, namely 30º, 45º, 50º, 60º, 75º, 90º, 105º, 120º, 135º and 150º. CXG and XG samples were prepared at different concentrations (i.e. 0.5 mg/ml, 1 mg/ml, 1.4 mg/ml, 2 mg/ml, 2.5 mg/ml) in MilliQ water. The measurements were performed at 20 °C ± 0.1 °C. The weight-average molecular weight (Mw) was determined from a Zimm plot analysis.[20]

For dynamic light scattering (DLS), all the analysed solutions were prepared starting from 0.1%wt aqueous solutions of XG and CXG.

For the study of interactions between CXG and positively charged molecules, CXG, PDL, PEI and PA-H3 0.1 %wt aqueous solutions were prepared and then mixed in different weight ratios to prepare CXG/polycation systems. Compositions of the analysed systems are reported in Tab. 5.1.

Tab. 5.1 Composition of CXG or XG and polycations (i.e. PDL, PEI or PA-H3) mixtures

System	Composition	CXG/Polycation w/w
CXG	CXG 1 mg/ml	-
XG	XG 1 mg/ml	-
PDL	PDL 10 µg/ml	-
PA-H3	PA-H3 10 µg/ml	-
CXG/PDL 100:1	CXG 1 mg/ml + PDL 10µg/ml	100
CXG/PDL 50:1	CXG 1 mg/ml + PDL 20µg/ml	50
CXG/PDL 25:1	CXG 1 mg/ml + PDL 40µg/ml	25
XG/PDL 100:1	XG 1 mg/ml + PDL 10µg/ml	100
XG/PDL 50:1	XG 1 mg/ml + PDL 20µg/ml	50
XG/PDL 25:1	XG 1 mg/ml + PDL 40µg/ml	25
CXG/PEI 100:1	CXG 1mg/ml + PEI 10 µg/ml	100
CXG/PEI 50:1	CXG 1mg/ml + PEI 20 µg/ml	50
CXG/PEI 25:1	CXG 1mg/ml + PEI 40 µg/ml	25
CXG/PA-H3 100:1	CXG 1mg/ml + PA-H3 10 µg/ml	100

All the solutions analysed through SLS and DLS were filtered with 1.2 µm syringe filters to remove gross contaminants and artefacts from the solution.
For single measurements performed at 90° scattering angle and at 20°C the method of cumulant[21] and/or the exponential stretched method were compared to obtain information on the apparent hydrodynamic size and width of the size distribution.
Further details on the instrumentation of both SLS and DLS and on the fitting methods are described in Appendix A.2.8.

Shear viscosity measurements

Shear viscosity measurements of CXG and XG 4%wt solutions were performed in rotation mode at 20 °C. Details are discussed in Appendix A.2.2.
Due to the different viscosities of the systems, the plate-cone geometry was chosen for CXG 4 %wt, while for XG 4 %wt the plate-plate geometry was preferred.

Z-potential measurements

For ζ-potential measurements, XG, CXG, PDL, PEI and PA-H3 solutions 0.1 %wt solutions were prepared in MilliQ water and performed using a Malvern Nano ZS-Series Zetasizer.

Thermal analysis

Thermal-gravimetric analysis (TGA) was conducted using a TA Instruments Q500. Pre-conditioned samples were analysed in a temperature range of 20−500°C at a heating rate of 10°C/min. For other details see Appendix A.2.4.
Differential Scanning Calorimetry (DSC) was performed with a Perkin-Elmer DSC4000 calorimeter. The samples (7-10 mg) were weighed in aluminium pans and Scans were recorder during a heating /cooling cycle carried out in a range of 25−300 °C under nitrogen atmosphere at a heating rate of 10°C/min. A detailed description of the setting parameters is provided in Appendix A.2.9.

Biological evaluations

Cell culture of adenocarcinomic human alveolar basal epithelial cells (A549), mouse embryonic fibroblasts (NIH-3T3), keratinocyte cell line (HaCat) is described in Appendix A.3.1.

Cell viability test

Preliminarily, cell viability was measured by MTS assay described in Appendix A.3.2. Different concentrations (0.5, 0.3, 0.6 and 1.25 mg/ml) of XG and CXG have been tested and these solutions have been seeded on a A549 monolayer in a 96-well flat-bottom plate and incubated for 48 hours. Results were expressed as the percentage of MTS reduction relatively to the control.

Other evaluations on the cytocompatibility with cells from the skin, namely fibroblasts (NIH-3T3) and keratinocytes (HaCat), were performed.

Cells were seeded in a 98 well-plate at a concentration of $10*10^3$ per well and incubated with 2.5 mg/ml CXG solution at 37°C in a humidified atmosphere with 5% CO_2 and 95% air. The experiment was made in triplicate and cell monolayers were used as control. After 3 days of incubation cells, the medium was removed and cells were stained with the LIVE/DEAD® (4μM μg/ml calcein and 2 μM ethidium homodimer) viability/cytotoxicity kit from Thermo-Fisher Scientific. Viability was then qualitatively assessed using a Leica TCS SP2 Confocal and Multiphoton microscope.

5.3. Results and discussion

5.3.1. Carboxylated xyloglucan physico-chemical characterisation

The presence of carboxyl groups after the TEMPO-catalysed regioselective oxidation was evaluated by FTIR spectroscopy measurements. In Fig. 5.1 the spectrum of native XG is compared with spectra of CXG both in dissociated (Fig. 5.1a-b) and protonated form (pH 7 and pH 3, respectively) (Fig. 5.1c-d).

XG spectra, both at neutral and acidic conditions, are characterised by the broad band at 3600-3200 cm^{-1} that refers to the stretching of the O-H bond from free and bound water and polymeric hydroxyl groups, also involved in hydrogen bonding. The band at 2925 cm^{-1} is attributed to the asymmetric stretching of C–H while the bands at 1150 cm^{-1} and at 1050 cm^{-1}, very common in all polysaccharides, are due to C-O and C-C stretching vibrations of pyranose rings.[22]

The spectra of CXG in the fully protonated and partially deprotonated forms show some differences compared to the native XG. In the partially deprotonated form, CXG displays a peak at 1620 cm^{-1} attributable to the asymmetric stretching of the carboxylate anions. In the fully protonated form, the new peak at 1737 cm^{-1} is assigned to stretching of the carboxyl groups. [23] These are clear evidences of the successful derivatization of some of the XG hydroxyl groups into carboxyl groups.

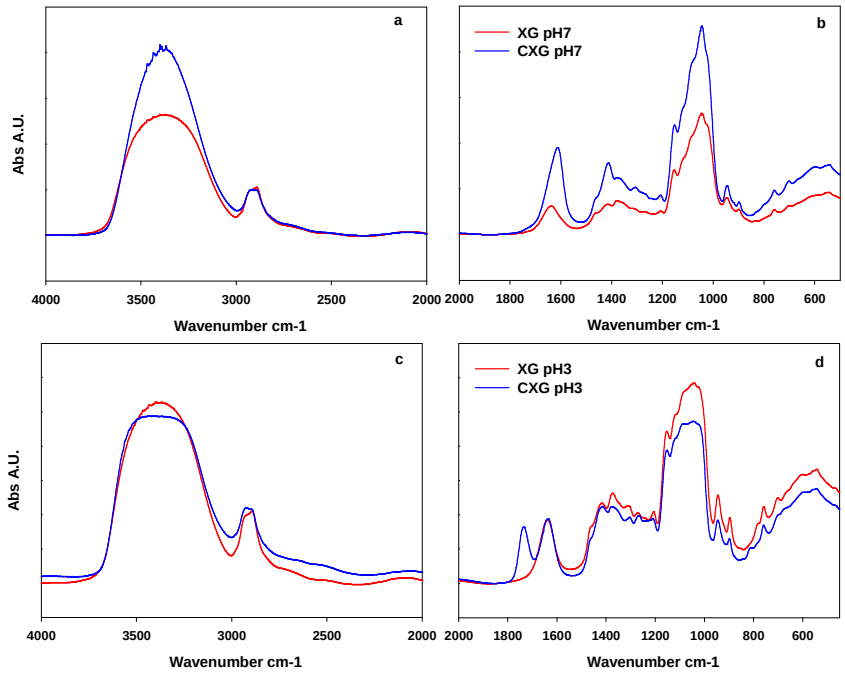

Fig. 5.1 FTIR spectra of XG and CXG in the 4000-2000 cm^{-1} (a, c) and 2000-400 cm^{-1} (b, d) ranges, with CXG in its partially dissociated (a, b) and fully protonated (c,d) forms

The carboxyl groups content of CXG was determined by pH-metric titration. The titration curves (not shown), typical of a weak acid, indicate a concentration of carboxyl groups of ca. 1.0 - 1.2 $mmol_{-COOH}/g_{CXG,}$ corresponding to the conversion of about 70 ± 5% of the primary hydroxyl groups present in the polymer.

It is expected that the presence of carboxyl groups in the oxidised xyloglucan causes a modification of the surface electrical charge of the polysaccharide chains in water. Indeed, the ζ-potential values (Tab. 5.2) of CXG dispersion measured in MilliQ water (at pH 6.5) are negative, while for XG were about zero.

Tab. 5.2 ζ-potential values obtained in MilliQ water

Sample	pH	Z Potential (mV)
XG	6.5	0.118 ± 3.75 mV
CXG	6.5	-21.6 ± 8.69 mV

Furthermore, it is expected that the oxidation reaction induces a modification of the molecular weight distribution of the polymer. GFC chromatography of XG and CXG are reported in Fig. 5.2. The CXG chromatogram is shifted towards the higher elution times with respect to XG, which correspond to lower molecular weights.

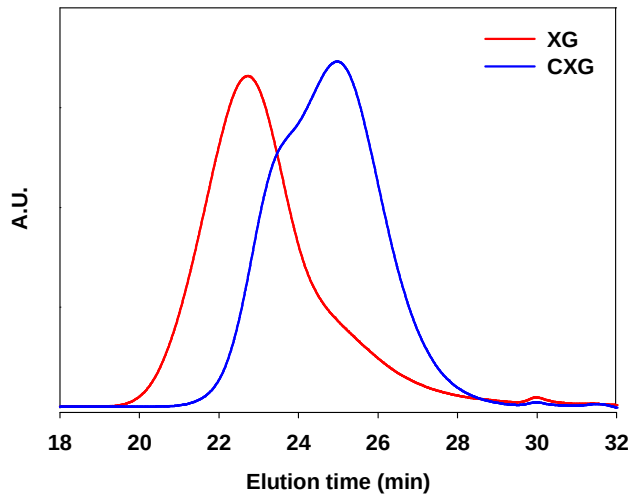

Fig. 5.2 GFC chromatograms of XG and CXG

More detailed information on the molecular weight distribution of CXG was obtained by comparing XG and CXG chromatograms with pullulan standards (Fig. 5.3). While XG shows a chromatogram overlapping pullulan standards from 2560 kDa to 400 kDa (Fig. 5.3a), CXG chromatogram envelops pullulan standards between 200 kDa and 800 kDa (Fig. 5.3b).

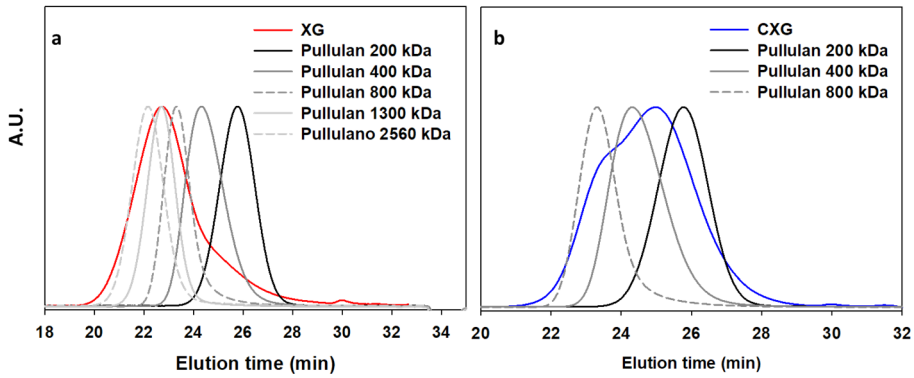

Fig. 5.3 Chromatograms of XG (a) and CXG (b) compared with pullulan standards

This reduction of the Mw was also confirmed by Zimm plots derived from static light scattering measurements at different angles, which are reported in Fig. 5.4a-b. The average weight molecular weights of XG and CXG resulted 1185 ± 85 kDa and 400 ± 86 kDa, respectively.

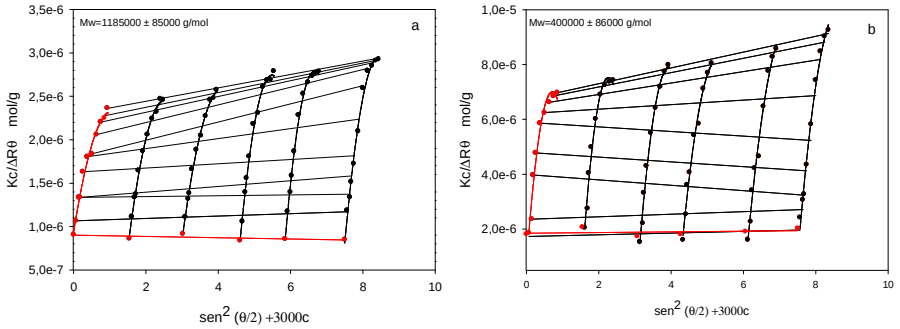

Fig. 5.4 Zimm plots XG (a) and CXG (b)

DLS measurements were performed at 20°C on both CXG and XG 0.1 %wt solutions. The stretched exponential fitting method was applied to obtain information on the apparent hydrodynamic size and width of the size distribution. This fitting method allows to calculate the average relaxation time (τ_c) and the stretched coefficient (β), giving information on the apparent hydrodynamic size and width of the size distribution or changes in the interactions among the objects in solution, respectively. Higher τ_c are generally related with objects or particles with higher apparent hydrodynamic size, while β coefficient is comprised between 0 and 1, with smaller values corresponding to wider distributions.

Decay curves of CXG and XG and parameters obtained after the fitting are reported in Fig. 5.5 and in Tab. 5.3, respectively. The stretched exponent β is lower for CXG than for XG. This could mean that CXG solution contains objects in a wider range of different hydrodynamic volumes (higher polydispersity), or since this parameter may also reflect a change in the interactions as a result of the structural and molecular modifications occurred upon oxidation, it can probably be interpreted as attenuation

of the attractive (mainly hydrophobic) interactions among polysaccharide chains owing to the establishment of repulsive electrostatic interactions due the presence of carboxylate anions.

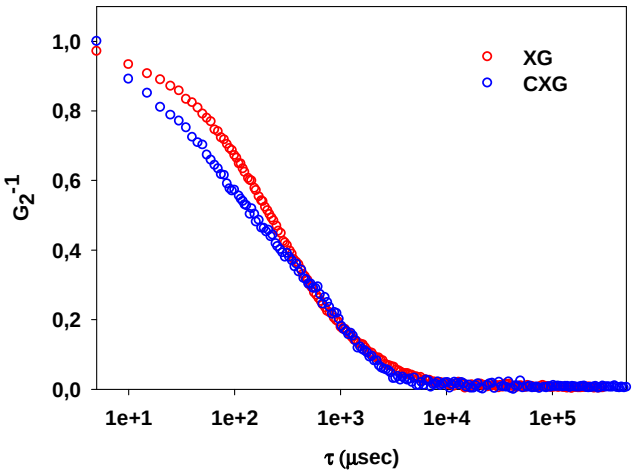

Fig. 5.5 Decay curves of functionalized XG and XG obtained by DLS measurements

Tab. 5.3 Stretched exponential fitting parameters for non-functionalized xyloglucan and after oxidation reaction

System	τ_c (µsec)	β
XG	904.55	0.61
CXG	1104.39	0.45

The effect of the oxidation on the viscosity of the two polymer solutions was also analysed. In Fig. 5.6 shear viscosity as function of shear rate for XG 4 %wt (Fig. 5.6a) and CXG 4 %wt (Fig. 5.6b) aqueous solutions are reported.

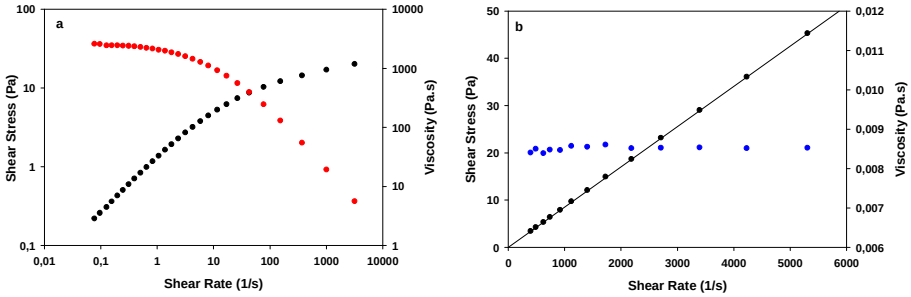

Fig. 5.6 Shear viscosities of XG 4 %wt (a) and CXG 4 %wt (b) aqueous solutions

While for XG solution the flow curve is dominated by the characteristic shear thinning behaviour, [24] CXG shows the typical behaviour of a Newtonian fluid with a constant viscosity in the whole analysed shear rate range. This result can be related to the decrease of the molecular weight of CXG that accompanies the oxidation reaction, but also to the electrostatic repulsion between the charged groups introduced in the polymer chains, which may limit chain entanglements.

Thermogravimetric analysis on XG and CXG was performed and results are reported in Fig. 5.7a-b.

As observed in Chapter 4 (paragraph 4.3.1), XG shows an extremely good thermal stability; the onset of thermal decomposition is at 310 °C (T_{max} of DTG curve), followed by a steep mass loss that is almost completed at 370°C with a residual mass of about 34% (Fig. 5.7a). This uncommon thermal stability has been attributed to a "hyper-entangled" supramolecular conformation, which confers relatively high stiffness and local high chain packing density to the long polymer molecules.[25]

CXG shows a significantly different degradation profile: the onset of degradation occurs at about 225 °C, the mass loss is very smooth and the residual mass is higher (Fig. 5.7a). The reduction of CXG molecular weight can be responsible of the decrease of onset of degradation; indeed, generally as the units in a chain increases the thermal stability of the polymer increases. The degradation process of CXG occurrs in a much

wider range of temperature, with a main peak of the DTG curve at 250°C and a long tail that stretches at 350°C. The T_{max} of the second event is closer to the T_{max} of the native XG. This may suggest that there is a chain-to-chain variability of the oxidation degree. The CXG early onset of degradation can be explained with a possible loss of the hyper-entagled supramolecular structure and decarboxylation.[26]

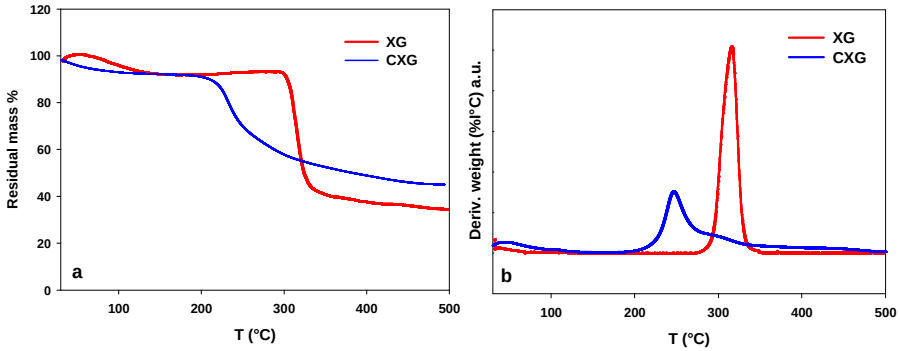

Fig. 5.7 Thermo-gravimetric analysis of XG and CXG polymer powders (a) and correspondent derivative curves (b)

The difference in the percentage of residual mass, 34% for XG and 40% for CXG, suggests that CXG generates a more stable degradation product. This result has been shown also by Freitas et al. for the carboxylation of *Hymenaea courbaril* xyloglucan. They observed a correlation between the residual mass and the level of xyloglucan oxidation, showing that the higher is the level of oxidation, the lower is themperature of the onset of degradation and the higher is the residual mass, due to increasingly stable products of degradation.[27]

DSC thermograms of XG and CXG are reported in Fig. 5.8. Both XG and CXG show a broad peak between 85 °C and 100 °C. These thermic events can be related to the evaporation of the water retained inside the samples. Indeed, a heating/cooling/heating cycle between 30°C and 200°C has shown that this peak is not present when the samples are heated for the second time, thus confirming that is

attibutable to the evaporation of water. Interestingly, the evaporation of moisture is shifted to higher temperatures in CXG with respect to XG. Since the polymers have been conditioned in the same way before the analysis, this suggests that the percentage of "bound water" is higher for CXG than for XG, as a result of the increased hydrophilicity of the carboxylated polysaccharide.[28]

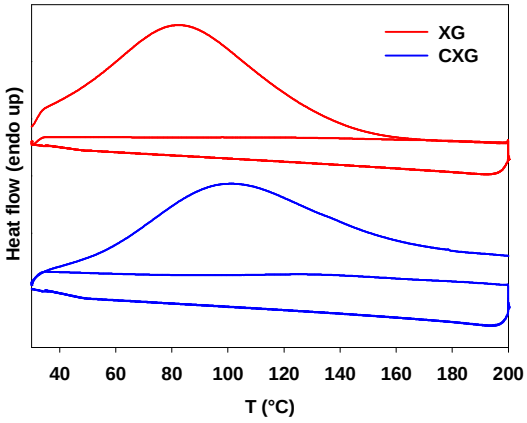

Fig. 5.8 DSC thermogram for native xyloglucan and CXG

5.3.2. Biological evaluation

As already mentioned, carboxylated xyloglucan was produced for the fabrication of co-assembled structures to be used as scaffolds for wound regeneration. Preliminary cytotoxicity evaluations were performed to determine the CXG suitability for the application.

MTS assay on adenocarcinomic human alveolar basal epithelial cells A549 incubated with CXG at 1.25 mg/ml, 0.6 mg/ml, 0.3 mg/ml and 0.15 mg/ml reveals that after 48h of incubation cells are 100% viable at all the tested concentrations (Fig. 5.9).

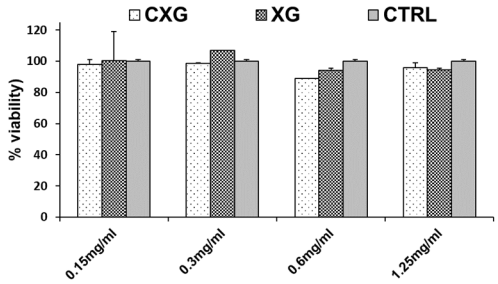

Fig. 5.9 Cell viability percentage of A549 cells incubated with CXG and XG at 0.15 mg/ml, 0.3 mg/ml, 0.6 mg/ml and 1.25 mg/ml compared with a cell monolayer (CTRL) used as control

This result encouraged to perform other viability tests on cells from the skin, namely NIH/3T3 and HaCat.

After 3 days of *in vitro* cell culture, cells were stained with LIVE/DEAD® staining and the confocal images were recorded. Representative images are reported in Fig. 5.10. No significant differences between the non-treated cells (control) and the cells incubated with CXG can be observed. The same result was obtained for all the tested cell types. This result, although only preliminary, encourage to proceed with the use of this polymer for the fabrication of skin scaffolds through co-assembly.

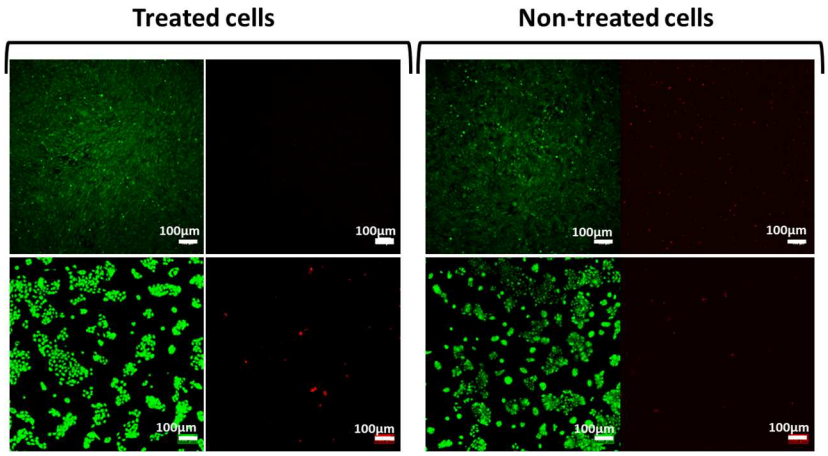

Fig. 5.10 Confocal images of NIH/3T3 and HaCat cells incubated with 2.5 mg/ml CXG solution (dead-red; live-green)

5.3.3. Preliminary study on interactions between CXG and polycations through DLS

In the perspective of using CXG to prepare scaffolds through co-assembly with oppositely charged molecules, a preliminary study of its ability to interact with positively charge polyelectrolytes was performed.

Molecules chosen for this study are poly-D-lysine and poly(ethylenimine) and peptide amphiphile. These three molecules were chosen as representatives of possible different co-assembly scenarios. Indeed, PDL is a linear macromolecule with a relatively high molecular weight, PEI is a small and branched molecule and a peptide amphiphile sequence (PA-H3) that is a small molecule that self-assemble in nanofibers (diameter around 6-8 nm) characterised by a marked surface charge density. The latter will be presented in detail in the following chapter (Chapter 6).

Their ζ-potentials values are reported in Tab. 5.4, together with the value of CXG.

Tab. 5.4 ζ-potential values of CXG, PDL, PEI and PA-H3 in MilliQ water

Molecule	pH	ζ potential (mV)
CXG	6.5	-21.6 ± 8.69
Poly-D-Lysine (PDL)	6	+62.4 ± 4.88
Poly(ethylenimine) (PEI)	6.5	+19.5 ± 2
Peptide amphiphile (PA-H3)	5	+46.0 ± 1.45

Dynamic light scattering (DLS) analysis of CXG solution (0.1 %wt) with small quantities of the various polycationic molecules was carried out to investigate if conformational changes and/or aggregation phenomena occur.

The scattered light intensity decay curves of CXG in presence of polycations are reported in Fig. 5.11, 5.12 and 5.13. All the curves were fitted according to the stretched exponential method and when possible also with cumulant method to

determine the apparent average hydrodynamic diameter (D_h) of the objects in solution and the polydispersity index (PI).

Hence, a comparison among CXG, PDL and their mixtures at different weight ratios is reported in Fig. 5.11a and parameters obtained from the fitting of the decay curves are reported in Tab. 5.5. PDL solution has a lower average relaxation time and a higher stretched exponential with respect to CXG. These parameters correspond to a system, containing smaller objects and in a narrower range of hydrodynamic volumes. In particular, it was possible to calculate the hydrodynamic diameter of these objects with cumulant fitting and it resulted of about 151 nm with a PI equal to 0.34 (see Tab. 5.5).

The addition of a small amount of PDL to a CXG solution causes a significant change of the decay curve of CXG. In particular, stretched exponential fitting of CXG/PDL 100:1 system shows that there is a significant increase of the average relaxation time of the binary system compared to the precursors solutions of CXG and PDL (values reported in Tab. 5.5). This change can be attributed to the interactions between the two molecules which lead to the formation of objects in solution, having an apparent hydrodynamic diameter of about 511 nm. A further addition of PDL (CXG/PDL 50:1) provokes an increase of both τ_c and β which can be translated into a decrease of the heterogeneity of the objects in solutions with respect to the system with weight ratio 100:1, having also a smaller D_h of about 469 nm. Furthermore, it was observed that a further increase of PDL content to 25:1 weight ratio seems to follow the same trend (decay curve not shown). However, it was believed that the observed decrease of the hydrodynamic size of objects in solution was actually related with the phenomenon of multiple scattering. This phenomenon is characteristic of larger particles systems with high refractive index contrast in which photons are scattered multiple times by the sample before to being detected. This hypothesis was confirmed by the observation that a further increase of PDL content (10:1 weight ratio) causes the

formation of dense aggregates visible with naked eyes, making the solution opalescent and thus not suitable for DLS analysis.

The same study was repeated using the neutral XG (ζ-potential= 0.118 ± 3.75 mV) at the place of CXG and decay curves are reported in Fig. 5.12b. All the XG/PDL systems analysed shown similar decay curve with no significant variation of the β coefficient with respect to XG, while it was registered a slight increase of τ_c probably due to the sum of the scattering of the two separate molecules rather than to interactions between the two components.

This result suggests that the interactions between CXG and PDL are mainly electrostatic, confirming the importance of introducing carboxyl groups into XG polymer chain in order to promote assembly with oppositely charged molecules.

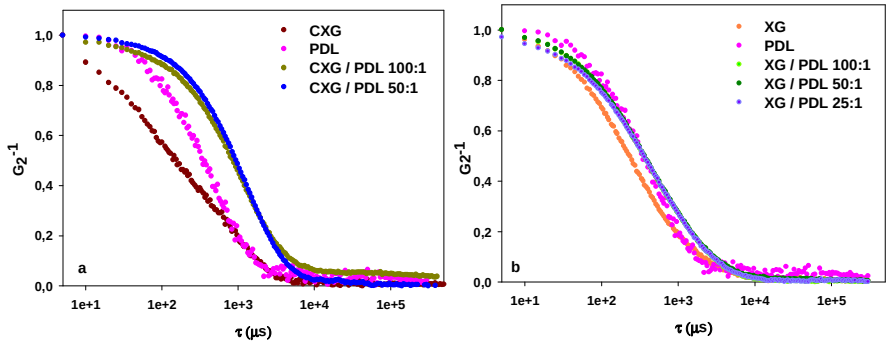

Fig. 5.11 Decay curves obtained by DLS measurements of CXG/PDL (a) and XG/PDL systems (b)

Tab. 5.5 Fitting parameters of the decay curves reported in Fig. 5.12; "n.a" = fitting method non-applicable

System	τ_c	β	D_h (nm)	PI
CXG	1104.39	0.44	n.a.	n.a.
XG	904.55	0.61	n.a.	n.a.
PDL	866.96	0.88	151.58 ± 44.2	0.34
CXG/PDL 100:1	2109.42	0.81	511.16 ± 193.0	0.57
CXG/PDL 50:1	2696.15	0.88	461.71 ± 179.3	0.5
XG/PDL 100:1	1562.64	0.61	n.a.	n.a.
XG/PDL 50:1	1470.56	0.63	n.a.	n.a.
XG/PDL 25:1	1592.73	0.64	n.a.	n.a.

Once established the importance of electrostatic interactions, it was decided to study how these CXG/PDL aggregates formed in solution are modified or perturbed by changing the pH that, modifying the protonation/deprotonation equilibria, strictly affect the surface charge of molecules.

Hence, for this study, increasing amounts of HCl were added to CXG/PDL 50:1 and decay curves of the resulting systems are reported in Fig. 5.12a.

Very small amount of HCl (1mM) do not cause any change in the system. While, increasing 10 times the concentration of HCl (10 mM), CXG/PDL system shows significant increase of the average relaxation time and a drastic decrease of the β coefficient (see Tab 5.6). Both these two parameters progressively decrease with further addition of HCl (15mM and 20 mM, respectively).

These results should indicate that the acidification (final pH with HCl 20 mM =2-3) cause the protonation of CXG, which lead to a decrease of the negative charges carboxyl groups with a subsequent weakening of electrostatic interactions with PDL. In particular, it is hypothesized that the objects formed by CXG and PDL are not affected by the small addition of HCl (1mM), while after the addition of HCl (10 mM) these objects start to disassemble, resulting in an increase of the hydrodynamic dimensions. The disassembly results then more evident after the addition of HCl 15

mM and 20 mM, having a decay curve that is intermediate between those of precursors molecules (Fig. 5.12b).

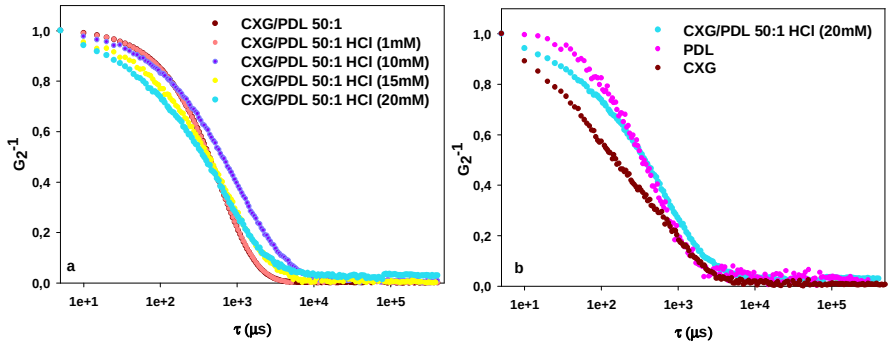

Fig. 5.12 Decay curves obtained by DLS measurements of CXG/PDL system with increasing amount of HCl (1 mM, 10 mM, 15 mM and 20 mM) (a) and the comparison between CXG/PDL system with HCl 20 mM (pH 2-3)

Tab. 5.6 Fitting parameters of the decay curves reported in Fig. 5.13

System	τ_c	β	D_h (nm)	PI
CXG/PDL 50:1	1247.55	0.95	254.89 ± 57.58	0.20
CXG/PDL 50:1+HCl (1 mM)	1289.78	0.93	254.89 ± 57.58	0.20
CXG/PDL 50:1+HCl (10 mM)	2482.09	0.68	n.a.	n.a.
CXG/PDL 50:1+HCl (15 mM)	1929.81	0.66	n.a.	n.a.
CXG/PDL 50:1+HCl (20 mM)	1234.54	0.61	n.a.	n.a.

A similar investigation was performed using polyethilenimine (PEI, MW= 800 Da) as polycation with a significantly lower molecular weight with respect to PDL (MW = 150-300 kDa).

Decay curves of CXG/PEI systems and the corresponding fitting parameters are reported in Fig. 5.13 and Tab. 5.7, respectively. DLS measurement of PEI is not shown because at the investigated concentrations it does not produce any scattered light due to its low molecular weight.

The addition of PEI to CXG solution causes a significant decrease of the average relaxation time accompanied by an increase of stretched coefficient with respect to CXG solution, corresponding to a decrease of the heterogeneity (or polydispersity) of the system.

The comparison among all the investigated CXG/PEI weigh ratios, reveals that increasing the content of PEI in the system, causes a slight increase of τ_c (not significant) as well as an increase of β, corresponding to objects in a narrower range of hydrodynamic sizes. In particular, hydrodynamic diameters of objects formed by CXG/PEI 50:1 and 25:1 are very similar, and they were estimated of about 108 nm and 105 nm, respectively.

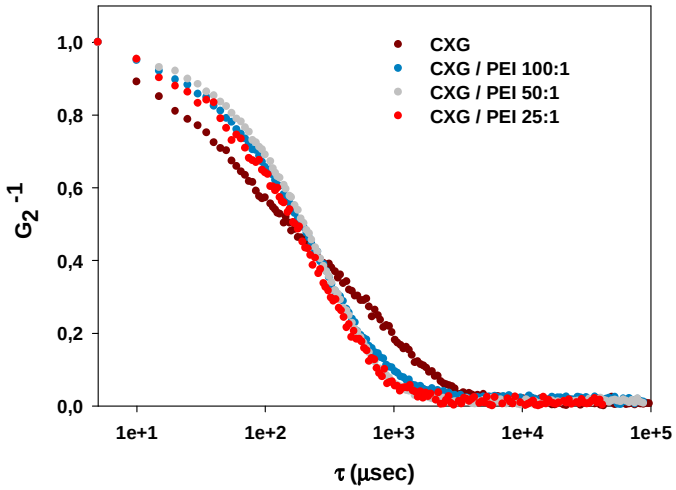

Fig. 5.13 Decay curves obtained by DLS measurements of CXG/PEI systems

Tab. 5.7 Fitting parameters of the decay curves reported in Fig. 5.14

System	τ_c	β	D_h (nm)	PI
CXG	1104.39	0.44	n.a.	n.a.
CXG/PEI 100:1	536.22	0.75	n.a.	n.a.
CXG/PEI 50:1	541.38	0.88	108.3 ± 38.5	0.50
CXG/PEI 25:1	572,60	0,88	105.8 ± 38.8	0.54

Finally, interactions between CXG and peptide amphiphile PA-H3 were studied. Decay curves of CXG, PA-H3 and CXG/PA-H3 system are reported in Fig. 5.14. PA-H3 is characterised by a low average relaxation time and a high stretched exponential that are related with a system containing objects in a narrow range of different hydrodynamic volumes (low polydispersity). In particular, the estimated apparent hydrodynamic diameter of PA-H3 assembled objects is of about 89 nm (see Tab. 5.8). The addition of a small amount of PA-H3 to CXG solution (CXG/PA-H3 100:1 weight ratio) provokes a very significant increase of the τ_c and an increase of β with respect to both CXG and PA-H3 (fitting parameters reported in Tab. 5.8) as effect of the interactions between CXG and the peptide amphiphile. The further increase of PA-H3 content (50:1 weight ratio) in the system causes the formation of an opalescent dispersion that was not analysable through DLS.

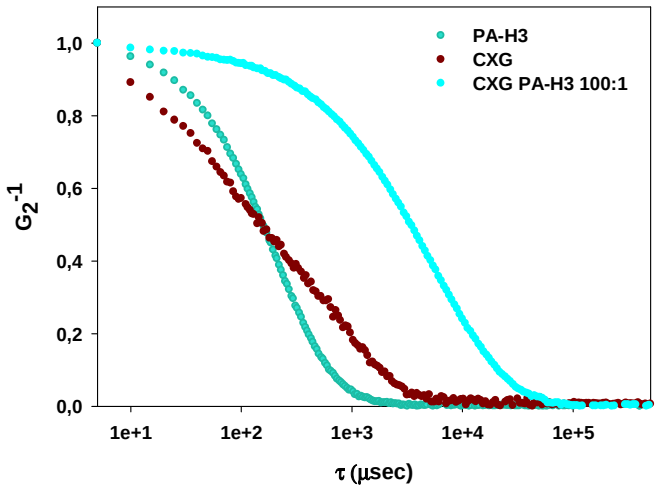

Fig. 5.14 Decay curves obtained by DLS of CXG/PA-H3 system

Tab. 5.8 Fitting parameters of the decay curves reported in Fig. 5.14

System	τ_c	β	D_h (nm)	PI
CXG	1104.39	0.44	n.a.	n.a.
PA-H3	459.47	0.88	83.9 ± 29.6	0.49
CXG/PA-H3 100:1	14,970.5	0.68	n.a.	n.a.

A comparison among all the analysed systems having the same CXG/polycation weight ratios (100:1) is provided in Fig. 5.15.

The three molecules PDL, PEI and PA-H3, due to their diverse molecular structures, molecular weights and assembly in solution, interact with CXG in a different way. From decay curves in Fig. 5.15, it is possible to argue that the interaction of CXG with the small and branched molecule of PEI form the smallest objects, followed by objects formed by CXG and PDL that have a bigger apparent hydrodynamic dimension and by the very big objects formed by CXG and PA-H3.

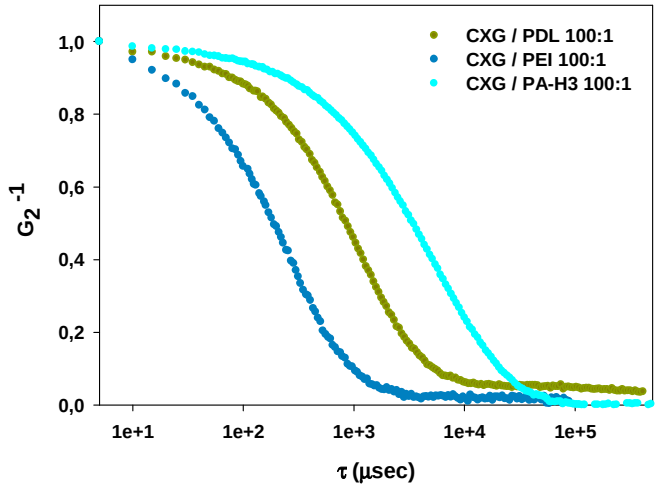

Fig. 5.15 Comparison of decay curves obtained by DLS of CXG/PDL, CXG/PEI and CXG/PA-H3 systems at 100:1 weight ratio

It is possible to hypothesize that PEI as small molecule can favour intramolecular "ionic crosslinking" points in CXG chains, resulting in very small objects. While PDL is a bigger linear molecule with a certain degree of flexibility and it can interpose between CXG chains inter- and intra-molecularly promoting a sort of "suture-line crosslinking" of CXG chains. On the other hand, the assembly of PA-H3 molecules in nanofibers exposing their multiple positive charges on their 3D nanostructure, can allow the "crosslinking" of more than two molecules on their surface resulting in significantly bigger objects. A pictorial representation of this hypothetic mechanism of interaction between CXG and the various polycations is presented in Fig. 5.16.

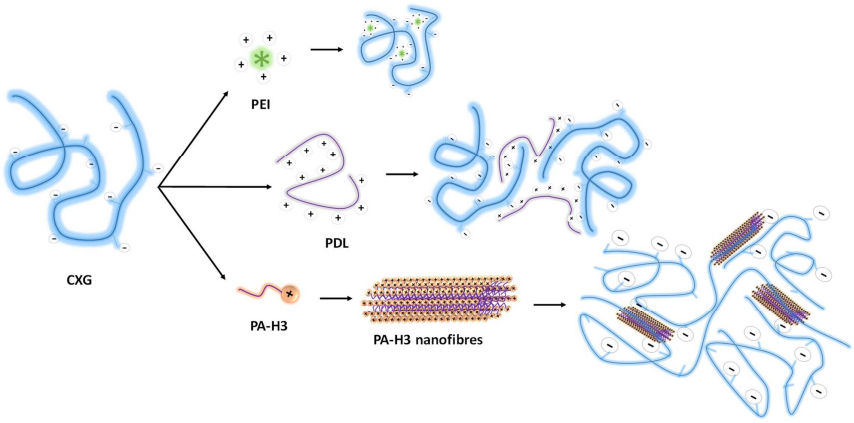

Fig. 5.16 Pictorial representation of the interactions between CXG and PEI, PDL or PA-H3 (all drawings are not in scale)

5.4. Conclusions

The overall results shown in this chapter demonstrate that xyloglucan extracted from Tamarind seeds was effectively carboxylated by the TEMPO-mediated oxidation reaction. It was found that after oxidation the molecular weight of CXG was significantly decreased and that properties, such as water solubility and thermal

stability, have been also altered resulting in an increase of solubility in water and a lowered thermal stability. Furthermore, the overall surface electrical charge of CXG chains in water resulted negative. CXG resulted non cytotoxic towards two different cell types, therefore suitable for the assembly of hybrid polymer matrices for tissue engineering. Preliminary study of the interactions between the negatively charged CXG and positively charged molecules (PEI, PDL and PA-H3) revealed the importance of electrostatic interactions for the formation of objects in solution in sub-micron scale of CXG and polycations. The interactions of CXG with these molecules was shown strongly affected by the nature of the polycation used. In particular, these results suggest that CXG is able to interact with oppositely charged small or macro-molecules as well as with self-assembled structures as the peptide amphiphile nanofibers.

Contribution

The author wishes to a highlight the contribution of Dr. Maria Antonietta Sabatino for GFC, SLS and carboxyl group titration measurements and for the support in the interpretation of all the reported results and Dr. Pasquale Picone for the MTS assay on adenocarcinomic human alveolar basal epithelial cells (A549).

References

[1] R. Manchanda, S.C. Arora, R. Manchanda, Tamarind Seed Polysaccharide and its Modifications- Versatile Pharmaceutical Excipients – A Review, Int. J. PharmaTech Res. 6 (2014) 412–420.

[2] P. Lang, G. Masci, M. Dentini, V. Crescenzi, D. Cooke, J. Gidley, C. Fanutti, J.S.G. Reid, Tamarind seed polysaccharide : preparation , characterisation and solution properties of carboxylated , sulphated and alkylaminated derivatives, Carbohydr. Polym. 17 (1992) 185–198. doi:10.1016/0144-8617(92)90003-9.

[3] H. Kaur, S. Yadav, M. Ahuja, N. Dilbaghi, Synthesis, characterization and evaluation of thiolated tamarind seed polysaccharide as a mucoadhesive polymer, Carbohydr. Polym. 90 (2012) 1543–1549. doi:10.1016/j.carbpol.2012.07.028.

[4] P. Goyal, V. Kumar, P. Sharma, Carboxymethylation of tamarind kernel powder, Carbohydr. Polym. 69 (2007) 251–255. doi:10.1016/j.carbpol.2006.10.001.

[5] I. Cumpstey, Chemical Modification of Polysaccharides, ISRN Org. Chem. 2013 (2013) 1–27. doi:10.1155/2013/417672.

[6] I. Shibata, A. Isogai, Depolymerization of cellouronic acid during TEMPO-mediated oxidation, Cellulose. 10 (2003) 151–158. doi:10.1023/A:1024051514026.

[7] V.C. Spier, M.R. Sierakowski, W.F. Reed, R.A. de Freitas, Polysaccharide depolymerization from TEMPO-catalysis: Effect of TEMPO concentration, Carbohydr. Polym. 170 (2017) 140–147. doi:10.1016/j.carbpol.2017.04.064.

[8] A.E.J. de Nooy, A.C. Besemer, H. van Bekkum, Highly selective tempo mediated oxidation of primary alcohol groups in polysaccharides, Recl. Des Trav. Chim. Des Pays-Bas. 113 (1994) 165–166. doi:10.1002/recl.19941130307.

[9] P.L. Bragd, H. van Bekkum, a C. Besemer, TEMPO-mediated oxidation of polysaccharides: survey of methods and applications, Top. Catal. 27 (2004) 49–66. doi:10.1023/B:TOCA.0000013540.69309.46.

[10] N. Lucyszyn, a. F. Lubambo, K.F. Matos, I. Marvilla, C.F. Souza, M.R. Sierakowski, Specific modification of xyloglucan from Hymenaea courbaril seeds, Mater. Sci. Eng. C. 29 (2009) 552–558.

doi:10.1016/j.msec.2008.10.001.

[11] E.F.L.J. Anet, 3-Deoxyglycosuloses (3-Deoxyglycosones) And The Degradation Of Carbohydrates, 1 (1965) 837–844.

[12] R. Tanaka, T. Saito, A. Isogai, Cellulose nanofibrils prepared from softwood cellulose by TEMPO/NaClO/NaClO2 systems in water at pH 4.8 or 6.8, Int. J. Biol. Macromol. 51 (2012) 228–234. doi:10.1016/j.ijbiomac.2012.05.016.

[13] R. Hiraoki, Y. Ono, T. Saito, A. Isogai, Molecular mass and molecular-mass distribution of TEMPO-oxidized celluloses and TEMPO-oxidized cellulose nanofibrils, Biomacromolecules. 16 (2015) 675–681. doi:10.1021/bm501857c.

[14] C.N. Sakakibara, M.R. Sierakowski, N. Lucyszyn, R.A. de Freitas, TEMPO-mediated oxidation on galactomannan: Gal/Man ratio and chain flexibility dependence, Carbohydr. Polym. 153 (2016) 371–378. doi:10.1016/j.carbpol.2016.07.114.

[15] J.J. Kochumalayil, Q. Zhou, W. Kasai, L.A. Berglund, Regioselective modification of a xyloglucan hemicellulose for high-performance biopolymer barrier films, Carbohydr. Polym. 93 (2013) 466–472. doi:10.1016/j.carbpol.2012.12.041.

[16] N. Stephanopoulos, J.H. Ortony, S.I. Stupp, Self-assembly for the synthesis of functional biomaterials, Acta Mater. 61 (2013) 912–930. doi:10.1016/j.actamat.2012.10.046.

[17] D.S. Ferreira, Y.A. Lin, H. Cui, J.A. Hubbell, R.L. Reis, H.S. Azevedo, Molecularly engineered self-assembling membranes for cell-mediated degradation, Adv. Healthc. Mater. 4 (2015) 602–612. doi:10.1002/adhm.201400586.

[18] R.M. Capito, H.S. Azevedo, Y.S. Velichko, A. Mata, S.I. Stupp, Self-Assembly of Large and Small Molecules into Hierarchically Ordered Sacs and Membranes, Science. 319 (2008) 1812–1816. doi:10.1126/science.1154622.

[19] K.E. Inostroza-brito, E. Collin, O. Siton-mendelson, K.H. Smith, A. Monge-marcet, D.S. Ferreira, R.P. Rodríguez, M. Alonso, J.C. Rodríguez-cabello, R.L. Reis, F. Sagués, L. Botto, R. Bitton, H.S. Azevedo, A. Mata, Co-assembly, spatiotemporal control and morphogenesis of a hybrid protein–peptide system, Nat. Chem. (2015) 1–8. doi:10.1038/nchem.2349.

[20] B.H. Zimm, The Scattering of Light and the Radial Distribution Function of High Polymer Solutions, J. Chem. Phys. 16 (1948) 1093–1099. doi:10.1063/1.1746738.

[21] D.E. Koppel, Analysis of Macromolecular Polydispersity in Intensity Correlation Spectroscopy: The Method of Cumulants, J. Chem. Phys. 57 (1972) 4814–4820. doi:10.1063/1.1678153.

[22] A. Mishra, A.V. Malhotra, Graft copolymers of xyloglucan and methyl methacrylate, Carbohydr. Polym. 87 (2012) 1899–1904. doi:10.1016/j.carbpol.2011.09.068.

[23] D. da Silva Perez, S. Montanari, M.R. Vignon, TEMPO-mediated oxidation of cellulose III, Biomacromolecules. 4 (2003) 1417–1425. doi:10.1021/bm034144s.

[24] K. Khounvilay, W. Sittikijyothin, Rheological behaviour of tamarind seed gum in aqueous solutions, Food Hydrocoll. 26 (2012) 334–338. doi:10.1016/j.foodhyd.2011.03.019.

[25] E.M. Bergstr̈m, L. Salmén, J. Kochumalayil, L. Berglund, Plasticized

xyloglucan for improved toughness-Thermal and mechanical behaviour, Carbohydr. Polym. 87 (2012) 2532–2537. doi:10.1016/j.carbpol.2011.11.024.

[26] P.R. Sharma, A.J. Varma, Thermal stability of cellulose and their nanoparticles: Effect of incremental increases in carboxyl and aldehyde groups, Carbohydr. Polym. 114 (2014) 339–343. doi:10.1016/j.carbpol.2014.08.032.

[27] R.A. Freitas, S. Martin, R.C. Paula, J.P.A. Feitosa, M.R. Sierakowskid, Effect of the oxidation level on the thermogravimetric kinetics of an oxidized galactoxyloglucan from Hymenaea courbaril (Jatobà) seeds, Thermochim. Acta. 409 (2004) 41–47. doi:10.1016/S0040-6031(03)00326-5.

[28] T. Hatakeyama, K. Nakamura, H. Hatakeyama, Determination of Bound Water Content in Polymers by DTA,DSC and TG, Thermochim. Acta Elsevier Sci. Publ. B.V. 123 (1988) 153–161.

6. Carboxylated xyloglucan-peptide amphiphile co-assembled scaffolds for wound healing

6.1. Introduction and aim

The term self-assembly refers to a spontaneous phenomenon that literary means ‘to put together or build’ (assembly) ‘without outside help or on its own’ (self). [1] Self-assembly of single molecules into supramolecular structures is driven by non-covalent interactions, namely hydrogen bonds, ionic bonds, hydrophobic interactions, van der Waals interactions, and water-mediated hydrogen bonds. These interactions can be relatively weak in isolation, but, when combined together, they give rise to very stable constructs.[2]

The simplest self-assembly systems are nano-sized materials composed of small molecules aggregated through short range interactions into supramolecular objects such as clusters of molecules,[3] ribbons,[4] tubes,[5] helices.[6]

More complex systems, as observed in biology, achieve higher levels of self-organization and form hierarchical structures. Indeed, biopolymers such as polypeptides, nucleic acids and polysaccharides are all capable to self-associate in structures of different levels of complexity.[7]

Self-assembly can be either static or dynamic. Static self-assembly involves systems that reach a global or local equilibrium state, like molecular crystals or folded proteins, and do not dissipate energy. In this case, the formation of the ordered structure may require energy at the beginning, but once the structure is formed, it remains stable. In dynamic self-assembly building blocks operate far from equilibrium and the interactions responsible for the formation of structures or patterns between components only occur if the system is dissipating energy. Any living organism is a perfect example of dynamic self-assembly.[8]

Co-assembly is a specific self-assembly mechanism that can be either static or dynamic and that occurs when different building blocks assemble simultaneously, leading to a synergic architecture, that could not be achieved by the isolated self-

assembly of either building block. Co-assembly offers the opportunity to incorporate multiple relevant molecules while generating new properties that go beyond the individual components and in particular the formation of novel hybrid materials exhibiting new architectures, higher and tunable mechanical properties, higher stability, and improved bio-functionality.[1]

Supramolecular self-assembly has gained in the last two decades increasing interest as powerful approach for fabricating novel supramolecular architectures for regenerative medicine, such as non-invasive, injectable scaffolds that are functionalised to be bioactive or used as delivery vehicle for cell therapies.[9,10]
A broad range of self-assembling systems have been explored as biomaterials for the fabrication of those scaffolds, either for healing existing damaged tissues in the body or to provide a favourable environment for externally transplanted components like stem cells.[11–13]
The use of biological components (i.e. peptides, proteins, polysaccharides) for self-assembly offers the additional benefit of high compatibility and low cellular toxicity, and are usually biodegradable and easily cleared from the body, allowing for "traceless" scaffolds.[2] However, the use of natural components for the fabrication of self-assembly materials has been hampered by the difficulty in controlling their conformation and nanoscale assembly with the precision required to form well-organized constructs with predictable structure and properties. This limitation has driven the development of simpler and more predictable peptide-based molecules such as peptide amphiphile (PA).[12]

PA molecules are naturally inspired and generally composed of four key structural features: (i) the first segment is a hydrophobic domain, typically consists of a long, traditionally saturated, alkyl tail; (ii) a second segment, immediately adjacent to the tail, consists of a short peptide sequence that promotes hydrogen bonding and the formation of intermolecular β-sheets secondary structures; (iii) a third segment

typically contains acidic or basic amino acids to provide charge and enhance solubility in water; and (iv) the fourth optional segment at the terminus opposite the hydrophobic tail is used to integrate within the molecule a bioactive signal, which may consist of an epitope to interact with cell receptors, a segment that binds proteins or biomolecules, or a pharmacological agent.[7,14]

The mechanism of PA self-assembly has been attributed to at least three energy contributions: hydrophobic interactions of the alkyl tails, hydrogen bonding among the middle peptide segments, and electrostatic repulsions between the charged amino acids. The first two are attractive forces that tend to promote the aggregation of PA molecules, whereas electrostatic repulsions from the charged components favour disassociation of PA molecules. The final assembly into high aspect ratio nanofibers reflects a delicate balance of each of these energy contributions (Fig. 6.1).[15]

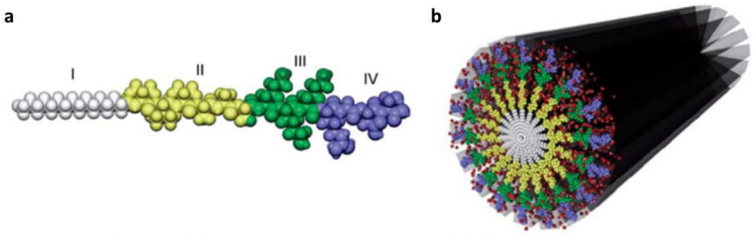

Fig. 6.1 Schematic representation of a peptide amphiphile (PA) molecule (a) and its assembly in nanofiber (b); figure adapted from Stupp et al.[7]

A canonical PA nanofiber is 6–12 nm in diameter depending on the PA sequence and up to several microns in length. Typical PA nanofibers are highly charged, which helps with solubility in water. Screening of PA nanofibers charges with ions, primarily divalent or higher valency, or reducing charge density through changes in pH results in the formation of viscous liquids or gels.[16]

When the bioactive epitope is incorporated in PA molecule, a useful strategy to guarantee spacing of epitopes for optimal recognition by proteins or receptors is the

mixing of an epitope-presenting PA with a shorter PA without the epitope, used as diluent molecule, which would allow the bioactive signal to be displayed protruding from the fibre surface. Such a strategy has been used to optimize RGDS epitope spacing and maximize cell adhesion to PA nanofibers.[11]

PAs can easily interact with several biologically active molecules, such as polyelectrolytes or proteins, thus enabling the design of well-defined and hierarchically ordered self-assembled structures exhibiting multifunctionalities.[15] The range of molecules used in co-assembly with PAs includes both proteins[17] and polysaccharides.[18–20] In particular, hyaluronic acid (HA) has been the most widely used polysaccharide to co-assemble with PAs.[13,18,21] This polysaccharide was shown able to co-assemble with PA in a broad range of different structures, such as sacs or membranes addressed to tissue engineering applications.[13] Co-assembled systems including PA can be also addressed to skin regeneration. For instance, co-assembled 2D membranes incorporating HA as a structural component of the skin extracellular matrix (ECM), and peptide amphiphiles presenting RGDS as biochemical signals to promote cell adhesion, have been proposed to mimic the skin tissue microenvironment.[22]
More recently, also alginate (Alg) has been reported to co-assemble with PAs and in particular to form multi-layered biomaterials for cell culture[19] and core-shell microparticles as targeted drug delivery system.[20]
In all the above mentioned reports it has been demonstrated that strong electrostatic interactions are the driving force of the co-assembly in interfacial systems.[17,23]

In this work, electrostatic interactions between functionalised XG variant (described in Chapter 5) and various peptide amphiphile molecules were exploited to obtain co-assembled hydrogels with the desired morphology.
In particular, co-assembly was aimed to the development of xyloglucan-based fibrous scaffolds for wound healing applications.

The fibrous microstructure is considered particularly interesting in the design of wound healing scaffolds, because of its efficiency to promote nutrients exchange and metabolic waste elimination.[24]

To achieve this goal, the ideal conditions for the co-assembly of these two building blocks were investigated. A PA sequence that co-assemble with CXG was identified among a selection of PA molecules synthesized for the scope.

Interactions between the two building blocks were characterized through different techniques (i.e. circular dichroism spectroscopy, IR spectroscopy, dynamic mechanical analysis, transmission and scanning electron microscopy,).

Biological *in vitro* evaluations were performed in order to evaluate the suitability of the co-assembled gel for tissue engineering applications, with a specific focus on wound healing.

Preliminary *in vivo* wound closure experiments using wild-type mouse model were performed in order to assess an eventual enhancement of the wound healing process. Because biological processes associated with wound healing are not fully clarified, the treatment of chronic wounds may require additional biological signals that should instruct cells to regenerate the tissue.[25]

For this reason, the incorporation of a bioactive epitope to the selected PA molecule that co-assemble with CXG is the ultimate goal in order to add bioactivity to the obtained scaffold.

QHREDGS peptide sequence was chosen as bioactive epitope suitable for wound healing. This sequence is an integrin-binding sequence from angiopoietin-1 and it has been reported to have effect on the treatment of chronic wound.[26] This epitope has also been extensively investigated for other regeneration medicine purposes such as angiogenesis, osteoblast differentiation, and for the treatment of myocardial infarction.[27,28] The effect of QHREDGS peptide in wound healing was to promoted keratinocyte adhesion and collective migration *in vitro*, as well as effect against H_2O_2 stress which is generally present in the wound site. Radisic et al. also tested the QHREDGS peptide immobilized to a chitosan–collagen hydrogel *in vivo*

on diabetic mice, reporting that the diabetic wound healing was accelerated by enhanced re-epithelialization and granulation tissue formation in presence of this small peptide.[26]

For this reason, a variant of the selected PA sequence including QHREDGS bioactive epitope to enhance wound healing in chronic wounds was synthesised and preliminarily characterised for its future incorporation in CXG/PA systems.

6.2. Materials and methods

6.2.1. Materials

Xyloglucan (XG) was purchased from Megazyme International (Ireland) (see Appendix A.4.1).

All the Fmoc-protected amino acids and rink amide resin were purchased from Novabiochem (USA). 1-Hydroxybenzotriazole hydrate (HOBT) and N,N′-diisopropylcarbodiimide (DIC) from Sigma Aldrich. Polydimethylsiloxane (PDMS) was prepared using SYLGARD® 184 kit from Sigma-Aldrich (see Appendix A.1.4).

6.2.2. Methods

Precursors of synthesis

Carboxylated-XG (CXG) was synthesized as described in Appendix A.1.2 and discussed in Chapter 5.

Peptide amphiphiles (PA) sequences synthesized and used in this study are reported in Tab. 6.1.

Tab. 6.1 PA sequences synthetized and tested for the co-assembly with CXG

	Nomenclature	Sequence
Positively Charged	PA-K2	C_{16}-$(Val)_3$ $Ala)_3(Lys)_2$
	PA-K3	C_{16}-$(Val)_3$ $(Ala)_3(Lys)_3$
	PA-K4	C_{16}-$(Val)_3$ $(Ala)_3(Lys)_4$
	PA-H2	C_{16}-$(Val)_3$ $(Ala)_3(His)_2$
	PA-H3	C_{16}-$(Val)_3$ $(Ala)_3$ $(His)_3$
	PA-H3$_{bio}$	C_{16}-$(Val)_{3(}Ala)_3(His)_3(Gly)_3$(Arg)(Glu)(Asp)(Gly)(Ser)
Negatively Charged	PA-E3	C_{16}-$(Val)_{3(}Ala)_3(Glu)_2$

All PA were synthesized by solid-phase peptide synthesis using standard fluoren-9-ylmethoxycarbonyl (Fmoc) chemistry on rink amide resin and purified using a preparative HPLC with an acetonitrile/water gradient containing 0.1%vol of trifluoroacetic acid. The PAs used for this work have a degree of purity of about 98%wt. Synthesis and purification procedures are described in detail in Appendix A. 1.3.

Molecular structures of two representative PA sequences among the ones tested are reported in Fig. 6.2 and in particular they are PA-K3 (Fig. 6.2a) and PA-H3 (Fig. 6.2b).

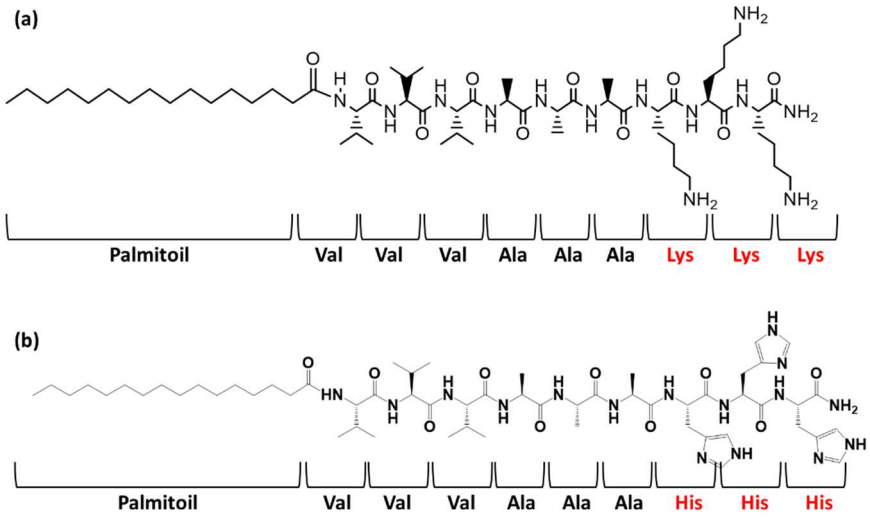

Fig. 6.2 Molecular structure of PA-K3 (a) and PA-H3 (b) as representative peptide amphiphile sequences among the ones synthesised and used in this chapter

Gel preparation

For a preliminary screening carboxy-xyloglucan (CXG) gels with all the PA sequences reported in Tab. 6.1 were prepared starting from CXG and PA solutions at 1 %wt in isotonic HEPES buffer.

The gels were obtained by injection of PA solution into CXG solution deposited on PDMS coated surface (see Appendix A.1.4) and were equilibrated at 28 ºC and relative humidity (RH) 38% for 24h.

Gels with the selected PA (PA-H3) were prepared starting from CXG and PA solutions at 1 %wt in isotonic HEPES buffer and using the same method of injection of PA-H3 into CXG solution on PDMS coated surface. CXG and PA-H3 solutions in HEPES buffer were at pH 8 and 4.5, respectively. For the characterisations, different variants of gels were prepared at different volume ratios between CXG and PA-H3 solutions both at 1 %wt, namely CXG/PA-H3 = 1:1, 2:1, 3:1 and 5:1 (also named in this chapter CXG_PA-H3 1:1, CXG_PA-H3 2:1, CXG_PA-H3 3:1 and CXG_PA-H3 5:1). Compositions of the gels that were used in this work are reported in Tab. 6.2.

Final concentration of the solid content is equal for all the samples (1 %wt), and weights ratios of CXG and PA-H3 are 1:1, 2:1, 3:1 and 5:1. The gel formation was visually captured using a Leica MZ 12-5 microscope (10x).

Tab. 6.2 composition of CXG/PA-H3 gels

Sample	CXG %wt	PA-H3 %wt	Solid content %wt in the gel
CXG_PA-H3 1:1	0.5 %wt	0.5 %wt	1 %wt
CXG_PA-H3 2:1	0.66 %wt	0.33 %wt	1 %wt
CXG_PA-H3 3:1	0.75 %wt	0.25 %wt	1 %wt
CXG_PA-H3 5:1	0.83 %wt	0.16 %wt	1 %wt

ζ-Potential

ζ-potential measurements of CXG and PA-H3 0.01 %wt solutions, were performed in MilliQ water at pH from 4 to 8 (adjusted by addition of small volumes of NaOH (1M) or HCl (1M)) and at a temperature of 20 °C. Results were averaged on three measurements. Details on the instrumentation used are discussed in Appendix A.2.10.

CD spectroscopy

CXG and PA-H3 solutions for CD analysis were prepared in isotonic 10mM HEPES buffer at 0.01 %wt. Mixtures were prepared mixing CXG and PA-H3 0.01 %wt HEPES solutions at different volume ratios 1:1, 2:1, 3:1 and 5:1, so that the systems reflect the composition in the gels but 100 times more diluted.

These mixtures were incubated 15 min before the measurement. Spectra were acquired in a range of wavelengths between 190-260 nm with a step size of 0.5 nm. Absorbance values of all the samples in the investigated range of wavelengths were all assessed below 1. Other details are discussed in Appendix A.2.11.

Fourier-Transform Infrared (FTIR) spectroscopy

For the FTIR measurements, CXG_PA-H3 1:1, 2:1, 3:1 and 5:1 gels were washed with MilliQ water, frozen in liquid nitrogen and freeze-dried. The freeze-dried gels were then mashed and diluted to about 2 %wt concentration in dehydrated KBr for the preparation of the tablets (see Appendix A.2.3).

Transmission electron microscopy (TEM)

Precursors solutions of CXG, PA-H3, hyaluronic acid (HA) and PA-E3 used to prepared TEM samples were all prepared at 0.05 %wt in isotonic 10mM HEPES and mixed at different volume ratios: i.e. CXG_PA-H3 at 1:1, 2:1, 3:1 and 5:1, HA_PA-H3 at 3:1, and CXG_PA-E3 at 1:1. Preparation of the samples grids for TEM is discussed in Appendix A.2.12.

Scanning electron microscopy (SEM)

Pre-formed CXG_PA-H3 1:1, 2:1, 3:1 and 5:1 gels were washed with MilliQ water to remove salts, frozen in liquid nitrogen and freeze-dried. Samples were coated with a gold layer before to image fracture surface morphologies of the gels. Other details are described in Appendix A.2.5.

Rheology

A TA Instruments AR-G2 rheometer was used to perform the measurements on all the pre-formed CXG_PA-H3 1:1, 2:1, 3:1 and 5:1 gels. A parallel plate geometry with 8 mm diameter was used for all measurements. The gels were placed carefully in the headspace with a spatula, and the geometry was then lowered to the pre-set 250 µm gap. Oscillatory frequency sweeps were performed in a range of angular frequencies between 1 and 100 rad/sec, using a fixed strain of 0.5 % and at 25 °C. The strain value was chosen within the linear viscoelastic region of the systems, previously determined by strain sweep tests performed at 1 Hz frequency. A gel of PA-H3 in PBS with the same solid content of the gels was used for comparison.

Compression test

CXG_PA-H3 1:1, 2:1, 3:1 and 5:1 gels, were used for the compression tests (Instron 5967 Tensile & Compression tester). The tests were carried out in culture media. A preload of 0.0005 N was used to contact the sample and determine the gauge length. The samples were compressed to 20 % strain at 1% per second and then held for 120 s. Videos of the compression test were used to obtain the gel area. The gel shape was approximated to a sphere. 1 %wt agarose sphere gels were used for comparison. A gel pf PA-H3 in PBS with the same solid content of the gels was used for comparison. Compression moduli reported are averaged on 8 measurements per type of sample.

Biological assessment

Cell culture description is provided in Appendix A.3.1.

Cell viability

For cell viability on top of gels, HaCat cells were seeded on the gels ($10*10^3$ cells, 96 well plate). After seeding, the samples were put under agitation for 30 min at 200 rpm and then maintained in a humidified 5% CO_2 atmosphere at 37 °C for a maximum period of 7 days. After 2 and 7 days, respectively, cells were stained with LIVE/DEAD® ThermoFisher assay (see Appendix A.3.3) for 30 minutes before analysis with a confocal microscope Confocal Laser Scanning Microscope (CLSM) (Leica Laser Scanning Confocal TCS SP2).

Cells encapsulation

For encapsulation of HaCat within CXG_PA-H3 gels, cells were suspended in a 1 %wt PA-H3 solution. Gels were rapidly formed in a 96-well plate by injection of PA-H3 solution containing $10*10^3$ cells into 1%wt CXG solution to form the gels. After 10 minutes, complete medium was added onto the gels. The constructs were maintained at 37 °C under 5 % CO_2 for 7 days with medium changes every two days. The cells were stained with LIVE/DEAD® staining (see Appendix A.3.3) after 2 and

7 days of culture, as described previously, and incubated for 30 min before the confocal analysis using a Confocal Laser Scanning Microscope (CLSM) (Leica Laser Scanning Confocal TCS SP2).

Cells attachment

For the cell attachment assay, HaCat cells were seeded in serum-free medium on top of the gels. After seeding, the samples were put under agitation for 30 min at 100 rpm at 37 °C and then maintained in static condition in a humidified 5% CO_2 atmosphere at 37 °C for 4h in serum free medium in order to allow cell attachment on gels surfaces without the influence of the proteins present on the serum. After 4h, serum-free medium was replaced with fresh complete medium. Samples were maintained in static condition in a humidified 5% CO_2 atmosphere at 37 °C ± 0.1 °C for 24h. Cells were then fixed using a 4 %wt paraformaldehyde (PFA) solution for 1h at room temperature. Samples were washed after fixation three times with PBS and stored in PBS at 4 °C until analysis. Before confocal analysis, samples were treated with DAPI at a 1/1000 dilution (nuclei staining) and with phalloidin 555 at a 1/1000 dilution (cytoskeleton staining). Details of the staining protocol are reported in Appendix A.3.4. Images of the cells were then acquired using a Confocal Laser Scanning Microscope (CLSM) (Leica Laser Scanning Confocal TCS SP2).

Scratch test

Effect of gels on HaCat cell migration was investigated by forming a scratch on a monolayer of cells. For this test, HaCat cells were marked with CM-Dil cell tracker (ThermoFisher sci.). Cells were incubated for 15 min with the cell tracker at a concentration of 4µM before trypsinisation. HaCat monolayers were then grown at $30*10^3$ cells/cm² and incubated until 98% confluence was reached. Complete medium was discarded, and cells were washed with HBSS solution (ThermoFisher sci.). A defined area was scratched with a pipette tip through the monolayer and the detached cells were gently washed away again with HBSS solution. Gels were carefully placed

on top of the scratch and gently pressed to have a good contact with the scratched area. Either complete medium or serum-free medium were then added. Monolayers were treated or not with 5µg/mL mitomycin C to inhibit the closure of the monolayer as a result of proliferation.

The images of the scratched area a t_0 i.e. scratched area before the placement of gels and at t_{24h} were acquired using Confocal Laser Scanning Microscope (CLSM) (Leica Laser Scanning Confocal TCS SP2). The size of the scratched area was calculated using ImageJ software (http://imagej.nih.gov/ij) (NIH, USA). Percentage of closure was estimated as described in Appendix A.3.5.

In vivo wound closure

Ten-week-old male CD1 mice were anesthetized by isofluorane inhalation, and the dorsal skin was shaved and sterilized with an alcohol swab. Two full-thickness circular 5 mm biopsy punch excisions (surface area of 19.63 mm^2) were made using a biopsy punch. The wounds were made approximately 1 cm apart on the dorsum of mice and left to heal by secondary intention. Wounds were left untreated or had a hydrogel added to the wound bed. The hydrogels were UV irradiated prior to application. The wounds were covered by Tegaderm (3M) transparent wound dressing, which was secured at the edges by Vetbond Tissue Adhesive (3M). Mice received a single intramuscular injection of analgesic immediately following surgery. Following the surgery, mice were housed individually with access to food and water ad libitum. Wounds were collected at day eight post-wounding. The horizontal and vertical diameters of the wounds were measured to permit calculation of the wound area. Wounds were excised and bisected using a scalpel. Half of each wound was snap frozen in liquid nitrogen and the other half was fixed in 10% Neutral Buffered Formalin for 24 hours followed by storage in 70% ethanol to permit histological analysis at a later time point. Other in-depth information are provided in Appendix A.3.6.

6.3. Results and discussion

6.3.1. Gel formation and characterisations

Peptide amphiphiles (PA) and carboxy-xyloglucan (CXG) were used as building blocks for the formation of co-assembled fibrous networks to be evaluated as scaffolds for wound healing applications.

A modified version of xyloglucan has been obtained through a TEMPO-mediated oxidation reaction in order to insert carboxyl groups in the polymer chain as ionisable functional groups that can promote electrostatic interactions with oppositely charged molecules. The XG carboxylation reaction and the properties of CXG have been already discussed in Chapter 5.

The PA molecule suitable to co-assemble with CXG was chosen among a range of different sequences, all characterised by three features: (i) the hydrophobic palmitoil tail, (ii) the β-sheet forming motif (-$(Val)_3(Ala)_3$-), and (iii) an ionisable amino acid sequence. In particular, the sequences tested have the same palmitoil tail and the β-sheet forming sequence and differ for the ionisable amino acid sequence. They were combined with CXG and incubated for 24h. HEPES buffer was chosen for the preparation of the CXG and PA precursors solutions, because it is a cell-friendly buffer that does not induce gelation of PAs.

ζ-potentials in HEPES buffer of the tested PA sequences are reported in Tab. 6.3.

Tab. 6.3 ζ-potentials values of the tested PA sequences in HEPES buffer at pH 7.4

Name	**ζ potential (mV)**
PA-K2	+38,12 ± 1,36
PA-K3	+34,77 ± 0,75
PA-K4	+35,62 ± 1,10
PA-H2	+8,8 ± 1,36
PA-H3	+15,9 ± 0,48
PA-E3	-29,94 ± 0,84

The selection of the suitable PA sequence as well as of the method to co-assemble CXG and PA were made on the basis of the visual assessment of structural integrity, uniformity and resilience of the obtained gels.

To establish a reproducible method of co-assembly, different methodologies were tried: (i) side-by-side contact of the CXG and PA solutions; (ii) dropping PA solution on top of the CXG solution or vice versa; and (iii) injecting the PA solution inside CXG solution and vice versa (Fig. 6.3). The first method leads to a membrane-like structure at the interface between the two components but not very uniform, while the second method leads to the formation of a donut-like structure. The third method leads to a uniform sphere-like gel, that is a preferred shape for this study.
Furthermore, it was observed that the formation of gels obtained by injection of PA inside CXG was much more reproducible than the injection of CXG inside PA and thus this approach was adopted for this work.

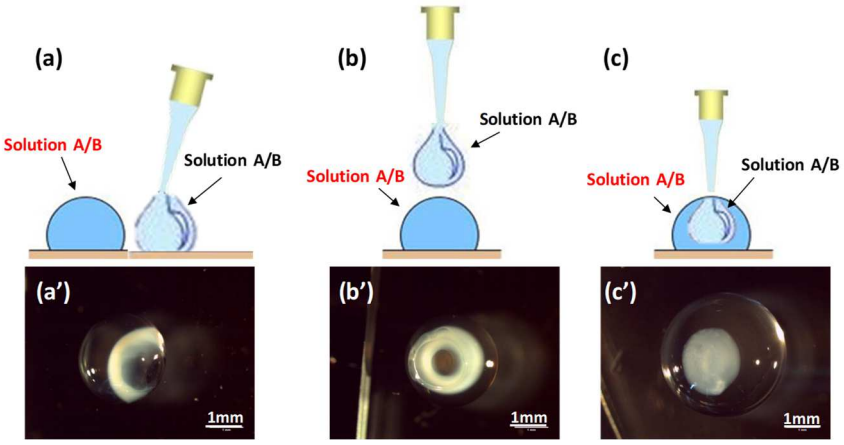

Fig. 6.3 Schematic representation of different co-assembly methodologies and pictures of the corresponding representative gel structures: side-by-side contact of the two solutions (a, a'); one solution drop above the other (b, b'); injection of one solution drop inside the other (c, c')

The chosen method of co-assembly was employed for the identification of the most suitable PA sequence, among all the sequences reported in Tab. 6.1, that co-assemble with CXG forming uniform and resilient constructs. Pictures of the obtained CXG/PA systems are reported in Fig. 6.4.

As expected, the use of the negatively charged PA-E3 reveals no visible interaction with CXG (Fig. 6.4a). All the positively charged PAs result in opaque constructs, more or less dense depending on the PA sequence used (Fig. 6.4b-f). In particular, both PA-H2 (Fig. 6.4e) and PA-H3 (Fig. 6.4f) form compact constructs, that are more uniform and resilient for PA-H3. For this reason, PA-H3 was selected for further characterisations.

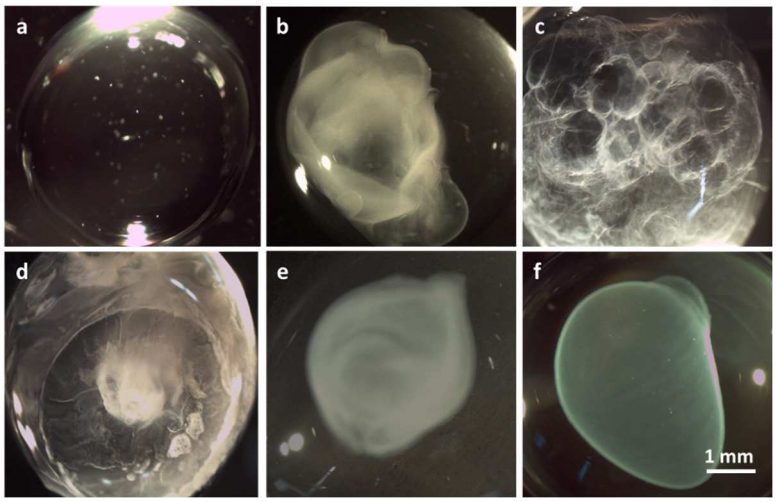

Fig. 6.4 Microscopy images showing the interaction between CXG and PA-E3 (a), PA-K2 (b), PA-K3 (c), PA-K4 (d), PA-H2 (e) and PA-H3 (f)

To the best of my knowledge the PA-H3 sequence has never been reported in the literature and never been used in co-assembly with polysaccharides. The sequence was proven cytocompatible thanks to a study conducted by Matagroup at Queen Mary University of London, that revealed that among all the sequences tested in this work, PA-H3 shows the best cytocompatibility (E.Collin et al., unpublished results). In the design of PA-H3, the β-sheet forming sequence was included to promote the assembly in nanofibers, as in the others studied PAs, and was also proven to be able to form gels in presence of PBS. This phenomenon, also reported for other PA sequences, has been attributed to the screening of the PA nanofiber surface charges by the buffer ions and/or by deprotonation as a result of the change of pH, thus resulting in nanofiber aggregation and gel formation.[7]

Electrostatic forces are needed in co-assembly and are believed the driving forces of the assembly in interfacial systems.[17] The electrical charges of polyelectrolytes are related with the degree of protonation or deprotonation of their ionisable groups, and

thus they are influenced by the pH. For this reason, the ζ-potential of the two building blocks was measured at different pHs. The ζ-potential values reported in Tab. 6.4, show that CXG surface charge is negative at neutral and alkaline pH (ca. -28 mV at pH 8), while PA-H3 is more markedly positive at pH acidic pH (ca. +43 mV at pH 4).

Tab. 6.4 ζ-potentials of CXG and PA-H3 in MilliQ water

Z-potentials (mV)						
Medium	**pH**	**4**	**5**	**6**	**7**	**8**
MilliQ water	**CXG**	-16.54 ± 1.5	-17.56 ± 1.4	-21.8 ± 0.6	-26.4 ± 1.7	-27.7 ± 1.2
	PA-H3	+42.9 ± 1.5	+46.0 ± 1.45	+7.2 ± 0.5	-12.01 ± 0.6	-13.2 ± 0.5

The influence of pH of the polymer solutions on the structural integrity of CXG/PA-H3 gels was investigated also by visual inspection (Fig. 6.5). Gels obtained from the co-assembly of PA-H3 solution at pH 4 or 5 and CXG solution at pH 7 or 8 resulted compact and resilient, while looser gels were obtained from PA-H3 solution at pH 6, 7 or 8 and CXG solution at pH 4, 5 or 6. As expected, the pH conditions that lead to the more compact gel were also those in which the ζ-potentials of CXG and PA-H3 in absolute value, were higher. This result confirms the important role of electrostatic interactions in the co-assembly. As observed in others co-assembled systems stronger constructs are obtained from strongly oppositely charge building blocks.[17,18]
On the basis of these results, HEPES buffer solutions of CXG at pH between 7 and 8 and PA-H3 at pH between 4 and 5 were used.

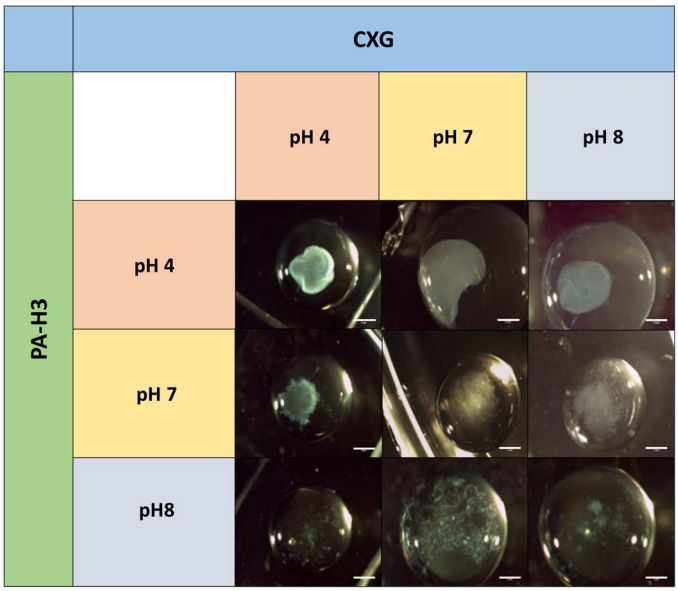

Fig. 6.5 Table reporting co-assembled structures of CXG and PA-H3 both prepared in HEPES buffer at different pHs (scale bar 1 mm)

The interaction between CXG and PA-H3, when are both prepared in HEPES buffer, and the PA-H3 solution is injected into the CXG solution, is very rapid at the interface but long times are required for the gel to reach its final "stable" condition (Fig. 6.6a). A construct forms immediately after the introduction of the PA-H3 solution into the CXG drop, but is very fragile and gradually evolves into a resilient and tough gel, reaching full maturation after 24h of incubation (28°C and 38% RH).

The interaction between CXG and PA-H3 was observed inside a PDMS channel (Fig. 6.6b). After the deposition of PA-H3 solution on one side of the channel, CXG solution was pipetted on the opposite side until it was in contact with the PA solution. Due to the different method of co-assembly, in this case a membrane is obtained at the interface of the two building blocks instead of a sphere-like gel, as described above (see Fig. 6.3a). As observed in the sphere-like construct, this membrane is immediately formed and it grows over time (Fig. 6.6b).

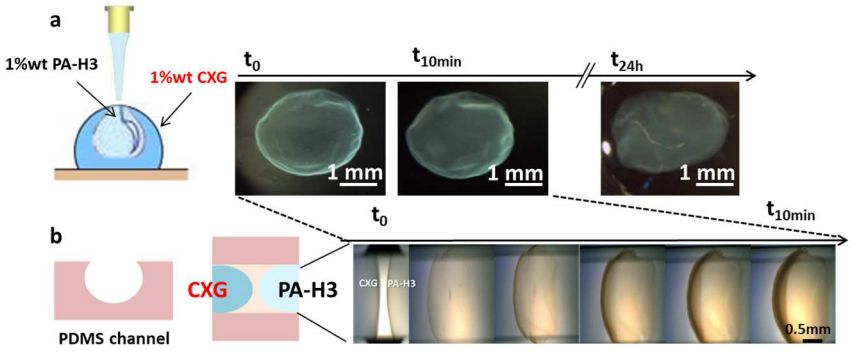

Fig. 6.6 Optical microscopy images of interaction of CXG and PA-H3 after injection of PA-H3 into CXG solution and follow up over time (a); CXG and PA-H3 solutions in contact inside a PDMS channel with a diameter of 3 mm (b)

Following these first assessments, CD was performed in order to investigate how the secondary structure of PA-H3 is affected by the interaction with CXG. In Fig. 6.7a-d the CD spectra of CXG_PA-H3 mixtures are reported. Since the concentration of PA-H3 in the various mixtures is different, each spectrum is compared with the spectrum of the corresponding PA-H3 system at the same concentration than in the mixtures.

CXG does not have a chromophore that absorbs in the 200 – 260 nm wavelength range, therefore no ellipticity was observed in this wavelength range. PA-H3 spectrum shows a negative peak near 220 nm and a positive peak at about 202 nm, indicating the presence of β-sheet secondary structure at all the reported concentrations.[29]

The CXG/PA-H3 mixtures show shifts of the β-sheet signal to higher wavelengths. CXG_PA-H3 1:1 shows a shift of the minimum from 220 nm to 224 nm, CXG_PA-H3 2:1 and 3:1 to 223 nm, and CXG_PA-H3 5:1 to 221 nm. The band becomes also progressively broader. These shifts suggest a possible modification of the β-sheet secondary structure, probably due to interactions between CXG and PA-H3. The higher is the relative amount CXG in the system, the lower is the β-sheet signal shift.

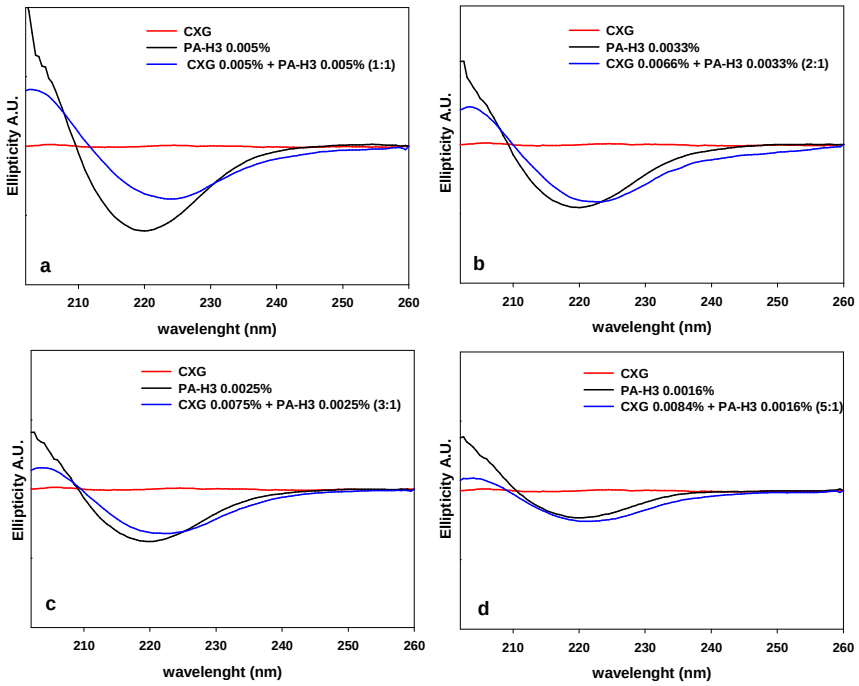

Fig. 6.7 CD spectra of mixtures of CXG/PA-H3, at volume ratios 1:1 (a), 2:1 (b), 3:1 (c) and 5:1 (d), having a total final concentration of 0.01%wt; each curve is supplied with the spectrum of PA-H3 at the same concentration than in the mixture. (%wt referred to CXG and PA-H3 in the various analysed system are reported in graphs' legend)

FTIR spectra of CXG, PA-H3 and of the CXG_PA-H3 1:1, 2:1, 3:1, and 5:1 gels are shown in Fig. 6.8a-c. The spectra were normalised at 1635 cm^{-1} for simplicity of representation.

The spectrum of CXG (Fig. 6.8a) shows the typical broad peak at 3400 cm^{-1} related to the stretching of –OH groups, the stretching of C-H at 2918 cm^{-1} and 2883 cm^{-1} with subdued intensity because of the cyclic nature of sugar rings, the peak at 1620 cm^{-1} t related to the stretching of the carbonyl groups in the deprotonated form and the band at 1040 cm^{-1} that is typical of glycosidic bonds. The spectrum of PA-H3 (Fig. 6.8a) is characterised by the broad peak at 3416 cm^{-1} and a peak at 3282 cm^{-1} that are related to the stretching of O-H and N-H, respectively. The peaks at 2960 cm^{-1} and at

2920 cm^{-1} are attributable to the C-H stretching of the alkyl tail. Furthermore, the peaks at 1635 cm^{-1} and 1541 cm^{-1} are related to the stretching of the C=O of the amide I, and the bending of N-H of amide II and both characteristic of the peptide sequences. Moreover, the three peaks in the finger print region at 965 cm^{-1}, 891 cm^{-1} and 851 cm^{-1} are typical of aromatic compounds, and referred to the bending of C-H of aromatic rings. Spectra of all the gels (Fig. 6.8b-c) look like the superimposition of the spectra of the two building blocks. Peaks at 1635 cm^{-1} and 1541 cm^{-1} related to amide bonds of PA-H3 are also present in gels spectra, which also display the CXG print in the characteristic glycosidic band at 1039 cm^{-1}.

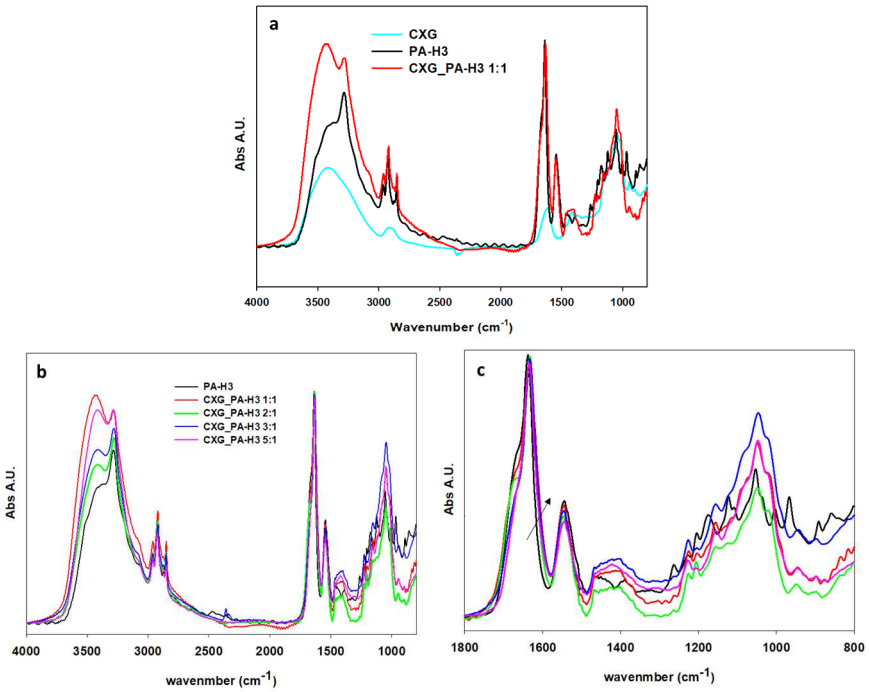

Fig. 6.8 FTIR spectra of solely CXG, PA-H3 and of CXG_PA-H3 1:1 (a); comparison between PA-H3 and CXG_PA-H3 gels 1:1, 2:1. 3:1 and 5:1 in the whole analysed range of wavelengths (b) and its zoom in a range between 1800 cm^{-1} and 800 cm^{-1}

The influence of the interactions between CXG and PA-H3 on the morphology of their supramolecular aggregates was investigated through TEM microscopy (Fig. 6.9). PA-H3 forms short and homogeneously dispersed fibres of about 10 nm diameter (Fig. 6.9a), while CXG has an amorphous structure (Fig. 6.9b). When the PA is combined with CXG in any of the ratios used, large fibrous aggregates form (Fig. 6.9c-f) with a significant increase of both the length and the diameter of the fibres. Furthermore, the absence of isolated fibres around these aggregates in all the CXG_PA-H3 systems suggests that CXG is able to sequestrate the PA-H3 fibres and incorporate them within its structure to form a non-covalently crosslinked network.

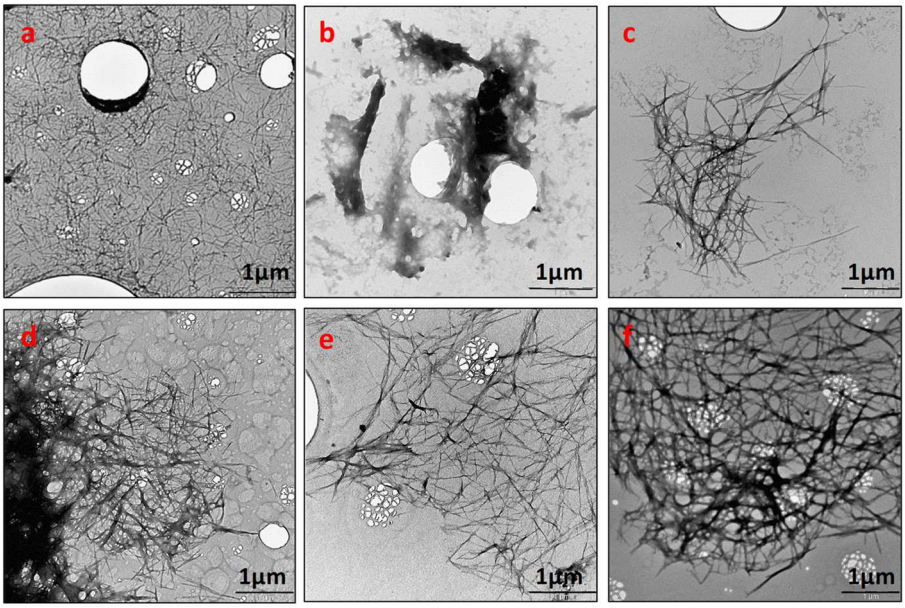

Fig. 6.9 TEM images of PA-H3 (a) and CXG (b), compared with CXG _PA-H3 mixture 1:1 (c), 2:1 (d), 3:1 v/v (e) and 5:1 (f) volume ratios

Furthermore, it was proved that negatively charged PA (PA-E3) was not able to form the same aggregates. PA-E3 fibres (Fig. 6.10a) are much longer than PA-H3 fibres;

when mixed with CXG they do not form aggregates appearing separate or covered by CXG deposits (Fig. 6.10b).

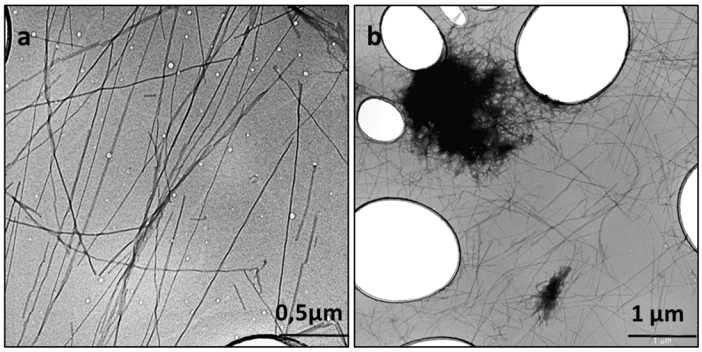

Fig. 6.10 TEM images of solely PA-E3 (a) and mixed with CXG mixed at 1:1 volume ratio (b)

The co-assembly of PA-H3 with hyaluronic acid (HA) was also observed by TEM. The chosen HA has a molecular weight of ca. 400 kDa, hence similar to CXG. In Fig. 6.11 TEM micrographs of PA-H3, CXG_PA-H3 3:1 and HA/PA-H3 at 3:1 are shown. The assembly of HA/PA-H3 (Fig. 6.11c) is different from the assembly of CXG/PA-H3 systems (Fig. 6.11b). HA promotes the formation of much longer and thicker fibres, which assemble in large bundles. The different behaviour in co-assembly can be ascribed to the different molecular structure of the two polymers, and charge density: linear and strongly anionic for HA, with short branches and less anionic for CXG.

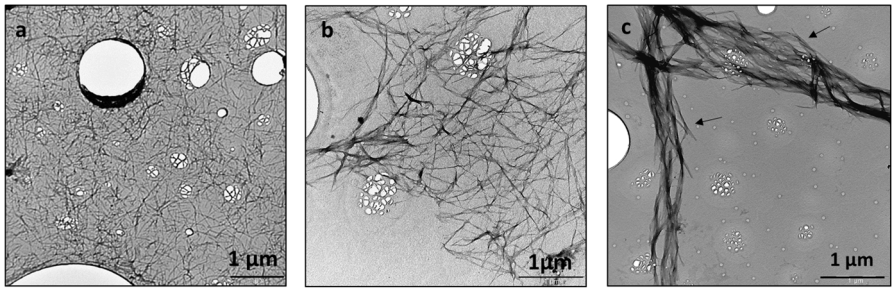

Fig. 6.11 TEM images of solely PA-H3 (a), CXG_PA-H3 3:1 system (b) and HA_PA-H3 system 3:1 volume ratio

Morphologies of CXG_PA-H3 gels were investigated through SEM and are reported in Fig. 6.12, together with the morphologies of CXG (Fig. 6.12a-a') and PA-H3 gel (Fig. 6.12b-b'). PA-H3 shows a non-porous structure as well as CXG but, differently from CXG, it is characterized by the presence of protruding fibers (Fig. 6.12b').

All CXG_PA-H3 gels look very similar, displaying a porous microstructure (Fig. 6.12c-f), characterized by a submicroscopic fibrous structure that can be attributed to the presence of PA-H3. CXG_PA-H3 1:1 and 2:1 (Fig. 6.12c-d) seems to have a smaller porosity with respect to CXG_PA-H3 3:1 and 5:1 (Fig. 6.12e-f). In particular, the gel with CXG_PA-H3 5:1 shows a structure that resembles the typical xyloglucan lamellar structure (see Fig. 4.8 in Chapter 4). Hence, the increased amount of CXG employed in the co-assembly, has an impact on the microstructure of the obtained gel. The thicker and longer fibers of CXG_PA-H3 2:1 and 5:1 (Fig. 6.12d' and f', respectively), already observed by TEM, are also clearly evident in the pore walls of the corresponding SEM micrographs.

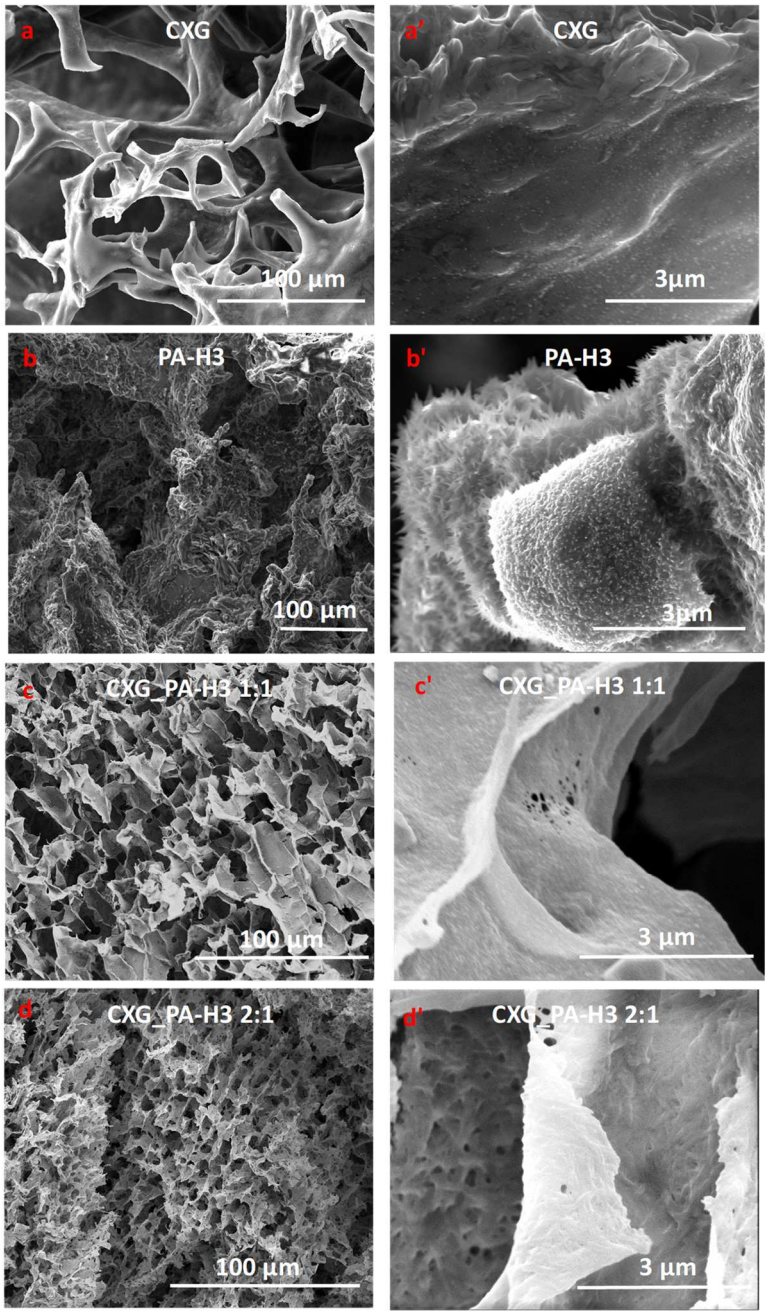
a
CXG
100 µm
a'
CXG
3µm
b
PA-H3
100 µm
b'
PA-H3
3µm
c
CXG_PA-H3 1:1
100 µm
c'
CXG_PA-H3 1:1
3 µm
d
CXG_PA-H3 2:1
100 µm
d'
CXG_PA-H3 2:1
3 µm

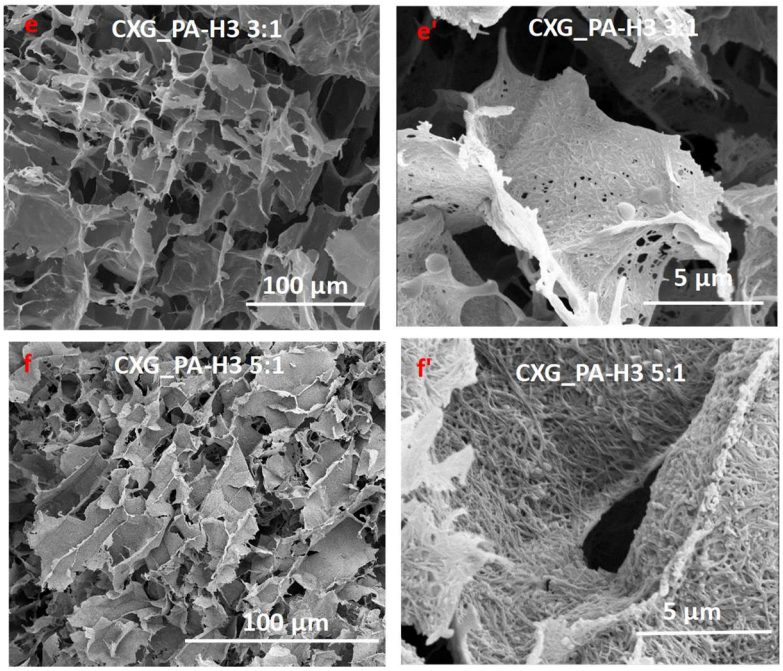

Fig. 6.12 SEM morphologies of CXG (a-a'), PA-H3 (b-b') and CXG_PA-H3 gels at different scale 1:1(c-c'), 2:1 (d-d'), 3:1 (e-e') and 5:1 (f-f') at different scale

Dynamic mechanical analysis was performed on PA-H3 gel formed in PBS and on the various CXG_PA-H3 gels and mechanical spectra are shown in Fig. 6.13. All gels show storage modulus (G') higher than loss modulus (G"), and G' and G'' that are almost invariant with frequency in the whole investigated range of frequencies, indicating a predominantly elastic behaviour, that is the typical behaviour of highly crosslinked, "strong" gels.[30] The pure PA-H3 gel has also the typical behaviour of a "strong" gel, yet it exhibits lower values of G' and G". The much higher values of G" for the CXG_PA-H3 gels actually support the general evidence gathered from handling these materials that tougher and more resilient materials were obtained when PA-H3 nanofibres where mixed with CXG.

The CXG_PA-H3 gels show higher G' values at the increase of CXG content. It can be expected that the ticker and longer fibres formed in the co-assembly reinforce the network, improving its mechanical properties.

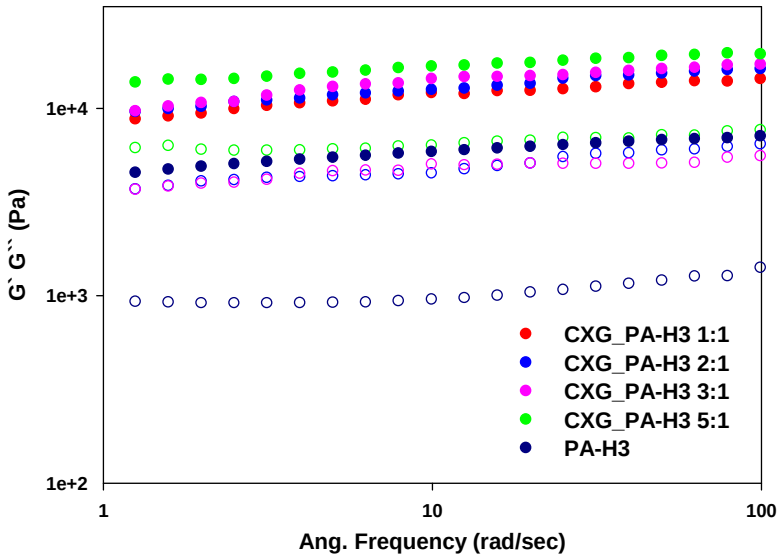

Fig. 6.13 Dynamic mechanical analysis in shear mode of PA-H3 gel compared with CXG_PA-H3 1:1, 2:1, 3:1 and 5:1 gels

CXG_PA-H3 gels were also subjected to uniaxial deformation during compression in culture media to simulate the biological microenvironment of the gel, when acting as scaffold. The tests were performed on both the PA-H3 gel formed in PBS and various CXG_PA-H3 gels and the measured compression moduli are reported in Fig. 6.14. An increase of the compression modulus is presented by all samples containing CXG with respect to PA-H3 gel. No significant differences can be appreciated among samples with different relative amount of the two polymers.

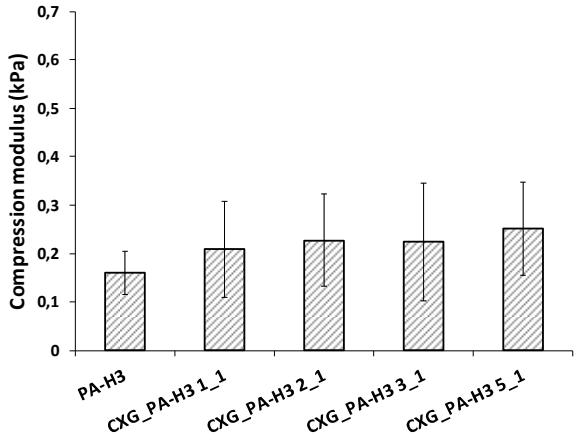

Fig. 6.14 Compression moduli (kPa) of PA-H3 gel, CXG_PA-H3 1:1, 2:1, 3:1 and 5:1 gels

6.3.2. Biological assessment

New biomaterials need to be firstly tested *in vitro* to ascertain that their cytotoxicity is not affected. Cell viability with and within the gels, attachment and migration have been studied in order to evaluate the suitability of the described gels as scaffolds for wound healing applications. Indeed, CXG/PA-H3 systems are able to form fibrous structure that resembles to the extracellular matrix (ECM) structure.

Prior to all biological assessments, all the gels, namely CXG_PA-H3 1:1, 2:1, 3:1 and 5:1, were incubated at 37 °C in complete cell culture medium to assess gels stability in cell culture conditions. Gels were observed over 45 days, with no dissolution of the co-assembled CXG/PA-H3 gels, while the control PA-H3 gel in PBS started to disassemble in small pieces after 10 days of incubation. (Fig. 6.15). CXG_PA-H3 1:1 was excluded from *in vitro* biological evaluations because among all the gels is the less tough.

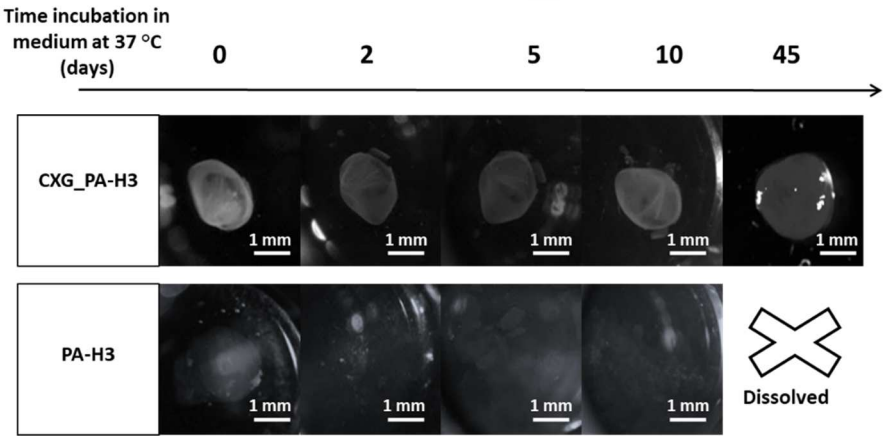

Fig. 6.15 Gel stability assessment in cell culture medium at 37 °C; optical microscopy images of a representative gel CXG_PA-H3 (top) and a PA-H3 gel in PBS (bottom)

Cell viability was investigated in two different settings: (i) cells were seeded on top of CXG_PA-H3 gels in order to assess their viability on the surface of the gels (Fig. 6.16a) and (ii) cells were encapsulated within the gels (Fig. 6.16b).

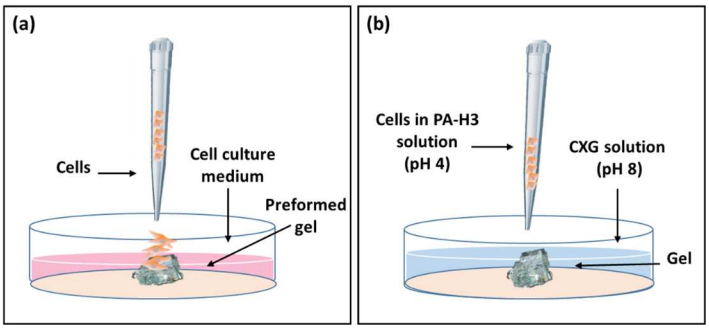

Fig. 6.16 Settings used for viability test: cells seeded onto preformed CXG_PA-H3 (a) and cells encapsulated within the gels (b)

In the first setting, cytotoxicity of CXG/PA-H3 gels was investigated by culturing HaCat cells onto the pre-formed gels. After 2 and 7 days, gels were stained with

LIVE/DEAD® assay staining (green - live cells, red - dead cells). The obtained results are summarized in Fig. 6.17. After 2 days, no cytotoxicity was detected for all gels and the different building blocks (CXG and PA-H3) which exhibit a viability comparable to non-treated cells (Non tt) (Fig. 6.17a). After 7 days, cells showed good viability without sigificative statistical difference between gels and non-treated cells (Fig. 6.17b).

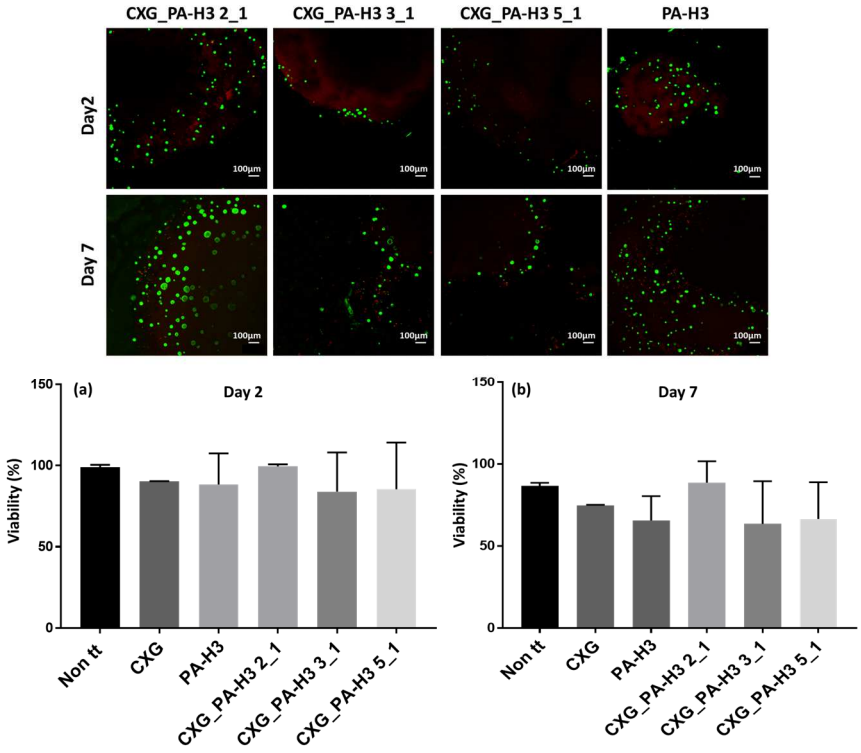

Fig. 6.17 Confocal images of HaCat cells stained with calcein-AM (live indicator; green) and ethidium homodimer-1(dead indicator; red) after 2 and 7 days post-seeding onto CXG_PA-H3 gels. Results of viability (percentage of alive cells) after 2 days (a) and 7 days (b) compared to cells seeded onto PA-H3 gel, cells treated with CXG and untreated cells

In the second setting, cytotoxicity of CXG/PA-H3 gels was investigated by encapsulating HaCat cells within CXG/PA-H3 gels. As described previously, after 2 and 7 days, gels were stained with LIVE/DEAD® assay. The obtained results are summarized in Fig. 6.18. Also in this case, a good viability was observed upon encapsulation within all the gels and with the control building blocks both after 2 (Fig. 6.18a) and 7 days (Fig. 6.18b) of culture.

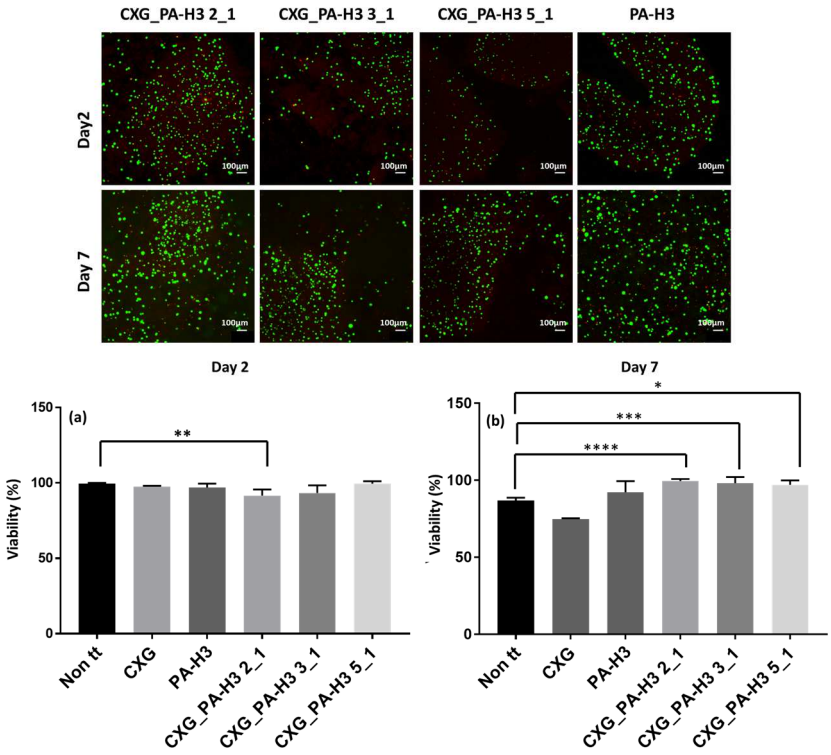

Fig. 6.18 Confocal images of HaCat cells stained with calcein-AM (live indicator; green) and ethidium homodimer-1(dead indicator; red) 2 and 7 days after encapsulation within CXG_PA-H3 gels. Results of viability after 2 (a) and 7 days (b) compared to cells seeded onto PA-H3 gel, cells treated with CXG and untreated cells

For the evaluation of cell attachment, cells were seeded onto the hydrogels. Control of cell attachment on CXG is not provided because conditions to gel CXG on its own was not explored in this study. After 24h, numerous cells were seen attached on the surface of the gels (Fig. 6.19). A significantly lower number of cells was found onto the PA-H3 gel used as control (Fig. 6.19a). This observation suggests an involvement of CXG molecules in cell attachment and in particular it can be related with the presence of CXG in the gels which seems to enhance cell attachment. A possible explanation of this behaviour can attributed to the presence of galectin-7 receptors in HaCat cells that can recognise galactose residues present in CXG branches. Galectins are a class of β-galactoside-binding receptors involved in the modulation of cell-matrix interactions and reepithelization of wounds by carbohydrate-based recognition.[31] This protein have also a role in wound healing process.[32] Indeed, they can promote reepithelization of skin by influencing cell migration and not cell proliferation.[31]

Cells on the surfaces of the gels adopted a spread morphology with a distribution in clusters.

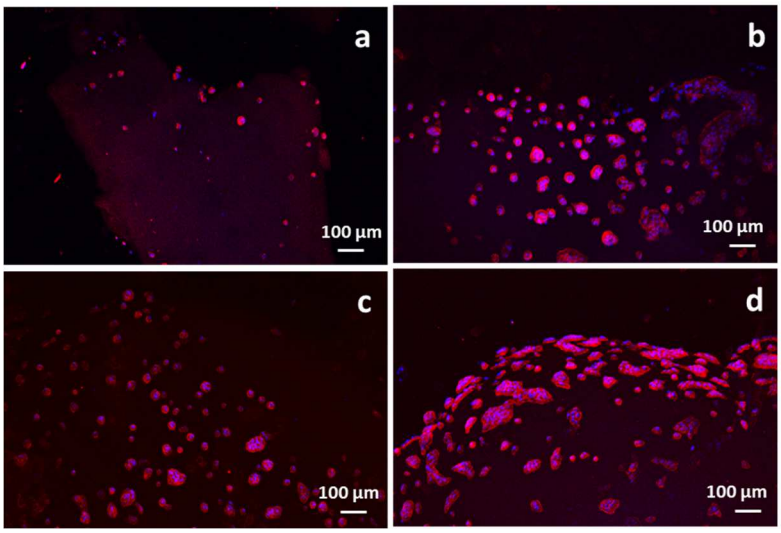

Fig. 6.19 Cells attachment on PA-H3 gel (a), CXG_PA-H3 2:1 (b), 3:1 (c) and 5:1 (d) gels

Closure of the scratched area of a HaCat monolayer after 24h was analysed and results are reported in Fig. 6.20. Scratched monolayers were incubated with CXG in solution, PA-H3 and CXG/PA-H3 hydrogel systems in presence or absence of mitomycin C as inhibitor of the proliferation. In this setting, the closure that occurred in samples with mitomycin was attributed to cell migration, while in samples without mitomycin, the closure was attributed to a combined effect of migration and proliferation.[33] In both analysed conditions, with and without mitomicyn, all the gels, including the control PA-H3, show poor scratch closure compared to non-treated cells (Non tt), while CXG shown a closure comparable with non-treated cells. This effect was attributed to the administration of CXG to cell monolayer as a solution, while all the others are gels could, in this setting, act as a barrier impairing the result.

For this reason, it is compared just the effect of all the gels as they are administered in the same physical form. Indeed, CXG_PA-H3 5:1 gel show a significant higher scratch closure compared to all the other gels in both conditions, with and without mitomycin.

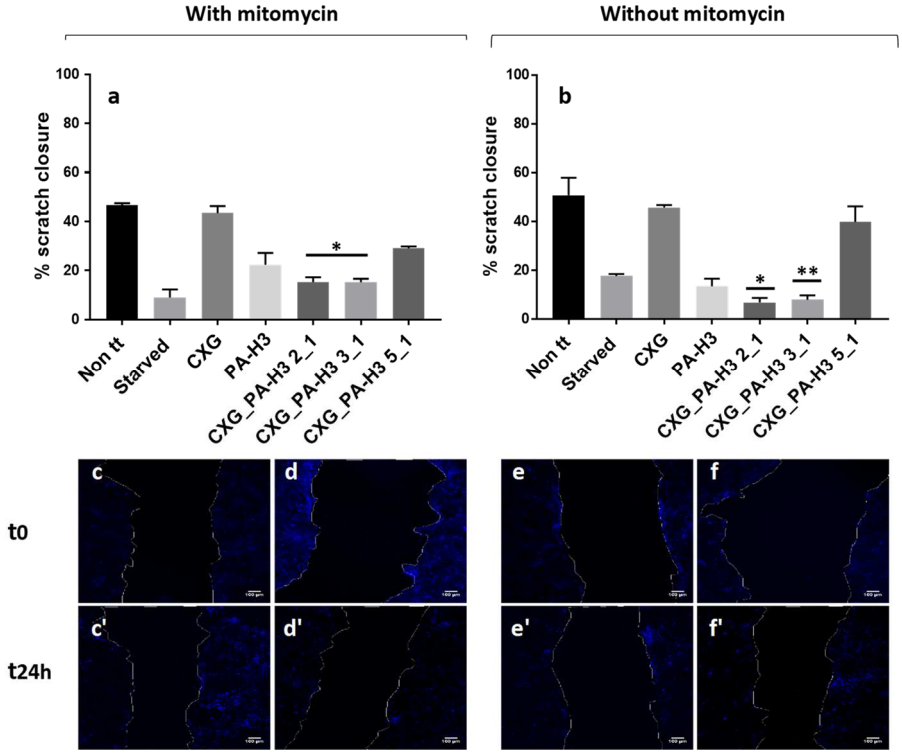

Fig. 6.20 Histogram reporting the percentages of scratch closure after 24h observation in presence of mitomycin (a) and without mitomycin (b); images of the scratch at t_0 and after 24h for CXG_PA-H3 2:1 (c-c') and 5:1 (d-d') in presence of mitomicyn; images of the scratch at t_0 and after 24h for CXG_PA-H3 2:1 (e-e') and 5:1 (f-f') without mitomicyn

In conclusion, from *in vitro* biological evaluations it was observed that CXG_PA-H3 2:1 and 5:1 hydrogels have better performance than the 3:1 CXG/PA-H3 ratio. CXG_PA-H3 2:1 shown a high viability percentage in both the tested setup and CXG_PA-H3 5:1 shown better cell adhesion and better capability to enhance *in vitro* wound closure. For this reason, these two gels were selected for *in vivo* testing.

Hence, a full-thickness excision wound was created on 10-week-old female CD-1 mice. The PA-H3 hydrogel alone without CXG and a no hydrogel/no peptide (Non tt)

were used as controls. A secondary dressing, Tegaderm film, was applied on top of the wound, with or without the hydrogel, to maintain a moist environment and the hydrogel in place. Image analysis of the wound gross morphology demonstrated faster wound closure after 7 days in presence of all the tested gels with respect to non-treated wounds and results are reported in Fig. 6.21. The similarity of the wound closure percentages between CXG/PA-H3 gels and solely PA-H3 gel may be due to the late time-point chosen in this experiment (7 days). Indeed, it was observed *in vitro* that after 24 hours CXG enhanced the closure on the scratch on cell monolayer. Furthermore, in previous reports the enhancement of *in vitro* scratch closure in presence of xyloglucan has been observed at early stages, namely between 24 and 48 hours.[34] Therefore, it is suggested that earlier data points are needed to conclude on the effect of CXG on wound closure in mice. Moreover, histology analysis (in progress) may as well reveal the effects of the presence of CXG in the gels.

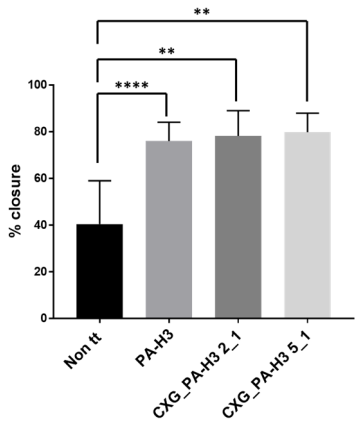

Fig. 6.21 Percentages of wound closure i*n vivo* after 7 days

6.3.3. Future perspective

A variant of PA-H3 with the addition of QHREDGS bio-signal peptide sequence was designed and synthesized and it will be named hereinafter PA-H3$_{bio}$. Looking at the chemical structures of PA-H3 (Fig. 6.22a) and PA-H3$_{bio}$ (Fig. 6.22b), the two PA

sequences have the same structure including alkil tail, -V_3A_3- β-sheet forming sequence, followed by the –H_3- polar sequence, but PA-$H3_{bio}$ include a further portion constituted by –G_3- and the -QHREDGS sequence. The –G_3- sequence between –H_3- polar and the bioactive peptide sequence, was introduced as a spacer.

It has been shown in previous report that a number of three aminoacids as spacer favour a good display of the biosignal on PA nanofibers. [11][35]

Glycine was chosen because it is the simplest amino acid and it does not have pendant group that could badly impact the assembly of the fibres. To the best of my knowledge, this is the first report of this peptide amphiphile sequence.

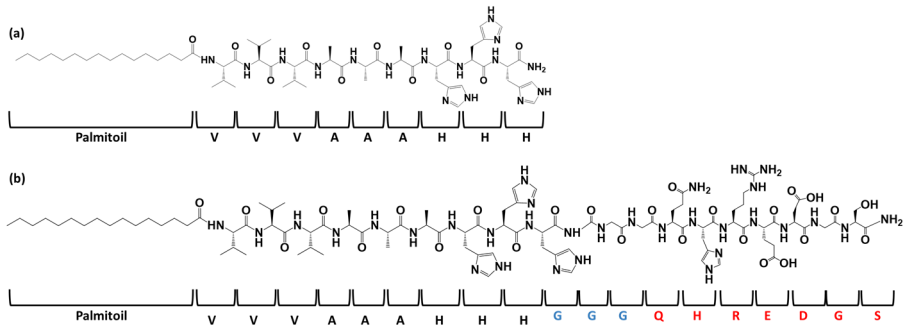

Fig. 6.22 Molecular structure of PA-H3 (a) and of PA-$H3_{bio}$, enriched with a spacer and biosignal sequences in blue and in red, respectively (b)

Some preliminary assessments were performed on this new PA-$H3_{bio}$.

Morphology of PA-$H3_{bio}$ was investigated through TEM (Fig. 6.23). Compared to PA-H3 fibres shown in Fig. 6.23a, PA-$H3_{bio}$ forms longer fibres (Fig. 7.23b-c) and promote the aggregation of those fibres into fused bundles, very clear in Fig. 6.23d (see the arrow). This different morphology on TEM could be correlated with the presence of the biosignaling sequence in the PA that strongly affect the assembly observed for PA-H3 sequence. This phenomenon has been already reported in literature for other PA sequences with bioactive motives.[16]

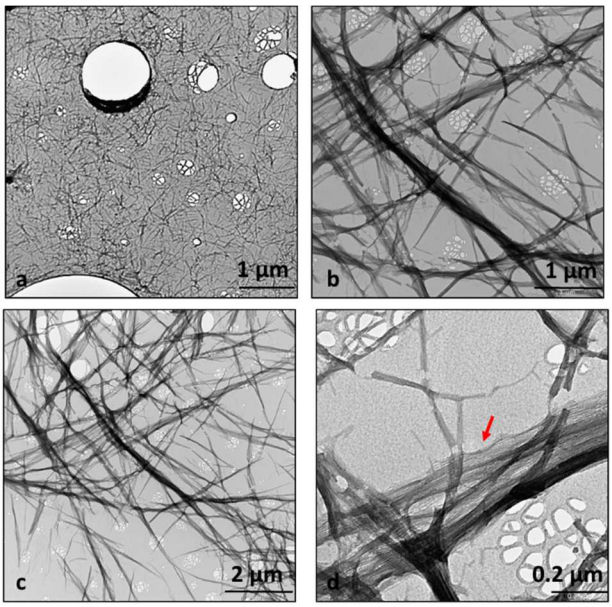

Fig. 6.23 TEM images of PA-H3 (a) and PA-H3$_{bio}$ at different scales (b,c and d)

Interactions between CXG and PA-H3$_{bio}$ were visually tested (Fig. 6.24). For this assessment, as used for CXG and PA-H3 systems, 1 %wt HEPES solutions of CXG and PA-H3$_{bio}$ were prepared and injecting PA-H3$_{bio}$ inside CXG solution, the interactions between these two components lead to a looser construct (Fig. 6.24a) with respect to the tough and resilient gel that was obtained with PA-H3 (Fig. 6.24b). This different result suggests that further investigations are needed before to proceed with the integration of this PA in CXG/PA-H3 gels

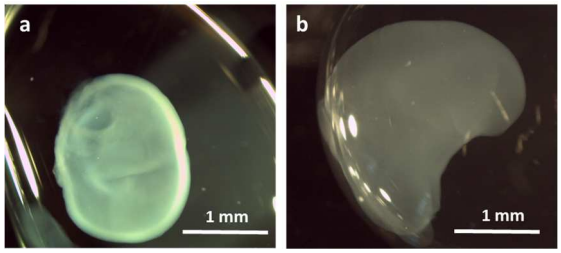

Fig. 6.24 Picture of CXG/PA-H3$_{bio}$ gel (a) and of CXG/PA-H3 gel (b)

Stupp et al. suggested to overcome the problem of different assembly using a bioactive PA, diluting the biosignal-presenting PA with a non-active shorter PA sequence. This strategy has been demonstrated a valid alternative to allow the epitope to be displayed protruding from the fibre surface, as described in the pictorial representation in Fig. 6.25. Indeed, they demonstrated that PAs displaying an RGDS epitope benefit from the presence of a diluent molecule to co-assemble with the epitope-presenting molecule and space the RGDS epitope for optimal cell recognition and adhesion.[11]

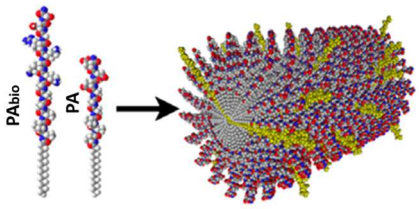

Fig. 6.25 Molecular graphics representations of binary PA fibers assembled from 90% non-active diluent and 10% PA_{bio} accented in yellow; figure adapted from [36]

Hence, the future plan for this work is to dilute PA-$H3_{bio}$ with the PA-H3. Firstly, the bioactivity of PA-$H3_{bio}$/PA-H3 gels has to be assessed and different ratios between PA-$H3_{bio}$ and PA-H3 have to be tested in order to identify the better conditions in which the biosignal give an optimal display and recognition by the cells. Secondly the selected PA-$H3_{bio}$/Pa-H3 could be assembled in presence of CXG, followed by physico-chemical characterisation of the new gels and subsequent biological assessments.

6.4. Conclusions

This study has demonstrated the ability of CXG to co-assemble with PA-H3, forming tough and resilient sphere-like gels with a fibrous microstructure.

Co-assembly resulted influenced by the pH of the precursors solutions and thus, by their electric surface charge density. The best gel was obtained mixing CXG at pH

between 7 and 8 and PA-H3 at pH 4 or 5. These were the pH conditions that allowed CXG and PA-H3 to be strongly oppositely charged. Co-assembly of CXG and PA-H3 led to the obtainment of a fibrous network, as observed by both TEM and SEM microscopies. The presence of CXG in the gels increased both storage modulus upon shear stress and compression modulus, in comparison to PA-H3 gels. The co-assembled gels were stable for longer (up to 1 month) when kept immersed in physiologic fluid and did not induce cytotoxicity after 2 and 7 days of incubation with HaCat cells.

Moreover, gels loaded with HaCat cells showed a good cytocompatibility both after 2 and 7 days of incubation. Cell attachment seems to be enhanced for the CXG_PA-H3 5:1 system and this gel also showed the best in vitro scratch closure enhancement. This is probably due to the recognition of galactose residues by galectin-7 receptors present in HaCat cells. Based on the in vitro results obtained, CXG_PA-H3 2:1 and CXG_PA-H3 5:1 were selected for in vivo studies of wound closure. An enhancement of the wound closure after 7 days was observed for all systems tested.

Furthermore, a PA-H3 variant including a QHREDGS peptide as biosignal to target chronic wounds was designed and synthesized. Its incorporation in CXG/PA-H3 systems will be studied in the future

Contributions

The author wishes to point out the contribution Carlos Redondo for the TEM measurements and for the synthesis and purification of the bioactive peptide amphiphile sequence and Dr Estelle Collin for the help in the design of biological experiments and the support in the interpretation of the results.

Reference

[1] G.A. Ozin, K. Hou, B. V. Lotsch, L. Cademartiri, D.P. Puzzo, F. Scotognella, A. Ghadimi, J. Thomson, Nanofabrication by self-assembly, Mater. Today. 12 (2009) 12–23. doi:10.1016/S1369-7021(09)70156-7.

[2] N. Stephanopoulos, J.H. Ortony, S.I. Stupp, Self-assembly for the synthesis of functional biomaterials, Acta Mater. 61 (2013) 912–930. doi:10.1016/j.actamat.2012.10.046.

[3] S.I. Stupp, V. Lebonheur, K. Walker, L.S. Li, K.E. Huggins, M. Keser, A. Amstutz, Supramolecular Materials : Self-Organized Nanostructures, Science (80-.). 384 (1997) 384–389. doi:10.1126/science.276.5311.384.

[4] E.R. Zubarev, M.U. Pralle, E.D. Sone, S.I. Stupp, Self-Assembly of Dendron Rodcoil Molecules into Nanoribbons, J. Amercan Chem. Soc. 123 (2001) 4105–4106. doi:10.1021/ja015653.

[5] J.P. Hill, W. Jin, A. Kosaka, T. Fukushima, H. Ichihara, T. Shimomura, K. Ito, T. Hashizume, N. Ishii, T. Aida, Self-Assembled Hexa-peri-hexabenzocoronene Graphitic Nanotube, Science (80-.). 304 (2012) 1481–1483. doi:10.1126/science.1097789.

[6] J.H.K.K. Hirschberg, L. Brunsveid, A. Ramzi, J.A.J.M. Vekemans, R.P. Sijbesma, E.W. Meijer, Helical self-assembled polymers from cooperative stacking of hydrogen-bonded pairs, Nature. 407 (2000) 167–170. doi:10.1038/35025027.

[7] S.I. Stupp, R.H. Zha, L.C. Palmer, H. Cui, R. Bitton, Self-assembly of biomolecular soft matter, Faraday Discuss. 166 (2013) 9. doi:10.1039/c3fd00120b.

[8] G.M. Whitesides, B. Grzybowski, Self-Assembly at All Scales, Science (80-.). 295 (2002) 2418–2421. doi:10.1126/science.1070821.

[9] J.B. Matson, S.I. Stupp, Self-assembling peptide scaffolds for regenerative medicine, Chem. Commun. 48 (2012) 26–33. doi:10.1039/C1CC15551B.

[10] C. Dispenza, S. Todaro, D. Bulone, M.A. Sabatino, G. Ghersi, P.L. San

Biagio, C. Lo Presti, Physico-chemical and mechanical characterization of in-situ forming xyloglucan gels incorporating a growth factor to promote cartilage reconstruction, Mater. Sci. Eng. C. 70 (2017) 745–752. doi:10.1016/j.msec.2016.09.045.

[11] H. Storrie, M.O. Guler, S.N. Abu-Amara, T. Volberg, M. Rao, B. Geiger, S.I. Stupp, Supramolecular crafting of cell adhesion, Biomaterials. 28 (2007) 4608–4618. doi:10.1016/j.biomaterials.2007.06.026.

[12] J.D. Hartgerink, E. Beniash, S.I. Stupp, Peptide-amphiphile nanofibers : A versatile scaffold for the preparation of self-assembling materials, 99 (2002) 5133–5138. doi:10.107/pnas.072699999.

[13] L.W. Chow, R. Bitton, M.J. Webber, D. Carvajal, K.R. Shull, A.K. Sharma, S.I. Stupp, A bioactive self-assembled membrane to promote angiogenesis, Biomaterials. 32 (2011) 1574–1582. doi:10.1016/j.biomaterials.2010.10.048.

[14] A. Dehsorkhi, V. Castelletto, I.W. Hamley, Self-assembling amphiphilic peptides, J. Pept. Sci. 20 (2014) 453–467. doi:10.1002/psc.2633.

[15] H. Cui, M.J. Webber, S.I. Stupp, Self-Assembly of Peptide Amphiphiles: From Molecules to Self-Assembly of Peptide Amphi, Pept. Sci. 94 (2009) 1–18. doi:10.1002/bip.21328.

[16] M.J. Webber, E.J. Berns, S.I. Stupp, Supramolecular nanofibers of peptide amphiphiles for medicine, Isr. J. Chem. 53 (2013) 530–554. doi:10.1002/ijch.201300046.

[17] K.E. Inostroza-brito, E. Collin, O. Siton-mendelson, K.H. Smith, A. Monge-marcet, D.S. Ferreira, R.P. Rodríguez, M. Alonso, J.C. Rodríguez-cabello, R.L. Reis, F. Sagués, L. Botto, R. Bitton, H.S. Azevedo, A. Mata, Co-

assembly, spatiotemporal control and morphogenesis of a hybrid protein–peptide system, Nat. Chem. (2015) 1–8. doi:10.1038/nchem.2349.

[18] R.M. Capito, H.S. Azevedo, Y.S. Velichko, A. Mata, S.I. Stupp, Self-Assembly of Large and Small Molecules into Hierarchically Ordered Sacs and Membranes, Science (80-.). 319 (2008) 1812–1816. doi:10.1126/science.1154622.

[19] J. Borges, M.P. Sousa, G. Cinar, S.G. Caridade, M.O. Guler, J.F. Mano, Nanoengineering Hybrid Supramolecular Multilayered Biomaterials Using Polysaccharides and Self-Assembling Peptide Amphiphiles, Adv. Funct. Mater. (2017) 1–14. doi:10.1002/adfm.201605122.

[20] T. Mcmahon, P.C.M. Van Zijl, A.A. Gilad, Alginate-peptide amphiphile core-shell microparticles as a targeted drug delivery system Job, NIH Public Access. 27 (2015) 320–331. doi:10.1002/nbm.3066.Non-invasive.

[21] A.C. Mendes, K.H. Smith, E. Tejeda-Montes, E. Engel, R.L. Reis, H.S. Azevedo, A. Mata, Co-assembled and microfabricated bioactive membranes, Adv. Funct. Mater. 23 (2013) 430–438. doi:10.1002/adfm.201201065.

[22] D.S. Ferreira, A.P. Marques, R.L. Reis, H.S. Azevedo, Hyaluronan and self-assembling peptides as building blocks to reconstruct the extracellular environment in skin tissue, Biomater. Sci. 1 (2013) 952. doi:10.1039/c3bm60019j.

[23] D.B. Carew, K.J. Channon, I. Manners, D.N. Woolfson, Polyelectrolyte–surfactant nanocomposite membranes formed at a liquid–liquid interface, Soft Matter. 7 (2011) 3475–3481. doi:10.1039/c0sm01075h.

[24] A.A. Chaudhari, K. Vig, D.R. Baganizi, R. Sahu, S. Dixit, V. Dennis, S.R. Singh, S.R. Pillai, Future prospects for scaffolding methods and biomaterials

in skin tissue engineering: A review, Int. J. Mol. Sci. 17 (2016) 1–31. doi:10.3390/ijms17121974.

[25] G. Han, R. Ceilley, Chronic Wound Healing: A Review of Current Management and Treatments, Adv. Ther. 34 (2017) 599–610. doi:10.1007/s12325-017-0478-y.

[26] Y. Xiao, L.A. Reis, N. Feric, E.J. Knee, J. Gu, S. Cao, C. Laschinger, C. Londono, J. Antolovich, A.P. McGuigan, M. Radisic, Diabetic wound regeneration using peptide-modified hydrogels to target re-epithelialization, Proc. Natl. Acad. Sci. 113 (2016) 201612277. doi:10.1073/pnas.1612277113.

[27] N. Feric, C.C.H. Cheng, M.C. Goh, V. Dudnyk, V. Di Tizio, M. Radisic, Angiopoietin-1 peptide QHREDGS promotes osteoblast differentiation, bone matrix deposition and mineralization on biomedical materials., Biomater. Sci. 2 (2014) 1384–1398. doi:10.1039/C4BM00073K.

[28] L.A. Reis, L.L.Y. Chiu, J. Wu, N. Feric, C. Laschinger, A. Momen, R.K. Li, M. Radisic, Hydrogels with integrin-binding angiopoietin-1-derived peptide, QHREDGS, for treatment of acute myocardial infarction, Circ. Hear. Fail. 8 (2015) 333–341. doi:10.1161/CIRCHEARTFAILURE.114.001881.

[29] N.J. Greenfield, Using circular dichroism spectra to estimate protein secondary structure, Nat. Protoc. 1 (2006) 2876–2890. doi:10.1038/nprot.2006.202.Using.

[30] J.C. Stendahl, M.S. Rao, M.O. Guler, S.I. Stupp, Intermolecular forces in the self-assembly of peptide amphiphile nanofibers, Adv. Funct. Mater. 16 (2006) 499–508. doi:10.1002/adfm.200500161.

[31] N. Panjwani, Role of galectins in re-epithelialization of wounds., Ann.

Transl. Med. 2 (2014) 1–11. doi:10.3978/j.issn.2305-5839.2014.09.09.

[32] J. Klíma, L. Lacina, B. Dvořánková, D. Herrmann, J.W. Carnwath, H. Niemann, H. Kaltner, S. André, J. Motlík, H.J. Gabius, J. Smetana, Differential regulation of galectin expression/reactivity during wound healing in porcine skin and in cultures of epidermal cells with functional impact on migration, Physiol. Res. 58 (2009) 873–884. doi:1624 [pii].

[33] W. Nie, a. M. Deters, Tamarind seed xyloglucans promote proliferation and migration of human skin cells through internalization via stimulation of proproliferative signal transduction pathways, Dermatol. Res. Pract. 2013 (2013) 1–14. doi:10.1155/2013/359756.

[34] S. Burgalassi, L. Raimondi, R. Pirisino, G. Banchelli, E. Boldrini, M.F. Saettone, Effect of xyloglucan (tamarind seed polysaccharide) on conjunctival cell adhesion to laminin and on corneal epithelium wound healing, Eur. J. Ophthalmol. 10 (2000) 71–76. doi:1120-6721/071.

[35] S. Sur, F. Tantakitti, J.B. Matson, S.I. Stupp, Epitope topography controls bioactivity in supramolecular nanofibers, Biomater. Sci. 3 (2015) 520–532. doi:10.1039/c4bm00326h.

[36] M.J. Webber, J. Tongers, M.A. Renault, J.G. Roncalli, D.W. Losordo, S.I. Stupp, Development of bioactive peptide amphiphiles for therapeutic cell delivery, Acta Biomater. 3 (2010) 3–11. doi:10.1016/j.actbio.2015.07.018.

7. RFID epidermal sensor including xyloglucan-based hydrogel films: wound dressing and wound monitoring applications

7.1. Introduction and aim

Nowadays, with the growing aging of people in many parts of the world and the increasing incidence of chronic diseases such as diabetes or obesity, chronic wounds and ulcers represent a very big economic and social issue for health care systems all over the world.[1] Chronic wounds and ulcers are particularly distressful for patients that suffer for restless and long-term pain, discomfort caused by the malodour, need of frequent inspections and medications. Foot ulcers, for example, occur in 25% of diabetics and are the leading cause in the 85% of the cases of non-traumatic limbs amputation.[2]

Wounds are typically managed as a co-morbidity of other conditions and there is still a lack of knowledge on the biochemical physiopathology of this type of wounds that has hampered the innovation in new therapies, diagnostics, clinical practices and procedures.[3,4]

Furthermore, the choice of the dressing is a challenging aspect of wound care since there is no single dressing suitable for all the different types of wounds (acute, chronic, burn etc.) and the wound healing pattern can be very diverse and complicated by comorbidity.[3]

In general, protection from infections and traumas is the most fundamental and traditional role of a wound dressings in the medical practice. Indeed, chronic ulcers are highly susceptible to infection.[5,6]

Further features have been added to the wound dressing in order to support or enhance the healing process, such as the ability to provide hydration,[7,8] to absorb wound fluids and exudates, release growth factors, prevent or treat infectious states through the incorporation of anti-microbial agents. Furthermore, it is important to prevent an excessive exudates accumulation that could inhibit cell proliferation and lead to skin irritation, especially in chronic wounds in which the elevated proteolytic activity of

exudates perpetuates wounds, damages the wound bed, degrades the extracellular matrix, causing peri-wound skin problems.[9]

Hydrogels represent a very promising category of materials for this purpose because they are hydrophilic networks, able to maintain a good balance between hydration of the wound and fluids absorption, generally non-adhesive to the skin and high conformable. This topic has been already treated in Chapter 2 (paragraph 2.3.2.1.4).

However, passive hydrogels are not sufficient to challenge the complex scenario of chronic wounds.

A possibility to improve hydrogel dressings could be the embedding of diagnostic tools to measure biologically relevant parameters.[10] Continuous or semi-continuous interrogations and readouts can be used to reduce the frequency of medical interventions, to detect potentially problematic conditions that require attention, but also to collect relevant data to resolve predictive trends and elaborate more efficacious therapies.

In particular, epidermal electronics is one of the most innovative and promising field of wearable devices which allows to operate in direct contact with the human skin.[10] While technologies that can detect specific markers of the wound healing process probably still need to await a clear understanding of the chronic wound biochemistry, there are parameters that have been already identified to be critical to healing, including level of hydration and temperature. Indeed, an optimal level of hydration is required for optimal wound management; excessive moisture results in maceration, while too little results in wound drying out and impaired tissue regrowth. On the other hand, an increase of the temperature of the wound may be an alert for the early detection of bacterial infections, avoiding frequent inspections of the wounds that cause dressing-change discomfort for the patient and also avoiding unnecessary administration of antibiotics.[6]

Ultra High Frequencies (UHF) radio frequencies identification (RFID) is the type of technology that envisages all the characteristic to fulfill the vision of “smart” plasters for wound monitoring that can gather and returns information about the wound

environment. RFID permits indeed to conjugate sensing and communication capabilities without the needs of local power supply or dedicated electronics, it is able to interact with human epidermis and wirelessly transmit data.[11] Furthermore, multifunctional sensing can be achieved through the use of a new family of RFID microchips equipped with an integrated temperature sensor. Parameters such as temperature and fluid loss could be locally detected by the "smart" plaster and remotely transmitted by using devices either incorporated into or near wound dressings. Furthermore, the possibility to directly modify the clinical therapy, e.g. by modulating the local release of drugs through on-demand heating of the device, according to the state of the wound, could open a promising opportunity in the management of chronic ulcers or infected acute wounds.

It is here proposed to couple the XG-PVA(GL1)_CX hydrogel film, already presented in Chapter 4, with an inexpensive, lightweight UHF RFID tag to produce a hydrogel wound dressing that can battery-less monitor temperature and moisture level of the bandage in contact with the wound.[11] The hydrogel film XG-PVA(GL1)_CX was selected for this study among all the formulations described in Chapter 4, because its chemical crosslinked structure guarantees the resistance to dissolution when in contact with aqueous media, it shown the higher swelling degree and its porous structure was preferred over the lamellar structure of XG-CX films. Furthermore, it shown good biocompatibility and hemocompatibility.

This work investigated the electrical properties and the radiofrequency response of the selected film. It also complements the characterization of this material with its biaxial mechanical properties and swelling behavior both in immersion and in contact through a porous membrane with simulated biological fluids. Furthermore, it was evaluated also the ability of the film to uptake and release a hydrophilic molecule and in particular a fluorescent probe, in the perspective of the film loading with a hydrophilic antibiotic. Then, the ability of the film to retain serum protein and to have a barrier effect against bacteria were *in vitro* evaluated.

7.2. Materials and methods

7.2.1. Materials

Xyloglucan (XG) was kindly provided by DSP Gokyo Food and Chemical Co. (Japan). Poly(vinylalcohol) (PVA, MW=16kDa, 98% degree of deacetylation), aqueous glutaraldehyde at 25%wt (GA, containing 3%wt monomer, 22%wt hemiacetal and oligomers), glycerol (GL), HCl (1M), NaOH (1M), NaCl, fetal bovine serum (FBS) and Atto 633 were all purchased from Sigma-Aldrich. All the reagents used in this work were employed as received.

7.2.2. Methods

Preparation of the hydrogel films

The preparation of XG-PVA(GL1)_CX film has been presented in Chapter 4 and described in detail in Appendix A.1.1. Briefly, XG(4 %wt)/PVA(2 %wt) at 50% volume ratio were reacted with glutaraldehyde in acidic environment for one hour at room temperature and under constant agitation. After this time, the solution was neutralised and glycerol was added under agitation. The homogeneous mixture was casted into a glass petri dish and air-dried.

Mechanical properties

The mechanical properties of the hydrogel wound dressing were evaluated by means of biaxial tension tests on a Bose® planar biaxial TestBench instrument equipped with four 250 N electromagnetic engines. From the hydrogel films, 20x20x0.6 mm specimens were obtained by means of a regular cutter and fixed to four clamps, each corresponding to one motor. The tests were carried out in displacement control by stretching the specimen, in each direction, at a speed of 1 mm/s. The forces in two directions were monitored through two 250 N load cells while the strains field at the specimen surface were obtained with a digital video extensometer (DVE) assuming as reference length the position of five markers (four at the corners and one at the centre) which displacements were monitored by a 1024x468 pixel digital camera with

a refresh rate of 50 Hz. Results obtained were averaged on 5 measurements of different samples.

Swelling degree

Swelling tests were carried out with two setups, upon immersion of the samples in the swelling medium (Fig. 7.1a), and by placing the samples on 6-well plate equipped with Transwell insert (Fig. 7.1b). Samples were pre-weighed after equilibration in air at 50% RH, exposed to the medium for determined periods of time, then removed from the swelling medium, blotted with filter paper and weighed. Temperature was kept at 25°C. The swelling degree was determined in different media, namely, distilled water, 0.9 %wt NaCl isotonic solution and fetal bovine serum (FBS) and it was assessed gravimetrically using the following equation:

$$SD\% = (W_s - W_d) / W_d \times 100$$

where W_s corresponds to the hydrated weight of the sample and W_d represents the sample "dry" weight.

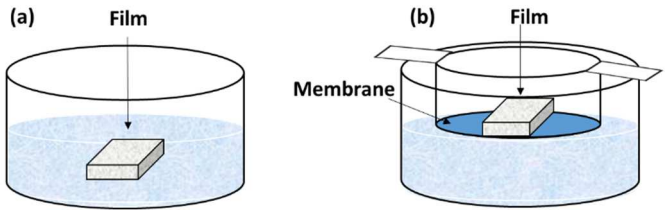

Fig. 7.1 Two different swelling setups for swelling degree measurements: film completely immersed in th swelling medium (a) and film in contact with the swelling medium through a porous membrane (b)

In vitro hydrolytic degradation

The *in vitro* degradation test was performed by the immersion of dry film samples in 15ml of PBS solution (pH 7.4) at 37ºC, during 6 weeks. At pre-determined periods, the samples were removed from the degradation medium, washed with distilled water to remove degrade fractions, freeze dried and then weighed.

Scanning Electron microscopy (SEM)

Surface morphology was imaged by a Field Emission Scanning Electron Microscope (FESEM-JEOL) at an accelerating voltage of 10 kV. Samples were previously swollen in MilliQ water or subjected to *in vitro* degradation, then frozen in liquid nitrogen and freeze-dried. Freeze-dried samples were cut to expose their inner structure, mounted on SEM aluminum stubs by means of a graphite adhesive layer and coated with a gold layer by JFC-1300 gold coater (JEOL) for 90 s at 30 mA before scanning.

Electrochemical Impedance Spectroscopy (EIS)

A Solartron FRA (Frequency Response Analyzer)-12558 instrument with a Dielectric interface-1249 equipped with a two-electrode cell was used to measure the electrochemical impedance of the XG-PVA(GL1)_CX hydrogel film. To perform the measurement, the dry film was cut in a disc having a diameter 2.1 cm and a thickness of about 0.5 mm. Then it was analysed in a range of frequencies between 10^{-2} and 106 Hz at room temperature, both in dry and wet condition, that means swollen at the equilibrium in water or in isotonic 0.9 %wt NaCl solution.

Radiofrequencies (RF) response characterisation

The dielectric-properties (permittivity and conductivity; ε_r and σ, respectively) of the XG-PVA(GL1)_CX based hydrogel films were investigated in the 200-1500 MHz band. A modified multilayer microstrip ring resonator was used.[12] The measurement setup, shown in Fig. 7.2, is composed by the ring and the ground plane/feed network, located in separate planes [13] at the purpose to enable the easy placement of an arbitrary sample between the two layers. Compared to conventional single-layer resonators, the multilayer structure enables also a stronger interaction between the sample and the ring fields, forcing the latter to physically cross the sample

before coupling with the ground plane. This feature is particularly important for thin film characterization, as in this case.

Dielectric properties of the XG-PVA(GL1)_CX film were estimated through a combined experimental and numerical procedure. Measurements of the measured/simulated scattering parameter (S_{12}) versus frequency were carried out by using a Vector Network Analyzer (Fig. 7.2b). In parallel, a numerical model of the multilayer ring resonator, including the sample, is computed by a Finite Element Method (in the FEKO implementation, https://www.feko.info). The peak frequency, f_R, and the quality factor ($Q=f_R/|f_{max}-f_{min}|_{-3dB}$) of the measured/simulated S_{12} intrinsically bring information about the unknown permittivity and conductivity of the sample.

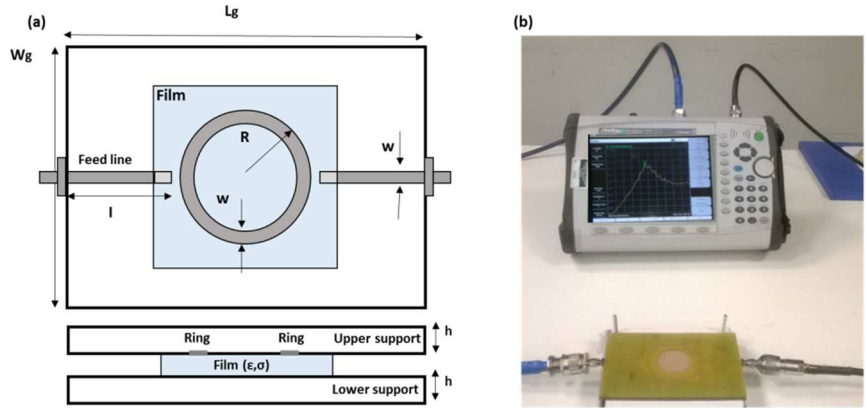

Fig. 7.2 Suspended ring resonator. Traces are etched over two FR4 PCBs (ε = 4.24, tanδ = 0.016). Size: L_g=136mm, W_g=90mm, g=0.25mm, R=25.9mm, w=2.2mm, l=40.75mm and h=1.575mm (a); measurement set up (b); inspired by Amendola et al.[14]

XG-PVA(GL1)_CX hydrogel film under test (thickness 0.17mm, diameter 8.5cm), was investigated both in the "as prepared" state and during a progressive absorption of isotonic NaCl solution emulating the release of the wound exudate.

Uptake and release of Atto 633 fluorescent probe

A weighed piece of XG-PVA(GL1)_CX film was immersed in the uptake PBS solution of Atto 633 (1,33 µg/ml). At pre-determined time, an aliquot of Atto 633 was collected and analyzed using a UV-670 Spectrophotometer (Jasco). After the measure, the collected aliquot of solution was returned to the uptake solution. For the release study, the loaded film was immersed in fresh PBS medium and again at predetermined time, an aliquot of the solution was analysed through UV spectrophotometry and this time it was replaced with fresh PBS medium. The concentration of Atto 633 both in the uptake and release solutions was determined measuring the absorbance at 629 nm through calibration curve.

Uptaken fractions were calculated as follow:

$$\%[Atto\ 633]_{Uptaken} = \frac{[Atto\ 633]_i - [Atto\ 633]_a}{[Atto\ 633]_i} x\ 100$$

Where $[Atto\ 633]_i$ is the initial concentration in the uptake solution and $[Atto\ 633]_a$ is the concentration of the probe in the analysed aliquot.

Released fractions were calculated as:

$$\%[Atto\ 633]_{Released} = \frac{[Atto\ 633]_{Released}}{[Atto\ 633]_{tot\ up.}} x\ 100$$

Where $[Atto\ 633]_{tot\ up.}$ is the total amount of Atto 633 that was uptake by the film and $[Atto\ 633]_{Released}$ is the amount of the molecules in the analysed aliquot.

Serum absorption test

Two pieces of the same size of XG/PVA film were soaked in fetal bovine serum (FBS) for 24h. After the incubation time, one piece of the film was stored (control) and the other piece was placed in a paper filter funnel and washed three times with PBS. Both the samples were dissolved in loading buffer at 95°C and resolved by 10% SDS-PAGE gel. The protein pattern was visualized by staining with Comassie brillant blue R-250. Band intensities were analyzed with a gel documentation system (BioRad) and the protein levels were expressed as densitometry and percentage of the control.

Antibacterial and bacterial retentivity tests

Antimicrobial activity of XG/PVA films was tested on *Escherichia coli* (*E. coli*), a gram negative bacterium. Depending on the test, bacterial strain was grown in typical Luria-Bertani broth (LB) medium or in LB agar plates. The day before the test, one colony was inoculated in LB medium and incubated at 37°C overnight (o.n.). An aliquot (100 µL) of an o.n. bacterial culture was added to two test tubes containing fresh LB medium and left to growth for 120 min. The exponential growth was determined by spectrophotometric measurement (600 nm). Then, UV sterilized XG-PVA(GL1)_CX (1 cm^2) was added only in one of the test tube and the absorbance was measured every 30 minutes up to two hours.

For the retentivity test 100 µl of an o.n. *E. coli* culture was spread onto LB agar plates in which some pieces of UV sterilized film (1 cm^2) were placed. After incubation at 37°C o.n., the film and the agar underneath the film were removed and separately incubated in LB liquid medium for 2 hours. Absorbance was measured at spectrophotometrically at 600 nm.

Bacterial infiltration test

E. coli was cultured in LB medium at 37°C o.n. then, 10 µl of the bacterial culture was gently dropped up the center of the film surface (ca.1 cm^2) placed on LB plate and 10 µl directly on LB plate (control) and incubated at 37°C o.n. Then, the piece of agar underneath the XG/PVA film and the agar control of the same dimension, were removed and incubated in LB medium. The bacterial growth was determined every 30 min by spectrophotometric measurement (600 nm).

7.3. Results and discussion

7.3.1. XG-PVA(GL1)_CX complementary characterisations

XG-PVA(GL1)_CX film was already presented in Chapter 4. Briefly, chemical crosslinking with a high yield was achieved by the use of glutaraldehyde as a

crosslinking agent. GA promotes the formation of acetal and hemiacetal bonds between XG chains, and between XG and PVA. Glycerol (GL) was added to the formulation before drying and provides the film with the required flexibility and water retention properties. GA continues to react also during the drying process and promotes some degree of glycerol grafting. In addition to covalent crosslinking, we expect hydrophobic association and hydrogen bonding to have a role in the formation of the network since XG/PVA solutions are able to gel when mixed with glycerol without addition of GA.

The mechanical properties of the film were investigated by biaxial tension tests. From the stress-strain curves (here not shown for brevity), a transversely isotropic mechanical behaviour is deduced. The plane of transverse isotropy is the cross-section of the specimen and, henceforth, two different elastic moduli for the two load directions (E11, E12) used in the mechanical tests were identified. In more detail, the membrane stress modulus avoiding the scattering of the specimen thickness that is not constant along the specimen. Fig. 7.3a shows the average values of the elastic moduli in the two directions with the confidence intervals obtained from the statistics of the analysis. The film resulted anisotropic along the load directions, in good agreement with the film morphology shown in Fig 7.3b.

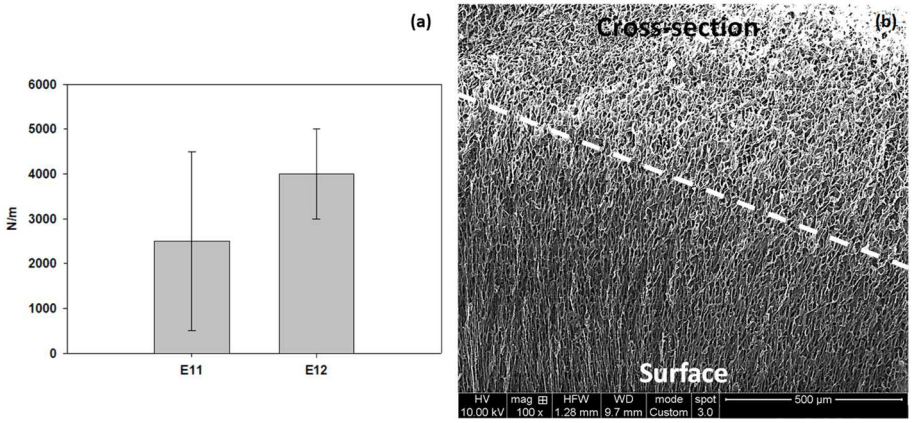

Fig. 7.3 Membrane elastic moduli in the two analysed directions (E11 and E12) (a) and SEM image of the cross-section and surface of the hydrogel film

In Fig. 7.4a the swelling curves for samples immersed in MilliQ water, isotonic NaCl solution or fetal bovine serum (FBS) are reported. Films swell more and faster in MilliQ water, reaching a plateau in about 8 h. The presence of NaCl in isotonic concentration, reduces both swelling rate and SD% at the plateaux, as expected, due to the decrease of the chemical potential of water in the swelling medium and, in turn, the osmotic contribution to the swelling pressure.[15] The swelling in a very complex medium as FBS reach in proteins, salts and other nutrients for cells does not change significantly the SD% but it drastically changes the consistence of the films that after 6 h become slimy and very difficult to handle; therefore the test was interrupted. This behaviour suggests the preferential uptake by the film of some components of the serum, as it will be discussed in the following.

When films are in contact with the different swelling media through a porous membrane (Fig. 7.4b), which better simulate the solvent exchange conditions of a wound dressing, they swell more slowly (especially in saline and FBS) and generally reach a plateau after 15 h of exposure to the fluid. The SD% at plateau for water is similar to the value measured upon immersion, while the SD% obtained for isotonic saline solution and FBS are slightly lower, probably due to the formation of a thin and

relatively dry skin on the top surface of the film that is exposed to air. The higher error bars for these measurements are caused by the difficulty in removing all the residual fluid present in the porous membrane used as support.

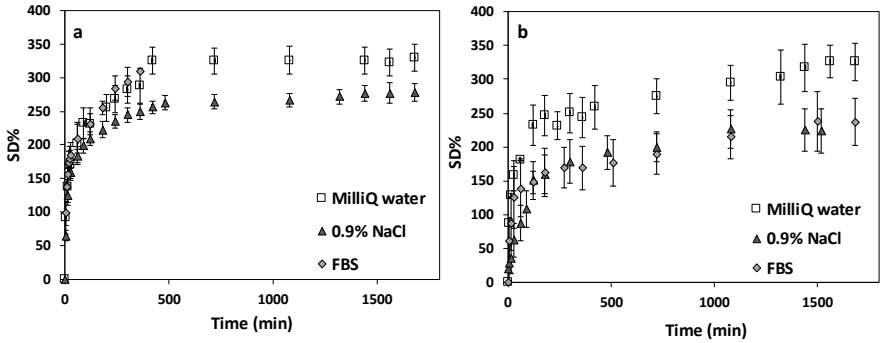

Fig. 7.4 Percentages of swelling degree upon immersion in the swelling medium (a) and in contact with the swelling medium (b)

XG-PVA(GL1)_CX was also subjected to *in vitro* hydrolytic degradation in PBS at 37 °C. The polymeric network weight loss was measured after 4, 8 and 12 days and after 6 weeks. During the first 4 days the polymer network loses 47% of the initial mass. Then, it does not show any significant change of residual weight in the following 8 days, reaching a total mass loss of ca. 67% after 6 weeks of incubation.

In Fig. 7.5 SEM images of the freeze dried hydrogel samples, before and after 8 days in vitro hydrolytic degradation, are reported. The “as prepared” XG/PVA film shows a finer and more heterogeneous microporous structure with an average pore size of 25 µm (Fig. 7.5a). After 8 days of immersion in PBS, the morphology of the films is characterised by a larger porosity (between 50 and 150 µm) (Fig. 7.5b). The micrographs obtained at higher magnification evidence thicker pore walls after incubation in PBS and the presence of small globules, probably due to the presence

of high crosslinking density regions. These globules are also present in the "as prepared" films (see Fig. 4.8 in Chapter 4).

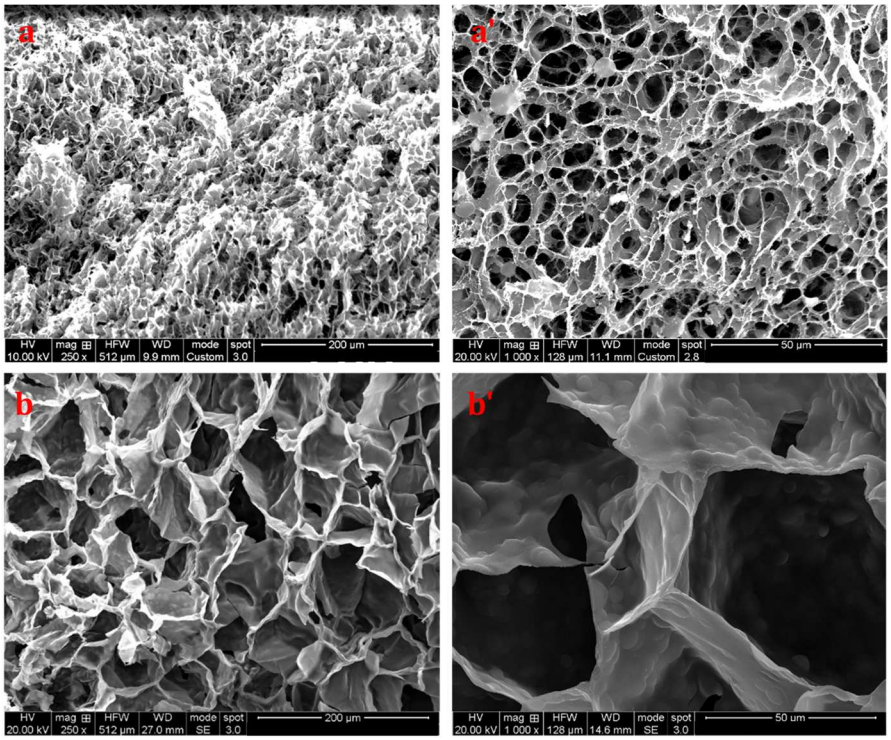

Fig. 7.5 SEM images of a prepared XG/PVA films (a, a') and after 8 days of incubation in PBS at 37°C (b, b')

The ability of the film to absorb and release a fluorescent hydrophilic dye, Atto 633 (Fig. 7.6a), was investigated through UV-Vis spectroscopy. Atto 633 uptake and release curves are reported in Fig. 7.6. Film specimens, previously swollen in water to their equilibrium state, incorporated ca. 80% of the dye present in the uptake solution within 24 hours and released ca. 98% of the loaded molecule in 24 hours (Fig. 7.6b).

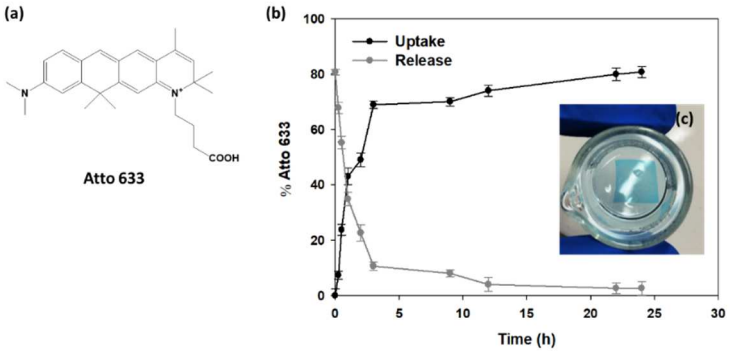

Fig. 7.6 Molecular structure of Atto 633 fluorescent dye (a), its uptake/release profile by XG-PVA (GL1)_CX (b) and a digital picture of the film after the uptake of the Atto 633 blue dye (c)

7.3.2. Electrical properties of the XG/PVA hydrogel film

The principle of functioning of an RFID device coupled to a hydrogel dressing is based on the change of electrical conductivity of the films upon absorption of wound exudates. Electric impedance spectroscopy was applied to measure the electric properties of the films in the "as prepared" condition and in the equilibrium swelling state either, in water or in simulated physiological fluid. As shown in Fig. 7.7a, Nyquist diagrams (Z" vs. Z') for the swollen films are distorted semicircles, sensibly smaller for the film swollen by the isotonic saline solution. Contrariwise, the "as prepared" film shows only a small portion of the semicircle (in the high frequency region), followed by a linear zone. These results indicate that the "as prepared" film has a mainly capacitive behaviour, while the swollen films are conductive, the resistivity being lower when the film is swollen by saline solution.

Fitting of the impedimetric spectra with different electrical equivalent circuits gave no satisfying results. Therefore, we adopted the formalisms of complex impedance, Z*, and permittivity, ε*, to describe the dielectric relaxation phenomena and determine the bulk conductivity of the films. [16–18]

According to this approach, the complex dielectric function can be calculated as:

$$\varepsilon^*(\omega) = \frac{Y^*}{i\omega C_0} = \frac{C}{C_0} - i\frac{G}{\omega C_0} = \varepsilon'(\omega) - \varepsilon''(\omega)$$

where $Y^*=[Z^*(\omega)]^{-1}$ is the measured complex admittance, C and G the measured capacitance and conductance, ω the angular frequency ($\omega=2\pi f$) and C_0 the equivalent capacitance of the free space. The frequency-dependent AC conductivity, $\sigma'(\omega)$, is then obtained as [17]:

$$\sigma'(\omega) = \varepsilon''(\omega)\omega\varepsilon_0$$

where ε_0 is the permittivity of free space and ε'' the imaginary part of complex permittivity.

Fig. 7.7b shows the $\sigma'(\omega)$ vs. frequency diagram for the different systems under 0.2 V. The plateau at intermediate to high frequencies (103-105 Hz) corresponds to the DC conductivity, σ_{dc}, of the films. The conductivity is mainly attributable to ion mobility: indeed, σ_{dc} is higher for the equilibrium swollen films that contain ca. 77% of water, with respect to the "as prepared" film, that has only 15% of water. The presence of sodium and chlorine ions causes an order of magnitude increase of σ_{dc}. The decrease of $\sigma'(\omega)$ at low frequencies could reflect both electrode polarization and diffusion phenomena (see the Nyquist plots of Fig. 7.7a).

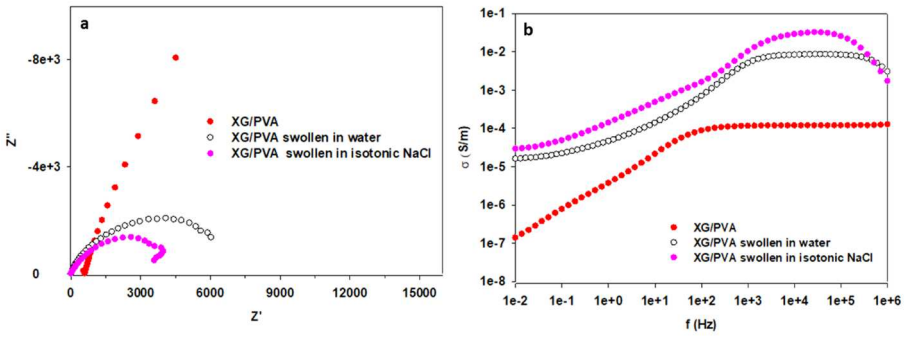

Fig. 7.7 Electric impedance spectroscopy of as prepared, water and saline swollen hydrogel films. Nyquist diagram (a); frequency-dependent conductivity (b)

Radio frequency (RF) response of the film was measured both in the dry state and during the exposition with simulated body fluids. The measured S_{12} scattering parameter corresponding to the dry membrane is shown in Fig. 7.8a. The estimated ε_r permittivity of the dry film is rather low, equal to 1.1, while the membrane exhibits a non-negligible conductivity (σ=3.2×10^{-2} S/m). The dynamic exposition to body fluid was induced by placing the hydrogel film on a synthetic sponge soaked with isotonic saline solution (ε_r=75.2, σ=1.67 S/m at 870MHz) for a fixed time interval (2 min). Then, it was placed between the two layers of the ring resonator and the S_{12} scattering parameter versus frequency was measured. This procedure was repeated four times up to the full immersion of the sample into the saline solution (for 2 min). A digital scale was used to further monitor the fluid dispersion by continuously weighing the membranes after each exposure to the fluid. The amount of absorbed fluid after each exposure was evaluated in terms of SD% of the membrane. The radiofrequency response of the membrane significantly changes at the increase of the SD%. The increase of the permittivity and the electric conductivity of the membrane produces a progressive shift of the S_{12} curves (Fig. 7.8b) that spans in the frequency range 985 < f < 780 MHz.

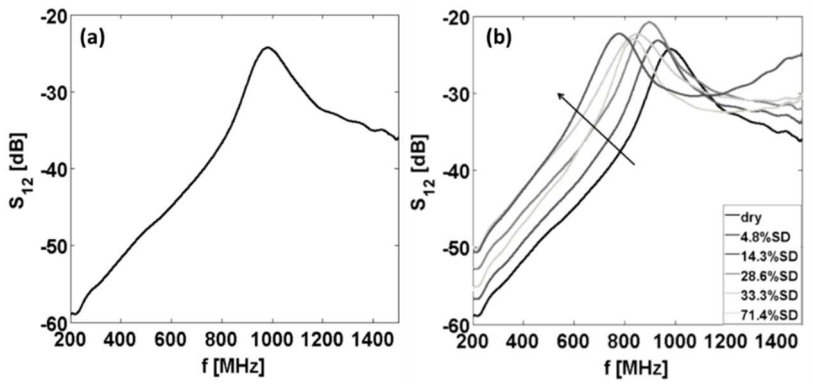

Fig. 7.8 Measured S_{12} for the dry membrane (a) and S_{12} measurements vs frequency during the progressive absorption of saline solution (b)

Dielectric properties of the XG-PVA(GL1)_CX estimated at different SD% are reported in Fig. 7.9. In the selected frequency band (200-1500 MHz), the hydrogel film exhibits a significant variation of permittivity up to 10 times its initial value and an increase of electrical conductivity, confirming that such membranes can be exploited for sensing applications.

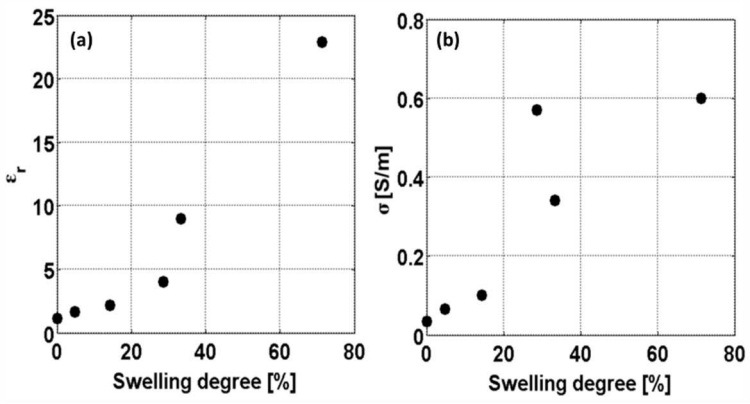

Fig. 7.9 Estimated dielectric properties of XG-PVA (GL1)_CX at different SD%: permittivity (a) and conductivity (b)

In order to verify the recovery capability of the sample, i.e. the capability to release the amount of the fluid absorbed by the film, the membrane was left to air-dry at room conditions. Its weight was then monitored every hour, until the membrane has recovered the initial weight. A comparison between the measured S_{12} in the case of the "as prepared" membrane and the S_{12} measured after the recovery process is shown in Fig. 7.10. Despite the slight frequency shift, denoting the need of a longer recovery time, the dielectric properties of the membrane are comparable.

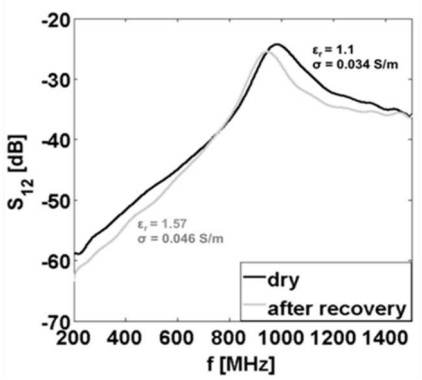

Fig. 7.10 Measured S_{12} in dry state and after recovery

By repeating the same procedure adopted above, the same XG-PVA (GL1)_CX film has been exposed to the isotonic saline solution in a second cycle of swelling, with the purpose of assessing the reproducibility of the electromagnetic features. The overlapped results related to the estimated dielectric properties with respect to SD% are shown in Fig. 7.11. In the early stages of the second cycle of swelling, values of ε_r and σ are in good agreement with values obtained from the first cycle, while increasing the degree of swelling these values start to differ. This phenomenon is probably due to irreversible modifications of the membrane structure during the first swelling cycle and to the leaching of the non-grafted glycerol, as observed in the *in vitro* degradation.

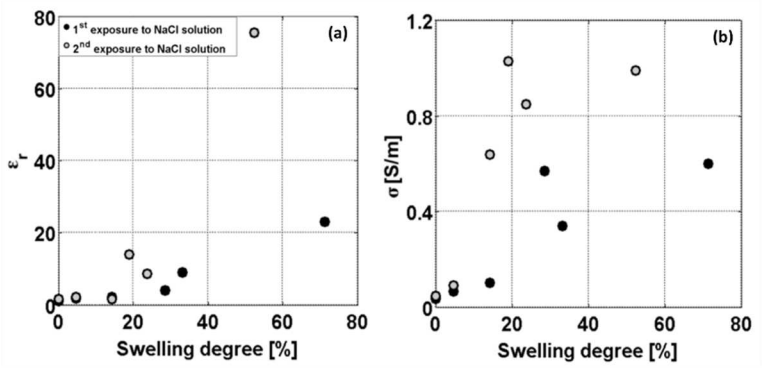

Fig. 7.11 The overlapped estimated dielectric properties of the sample vs SD% of the film in the case of two consecutive exposures to the saline solution

7.3.3. Serum absorption and antibacterial properties characterisations

The ability of the film to retain serum protein and to act as a barrier against bacteria were *in vitro* evaluated.

To assess the potential ability of XG-PVA(GL1)_CX film to absorb and retain proteins contained in the exudate, two pieces of film were immersed in FBS for 6 hours. After this time one of the films was washed and proteins retained within the film were analysed by electrophoresis. The other piece avoiding the washing step was used as control. In Fig. 7.12a it is shown the electrophoretic pathways of the two samples. The most intense band corresponds to the molecular weight of albumin. By optical density analysis (Fig. 7.12b) it is possible to assume that about 50% of the serum proteins have been retained in the hydrogel film after washing.

This result suggests that the film could be able to absorb and reduce exudate levels maintaining a balanced degree of wet and it may stimulate re-epithelization.

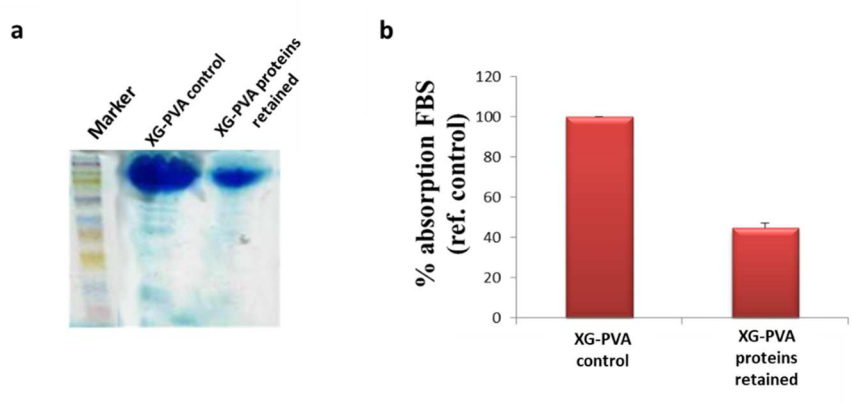

Fig. 7.12 XG-PVA (GL1)_CX film absorption of serum proteins. Electrophoretic pathway of FBS proteins retained within the film or protein adsorbed on film surface (a), and optical density analysis of the serum proteins (b)

An important function of an ideal wound dressing is the protection from infections, that especially in the case of chronic wounds are the major cause of mortality.

For this reason, the effect of XG-PVA(GL1)_CX film on bacterial growth was evaluated. For this test a non-pathogenic *E. coli* bacterium was chosen and thus an aliquot of overnight bacteria growth was incubated in two test tubes containing LB and left to growth for 120 min. The potential antimicrobial effect of XG/PVA film was estimated by measuring bacterial growth. Hence, XG/PVA film was added to only one of the test tube, while the other tube without film was used as control. Spectrometric measures of both samples were acquired at different interval of times up to 240 min. From results shown in Fig. 7.13 it is possible to argue that no difference in the growth curves between the control and the sample was detected, indicating that the dressing material have not intrinsic antibacterial effectiveness.

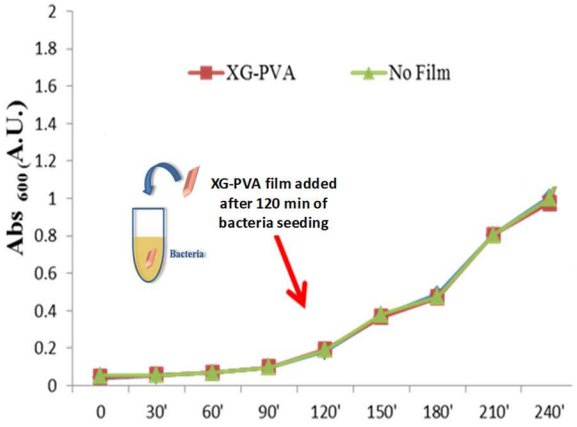

Fig. 7.13 Spectrophotometric measurements of XG-PVA(GL1)_CX film incubated with *E.coli* and the control without the film

Furthermore, the possibility that the wound dressing here studied could have bacterial retentivity was investigated. Indeed, *E. coli* were seeded on a LB agar plate and pieces of XG/PVA film of the same dimensions were place on this plate and incubated overnight to allow the bacterial growth. In agreement with the above results, bacterial growth was not inhibited (Fig. 7.14a). Subsequently, the XG/PVA film, the portion of LB agar under the film and a portion of LB agar far from the film of the same size (control) were separately incubated in a fresh LB medium and after 120 minutes the growth was measured (Fig. 7.14a). The experimental results (Fig. 7.14b), indicate that the number of bacteria was significantly higher in the sample containing the film with respect to the one with agar underneath the film, indicating that the wound dressing may have bacteria retention properties.

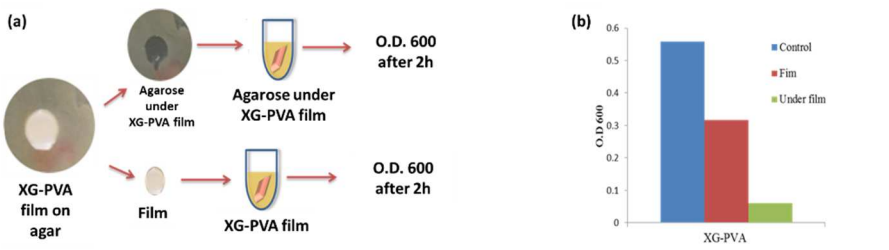

Fig. 7.14 Schematic representation of bacterial retention test on XG-PVA(GL1)_CX (a) and results from optical density (O.D.) of an agar piece collected far from the film, the film and the piece of agar under the film (b)

Moreover, the ability of XG-PVA(GL1)_CX film to provide protection against bacterial infiltration was further investigated. Hence, XG/PVA film was placed on a LB agar plate and 10 µl of *E. coli* were gently dropped in the centre of the film's surface as depicted in Fig. 7.15a. After 24 hours the agar below the film and a piece of agar with bacteria collected far from the film were cut and incubated in LB medium, and the bacterial growth was measured every 30 minutes. For this analysis a piece of solely agar without bacteria was used as control. The proliferation curves, shown in Fig. 7.15b, clearly indicate that the piece of agar under XG/PVA film does not show any bacterial growth, being comparable to the control without bacteria. This result suggests that the film is able to prevent bacterial infiltration and it can act as a barrier against infections when used as wound dressing.

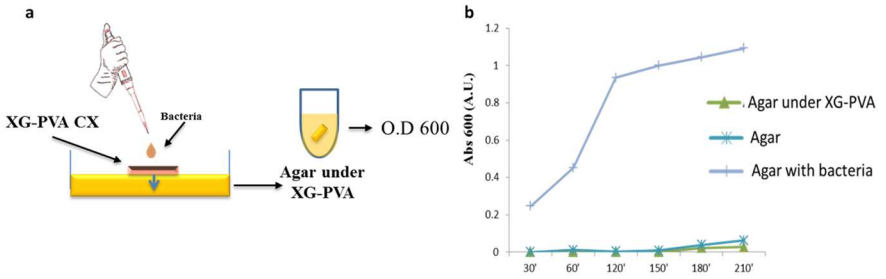

Fig. 7.15 Schematic representation of bacterial infiltration experiment (a) and optical density spectra (b)

However, XG-PVA(GL1)_CX film does not contain any active compound and its antibacterial activity may be improved by the incorporation of an antimicrobial or antibiotic.

7.4. Conclusions

In the present study, it was demonstrated the feasibility of integrating passive RFID sensor tags in XG-PVA-based hydrogel films in the perspective of developing "smart" plasters to monitor fluid loss and temperature of a wound. Swelling ability of XG-PVA(GL1)_CX was measured using a setup that could emulate the conditions of a dressing on an exuding wound and thus its ability to absorb simulated exudates (FBS) was estimated to be around 200% of its initial weight. The ability of the film to retain about the 50% of proteins contained in the simulated exudates, could prevent the side effects due to proteolytic activity of excessive exudate in the wound site.

The electrical characterization at frequencies between 10^{-2} and 106 Hz, revealed the conductivity of the film increases when swollen in saline solution, essentially due to the presence of the ionic species. RF characterisation revealed that the film is able to change RF response of the tag depending on its swelling degree and its dielectric properties, permittivity and conductivity, are increased at the increase of SD% at the high frequencies range confirming the possibility to exploit this device for sensing applications and in particular to monitor exudate loss in a wound.

Furthermore, XG-PVA(GL1)_CX film was found able to absorb and release a hydrophilic fluorescent probe and this results suggest the investigation about loading and release ability of this film with relevant active molecule (e.g. antibiotic). Finally, the film was demonstrated to have good ability to act as barrier against bacteria and thus in an application as wound dressing it can protect the wound from infections.

Contributions

The author wishes to point out the contribution of Dr. Maria Antonietta Sabatino for EIS spectroscopy characterisation, Dr. Cecilia Occhiuzzi and Prof. Gaetano Marrocco for RFID characterisations, Prof. Massimiliano Zingales for mechanical testing, Dr. Pasquale Picone for biological evaluations presented in this chapter.

Reference

[1] K. Järbrink, G. Ni, H. Sönnergren, A. Schmidtchen, C. Pang, R. Bajpai, J. Car, The humanistic and economic burden of chronic wounds: a protocol for a systematic review, Syst. Rev. 6 (2017) 1–7. doi:10.1186/s13643-016-0400-8.

[2] M. Turns, The diabetic foot: an overview of assessment and complications., Br. J. Nurs. 20 (2011) S19–S25. doi:10.12968/bjon.2011.20.Sup8.S19.

[3] J.S. Boateng, K.H. Matthews, H.N.E. Stevens, G.M. Eccleston, Wound Healing Dressings and Drug Delivery Systems: A Review, J. Pharm. Sci. 97 (2008) 2892–2922. doi:10.1002/jps21210.

[4] Z. Moore, S. Cowman, The need for EU standards in wound care : an Irish survey, Wounds UK. (2002) 20–28.

[5] R.G. Frykberg, J. Banks, Challenges in the Treatment of Chronic Wounds, Adv. Wound Care. 4 (2015) 560–582. doi:10.1089/wound.2015.0635.

[6] A.R. Siddiqui, J.M. Bernstein, Chronic wound infection: Facts and

controversies, Clin. Dermatol. 28 (2010) 519–526. doi:10.1016/j.clindermatol.2010.03.009.

[7] G.D. Winter, J.T. Scales, Effect of Air drying and Dressings on the Surface of a Wound, Nature. 4862 (1963) 91–92. doi:10.1038/197091b0.

[8] G.D. Winter, Formation of the Scab and the Rate of Epithelization of Superficial Wounds in the Skin of the Young Domestic Pig, Nature. 193 (1962) 293–294. doi:10.1038/193293a0.

[9] M. Romanelli, K. Vowden, D. Weir, Exudate management made easy, Wounds Int. 1 (2010) 1–6.

[10] T.R. Dargaville, B.L. Farrugia, J. a. Broadbent, S. Pace, Z. Upton, N.H. Voelcker, Sensors and imaging for wound healing: A review, Biosens. Bioelectron. 41 (2013) 30–42. doi:10.1016/j.bios.2012.09.029.

[11] C. Occhiuzzi, A. Ajovalasit, M.A. Sabatino, C. Dispenza, G. Marrocco, RFID Epidermal Sensor including Hydrogel Membranes for Wound Monitoring and Healing, in: 2015 IEEE Int. Conf. RFID, 2015: pp. 227–233.

[12] S. Amendola, C. Occhiuzzi, A. Ajovalasit, M.A. Sabatino, C. Dispenza, G. Marrocco, Dielectric Characterization of Biocompatible Hydrogels for Application to Epidermal RFID Devices, in: Microw. Conf., 2015: pp. 379–382.

[13] I. Waldron, S.N. Makarov, S. Biederman, R. Ludwig, Suspended ring resonator for dielectric constant measurement of foams, IEEE Microw. Wirel. Components Lett. 16 (2006) 496–498. doi:10.1109/LMWC.2006.880708.

[14] S. Amendola, C. Occhiuzzi, A. Ajovalasit, M.A. Sabatino, C. Dispenza, G. Marrocco, Dielectric characterization of biocompatible hydrogels for application to Epidermal RFID devices, in: Eur. Microw. Week 2015 “Freedom Through Microwaves”, EuMW 2015 - Conf. Proceedings; 2015

45th Eur. Microw. Conf. Proceedings, EuMC, 2015: pp. 379–382. doi:10.1109/EuMC.2015.7345779.

[15] J.H. Northrop, M. Kunitz, The Swelling and Osmotic Pressure of Gelatin in salt solutions, J. Gen. Physiol. (1926) 317–337. doi:10.1016/0008-8846(79)90050-4.

[16] P. Pissis, A. Kyritsis, Electrical conductivity studies in hydrogels, Solid State Ionics. 97 (1997) 105–113. doi:10.1016/S0167-2738(97)00074-X.

[17] B. Macdonald, J. Evgenij, Ross, eds., Impedance Spectroscopy: Theory, Experiment, and Applications, Wiley, 2005.

[18] C. Dispenza, C. Lo Presti, C. Belfiore, G. Spadaro, S. Piazza, Electrically conductive hydrogel composites made of polyaniline nanoparticles and poly(N-vinyl-2-pyrrolidone), Polymer (Guildf). 47 (2006) 961–971. doi:10.1016/j.polymer.2005.12.071.

CONCLUSIONS

This PhD project has given a contribution to the development of new materials addressed to an advanced wound management.

In particular, this research:

- introduced a new platform of materials for wound healing applications, which uses as main component a polysaccharide readily available at low cost, usually employed in food industry but with great potential for biomedical applications thanks to its intrinsic active properties which could enhance the healing process;
- produced new hydrogel films stable in contact with fluids, transparent, thus allowing the inspection of the wound without dressing removal, wearable thanks to their flexibility and resilience, and with tunable swelling degree and microstructure;
- used for the first time - to the best of my knowledge - a carboxylated XG to obtain new co-assembled materials suitable for biomedical applications and in particular for wound healing;
- investigated for the first time the co-assembly of peptide amphiphile with CXG as method to produce fibrous and cytocompatible scaffolds that promote cell adhesion and that are able to enhance the healing process *in vivo*;
- proved the concept of the integration of a hydrogel film with an RFID antenna to develop a sensor that can monitor fluid loss and temperature of a wound bed.

FUTURE DEVELOPMENTS

This study may provide inspiration for future research projects focused on the development of the here presented materials and device (Fig. II).

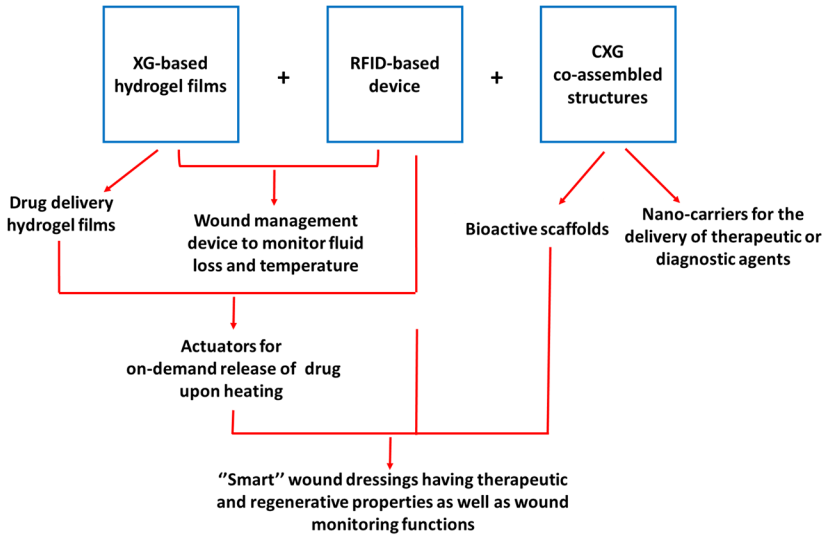

Fig.II Future developments of the here presented platform; red lines represent possible improvements of the new materials and device developed as part of my thesis (in blue boxes)

In particular,

- a more detailed *in vitro* and *in vivo* biological characterisation for the application of the xyloglucan-based films as wound dressings and for the validation of the polysaccharide intrinsic properties to the benefit of wound healing;
- the influence on the healing process of the XG-based films (with no PVA) semi-ordered microstructure on cell growth;
- the possibility of loading drugs, growth factors and/or cells on the dressing, to exploit scaffolding properties;

- the development and further optimisation of the RFID-based sensor, that could become also actuators if the hydrogel film would be loaded with an active molecule, or be applies in other fields than advanced wound dressings;
- CXG/polycations interactions could be explored to design multifunctional carriers for therapeutics or diagnostic purposes.

APPENDIX A

Experimental

A.1. Preparation procedures

A.1.1. Preparation of XG and PVA solutions

Xyloglucan aqueous solution (4 %wt) was prepared by adding the dry biopolymer to MilliQ water and stirring overnight at room temperature, while PVA (2 % wt) was dissolved in MilliQ water at 80°C for about 1 hour.

A.1.2. Xyloglucan functionalisation protocol

Carboxylation reaction was conducted on XG dispersed in water at 0.2 %wt. Polymer solution was initially de-oxygenated with N_2 for 30 minutes. The reaction was performed on 150 ml of polymer solution, by adding 3 mg (or 0.128 mM) TEMPO, 12.5 mg (or 0.81 mM) NaBr and 720 µl of 15% sodium hypochlorite solution (NaOCl) at 5°C under inert atmosphere and providing continuous magnetic stirring. Both pHmeter and temperature probes (HI 2211 pH/ORP Meter, Hanna Instrument) were assembled inside the bottle and pH was constantly measured (Fig. A.1). Thus, during the oxidation process small volumes of NaOH 0.1 M were added to maintain the pH around 9. The reaction was stopped after 4 hours, by adding 22.8 mg (or 4 mM) $NaBH_4$ powder. Functionalized polymer was recovered by precipitation in ethanol followed by freeze drying.

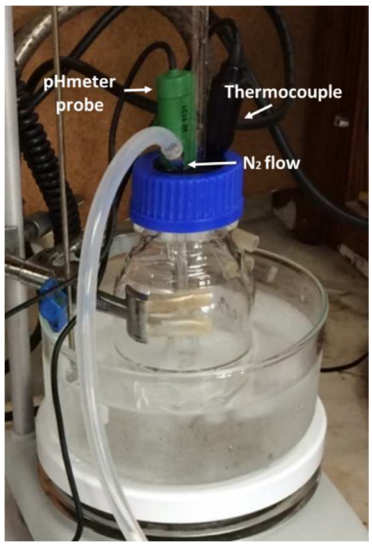

Fig. A.1 Reaction setup: pH and temperature probes were assembled inside a reaction bottle, providing a constant flux of N_2 and inside an ice bath to maintain the temperature below 5 °C

A.1.3. Peptide amphiphile synthesis and purification

Peptide synthesis and purification was performed at Queen Mary University of London.

Peptides were prepared on a 0.5 mmol scale using modifications of previously published protocols. (MBHA) Rink Amide resin (Novabiochem Corporation, UK) was used to generate a terminal amide.

All the amino acids and other reagents were dissolved in N,N-dimethylformamide (DMF).

Amino acid couplings were performed using four equivalents (4mmol) of Fmoc-protected amino acids (Novabiochem Corporation), four equivalents of 1-hydroxybenzotriazol (HOBT, Carbosynth Limited) and six equivalents of N,N'-diisopropylcarbodiimide (DIC, Sigma–Aldrich) for 1h. Fmoc was removed with 1-hour treatment of 20% v/v piperidine (Sigma–Aldrich) in DMF. After treatment with piperidine, Kaiser test (phenol, 80% in ethanol, KCN in H_2O/ pyridine and

Ninhydrin, 6% in ethanol, Sigma-aldrich) was used to check the effectiveness of the Fmoc deprotection at each aminoacid coupling. Following Fmoc removal from the last amino acid residue of the desired sequence, an alkyl tail moiety of palmitic acid ($C_{16}H_{32}O_2$, Calbiochem) was conjugated to the free N-terminus. The alkylation reaction was performed using four equivalents of the fatty acid, four equivalents of HOBT, and six equivalents of DIC in DMF/dichloromethane and the reaction was carried out overnight. The reaction was stopped when a negative Kaiser test was obtained.

After the reaction was finished, the resin was washed several times with DCM before cleavage from the resin. Cleavage of peptide amphiphile from the resin and deprotection were carried out with a mixture of trifluoracetic acid (TFA, Sigma-Aldrich)/triisopropylsilane (TIS, Alfa Aesar)/water (95:2.5:2.5) for 3h at room temperature. The solution was then collected by filtration and all washings were combined and rotoevaporated to remove residual TFA. The viscous peptide solution was precipitated by addition of cold diethyl ether. The precipitate was collected by centrifugation and was washed several times with cold ether followed by drying overnight under vacuum.

For peptide purification, freeze dried peptide amphiphile was dissolved in deionized water at 5 mg/ml concentration and purified using a 2545 binary gradient preparative High-Performance Liquid Chromatography (Waters, USA) with a 2489 UV/Visible detector (Waters, USA) using a C18 column (Atlantis Prep OBD T3 Column, Waters, USA) and a water/acetonitrile gradient containing 0.1%v TFA.

Purified fractions of peptide in solution were frozen and then lyophilized to collect the pure peptide. The mass of the peptides was confirmed by electrospray ionisation (ESI, Thermo LXQ, Thermo Scientific, USA) and matrix-assisted laser desorption ionisation-time of flight mass spectrometry (MALDI-TOF MS, Applied Biosystems 4800 Proteomics Analyzer (TOF/TOF) mass spectrometer).

A.1.4. Preparation of PDMS surfaces

To prepare polydimethylsiloxane (PDMS) (Sylgard 184, Dow Corning, USA) surfaces used for the preparation of CXG/PA-H3 gels it was used the following protocol: the desired amount of elastomer was weighed inside a glass beaker, 10 %wt of the curing agent was added to the elastomer and the mixture was manually stirred. Once the mixture was homogeneous, it was poured into plastic petri dishes. To prepare PDMS channel, a cylindrical aluminium stick with a diameter of 3 mm was placed on the precursors mixture. Then the petri was placed in a pre-heated oven at 60°C for at least 1 hour.

A.2 Characterisations

A.2.1. Unreacted glutaraldehyde evaluation

A weighted amount of "dry" XG or XG/PVA crosslinked hydrogel films was immersed in MilliQ water for 20 minutes. After this time, an aliquot of MilliQ water in which the film was immersed was analysed using a UV-670 Spectrophotometer (Jasco). This procedure was repeated several times, until complete disappearance of the characteristic glutaraldehyde absorption peak at 280 nm. A calibration curve of GA was built for the quantitative analysis of the GA released by the films.

A.2.2. Shear viscosity measurements

Shear viscosity measurements presented in Chapter 4 and Chapter 5 were performed in a stress-controlled Rheometer Ar G2, TA Instruments (Bipohysics Institute Palermo Unit, National Research Council) in rotational mode. Low concentrated samples were analysed with an acrylic plate-cone geometry (angle < 0.0174 rad, radius 20 mm, truncation 30 μm) and a gap of 30 μm, while concentrated samples were analysed with an acrylic plate-plate geometry (diam. 4 cm) and a gap of 500 μm. Shear viscosity measurements were performed at 25 °C and the duration of

measurements was chosen according to the explored shear rate range. Temperature control was provided by a Peltier plate.

A.2.3. Fourier-transform infrared spectroscopy (FTIR)

FTIR analyses were carried out with a Perkin Elmer-Spectrum 400 apparatus at the University of Palermo. Samples of XG-based films (Chapter 4) were prepared by freezing and freeze-drying the film samples. The freeze-dried products were mashed and diluted with potassium bromide anhydrous powder to have final concentration of the sample of about 3 %wt; then they were compressed into pellets.

CXG samples presented in Chapter 5 having carboxyl groups in dissociated form, were prepared dissolving an amount of CXG in MilliQ water before the analysis and assuring that pH was around 6-7. While samples of CXG with carboxyl groups in undissociated form, namely in the protonated form, were prepared dissolving CXG in MilliQ and adjusting pH to about 3 by addition of HCl (1M); both solutions were subsequently lyophilised and then mashed with KBr (final conc of the sample 3 %wt) for the preparation of a tablet. All the spectra were collected by accumulation of 32 scans between 4000 and 400 cm^{-1}, with a resolution of 4 cm^{-1} and normalised to do the comparison.

FTIR measurements of CXG/PA-H3 mixtures (Chapter 6) were performed at Queen Mary University of London using a Brukler Tensor 27 FTIR spectrometer. CXG/PA-H3 gels were freeze dried and then mashed in presence of KBr so that the samples had a concentration of 2-3 % in the analysed tablets. Spectra were acquired by accumulation of 32 scans between 4000 and 800 cm^{-1}, with a resolution of 4 cm^{-1}.

A.2.4. Thermal gravimetric analysis (TGA)

For XG- and XG/PVA-based films (Chapter 4), thermal-gravimetric analysis of (TGA) was conducted with a Setaram, Labsysevo, TGDTA/DSC at University of

Palermo. Samples were pre-conditioned at 20 °C and 11 % RH, and tested in a temperature range of 20−500 °C at a heating rate of 10 °C/min. The characteristic temperatures associated to the various phenomena are calculated as the peak temperature of the first derivative function (DTG).

TGA analysis on XG and on CXG (Chapter 5) was performed with a TA Instruments Q500 at Queen Mary University of London. Samples were pre-conditioned at 20 °C and 10 % RH and then loaded on platinum sample holder and tested in a temperature range of 20−500°C at a heating rate of 10°C/min under constant nitrogen flux.

A.2.5. Scanning electron microscopy (SEM)

Fracture surface morphology was imaged by a field emission scanning electron microscopy (FESEM) system (JEOL) at an accelerating voltage of 10 or 20 kV. Freeze-dried samples were mounted on SEM aluminium stubs by means of a graphite adhesive layer. Then, samples were coated with a gold layer by JFC-1300 gold coater (JEOL) for 50 s at 30 mA for 60 or 120 seconds, depending on the porosity of the sample, before scanning.

A.2.6 Carboxyl-groups titration

A volume of 15 ml of CXG 0.1 %wt was poured in a glass beaker containing a pHmeter probe (HI 2211 pH/ORP Meter, Hanna Instrument). Titration was performed under constant agitation using a standardized NaOH 0.05M solution as titrant. The equivalent point was detected when pH reached 7. The amount of carboxyl groups was subsequently calculated equal to moles of NaOH added at the equivalent point.

A.2.7. Gel filtration chromatography (GFC)

Gel filtration chromatography is a size exclusion chromatography in which water is used to transport the sample through the column. The chromatographic profiles of XG and CXG (Chapter 5) were obtained by using two Shodex SB HQ columns in series (806 and 804) connected to an Agilent 1260 Infinity HPLC and equipped with a 50 µl sample loop (equipment belonging to University of Palermo). Samples were filtered with 1.2 µm cellulose acetate (Millipore) syringe filters before analysis to eliminate contaminants. All samples were eluted with 0.02%wt sodium azide solution at 0.6 ml/min and the refractive index was recorded with a Smartline RI detector 2300 Knauer.

A.2.8 Static and dynamic Light Scattering (SLS, DLS)

Both for static and dynamic light scattering measurements presented in Chapter 5, samples were placed into a thermostated cell compartment of a Brookhaven Instrument BI200-SM goniometer (equipment belonging to Biophysics Institute, Palermo Unit, National Research Council). The temperature was controlled to within 0.1°C using a thermostated recirculating bath.

The light scattered intensity and time autocorrelation function (TCF) were measured by using a Brookhaven BI-9000 correlator and a 100mW solid-state laser (Quantum-Ventus MPC 6000) tuned at λ = 532 nm or a 50mW He–Ne tuned at λ = 632.8 nm. Measurements were taken at different scattering vectors $q=4\pi n \lambda_0\text{-}1/\sin(\theta/2)$, where n is the refractive index of the solution, λ_0 is the wavelength of the incident light, and θ is the scattering angle. For both SLS and DLS, samples were filtered through 5 or 1.2 µm cellulose acetate (Millipore) syringe filters before the measurements to remove gross contaminants and big aggregates.

Dynamic light scattering (DLS): In DLS experiments the correlator operated in the multi-τ mode and the experimental duration was set to have at least 2000 counts on the last channel of the correlation function.

Stretched exponential or cumulants fittings were used to analyse the obtained decay curves. For single measurements performed at 90° scattering angle and at 25°C the method of cumulant [1] and the exponential stretched method were compared to obtain information on the apparent hydrodynamic size and width of the size distribution. According to the cumulant method, the logarithm of electric field autocorrelation function can be expanded in terms of the cumulants of the distribution:

$$\ln[g(\tau)] \equiv K(-\tau, \Gamma) = -\Gamma\tau + \frac{k_2}{2!}\tau^2 - \frac{k_3}{3!}\tau^3 + \frac{k_4}{4!}\tau^4 \ldots$$

The fitting of the auto-correlation function to a stretched exponential is given by

the equation:

$$g(\tau) = A\exp(-\left(\frac{t}{\tau}\right)^{-\beta})^2$$

where τ is the relaxation time and β is the stretched exponential and it is related to the width of the relaxation time distribution. β values are in the range 0-1, with smaller values corresponding to wider distributions.

The average relaxation time τ_c can be calculated by:

$$\tau_c = \frac{\tau}{\beta}\,\Gamma\left(\frac{1}{\beta}\right)$$

Where Γ is the decay rate.

Static light scattering (SLS): For SLS, data were corrected for the background scattering of the solvent and normalized by using toluene as calibration liquid.

Determination of CXG and XG weight-average molecular weight from SLS was obtained from Zimm equation [2]:

$$\frac{K_c}{\Delta R_{(\theta,c)}} = \frac{1}{M_w}\left(1 + \frac{q^2\ {R_g}^2}{3} + O(q^4)\right) + 2A_2c + O(c^2)$$

A Zimm plot is built from a double extrapolation to zero angle and zero concentration from many angle and many concentration measurements. In the simplest form, the Zimm equation is reduced to:

$$\frac{K_c}{\Delta R_{(\theta,c)}}\ (\theta \to 0, c \to 0) = \frac{1}{M_w}$$

for measurements made at low angle and infinite dilution since P(0)=1. Experiments were performed at 10 different angles (i.e. 30°, 45°, 50°, 60°, 75°, 90°, 105°, 120°, 135°, and 150°) which satisfy condition $qR_g < 1$ and 5 different concentrations (i.e. 0.5 mg/ml, 1 mg/ml, 1.4 mg/ml, 2 mg/ml, 2.5 mg/ml).

A.2.9 Differential scanning calorimentry (DSC)

DSC of CXG and XG (Chapter 5) was performed with a Perkin-Elmer DSC4000 calorimeter belonging to University of Palermo. XG and CXG samples of about 7-10 mg were weighed in aluminium pans that were sealed and a hole was made in the center of the lid. Heating/cooling cycle was carried out (i) heating the samples from 30 °C to 200 °C at a heating rate of 10 °C/min under constant nitrogen flow, (ii) holding the temperature for 5 minutes, then (iii) cooling from 200 °C to 30 °C at a rate of 10°C/min, and finally (iv) the first heating step was repeated.

A.2.10 ζ-potential measurements

ζ-potential measurements presented in Chapter 5 and Chapter 6 were performed using a Zetasizer Instrument (NANO-ZS ZEN3600, Malvern Instruments) belonging to Queen Mary University of London (UK), on 0.1 %wt solutions. When required, pH of the samples was adjusted adding small amount of HCl (1 M) or NaOH (1M) to reach a desired value. Samples were let to equilibrate for 120s before measuring

the ζ-potential, using an applied voltage of 50.0 V. The results presented are the average over three measurements.

A.2.11 CD spectroscopy

CXG and PA-H3 solutions for CD analysis were prepared in isotonic 10mM HEPES buffer at 0.01 %wt. Mixtures were prepared mixing CXG and PA-H3 0.01 %wt HEPES solutions at different volume ratios 1:1, 2:1, 3:1 and 5:1. Absorption of the sample was firstly assessed below 1. CD spectra were recorded under a constant flow of nitrogen at a constant pressure of 0.7 MPa and temperature of 25°C with a Pistar-180 spectrophotometer from Applied Photophysics (equipment belonging to Queen Mary University of London,UK) in a range from 190 nm to 260 nm at a step size of 0.5 nm. Data were averaged over three spectra for each sample.

A.2.12 Transmission electron microscopy (TEM)

Samples were casted onto carbon film coated copper TEM plasma etched holey carbon-coated copper grids (Agar Scientific) and incubated for 5 min. Excess was removed on filter paper before incubation with 2 %wt uranylacetate filtered solution for 30 seconds. Grids were then washed with ultrapure water for 30s and air dried for 24h at room temperature. Bright-field TEM imaging was performed on a JEOL 1230 Transmission Electron Microscope operated at an acceleration voltage of 80 kV (equipment belonging to Queen Mary University of London, UK). All the images were recorded by a Morada CCD camera (Image Systems). At least three images were taken per samples for further analysis.

A.3 Biological evaluations

A.3.1 Cell culture

Biological assessments presented in Chapter 4, Chapter 7 and part of the evaluations presented in Chapter 5 were performed at the Institute of biomedicine and

immunology (IBIM) of the National centre of Research (CNR) of Palermo (Italy), using adenocarcinomic human alveolar basal epithelial cells (A549) and human neuroblastoma cell line (LAN5). These cell lines were cultured with RPMI 1640 medium (Celbio srl, Milan, Italy) supplemented with 10 % fetal bovine serum (FBS) (Gibco-Invitrogen, Milan, Italy), 2 mM glutamine, 1 % penicillin and 1 % streptomycin (50 mg/ml). Cells were maintained in a humidified 5 % CO_2 atmosphere at 37 ± 0.1 °C. Confluent cells were detached using 0.25% (wt/v) trypsin-EDTA.

Other experiments presented in Chapter 5 and all the evaluations presented in Chapter 6 were performed at Queen Mary University of London, using keratinocyte cell line (HaCat).

HaCat were cultured in 75 cm^2 cell culture flask in Dulbecco's Modified Eagle's Medium (DMEM) from ThermoFisher sci. supplemented with 10% fetal bovine serum (FBS) from ThermoFisher sci. and antibiotic solution (streptomycin 100 mg/mL and penicillin 100 U/ml, Sigma Chem). Cells were maintained in a humidified 5 % CO_2 atmosphere at 37 ± 0.1 °C. Confluent cells were detached using 0.25% (wt/v) trypsin-EDTA.

A.3.2 MTS assay

Cell viability was measured by MTS assay (Promega Italia, S.r.l., Milan, Italy). MTS [3 - (4,5-dimethylthiazol-2-yl) – 5 - (3-carboxymethoxyphenyl) - 2 - (4 - sulphophenyl)-2H-tetrazolium], utilized according to the manufacturer's instructions. The absorbance was read at 490 nm on the Microplate reader Wallac Victor 2 1420 Multilabel Counter (PerkinElmer, Inc. Monza, Italy). Results were expressed as the percentage of MTS reduction relatively to the control.

A.3.3 LIVE/DEAD® viability test

For the evaluation of cell viability presented in Chapter 5 and Chapter 6, cells were stained with 10 mM calcein AM and 1 mM ethidium homodimer-1 (Life Technologies, UK), incubated 30 minutes with the staining before the analysis. Stained samples were then visualized on an inverted Confocal Laser Scanning Microscope (CLSM) (Leica Laser Scanning Confocal TCS SP2) belonging to Queen Mary University of London (UK). Viability percentage was estimated from confocal images, using ImageJ-Fiji macro processing and averaged on three different experiments ((http://imagej.nih.gov/ij) (NIH, USA).

A.3.4 Cytoskeleton and nuclei staining

For cell attachment evaluations presented in Chapter 6, HaCat cells attached on the gels were fixed with 4% paraformaldehyde (PFA) for 1 hour at RT. Afterward, cells were washed again 1 or 2 times with PBS buffer to remove PFA and incubated for 5 minutes at 0°C with the permeabilising solution (1ml Triton x-100, 0.028 g NaCl, 0.003 g $MgCl_2$, 1.099 g sucrose in 20 ml of PBS). After this time, samples were washed three times with PBS prior treatment with (4',6-diamidino-2-phenylindole (DAPI) 1/1000 dilution for the staining of the nuclei and with phalloidin 555 1/1000 dilution for the staining of the cytoskeleton for 40 minutes. Samples were finally washed from the staining agents with PBS and stored in PBS at 4°C. Stained samples were then visualized on an inverted Confocal Laser Scanning Microscope (CLSM) (Leica Laser Scanning Confocal TCS SP2) belonging to Queen Mary University of London (UK).

A.3.5 Scratch test

Scratched areas were then estimated using ImageJ-Fiji software, ((http://imagej.nih.gov/ij) (NIH, USA).

The percentage of scratch closure was calculated as follow:

$$\frac{A_i - A_{24h}}{A_i} \; x \; 100$$

Where, A_i is the initial scratched area, A_{24h} is the scratched area after 24h.

A.3.6 *In vivo* wound closure

Ten-week-old male CD1 mice were anesthetized by isofluorane inhalation, and the dorsal skin was shaved and sterilized with an alcohol swab. Two full-thickness circular 5 mm biopsy punch excisions (surface area of 19.63 mm^2) were made using a Biopsy Punch (Stiefel). The wounds were made approximately 1 cm apart on the dorsum of mice and left to heal by secondary intention. Wounds were left untreated or had a hydrogel added to the wound bed. The hydrogels were UV irradiated (300,000 microJoules per cm^2) prior to application. The wounds were covered by Tegaderm (3M) transparent wound dressing, which was secured at the edges by Vetbond Tissue Adhesive (3M). Mice received a single intramuscular injection of buprenorphine (Vetergesic) at 0.03 mg/kg immediately following surgery as an analgesic. Following the surgery, mice were housed individually with access to food and water ad libitum. All experiments were reviewed and approved by the animal use committee at Queen Mary University of London and were conducted in accordance with licenses granted by the United Kingdom Home Office. Wounds were collected at day eight post-wounding. The horizontal and vertical diameters of the wounds were measured to permit calculation of the wound area. Wounds were excised and bisected using a scalpel. Half of each wound was snap frozen in liquid nitrogen and the other half was fixed in 10% Neutral Buffered Formalin for 24 hours followed by storage in 70% Ethanol to permit histological analysis at a later time point.

A.3.7 Statistical analysis

Numerical data were expressed as mean ± standard deviation or ± standard error of the mean. All experiments were repeated at least three times. Analysis was performed using GraphPad Prism 15 (La Jolla, USA). One-way analysis of variance (ANOVA) for multiple comparisons were employed. Non parametric statistics were

used when the samples did not present a normal distribution (Mann-Whitney test). Statistical significance was accepted when $p<0.05$.

A.4 Supplementary information

A.4.1 Gel filtration chromatograms of xyloglucan purchased from DSP Gokyo (Japan) and xyloglucan purchased from Megazyme

From GFC chromatography (Fig. A.2) the two batches of xyloglucan resulted comparable and they were use indifferently in this thesis.

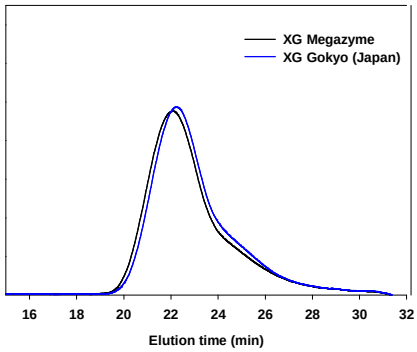

Fig. A.2 GFC chromatogram of XG from Megazyme vs. XG from Gyko (DSP)

References

[1] D.E. Koppel, Analysis of Macromolecular Polydispersity in Intensity Correlation Spectroscopy: The Method of Cumulants, J. Chem. Phys. 57 (1972) 4814–4820. doi:10.1063/1.1678153.

[2] B.H. Zimm, The Scattering of Light and the Radial Distribution Function of High Polymer Solutions, J. Chem. Phys. 16 (1948) 1093–1099. doi:10.1063/1.1746738.